Développement de liquides synoviaux synthétiques bio-inspirés

par

Jimmy Faivre

Thèse effectuée en cotutelle

à la

Faculté de Pharmacie

Université de Montréal

et au

Laboratoire Ingénierie des Matériaux Polymères

Université Claude Bernard Lyon 1

Thèse présentée à

la Faculté des études supérieures et postdoctorales de l'Université de Montréal en vue de l'obtention du grade de Philosophiae Doctor (Ph.D)
en Sciences Pharmaceutiques

et à

l'École Doctorale Matériaux ED 34 de l'Université Claude Bernard Lyon 1 en vue de l'obtention du grade de Docteur
en Matériaux

Juillet, 2018

Résumé

La bioinspiration consiste à analyser les systèmes naturels qui se sont adaptés parfaitement à leurs environnements pour développer des solutions ingénieuses. Ce projet de thèse aborde la thématique de la lubrification articulaire dans le but de développer un traitement contre l'*ostéoarthrite* (OA). Nous nous sommes inspirés des articulations synoviales, systèmes tribologiques très performants grâce aux interactions synergiques entre la structure unique du cartilage et les molécules lubrifiantes (ML) du fluide synovial (SF). Cependant, lors de l'OA des mécanismes inflammatoires et d'érosion mécanique aboutissent à la dégénérescence progressive du cartilage et la dégradation spécifique des ML du SF (aggrécane et lubricine). Des mimes des ML du SF ont été synthétisés reprenant leur structure particulière dite en écouvillon moléculaire (BB), structure responsable de la lubrification. Des tests tribologiques (SFA, tribomètre) ont montré que les BB garantissent à la fois une faible friction et une résistance à l'usure sur des surfaces dures de mica. Ceci est dû à la présence, sur nos EM, de groupements d'ancrage spécifiques assurant l'adsorption sur la surface de mica et à la formation d'enchevêtrements et d'interactions intermoléculaires avec l'acide hyaluronique de haut poids moléculaire, composant essentiel du SF. Des mimes de cartilage à base d'hydrogels de chitosane multicouches ont été également réalisés reprenant les principales propriétés architecturales du cartilage. En combinaison avec nos EM, ces hydrogels, matériaux poroélastiques fragiles, sont capables d'être lubrifiés avec une friction dans la gamme physiologique et une nette amélioration de leur usure.

Mots clés : écouvillon moléculaire, acide hyaluronique, tribologie, friction, lubrification, usure, hydrogel, articulations, liquide synovial, cartilage.

Abstract

Bioinspiration consists in the design of materials inspired by biological systems which have developed ingenious solutions to suit their environment. This project deals with bioinspiration for joint lubrication and in particular for the development of treatments for patients suffering from osteoarthritis (OA). To do so, we took our inspiration from joints which are amongst the most efficient aqueous tribological systems. Their unique properties arise from the complex synergistic interactions between cartilage structure and the lubricant macromolecules of the synovial fluid (SF). However, during OA, inflammatory mechanisms as long as mechanical erosion result in the degeneration of cartilage and lubricant macromolecules (aggrecan and lubricin). Polymeric mimes of the SF have been synthesized based on the bottle-brush (BB) architecture of LUB and AGG which is responsible for the joint lubrication. Tribological tests (SFA, tribometer) showed that BB polymers provided mica surfaces with a low friction and a wear protection up to several megapascals, typically in the range of natural joints. This wear protection was essentially due to the incorporation of anchoring groups specific to mica tribopairs on the BB polymers and the intermolecular bridging and entanglements emerging between BB polymers and high molecular weight HA, another main SF component. Cartilage mimes composed of multilayered chitosan hydrogels were designed to mimic the basic features of cartilage. Along with our BB polymers, the hydrogels, which are poroelastic and fragile materials, provided a low friction and a great decrease of wear.

Key words: bottle-brush polymers, tribology, friction, lubrication, wear, hydrogel, joints, synovial fluid, cartilage.

Table des Matières

Liste des illustrations

Chapitre 1

Chapitre 2

Chapitre 3

Chapitre 4

Listes des schémas

Liste des tableaux

Liste des abréviations

ACLT	Coupe transversale du ligament croisé antérieur (Anterior Cruciate Ligament transection)
AdG theory	Théorie d'Alexander - de Gennes
AFM	Microscopie à force atomique (Atomic Force Microscopy)
AGG	Aggrécane
ATRP	Polymérisation radicalaire par transfert d'atome (Atomic Transfer Radical Polymerization)
BB	Architecture en "écouvillon moléculaire" (Bottle-Brush)
CLSM	Microscopie confocale (Confocal Laser Scanning Microscopy)
CoF ou μ	Coefficient de friction (Coefficient of Friction)
C_p	Concentration en chitosan
D	Distance de séparation
DA	Degré d'acétylation (Degree of Acetylation)
DMA	Analyse mécanique dynamique (Dynamic Mechanical Analysis)
DMAEMA	Méthacrylate de diméthyle amino éthyle (Dimethyl Amino Ethyl Methacrylate)
DP	Degré de polymérisation (Degree of Polymerization)
DPPC	1,2-Dipalmitoylphosphatidylcholine
DZ	Zone profonde (Deep Zone)
E	Module d'Young
EBiB	α-bromoisobutyrate d'éthyle (Ethyl α-bromoisobutyrate)
ECM	Matrice extra-cellulaire (Extra-Cellular Matrix)
FECO	Franges d'ordre chromatique égal (Fringes of Equal Chromatic Order)
FITC	Fluorescéine isothiocyanate
F_N	Force normale
FRAP	Redistribution de la fluorescence après photoblanchiment (Fluorescence Recovery After Photobleaching)
F_s ou F_t	Force tangentielle
G	Domaine globulaire
G', G"	Module de conservation, Module de perte
GAG	Glycosaminoglycane
GPC	Chromatographie par perméation de gel (Gel Permeation Chromatography)

HA	Acide hyaluronique (hyaluronic acid)
HEMA-TMS	2-(trimethylsilyloxy)ethyl methacrylate
HEPES	Tampon à base de 4-(2-hydroxyéthyl)-1-pipérazine éthane sulfonique (pH 7.4, 150 mM NaCl) (Phosphate Buffer Saline)
IPN	Réseaux hydrogels interpénétrés (interpenetrated Network)
k	Constante de cinétique
k_b	Constante de Boltzmann
KF	Fluorure de potassium (Potassium Fluoride)
K_{gel}	Perméabilité du gel
L_c	Longueur d'une chaine de polymère totalement étendue (Contour Length)
LUB	Lubricine
MI	Macroinitiateur (Macroinitiator)
MMA	Acide méthacrylique (Methylmethacrylate Acid)
M_n	Masse molaire en nombre d'un polymère
MPC	2-méthacryloyloxyethyle phosphorylcholine
M_w	Masse molaire en poids d'un polymère
MWCO	Masse molaire la plus basse pour laquelle 90 % du soluté sera retenu par une membrane de dialyse (Molecular Weight Cut-Off)
MZ	Zone médiale (Middle Zone)
NMR	Spectroscopie de résonnance magnétique nucléaire (Nuclear Magnetic Resonance)
OA	Ostéoarthrite ou arthrose (Osteoarthritis)
P*,P_c ou σ_c	Pression critique
P, σ	Pression (stress)
PAA	Polyacrylic acid
PAM	Polyacrylamide
PAMPS	poly(2-acrylamide-2-methylpropane sulfonic acid)
PBiBEM	Poly(2-bromoisobutyryloxyethyl methacrylate)
PBS	Tampon phosphate (pH 7.4, 150 mM NaCl) (Phosphate Buffer Saline)
PdI	Polydispersité
PDMS	Polydimethylsiloxane
PEG	Poly(ethylene glycol)

PEGMA	Poly(ethylene glycol) methacrylate
PEX	Haemopexine
PG	Protéoglycane
pH	Potentiel Hydrogène
PHEMA	Polyhydroxyethylmethacrylate
PLL	Poly(*L*-lysine)
PMAA	Polymethacrylic acid
PMETAC	Poly[(2-(methacryloyloxy)ethyl) trimethylammonium chloride]
PMMA	Poly(Methylmethacrylate Acid)
PMPC	Poly(2-methacryloyloxyethyl phosphorylcholine)
PNIPAM	Poly(N-isopropylacrylamide)
PRG4	Protéoglycane 4
PSBMA	Poly(sulfobetaine methacrylate)
PSPMA	Poly(3-sulfopropylmethacrylate potassium salt)
PVA	Poly(vinyl alcohol)
PVP	Poly(N-vinylpyrrolidone)
R	Rayon de courbure
R_g	Rayon de gyration
SEC	Chromatographie par exclusion stérique (Size Exclusion Chromatography)
SEM	Microscopie électronique à balayage (Scanning Electron Microscopy)
SF	Fluide synovial (synovial fluid)
SFA	Appareil de forces de surface (Surface Forces Apparatus)
SMB	2-somatomedine B
SSF	Fluide synovial synthétique
SZ	Zone superficielle (Superficial Zone)
T	Température
t	Temps
TBAF	Fluorure de tétrabutylammonium (Tetrabutylammonium Fluoride)
THF	Tétrahydrofurane
UHMWPE	Polyethylene de masse molaire très élevée (Ultra High Molecular Weight Polyethylene)
v	vitesse
VP-ITC	Calorimètre de titration isotherme (Isothermal Titration Calorimeter)

Γ, z	Densité de greffage
ε	Déformation (Strain)
η	viscosité
Π_0	Pression osmotique
τ	Temps caractéristique

À toi, mon petit Bonhomme, mon Étoile !

Remerciements

Cette thèse de doctorat a été effectuée en cotutelle de thèse entre l'Université de Montréal, Canada et l'Université Claude Bernard Lyon 1, France au sein des laboratoires Biomaterials and structured Interfaces du Pr Xavier Banquy et Ingénierie des Matériaux Polymères avec les Pr Laurent David et Thierry Delair.

Mes remerciements s'adressent en premier lieu à mes directeurs de thèse. Je remercie le Pr Xavier Banquy qui m'a proposé ce projet alors que j'étais en stage au sein de son laboratoire. Je le remercie de m'avoir fait confiance pour ce projet ambitieux, mais également pour toutes les riches discussions que nous avons eues et son aide précieuse tout du long de ces quatre années de doctorat. Je remercie également les Pr Laurent David et Thierry Delair de m'avoir accueilli avec enthousiasme, d'avoir enrichi ce projet de leurs précieuses expertises et d'avoir initié des collaborations pour mon projet. Leurs suggestions, leur aide et leurs conseils sont de précieux atouts qui me guideront dans ma vie de scientifique.

Je tiens à remercier Mesdames Anne Jonquières et Anne Rubin, rapporteures, Mesdames Antonella Badia et Daria Camilla Boffito et Messieurs Eric Allémann et François Lux, examinateurs, ainsi que mes directeurs et codirecteurs de thèse pour le temps passé à la lecture de cette thèse de doctorat.

Je remercie les coauteurs des articles scientifiques présentés dans ce manuscrit pour leur aide scientifique et technique. Sans leur aide, ce travail n'existerait pas.

Je remercie plus particulièrement le Dr Buddha Ratna Shrestha pour son aide, ses discussions toujours intéressantes et ses conseils.

J'ai une pensée particulière pour le Pr Krzysztof Matyjaszewski. Ce fut un privilège d'avoir pu collaborer avec son laboratoire. Sa rapidité de réponse à nos questions et de relecture d'articles m'ont impressionné. Je remercie particulièrement le Dr Guojun Xie pour son enthousiasme et sa rapidité que ce soit pour la synthèse de polymères, la relecture d'articles ou la réponse à de simples questionnements.

Je voudrais également remercier le Pr Stéphane Benayoun de m'avoir proposé de venir effectuer mes tests tribologiques dans son laboratoire et pour son expertise essentielle à la rédaction de mes articles. Son aide m'a permis d'enrichir mon travail. Je remercie également Matthieu

Guibert d'avoir conçu, tout spécialement pour ce projet, le tribomètre faible charge si utile à mon travail et également Thomas Malhomme pour son temps à m'aider en interférométrie.

Merci au Pr Moldovan de m'avoir permis d'aborder des thématiques d'études *in vitro* et *in vivo* au sein de son laboratoire. Sa gentillesse et son aide m'ont permis de découvrir de nouvelles techniques et d'apporter une plus-value indéniable à ce travail. Je remercie également tous les membres de son laboratoire pour leur aide et leur temps à me former.

Je remercie particulièrement les Drs Alexandra Montembault et Guillaume Sudre pour leur disponibilité et aide en tout temps de cette thèse. Vos conseils me sont très précieux. Merci pour le temps passé à répondre à mes questions auxquelles vous avez toujours répondu avec plaisir et pertinence.

Je remercie également les Pr Valérie Gaëlle Roullin et Jeanne Leblond Chain pour leurs rôles essentiels dans ma formation de doctorant en tant, notamment, que membres de mon comité de suivi de thèse, mais également pour le temps pris à discuter sur des sujets hors projet et tout aussi importants.

Je remercie spécialement les organismes subventionnaires qui m'ont également soutenu financièrement durant ces quatre années en plus des fonds de mes directeurs de thèse : la Société de l'Arthrite, le programme Avenir Lyon Saint-Étienne de l'Université de Lyon, le programme Frontenac du consulat général de France à Québec, le conseil Franco-Québécois de Coopération Universitaire, la Faculté de Pharmacie de l'Université de Montréal et la Faculté des Études Supérieures de l'Université de Montréal.

J'adresse mes remerciements à tous les membres des laboratoires français et canadien. Côté Canadien, je remercie le Pr Leclair, pour m'avoir permis d'enseigner les sciences pharmaceutiques aux étudiants de la Faculté de Pharmacie, le Pr Hildgen, pour sa gentillesse et ses réponses riches de son expérience. Je remercie les membres extraordinaires de la plateforme de l'axe formulation et analyse du médicament, Martin, Michaela, Amandine et Isabelle toujours disponibles et très agréables. Je remercie chaque étudiant au doctorat, à la maitrise, en stage, en post-doctorat et les permanents du "4ème" qui de près ou de loin m'ont aidé à réaliser ce doctorat dans les meilleures conditions : Alex, Hugo, Wided, Lucie et Suzanne pour leur aide avec les surfaces de mica, Cloé, Ina, Florian, Ophélie, Mouna, Teresita, Vahid, Frédéric, Soudeh, Jean-Michel, Lorine, Aline, Guillaume, Shaker, Mirza, Warren, Amira, Aurore,

Araceli, Arnould, Cyrielle, Nicolas, Audrey, Alexander, Johanne. Vous êtes géniaux, restez comme vous êtes ! J'ai une pensée toute particulière envers mon collègue de bureau, interlocuteur scientifique, partenaire de sport et de jeux et tout simplement ami Pierre-Luc. Ces années passées au Québec n'auraient pas eu cette saveur si particulière sans lui. Côté Français, je remercie chaque personnel permanent pour leur aide. Plus particulièrement, je remercie Agnès Crépet pour son aide précieuse en GPC, Pierre Alcouffe pour le temps passé en SEM et le Dr Béatrice Burdin, pour son expertise en CLSM. Tout comme mes collègues et amis canadiens, je remercie chaque étudiant du laboratoire IMP. Vous comptez beaucoup pour moi : Christophe, Guillaume, Pierre, Mona, Sarra, Dimitri, Luisa, Injee, Yann, Mélanie, Anatole, Michaël, Florian, Antoine, Claire, Orianne, Mo, Imed, Marjo, Nico, Fabien, Antoine, Mathilde, Amani, Gautier, Margarita, Renaud, Benjamin, Manon, Noémie, Hubert, Thouaiba, Marwa, Maxime, Aurélie, Adrien, Paula, Maud, Anais, Anthony, Laura, Bryan, Hend, Amira, Chloé, Mathieu, Baptiste, Soline, Pierre, Thibaut, Clémence, Laurent, Quanyi, Marie et les nombreux stagiaires de l'IMP.

Mes plus tendres remerciements vont à ma famille, notamment mes très chers parents qui m'ont sans cesse encouragé et soutenu au-delà de mes espérances. Sans leur aide, je ne serais pas la personne que je suis maintenant. Je pense à ma chère tante qui m'a insufflé cette persévérance et le désir de toujours viser plus haut. Je pense également à mon frère et à sa famille. Mille mercis à mes beaux-parents et à ma belle-famille si riches d'amour et d'entraide, toujours présents et disponibles. Yaël, Sixtine, Ulysse, Constance, Albin, Céleste et Alexis, mes nièces, neveux et mon filleul, je vous souhaite joie et plein succès pour votre futur.

Enfin, je souhaite remercier de tout mon cœur ma très chère femme Augustine. Ton amour, ton courage et ton soutien n'ont pas de limites et me transcendent chaque jour. Merci pour tout et bien plus encore.

« L'Homme ne trouvera jamais une invention plus belle, plus simple ou plus directe que la nature, car dans ses inventions rien ne manque et rien n'est excessif. »

«Prenez vos leçons dans la nature, c'est là qu'est notre futur… »

- Léonard De Vinci

CHAPITRE I - INTRODUCTION

-Chapitre I-

Introduction

Introduction générale du Chapitre I

La lubrification de surfaces permet d'assurer la longévité et le bon fonctionnement des pièces en mouvement dans de nombreux systèmes mécaniques. Sans exception, le monde du vivant possède une multitude de systèmes lubrifiants indispensables pour la locomotion, la protection des muqueuses, le transit alimentaire, le fonctionnement des yeux, etc[1].

Parmi les systèmes biologiques fournissant une faible friction **et** résistant à l'usure, les articulations synoviales sont probablement les plus perfectionnées. En effet, elles garantissent une excellente mobilité du squelette des vertébrés tout en protégeant les zones en mouvement tout au long de la vie d'un individu et parfois dans des conditions extrêmes lors, par exemple, de sauts, courses ou appuis. Pour donner un aperçu de cette efficacité, le genou d'une personne effectue plusieurs dizaines de millions de cycles de flexion sur toute une vie, avec des contraintes normales très élevées de plusieurs mégapascals[2].

Les articulations synoviales peuvent se décomposer en éléments tribologiquement fonctionnels : le cartilage et le liquide synovial. Le cartilage, composé de fibrilles de collagène structurées, principalement de type II (90 % en masse) (mais aussi des collagènes mineurs de type XI qui régule du diamètre de la fibrille de collagène de type II et de type IX qui lie le collagène type II et l'ECM assurant la cohésion du cartilage)[3-4] piégeant des protéoglycanes, est responsable des propriétés de résistance aux contraintes mécaniques des articulations tandis que les composantes du liquide synovial garantissent la lubrification et une protection contre l'usure du cartilage. Cependant, malgré un siècle d'études intensives sur ces systèmes, les mécanismes de lubrification ne sont toujours pas complètement élucidés comme le reflètent la quarantaine de théories proposées sur le fonctionnement des articulations[5-6]. En effet, les systèmes biologiques responsables de la lubrification et/ou de la protection contre l'usure des tissus et des êtres vivants peuvent être multiples, et relèvent de domaines d'études multidisciplinaires: biologie, chimie, mécanique, biomécanique, sciences des matériaux, sciences des interfaces et tribologie.

Cependant, quand des lésions apparaissent, dues, par exemple, à des traumatismes, une inflammation, ou à cause d'un surpoids ou une chirurgie touchant l'intégrité du cartilage, les très faibles propriétés de régénération (absence de vascularisation et d'innervation) du cartilage n'empêchent pas leur progressive dégénérescence. Cette dégénération est amplifiée par des mécanismes inflammatoires et d'érosion jusqu'à l'atteinte osseuse et l'apparition de douleurs aigües. Ainsi l'ostéoarthrite (OA), ou arthrose, touche actuellement 10 millions de Français et 4.4 millions de Canadiens (environ 10-15 % de la population de chaque pays). L'OA représente une des premières maladies invalidantes des pays développés et un fardeau économique pour les systèmes de santé puisqu'il n'existe aujourd'hui aucun traitement de l'OA. Les seuls traitements existants sont symptomatiques : traitements non pharmacologiques (nutrition, exercices, rééducation), traitements pharmacologiques (anti-inflammatoires (voie orale, cutanée et intra-articulaire), viscosupplémentation, ou chirurgicaux (débridement, forage/microfracture, greffe autologue de cartilage, pose de prothèse)[7-8]. Certains traitements symptomatiques ont des résultats cliniques assez controversés, car les résultats sont souvent limités[9]. Les prothèses articulaires ont une durée de vie limitée, mais en constante augmentation, grâce aux nouveaux matériaux et aux nouvelles techniques chirurgicales (environ une vingtaine d'années actuellement)[10], de plus, de nombreuses complications peuvent intervenir (complications mécaniques : descellement aseptique, usure et formation de débris provoquant de l'inflammation, désaxation, fracture, complications non mécaniques : infections, raideurs, troubles hémorragiques), et il devient alors nécessaire de recourir à des chirurgies de pose de dispositifs de deuxième intention, pratique très invasive[11]. **Il est donc nécessaire de proposer des stratégies en amont de la pose de prothèse, soit pour différer leur pose, soit pour éviter complètement ces approches invasives.**

Une stratégie envisageable est l'utilisation de systèmes lubrifiants biocompatibles en voie aqueuse qui seraient directement utilisés au niveau de l'articulation afin de ralentir l'avancée de l'OA. Afin de concevoir des systèmes lubrifiants en voie aqueuse, réduisant la friction et/ou protégeant contre l'usure, pour des applications biomédicales (revêtement de prothèses, lentilles cornéennes, viscosupplémentation), une première approche consiste à s'intéresser à la détermination des mécanismes responsables de la réduction de la friction et/ou de l'usure dans le monde vivant (animaux, végétaux, insectes, champignons, bactéries et virus) et à en élucider les mécanismes sous-jacents. En effet, ces mécanismes développés au cours de l'évolution confèrent des capacités extraordinaires d'adaptation à un environnement

particulier[12]. Nous pouvons citer par exemple, les denticules de la peau des requins qui améliorent leur aérodynamisme dans l'eau, ou encore les fonctions lubrifiantes et de protection des larmes des yeux composées de protéoglycanes et de lipides. Ceci a conduit les chercheurs à fonder leurs recherches sur les concepts de biomimétisme et de bioinspiration qui consistent à adapter des systèmes naturels à des systèmes artificiels ou synthétiques, d'ores et déjà utilisés dans de nombreuses technologies[13].

Définitions

Avant de détailler les recherches sur la bioinspiration pour la lubrification et la résistance à l'usure, nous allons revenir rapidement sur des concepts clés qui seront abordés dans cette thèse, à savoir la tribologie, la friction, l'usure et la lubrification.

La tribologie est la science qui étudie les phénomènes de frottement se produisant entre deux substrats en contact direct ou séparé par un fluide lubrifiant. En ce sens, la tribologie regroupe les concepts de friction, d'usure et de lubrification.

La friction est définie comme la résistance tangentielle à un mouvement d'un objet par rapport à un autre[14]. Elle peut être caractérisée par le coefficient de friction (CoF) qui est le rapport de la force tangentielle sur la force normale appliquée (IUPAC Gold Book, https://doi.org/10.1351/goldbook.F02530).

L'usure, d'un point de vue tribologique, est le phénomène par lequel deux matériaux frottés l'un par rapport à l'autre perdent progressivement de la masse à cause de l'abrasion, de l'adhésion des matériaux, de la fatigue des matériaux et/ou de l'usure chimique ou corrosive[14].

Finalement, la lubrification est un procédé destiné à réduire la friction **et/ou** l'usure entre deux matériaux qui se frottent par l'ajout d'un fluide séparant les surfaces ou en modifiant les surfaces en contact[5]. Un point important est que la friction et l'usure de matériaux à base de polymères sont des concepts qui ne sont pas simplement reliés[5, 14-16], d'où la distinction "friction **et/ou** usure".

Bioinspiration

Afin d'aborder la thématique de la bioinspiration pour la lubrification en voie aqueuse, nous avons réalisé une revue de la littérature intitulée : "**Biolubrication and Wear Resistance: from nature to bioinspired materials**". Cette revue est composée de deux parties : une première s'intéresse aux systèmes voués à réduire la friction à partir de systèmes

polymériques aux architectures bioinspirées. Une seconde partie traite de la bioinspiration dans le but de réduire l'usure de matériaux pour applications biomédicales grâce à leur combinaison avec des matériaux lubrifiants polymériques. Cette revue a été rédigée dans le cadre d'une collaboration de l'équipe de X. Banquy avec une équipe sud-coréenne dirigée par le Professeur Dong Woog Lee, Université Nationale de Science et de Technologie d'Ulsan, spécialiste dans le domaine de la bioinspiration, biotribologie et des phénomènes de surface. Le fonctionnement des articulations synoviales est abordé au début de la revue, ainsi que les techniques de mesure de la friction et de l'usure de biomatériaux afin de mieux comprendre les différentes méthodologies utilisées dans ce manuscrit. Finalement, dans cette revue comme tout au long de ce travail, nous avons choisi de soigneusement distinguer et aborder séparément la friction et l'usure de nos matériaux[16].

Biolubrication and Wear Resistance: from Nature to Biomimetism Engineering

1.1 Introduction

Engineering new materials is a current need to sustain new challenging tasks and environments such as in the aerospatial industry, construction industry, robotics or health area. To help designing efficient structures able to resist severe and specific working conditions, researchers has often found their inspiration from natural biological architectures. Living systems have indeed adapted their specific, sometimes drastic, environments through millions of years to perfectly thrive and reproduce. Thus, bioinspiration is now the source of intense research since it is now possible to analyze in-depth the basic structure of biological systems from macro to nano-scales and adapt them in daily materials making them able to last longer, to be stronger or to suit better their environments. Among all the newly developed bioinspired technologies[12], the design of efficient lubricants is of paramount importance to ensure efficient motion without any wear of mechanical or biological moving systems.

Friction reduction is crucial in living systems for locomotion, feeding, cell signaling or self-protection. This is generally achieved by the presence of a lubricating fluid at the rubbing contact (presence of glycoproteins (mucins), proteoglycan, lipids) and/or the topography of the contact surfaces (patterned surfaces). Glycoproteins or mucins are hydrophilic and heavily glycosylated proteins due to the linkage of sugar units (galactose, sialic acid) to hydroxy-terminated aminoacid from the backbone[17] (Fig. 1.1). They bear cysteine-rich regions allowing their self-assembly into a dense gel covering the mucosa. They can also form hydrophobic interactions due to hydrophobic amino acids, electrostatic interactions due to charged amino-acids and hydrogen bondings[17]. Similarly, proteoglycans are composed of a core protein heavily glycosylated with glycosaminoglycans (GAG)[18]. GAG are long, linear and negatively-charged carbohydrate polymers due to the presence of sulfate groups on sugar units. They bind in the extra-cellular matrix (ECM) with hyaluronic acid (HA) or collagen. Both macromolecules, glycoproteins and proteoglycans, exhibit a unique architecture referred as a bottle-brush (BB) with regions that can be firmly anchored to substrates at one end of the molecule and provide extremely low coefficient of friction (CoF) in the brush or mucin-like domains due to weak interpenetration and the high steric hindrance generated by the pendant

chains. This repulsive force also originates from the osmotic pressure due to highly hydrated moieties (charged sialic acid or GAG) creating hydration forces[19-21].

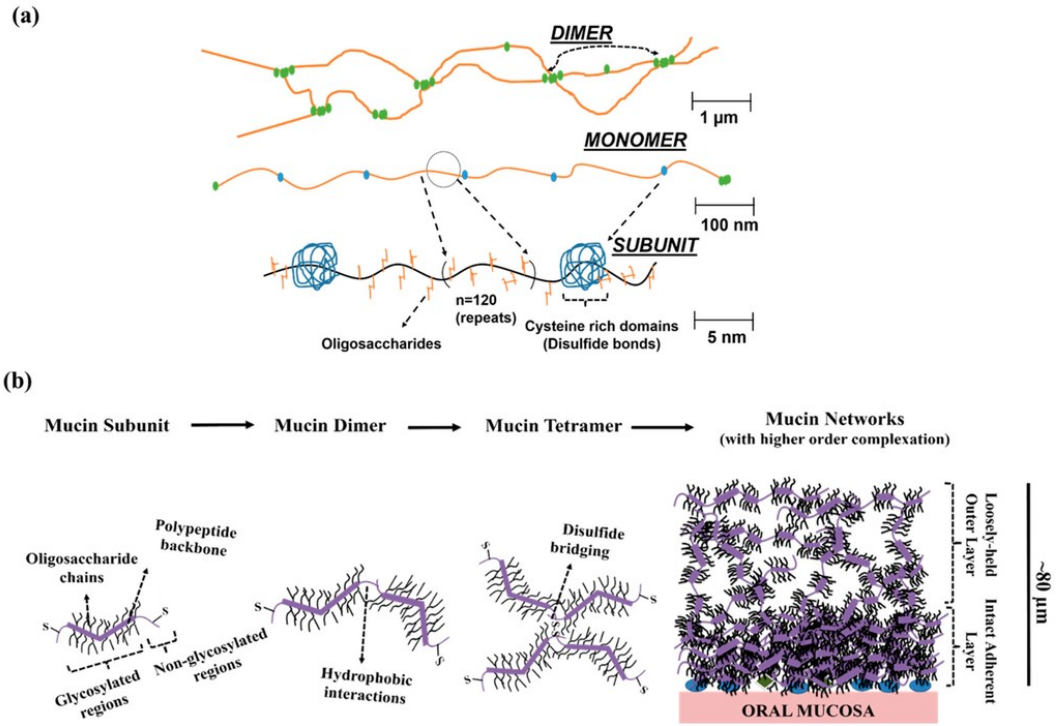

Figure 1.1. *Structure of a mucin-like glycoprotein and its self-assembling in mucosa. (A) Basic structure of a glycoprotein subunit made of oligosaccharides pendant chains densely grafted on a protein core and cysteine rich domains. This repetition leads to the glycoprotein monomer which can self-assemble to form a dimer; (B) Illustration of the successive aggregation steps of glycoproteins mediated by hydrophobic interactions and cysteine moieties (disulfide bridging) to form the oral mucosa. From reference*[17].

For instance, terrestrial gastropods adhesive locomotion is unique and has guided the design of biomimetic robots moving on a large variety of surfaces. These animals are able to move forward on horizontal or vertical surfaces and even upside down on ceilings thanks to the complex wave-like succession of muscle contractions and the thin mucus layer secreted by the animal[22]. The mucus, composed of 93 % water and 7 % glycoproteins, behaves as a viscoplastic non-newtonian fluid with the viscosity drastically decreasing with the increase of shear rate[23-24]. The combination of lubricant and adhesive properties allows the snails to adapt any surfaces. Earthworms also secrete, around their body, mucus with thixotropic properties reducing friction during their motion in the ground. This application could be of great interest for the development of machines, reducing energy consumption while moving in soil[25]. The mucilage of the aquatic plant *Brasenia Schreberi*, meant to protect itself from herbivores, is

composed of a polysaccharide gel forming 75 nm-thick nanosheets and exhibiting a CoF as low as 0.005 when adsorbed on glass substrate[26-27]. This mucilage is of great interest, for example, for the development of lubricating pills coatings for oral drug administration[26]. The hind leg joints of jumping insects such as katykids exhibit a CoF of 0.053 thanks to the combination of micro/nanopatterned articular surfaces, lowering the contact area and thus adhesion, and lubricating lipids[28]. Shark skin has also proved to be an efficient drag-reducing coating in liquids due to the ribbed structure of its denticles and has many applications for the design of drag-reducing materials for transportation and swimming[29-30] as well as the micro/nanoprotrusions of the surface of lotus leaf for the design of hydrophobic and self-cleaning coatings[31]. The human body also uses lubricating systems mandatory for its survival as illustrated by the numerous different mucins found in different epithelia[32]. Every mucosal surface is meant to protect an epithelium, modify the permeability of molecules and pathogens, hydrate or lubricate. Accordingly, the synovial joint lubrication[6] is designed to facilitate macroscopic motion of the skeleton by means of glycoproteins like lubricin (LUB), proteoglycan like aggrecans (AGG), phospholipids and the unique cartilage material structure[6, 33], the eye and lid surfaces lubricated by the lacrimal system[34] helps the drainage of impurities, the mucus clearance in the airways mediated by mucins prevents the inhalation of pathogens or hazardous products[35] or the salivary mucins coating on the skin of comestible foods improves the swallowing process[36-37]. The mucins are also essential in the gastrointestinal tract[38], reproductive tract[37] or the bladder[39]. In turn, any defects in the mucus secretion or in the macromolecular synthesis are related to inflammation diseases such as OA, cystite, xerostomia, dry eye syndrom, cystic fibrosis and a higher rate of respiratory and gastrointestinal infections[40]. Strategies to restore the rheological properties of mucins are also being considered[41]. Nevertheless, in a large number of applications, there is a need to find a replacement for the biological lubricant.

Biological surface wear protection is another vital parameter of living systems for feeding, defending or moving in abrasive environments. The anti-wear structures are often the result of organic materials structuring with or without the presence of biominerals yielding mechanical properties from kPa to GPa such as teeth, claws, shells, exoskeletons, nacre or enamel. For instance, the inner shell of seashells, nacre, designed as a protective armor against predators, is composed of a brick-and-mortar architecture composed of 95 % calcium carbonate glued by 5 % chitin and fibroin and yields to elastic moduli in the range of 1-100 GPa[42]. Another interesting wear-protecting materials are the bones. Bones exhibit exceptional mechanical

properties due to a complex organization of mineralized collagen fibrils glued together with an organic matrix. Upon severe deformation and shear, Ca^{2+}-mediated sacrificial bonds crosslinking the organic matrix and linking this glue to the collagen rupture first, dissipating a high amount of energy and drastically increasing the bone stiffness[43-44]. These bonds are reversible ensuring the self-healing properties of bones and were found to disappear when Ca^{2+} was replaced by Na^{+} ions[45]. To have a better view about the wear resistant biological systems, readers are invited to refer to this interesting review which introduces material selection charts for a clear wear prediction of biomaterials[46].

The current work is aimed to analyze bioinspired materials designed to reduce friction and/or reduce wear of surfaces for biomedical applications with the focus on polymer-based materials since they are predominant in most of the living systems lubricants *via* glycoproteins and proteoglycans. As diarthrodial joint synovial fluids are outstanding aqueous lubricating systems thanks to molecules, macromolecules and structured interfaces acting in synergy to provide exceptional wear protection **and** low friction [6, 47-52], they have fostered bioinspired research to design specific features to improve biolubrication. After reviewing the basic features of joints, their composition and their mechanisms of action, the common techniques of friction and wear assessment will be presented as long as their main drawbacks. A review of natural, synthetic and artificial polymer-based lubricant will then be presented. A clear attention will be paid to explain how these materials actually behave under normal load and shear rates.

1.2 Synovial joint lubrication and wear protection

Healthy mammalian synovial joints are remarkable lubricated and antiwear systems able to provide excellent mobility over the lifetime of an individual. These tribological properties arise from the synergistic behavior of the cartilage (a 0.5 to 6 mm thick poroelastic scaffold covering the articulating bone) with the bathing synovial fluid acting at different regimes throughout the motion process (Fig 1.2). Cartilage and the interstitial synovial fluid are often described as a biphasic structure[33]. Many studies attempted over a century to give better insights in the function of synovial joints. In this view, interesting reviews have been published[6, 47].

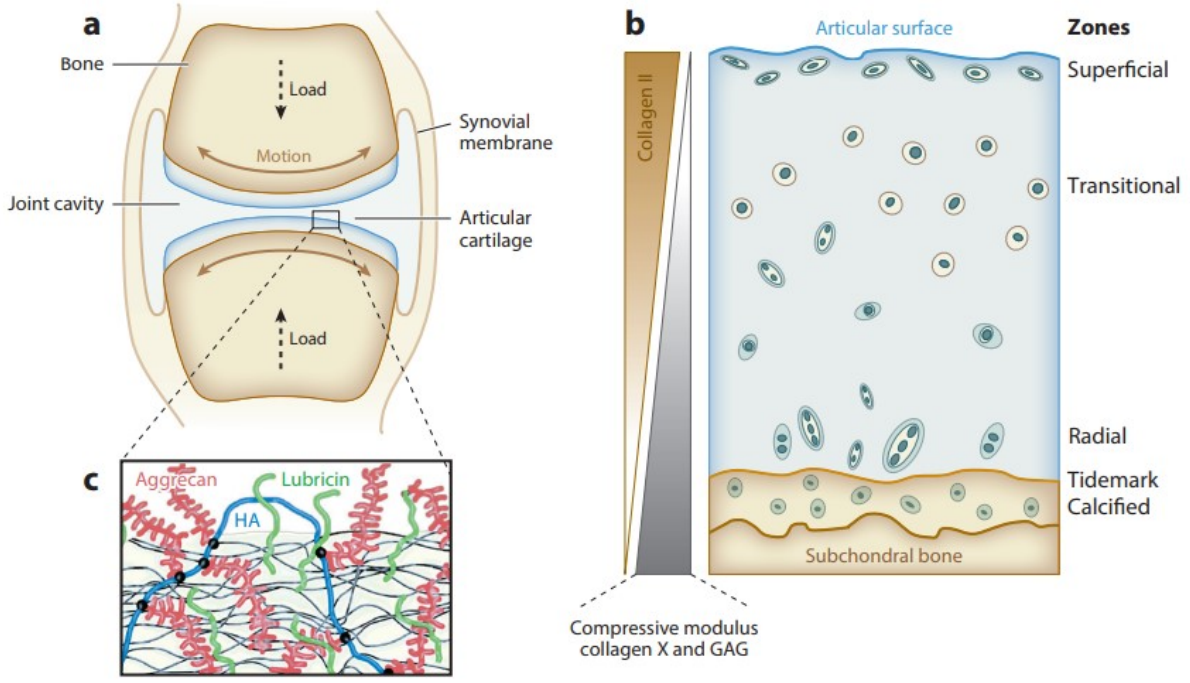

Figure 1.2. *Schematic of diarthrodial joints structure from macroscopic to molecular scales. (A) Two opposing bones are covered by a layer of cartilage. The joint cavity is filled by the synovial fluid which baths the cartilage. (B) Structure of the osteochondral junction in four distinct zones: calcified, radial, transitional and superficial zones from the bone to the surface. The type II collagen concentration increases whereas the compressive modulus, type X collagen concentration and GAG concentration decreases from the bone to the articular surface (C) Molecular composition of the joints surface with the macromolecules, lubricin, aggrecan and hyaluronic acid, involved in the joint lubrication. From reference[6].*

1.2.1 Articular cartilage

Articular cartilage is a highly hydrated and well-organized extra cellular matrix composed of mainly type-II collagen fibers entrapping proteoglycans, lipids and electrolytes[6, 33, 47]. Water and electrolytes represent up to 80 % of the cartilage wet weight near the superficial zone and 65 % in the radial zone while collagen accounts for 10-20 % and proteoglycans 5-15 % of the wet weight[6, 33]. Phospholipids, mainly *L*-α-dipalmitoylphosphatidylcholine (DPPC) and proteins such as link protein, albumin or fibronectin are the other main components of the cartilage. This structured extracellular matrix is produced by specialized cells named chondrocytes. Four different zones can be defined throughout the cartilage depth (Fig. 1.3). From the bone to the articular surface, the calcified cartilage zone makes the transition from the hyaline cartilage to the bone by attaching collagen fibrils within the articulating bone. A tidemark separates the calcified zone from the deep/radial zone which is structured with collagen fibrils perpendicularly aligned to the articulating bone (Fig. 1.4). This zone, representing ~ 30 % of total cartilage thickness is mainly responsible for the mechanical resistance of cartilage to compression. Immediately up to this region is the medial/transitional zone representing ~ 40-60% of the cartilage thickness which has more randomly orientated collagen fibers forming hemispherical arcades toward the superficial zone[53]. The superficial zone, representing ~ 10-20 % of cartilage thickness, has thin and densely packed collagen fibers orientated parallel to the surface designed to protect cartilage from shear stresses. This is composed of two thin layers: a superficial acellular layer covering a cellular layer embedding flattened chondrocytes. On top of this superficial zone and in direct contact with the opposite cartilage surface is the lamina splendens, devoid of collagen fibrils and rich in proteoglycan, phospolipids, HA and proteins[53-54]. Moreover, the composition of each zone closely follows the proximity to the chondrocytes and three different regions can be ascribed[55] (Fig. 1.3 C). The pericellular region surrounds the chondrocytes and is composed of proteoglycans and non collagenous proteins[33, 47, 55] forming the chondron. It is supposed to play a role of signal transduction under compressive and shearing stimuli[55]. The territorial region is composed of chondrons and collagen fibrils and may protect the chondrocytes against high loads. Finally, the interterritorial region is the gathering of large collagen fibrils entrapping chondrons forming the cartilage structure, rich in proteoglycans.

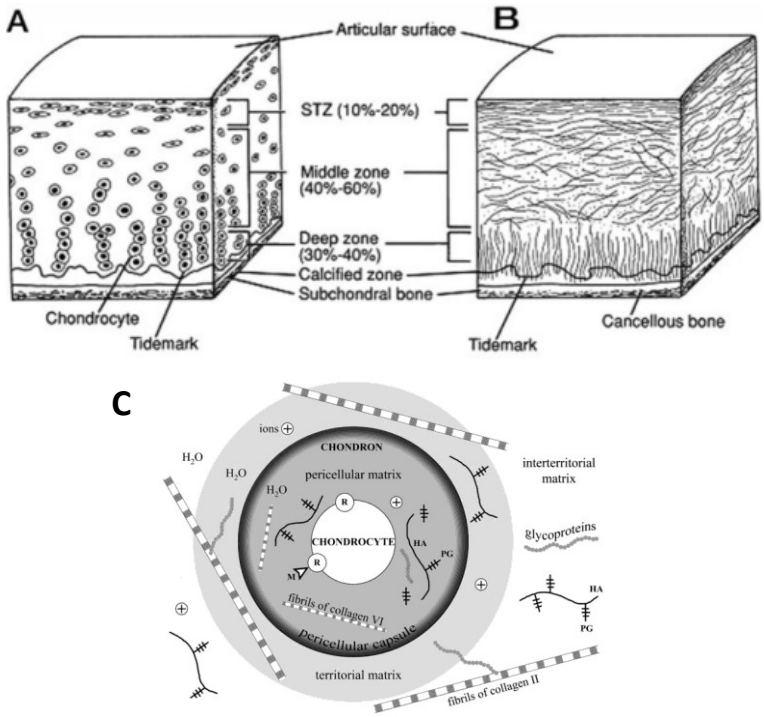

Figure 1.3. *Schematic of cartilage structure. (A) Organization of chondrocytes and (B) organization of the collagen throughout the cartilage thickness.(C) Localization of the three regions found in the cartilage from the chondrocyte to the cartilage basic structure: the pericellular, territorial, and the interterritorial regions. From references*[33, 56].

Amongst the proteoglycans present in synovial joints, aggrecan is a major component, present at a concentration close to 100 µg/mL in healthy joints[57] (Fig. 1.5 A). A ~ 250 kDa core protein bears anionic GAG pendant chains made of ~ 100 chondroitin sulfate and ~30 keratan sulfate, adopting a bottle-brush structure[58]. Globular domains, G1, G2, and G3, are present at the C and N-termini of the aggrecan. Interestingly, in synovial joints, aggrecan is the most abundantly present in the cartilage deep zone and forms large aggregates with high molecular weight HA stabilized by the link protein *via* the G1 domain composed of two HA-binding motifs (PTR). The presence of anionic and highly hydrated HA/aggrecan complexes generates a strong osmotic pressure of 2-3 atm constrained in the collagen matrix and enhances the cartilage mechanical properties under compression and ensures its rapid recovery[59].

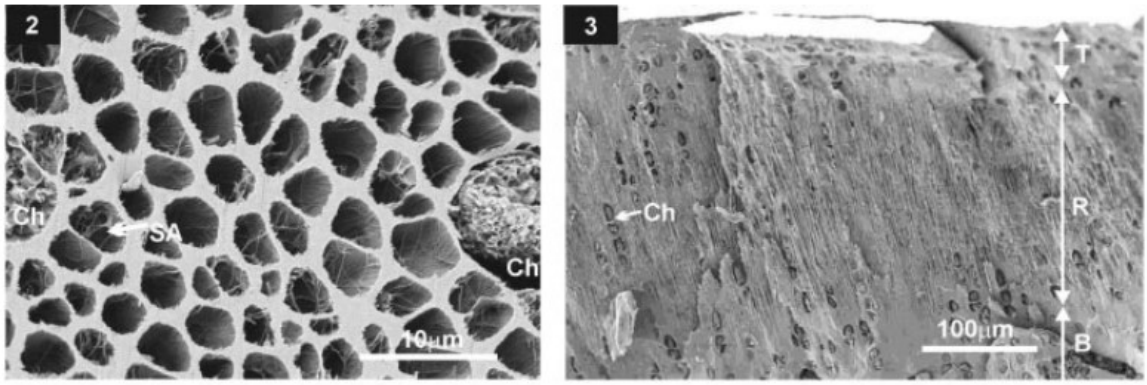

Figure 1.4. *SEM imaging of cartilage from rabbit tibial plateau. (2) Transection of the deep radial zone, showing the tubular structure of few microns of the radial zone and few chondrocytes (Ch) embedded in the collagen matrix. (3) Longitudinal fracture of the cartilage exhibitng the different cartilage zones from the bone (B) to the articular surface (T). Collagen fibrils arranged in micron-sized tubules are noticeable in the R zone. From reference*[60].

1.2.2 Synovial fluid constituents

SF is an dialysate of blood plasma with the addition of molecules from the synovium which is the capsule where the fluid is entrapped. SF plays a crucial role in the tribological properties of the unnerved and unvascularized cartilage as well as in the diffusion of nutrients to the chondrocytes. It is composed of high molecular weight HA, different types of lubricins gathered in one term: proteoglycan 4 (PRG4), and phospholipids which interacts with each other at the lamina splendens[61-62].

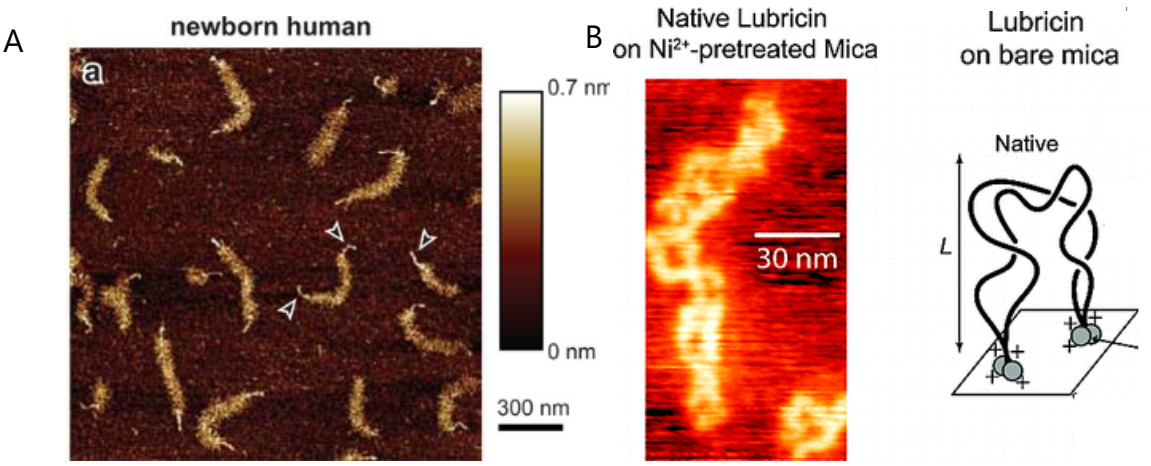

Figure 1.5. *(A) AFM image of aggrecan from newborn human femoral condyle, adapted from reference*[58]. *(B) AFM image of a lubricin dimer exhibiting the loop conformation highlighted by the lubricin schematic on bare mica, adapted from reference*[63].

HA, produced by synoviocytes, cells of the articular membrane named synovium, is abundantly present in SF at the range of few mg/mL and a molecular weight of few MDa[64]. This leads to the hydrodynamic properties of the SF, but is not responsible for the boundary lubrication mode as SF still lubricated surfaces after HA digestion by hyaluronidase[62]. PRG4 owns a central mucin domain, anionic and highly glycosylated pendant chains flanked by two somatomedin B-like domains at the *N*-terminus and a haemopexin-like domain at the *C*-terminus[65]. The *N*-terminus is able to promote disulphide bonding creating PRG4 dimers (Fig. 1.5 B). Lubricin, present at a concentration of about 200 µg/mL, adsorbs to articular surfaces and works in synergy with HA [66] and phospholipids[67] to provide low COF. Lubricin owns a promising lubricating and joint protection properties since it was successfully used in an intra-articular injections into ACLT knees and showed lower OARSI scores, chondrocyte apoptosis, radiographic and histologic scores of cartilage damage than PBS and HA alone as controls[68-69]. Patients with camptodactyly-arthropathy-coxa vara-pericarditis syndrome caused by truncating mutations in the gene PRG4 do not have lubricin expression or functionality, and thus, are characterized by a precocious joint failure and abnormal high CoF[64, 70]. DPPC is the most abundant phospholipid representing 41 % of their content in the SF[71]. Lubricin bears ~ 10 % by weight DPPC at the cartilage surface[67] and DPPC liposomes in combination with HA intra-articularly injected in ACLT rabbit knees exhibited less damage and a CoF similar to the control group compared to no treatment or HA alone treatment groups after 8 weeks of weekly injection[72]. DPPC is also suspected to be carried and anchored to the articular surface to provide efficient CoF. Despite intense efforts addressed to elucidate the role of each SF components on friction, their mechanistic role is still a matter of debate[73-74].

1.2.3 Friction and wear protection properties of cartilage

Under working conditions, joints can provide CoF in the range of 10^{-3} to few 10^{-1} depending on the measurement setup, the tribopairs, the studied lubrication regime, the location of the cartilage sample and the preparation of cartilage explants[6, 75] at shear rates up to ~ 10^5-10^6 Hz[75], and normal contact stresses in the range of 0.5-5 MPa across vertebrate species, rising up to 20 MPa in some joint disorders[76]. Frictional properties are classified in different regimes which can be defined by the tribopair separating distance or the lubricant film thickness. At large separating distances, thus at high sliding velocity and low load, the rheological properties of the separating lubricant are responsible for the frictional behavior, reported as fluid-film lubrication. At short separating distances close to few molecular layer thicknesses, thus at low shear rate and high load, the chemical properties of the substrate surfaces as well

as the tightly absorbed lubricant molecules lately described, largely or solely influence the friction, reported as the boundary lubrication[77]. In between this separating distance and due to the substrate roughness, a mixed mode of lubrication can occur with pockets of lubricant and substrate contact in the same surface area.

Under fluid-film lubrication, the synovial fluid exerts a hydrostatic lubrication or squeeze film lubrication due to the viscous pressurized fluid being expelled from the contact and shortly keeping the cartilage surface apart. A hydrodynamic lubrication process occurs upon articular surfaces relative motion, dragging the fluid to the non-contacting zones and thus generating a flow-induced pressure lifting the opposite surfaces[6, 77]. Upon fluid film lubrication, the applied load eventually forces the elastic deformation of the articular cartilage leading to a higher contact area, a higher SF retention and viscosity, phenomenon denominated as the elastohydrodynamic lubrication[78].

Under boundary lubrication, the firmly anchored SF's molecules accumulates at cartilage surface and provide extensive lubrication and wear protection[79-80]. Under such conditions, hydration lubrication mechanism was proposed to explain the excellent CoF even if few molecular layers still remain[19, 21]. Water sheaths still remain under drastic shear and load stresses surrounding charges or highly hydrated moieties due to the presence of ions[19] and polyelectrolytes[81], or zwitterions[82-84] such as HA, PRG4 and phospholipids. These bonded water molecules resist from squeezing out, but remain highly mobile with an exchange rate with the bulk of 10^{-9} s[19].

Finally, the mixed lubrication regime occurs in between the previously exposed lubrication regimes, namely, the fluid-film lubrication and the boundary lubrication. Different theories were exposed over a century to understand the complex mechanism of this lubrication regime between SF molecules and cartilage structure[5]. The weeping lubrication considers an asperity on the opposite cartilage contact leading to local ECM pressurization and interstitial fluid flow, shortly preventing cartilage on cartilage contacts[82]. The boosted or ultrafiltration lubrication postulates that under loading, SF macromolecules cannot penetrate the cartilage network contrary to water molecules, resulting in the local concentration increase of lubricating molecules at the stressed contact, once again preventing direct cartilage contact[85].

1.3 Friction and Wear characterizations

Prior to explain how scientists can obtain enhanced tribological properties by mimicking the nature solutions, a review on how it is possible to efficiently probe friction and wear at different scales is provided. Indeed, every tribological device can lead to different results for a identical studied system.

1.3.1 Friction characterizations

Friction is a nonconservation force generating a motion resistance of one body sliding over another in direct or close contact, resulting in an energy transfer. It can be characterized by the coefficient of friction (CoF or μ), a dimensionless parameter defined by the ratio of the sliding or friction force over the normal/compression force applied. This useful parameter allows to compare tribological systems (a body sliding on another in presence of a lubricant in between) even though it does not directly inquire the origins of the friction. Usually, two different CoF are used depending on the application: the static and the kinetic CoF. The static CoF is defined by the force needed to set the moving body in motion over another one divided by the applied load whereas the kinetic CoF is defined by the force opposed to the body motion divided by the applied load. In this thesis, we have only taken the kinetic CoF in consideration for polymeric materials since viscoelastic materials can provide different static CoF depending on their contact time due to entanglements, bridging, changing contact area.

Many different alternatives can be used to assess the CoF, and thus the friction, between surfaces designed for biomedical applications and have been recently reviewed[86]. Friction measurements can be split into categories depending on the scale of friction measurements: the macro, the micro and the nano-scale (Fig. 1.6). Usually, pin-on-disk or ball-on-disk tribometers are implemented in the sliding or rolling regime in a circular or back-and-forth motion for macroscale friction measurements. At micro/nano-scale, atomic force microscopy (AFM), lateral force microscopy (LFM) or surface forces apparatus (SFA) techniques are commonly used.

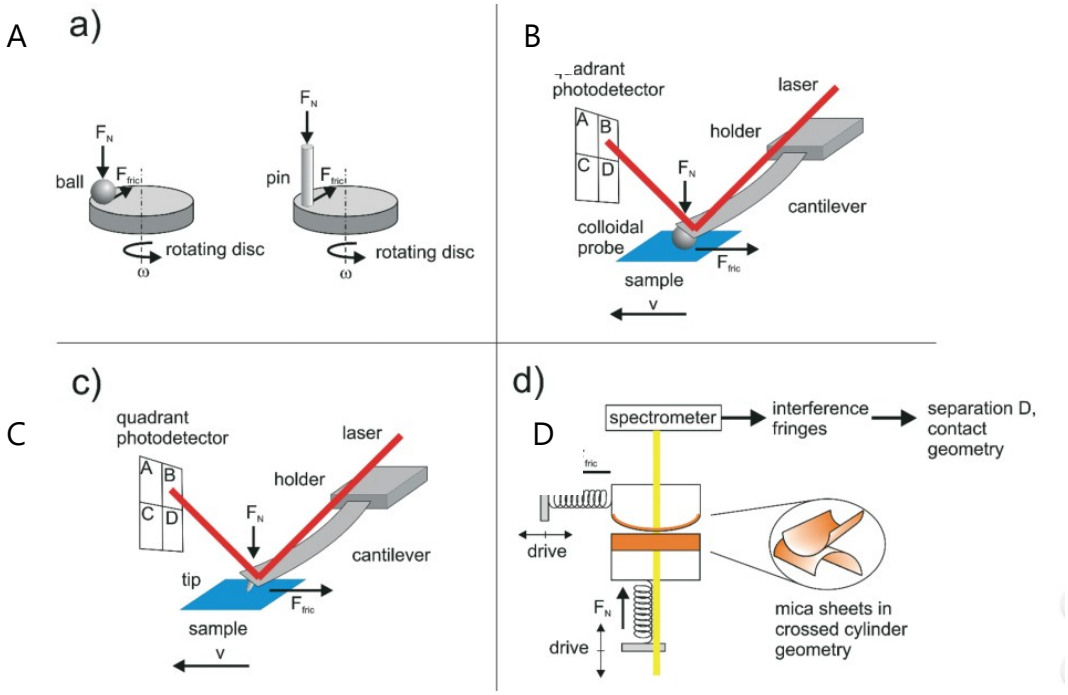

Figure 1.6. *Schematics of the common tribological techniques used to probe the CoF. (A) Ball or pin-on-disk geometries used for macro-scale friction measurements. (B) AFM friction measurement using the colloidal probe technique, (C) lateral force microscopy and (D) surface forces apparatus for micro-scale friction measurements. From reference*[86].

The interest of micro-nano scale measurement is to avoid any influence of surface roughness because the area of contact is considered as a single asperity contact[86]. To study the lubricating ability of a fluid or a substrate, the used technique largely influence the tribological measurements. For instance, in a comparative study between colloidal probe AFM (glass ball/mica), LFM (nitride tip/mica) and SFA (mica cylinders) coated with PFPE or PDMS as lubricant, the authors showed that decreasing contact areas (from SFA 0-125 µm to AFM 0-200 nm and LFM 0-25 nm) lead to different CoF values (from $\mu_{PFPE} << \mu_{PDMS}$ for SFA to $\mu_{PFPE} \sim \mu_{PDMS}$ for AFM and LFM)[87]. Another example using two different machines at macro-scale: a ball-on-disk machine with a rolling contact and a pin-on-disk machine with a sliding contact was conducted with glass/steel tribopairs and PEGylated polymer brushes as lubricants[88]. The CoF was higher for poly(allylamine)-*graft*-poly(ethylene glycol) (PAAm-*g*-PEG) than poly(l-lysine)-*graft*-poly(ethylene glycol) (PLL-*g*-PEG) in a sliding contact configuration whereas they showed similar friction behavior in a rolling contact configuration. A friction study was performed characterizing polyacrylamide (PAM) hydrogels using glass on PAM, PAM on glass and PAM on PAM tribopairs mounted in a reciprocating microtribometer. Every studied systems exhibited a different frictional behavior

since a glass ball rubbing over a flat hydrogel (hydrogel migrating contact) showed a sliding speed frictional dependence, the reverse system (hydrogel stationary contact) showed a CoF dependence over time whereas the hydrogel-hydrogel tribopairs showed little dependency over time and on sliding speed and reaching lower CoF than glass-hydrogel tribopairs[89]. Freely adsorbed HA was tribotested on mica surfaces using SFA or cartilage surfaces using different tribometers. Using SFA, HA was readily squeezed out from the mica surfaces leading to high friction and mica wear[90] whereas on cartilage, HA significantly reduced friction when increasing HA concentration and molecular weight[61, 91]. These different experiments show how difficult it is to compare tribological results since the nature of the substrates, their roughness and viscoelastic properties, the nature of the lubricant, its concentration, its propensity to resist drastic coercions, the load and the sliding speed applied as well as the time of experiment or the production of wear debris influence the CoF. In other words, all the experimental parameters should be mentioned in order to have a possible comparison.

1.3.2 Wear characterizations

Wear is more scarcely studied than friction for biomaterials especially potential cartilage substrates or contact lenses such as hydrogels due to the difficulty to quantify wear for deformable poroelastic structures. As, in this review, we attached great importance to systematically separate friction and wear, we propose a review of common techniques able to assess wear of biomaterials and notably hydrogels. Wear is usually probed using qualitative techniques using visual observations or quantitative techniques such as gravimetric (mass loss), volumetric (volume, width, depth of wear tracks) or dosage (release of wear debris) techniques. Characterizing deformable biomaterials such as hydrogels is challenging since their high deformability, and the low contrast of the polymer matrix to its interstitial water for microscopic visualizations, render these common techniques difficult to implement.

1.3.2.1 Qualitative observations

Visual observations offer qualitative appreciations of wear using optical or electronic microscopy[92-97]. For SEM experiments, gels are pre-treated to immobilize the structure using aerogels obtained from fast freezing in liquid nitrogen and drying[98-99], from successive solvent exchanges from hydrogel, alcoholgel to supercritical CO_2 aerogel [95] and then metal sprayed. Wear can also be assessed upon drastic friction change when using micro-nano-scale apparatus. For instance, many SFA studies characterized wear of polymer brush layer at the

pressure from which friction drastically increased, verified by the appearance of deformation or rupture on the FECO fringes as well as the brush thickness abrupt decrease (polymer film rupture) or increase (aggregation and debris accumulation)[79, 100-104].

1.3.2.2 Quantitative evaluations

Gravimetric studies can directly probe the wear loss or the wear rate. For stiff materials, direct weight loss was possible to assess[105-106] after surface drying using absorbent tissues, sometimes corrected by a load soak control due to fluid adsorption by continuous loadings using standardized procedures[107]. However, due to the presence of surrounding water, hydrogel weighing could be challenging notably due to water exudation which is a different phenomenon than wear. To avoid this phenomenon, one could rehydrate the compressed gel into water before surface drying using absorbent tissue and weighing[108]. Some alternatives propose to dry the hydrogels under vacuum and weight them before and after wear tests, so that, a kinetic of gel weight loss can be converted to a wear rate avoiding the effect of the solvent[109] or to weight hydrogels directly in water by submerging a basket equipping a precise balance[110].

Volumetric studies are frequently used in materials science to characterize the height, the depth, the width, and thus the volume of wear tracks as well as the surface roughness. The wear of a library of poly(vinyl alcohol)-poly(ethylene glycol) (PVA-PEG) charged with graphene oxide (GO) composites was analyzed using white-light interferometry[111]. The wear depth was ~ 150 µm for PVA-PEG whereas PVA-PEG charged with 1.5 $\%_{wt}$ of GO lead to almost no wear track. Chitosan gels have low contrast between water and the polymer matrix for interferometry, so gels disks were beforehand surface dried using compressed air to increase the contrast of the polymeric matrix and make cracks appear to assess surface roughness[95, 101]. Similarly, laser confocal microscopy was used to assess the wear depth as well as gel roughness from the top of the gel or from a vertical slice to observe a wear profile[112-113]. Profilometry has also been used to probe wear depth on hydrogel surfaces[114] as well as on the surface replica of a torn gel[115].

Dosage or visualization of wear debris are also a useful parameter of wear evaluation. Moreover, wear debris of biomaterials can in turn induce inflammation or infections used as contact lenses or prosthetics[116-117]. Wear can be assessed for biomaterials as well as the tissue counterpart such as in the case of a hemiarthroplasty requiring a biomaterial to interact with cartilage. Hydroxyproline (HYP) is an amino acid specific of cartilage collagen and is

released upon cartilage wear. It was successfully quantified by HPLC by collecting the hydrating bath of the genipin-crosslinked cartilage tribopairs[118]. Similarly, glucose release from bacterial cellulose scaffold during tribological experiment was quantified by H_2SO_4 assay[119]. Enzyme-linked immunoabsorbent-inhibition assay (ELISA) is also of great interest when assessing wear. Keratan sulfate (KS), a glycosaminoglycan present in joints or at the eye surface was successfully quantified using a monoclonal antibody specific of KS by ELISA[120]. Serum cartilage oligomeric matrix protein, urine C-terminal telopeptide of collagen type II and I were also quantified by enzyme-linked immunoassay to assess the effect of weight loss on OA biomakers production in humans[121]. GAG degradation was also assessed by dimethylmethylene blue assay and the resistance to collagenase -mediated cartilage degradation was quantified by histological staining[122]. For a better understanding of the wear rate and process, a combination of these techniques are often required.

1.4 Human Alternatives to reduce friction for Biomedical Applications.

Lubrication of tissues or biomaterials is essential to ensure the mobility of the moving parts found in the body. For instance, eyes or joints require complex lubricating fluids to cover and protect their surfaces. The lubricating biological fluids are composed of macromolecules such as proteoglycanes, glycosaminoglycanes and small molecules such as phopsholipids and ions. The biolubrication process is then a complex synergistic mechanism depending on the surface topography and the surrounding fluid molecules which provides excellent lubrication even under boundary lubrication regime. Researchers have successfully used natural lubricating molecules, synthesized bioinspired macromolecules or manufactured bioinspired textured surfaces to provide low coefficient of friction and help natural or prosthetics surfaces work more efficiently *in vivo*[123-127].

1.4.1 Using natural materials

As the synovial joints are amongst the most exciting biotribological systems, many research teams started designing tribological systems by exploiting the synovial fluids components in the view to achieve a tribological properties similar to natural joints. A list of the main natural strategies found to develop biocompatible and hydrophilic lubricants is compiled in table 1.1.

1.4.1.1 Hyaluronic acid (HA)

HA is now well known not to be, alone, responsible for the frictionless properties of joints in the boundary lubrication regime, but is involved in synergistic mechanisms with LUB, AGG

and phospholipids[6, 50, 52, 128]. This polyelectrolyte is still administered *via* intra-articular injection in various forms as a viscosupplementation treatment to temporarily[129] restablish the viscoelastic properties of the degraded synovial fluid under inflammatory diseases such as OA[130-131]. Studies by Tadmor *et al*. showed that free HA was readily expelled from weakly negatively charged and hydrophilic mica surfaces [90, 132]. Another study showed little CoF dependency on HA molecular weight on mica[103]. In contrast, HA was found to exhibit a dose and a molecular weight-dependencies[61, 91] at cartilage interfaces to reach CoF close to 0.1 for the high molecular weight HA (Mw > 1MDa) at high concentration (~ mg/mL) which is similar to physiological conditions[133]. Such behavior may be explained by partial and weak entanglements of high molecular weight HA on the poroelastic cartilage surface, referred as the trapping mechanism[16], but also may be due to the presence of LUB which induces HA retention at the surface[61, 134]. HA is nevertheless essential for the joints lubrication properties since HA bounds other molecules to the cartilage surface[135-136]. Weakly physisorbed HA *via* electrostatic interactions thanks to adsorbed Ca^{2+} cations or lipid bilayers to mica surface lowered the CoF up to mild load and shear rates[132]. It was further demonstrated that anchored HA or even crosslinked hylan ensured a better lubrication of mica surfaces than free physisorbed HA[79]. HA was successfully chemically grafted to model surfaces using attachment groups such as biotin-streptavidin or EDC coupling on amine-functionalized surfaces[136], but exhibited intermediate lubrication properties with CoF ~ 0.2 up to mild pressures. A promising alternative was provided by Singh *et al.* who managed to bind HA to cartilage surface *via* a peptide spacer and provided low CoF to normal and osteoarthritic cartilage[135]. This concept can be expanded to numerous applications in ophthalmology where hydrophilic lubrication is needed such as contact lens and ocular coatings. Finally, crosslinked HA was shown to partially reduce the CoF either after injection between cartilage surfaces[137] or when bonded to a mica surface[136].

1.4.1.2 Polysaccharides

Polysaccharides in general are interesting candidates for biolubrication since they are mostly non-toxic, naturally-abundant[138] and offer alternatives to HA which is readily eliminated from joint cavity[139]. Free (hydroxy propyl)methyl cellulose (HPMC), pectin, and xanthan were able to decrease CoF close to 0.1-0.2 up to mild pressure conditions on a ball-on-disk tribometer using hydrophobic elastomer tribopairs [140-141]. Pectin ensured a better lubrication than xanthan or locus bean gum due to the formation of a thicker and highly hydrated polymeric layer[140]. Chitosan, a positively charged polyeletrolyte in acidic conditions, was able to provide a CoF

as low as 0.07 up to several atmospheres of normal pressure due to the presence of highly hydrated spheres around the polymer charges creating an osmotic pressure able to enhance the repulsion of opposing mica surfaces[142]. Interestingly, a polysaccharide extracted from red algae *Porphyridium sp.* was able to lubricate hydrophilic mica surfaces with a CoF of 0.015 up to 10 MPa of normal pressure with only a sub-nanometric polymer monolayer[100]. At boundary lubrication regime, the hydration decrease of this polysaccharide increased its number of intermolecular hydrogen bonding generating a more cohesive film[143].

1.4.1.3 Lubricine (LUB) and aggrecan (AGG)

An interesting review has been recently published about LUB properties[123]. LUB alone provided a low CoF close to 0.1 in a dose-dependence manner on cartilage[61, 91], slightly reduced hydrogel friction[144-145] and lowered CoF on mica up to mild pressures ($\mu \sim 0.03$)[146], but was not responsible on its own of the exceptional lubrication of cartilage surfaces. In a synergistic combination with HA, LUB provided low CoF similar to those found in natural joints in contrast to LUB alone on different surfaces [61, 79, 91, 144-145]. The main point here is that the anchoring of HA and LUB to the surface effectively improves the lubrication of model surfaces. Similarly to LUB, AGG was assessed in combination with HA and a link protein to successfully form AGG-HA aggregates[147-148]. CoF values close to 0.01 up to $P \sim 10$ - 15 atm in pure water and up to lower loads in saline buffers were obtained due to the screening of the AGG charges giving rise to the chain collapse and a lower hydration level due to a salting-out effect of AGG[147].

1.4.1.4 Phospholipids

Phospholipids, especially those composed of phosphatidyl choline, play also a significant role in joint lubrication[47, 128, 149-150]. DPPC liposomes were successfully used as boundary lubricant at cartilage surfaces. Upon shear, lipids form a lubricant layer able to provide CoF as low as $\mu = 10^{-4}$-10^{-5} at mica interfaces[149, 151] up to 6 MPa. These properties are due to the hydration lubrication process which provides hydration layers tightly bound to the charges of the anchored molecules[19-21, 152]. Once again, in combination with HA or LUB, DPPC liposomes were able to reach cartilage-like CoF[67, 72, 153]. It was observed that DPPC vesicles were able to rearrange and adsorb around HA and lubricin, then being immobilized at the contact interface, LUB acting as an immobilizing carrier of phospholipids at contact areas[67].

1.4.1.5 Ions

Another important constituents of SF are ionic species. As described by Klein *et al.*, the ions entrapped between oppositely charged surfaces generate a strong, short-range repulsive force, named hydration force[19, 154]. This phenomenon is also observed for polyelectrolytes in boundary lubrication regime whose fully hydrated charges generate an intermolecular repulsive force. The capacity of an ion to attract more water molecules leads to a CoF decrease[155]. A series of sodium salts were tested in the same friction conditions and the lubrication was better for citrate sodium salt ($\mu = 0.12$) than iodide sodium salts ($\mu = 0.30$) with the following Hofmeister series: $\mu_{iodide} > \mu_{nitrate} > \mu_{bromide} > \mu_{chloride} > \mu_{fluoride} > \mu_{phosphate} > \mu_{citrate}$ [155]. A similar study was carried out to explore the effect of cations on silica wafer. It was observed a better lubrication for Li^+ ions ($\mu = 0.09$) compared to Cs^+ ions ($\mu = 0.33$) due to the higher ability for smaller and more hydrated ions to retain water molecules[156]. Extremely low CoF ($2.10^{-3} < \mu < 2.10^{-4}$) were obtained at mica surfaces using sodium salts up to mean loads (450 nN) due to the exchange between K+ ions of mica and Na^+ ions which possess a larger hydration shell[152]. It was also shown that free HA, readily expelled from mica contact using SFA, provided excellent CoF close to 10^{-3} in a saline solution contrary to free HA in pure water due to the presence of adsorbed sodium ions from sodium hyalorunate on mica remaining at the boundary lubrication regime[101].

We observed that the complexity of the friction measurement strongly depends on the substrate, the friction tester and the operative conditions (load, shear rate, lubricant concentration). Through this section, the CoF of natural lubricants was systematically higher when the lubrication was assessed between flat and non porous surfaces such as mica, highlighting the paramount role of poroelastic materials used as tribopairs such as the cartilage or hydrogels on the lubrication process that we will discuss latter in this review. It was also noticed that it was difficult to reach friction properties as excellent as natural joints by just using SF components. This difficulty is due to the complex synergy arising between cartilage surface and the interactions between SF components[6, 33]. The main lubrication factor is then to successfully anchor highly hydrated molecules at the rubbing contact to ensure water molecules retention, and thus excellent lubrication.

Several techniques have been implemented to efficiently anchor lubricant molecules to surfaces using for example synergistic interactions between molecules such as the ability of lubricin and HA to interact with phospholipids[48, 67, 157], crosslinking, hydrogen bonding or specific interactions through peptides or link proteins[79, 135-136, 147-148].

Table 1.1. Tribological properties of natural lubricants

Lubricant	Substrate and friction tester	CoF	Operative parameters (Pressure or load, sliding rate)	Remarks	Refe-rences
Free HA in solution	Mica mounted in an SFA	n/a		HA does not adsorb on hydrophilic and slightly negatively charged mica surface	90
	Cartilage on cartilage in a rheometer	$\mu = 0.21$ to 0.12 from 110 µg/mL to 3.3 mg/mL HA solution	at 0.3 mm/s and a compression of 18 % of cartilage thickness	Lubrication follows a dose-dependent behavior	61
	Cartilage on cartilage in a rheometer	$\mu = 0.098$ to 0.079 from 20 kDa to 5MDa HA solution at 3.3 mg/mL,	0.3 mm/s and a compression of 18 % of cartilage thickness	Lubrication follows a Mw-dependent behavior	91
Polysaccharides	PDMS ball on disk mini traction machine	$\mu \sim 0.1$ for pectin, $\mu \sim 0.25$ for xanthan and $\mu \sim 0.7$ for locus bean gum	at a load of 4 N and v = 5 mm/s	Friction decreased with the increase of hydrated polymer layer	140
	Mica surfaces mounted in SFA	$\mu = 0.015$ for a polysaccharide extracted from red algae *Porphyridium sp.*	up to P = 10 MPa and v = 0.1-10 µm/s	Increased hydrogen bond formation under boundary lubrication regime with a film layer < 1 nm	100
	Bare silicium ball-on-disk tribometer	$\mu = 0.14$for HPMC	at 0.01 m/s at a load of 8 N		141
	Mica surfaces mounted in SFA	$\mu = 0.07$ for a 0.065 $\%_{w/v}$ chitosan solution	at v = 200 nm/s up to some atm	Enhanced lubrication due to the counterions osmotic pressures generated by the hydration heaths around the charged groups	142
Physisorbed HA	Mica mounted in an SFA	$\mu = 0.35$	at v = 0.12 µm/s and P = 5 atm	HA weakly adsorb on positively charged mica *via* Ca^{2+} bridging or surfactant bilayers but bridge both surfaces;	132
Covalently attached HA	Mica mounted in an SFA	$\mu = 0.27$		Biotinylated HA (b-HA) attached to streptavidin supported lipid bilayer	136
		$\mu = 0.19$	up to P = 3 atm	*Via* EDC coupling between HA and amino free groups supported-lipid bilayer	136
	Cartilage on cartilage plates mounted in a rheometer	$\mu \sim 0.05$	at v = 0.3 mm/s and a compression of 18 % of cartilage thickness on normal tissue and on osteoarthritic tissue	HA coupled with a binding peptide to a cartilage or a ocular surface *via* a heterobifunctional PEG spacer	135
		µ negligible but drastically increased	from P = 6 atm in an asymetric configuration with no salt (HA coated mica vs bare mica)	b-HA attached to avidin supported mica surface	147-148
		$\mu = 0.4$	In a symetric contact for P = 2 atm		
Crosslinked HA - Hylan	Mica mounted in an SFA	$\mu = 0.15$	up to P = 3 atm	Crosslinked HA supported-lipid bilayer	136
Hylan G-F-20	Bovine osteochond	$\mu = 0.05$ at 8 mg/mL	compression of 18 % of cartilage thickness	Synvisc® treatment composed of a mixture of crosslinked HA: weakly crosslinked HA-	131, 137

	ral cartilage in a rheometer			A of 6 MDa in a fluid form and highly crosslinked HA-B in a gel form at a ratio HA-A/HA-B 9/1	
Lubricin	Cartilage on cartilage in a rheometer	$\mu = 0.11$ in 450 µg/mL PRG4 solution	compression of 18 % of cartilage thickness	Lubrication follows a dose-dependent behavior	61
	Cartilage on cartilage in a rheometer	$\mu = 0.080$ in 450 µg/mL PRG4 solution	a compression of 18 % of cartilage thickness		91
	Cartilage/glass	$\mu = 0.093$ in 50 µg/mL PRG4 solution,	v = 0.33 mm/s and 30 % normal strain	Lubrication follows a dose-dependent behavior with a maximum of lubrication from the concentration 50 µg/mL	158
	Mica surfaces mounted in SFA	$\mu \sim 0.03$ -0.2	at P = 6 atm and v = 1 µm/s	Lubricin in readily rearranged when the load was increased and do not provide low CoF on positively charged and hydrophobized mica surfaces	146
Lubricin and HA	Cartilage in a rheometer	$\mu = 0.066$ in 3.3 mg/mL HA plus 450 µg/mL PRG4 solution	At v = 0.3 mm/s a compression of 18 % of cartilage thickness	Synergistic behavior of HA and PRG4	61
	Cartilage in a rheometer	$\mu = 0.040$ in 3.3 mg/mL of various M_w HA plus 450 µg/mL PRG4 solution	at v = 0.3 mm/s a compression of 18 % of cartilage thickness	Synergistic effect between HA and PRG4 is not dependent on HA M_w	91
	Mica mounted in SFA	$\mu = 0.23$ at 250 µg/mL PRG4, 2.5 g/L free HA	v = 3 µm/s up to P = 10 atm	Physisorbed HA plus free HA and PRG4 between the surfaces	79
	Mica mounted in SFA	$\mu = 0.09$ at 55.5 µg/mL PRG4 1.5 g/L free HA	v = 3 µm/s up to P = 40 atm	Grafted HA plus free HA and PRG4 between the surfaces	79
	Methacryloyloxy propyltris Trimethylsiloxy silane (pHEMA/TRIS) and dimethylacrylamide tris Trimethylsiloxy silane (DMAA/TRIS) hydrogel versus human cornea or eyelid in a rheometer	$\mu = 0.10$ for DMAA/TRIS hydrogel and $\mu = 0.17$ for pHEMA/TRIS hydrogel for HA and 300 µg/mL PRG4	at P < 30 kPa and v = 0.3-30 mm/s	HA and PRG4 alone did not improve significantly the lubrication, but the synergy between HA and PRG4 decreased the CoF	144-145
Mucins bovine submaxillary mucin and recombinant fusion PSGL-1/mIgG mucin dimer with an	PMMA surface in a colloidal probe AFM	$\mu = 0.02$-0.24 for PSGL-1/mIgG $\mu = 0.7$ for bovine mucin	Up to a P = 8-9 MPa at v = 4 µm/s	The mucin dimer anchored at a larger extend on the PMMA than the bovine mucin assessed by QCM. This reduced the opposite surface bridging and molecule drag and thus provided a lower friction	159

immunoglobulin anchoring groups(P-selectin glycoprotein ligand-1)					
C-P55 and C-PSLex made of PSGL-1/IgG produced in different cells	PMMA surface in a colloidal probe AFM	μ = 0.1-0.24	Up to P = 8 MPa	At low load, C-PSLex provided lower CoF due to longer side chains (higher glycosylation) providing higher hydration at contact. At higher load, the trend changed due to higher interpenetration for longer side chains	160
porcine gastric mucin	Hydrophobized (HB) mica mounted in SFA	$\mu \sim$ 0.05-0.4	Low friction up to P ~ 0.5-1 MPa at v = 80-820 nm/s	Friction was lower on HB mica than bare mica due to the anchoring of hydrophobic moieties of the mucin on HB mica and a higher amount of hydrophilic moieties exposed in the medium	161
Aggrecan plus HA	Mica mounted in SFA	μ = 0.01 for a solution of b-HA at 0.3 mg/mL, 0.2 mg/mL aggrecan and 4.9 µg/mL link protein with no salt for an asymetric configuration (Aggrecan-HA coated mica versus bare mica)	up to P = 16 atm	HA is grafted on mica surface and aggrecan is added overnight in addition with the link proteins to allow the formation of aggrecan-HA complexes. Addition of salt decreases the interaction lengths of the aggrecan-HA complexes leading to an increase in CoF and shorter pressure range	147
		μ = 0.014 in pure water and μ = 0.015 in saline conditions for a solution of b-HA at 0.3 mg/mL, 0.2 mg/mL aggrecan and 4.9 µg/mL link protein for a symetric configuration	up to P = 12 atm		148
phospholipids	Cartilage in a rheometer	μ = 0.17 at 200 µg/mL DPPC liposomes			61
	Cartilage on cartilage on a Pin-on-plate tribometer	0.06 < μ < 0.17 for a 200 mg/mL of DPPC at	P = 1.3 MPa and v = 4 mm/s	Dose dependency of DPPC on its lubrication. The friction significantly decreased compared to a control lubricated by Ringers solution	153
	Mica surfaces mounted in a SFA	$\mu = 2.10^{-5}$ up to 12 MPa in pure water and $\mu = 6.10^{-4}$ in 0.15 M $NaNO_3$ for 30 mM hydrogenated soy phophatidylcholine liposomes	up to P = 6 MPa	Hydration lubrication mechanism arising from the highly hydrated phosphoryl choline heads	151
	Bovine cartilage on steel in a	μ = 0.045 to 0.022 from 0 to 35.5	at P = 1MPa and v = 0.3 m/s	Dose dependency of DPPC on friction	97

	pin-on-disc rheometer	mg/mL DPPC			
Phospholipids and HA	Pendulum friction test with rabbit knees	$\mu = 0.015$	At P = 1 MPa	Addition of DPPC liposomes to high molecular weight HA solution allowed to reduce friction up to healthy control value compared to HA alone whose CoF significantly differed from the healthy control	72
	Cartilage on cartilage on a Pin-on-plate tribometer	$0.04 < \mu < 0.08$ for a 200 mg/mL of DPPC liposomes plus 10 mg/mL HA	at P = 1.3 MPa and v = 4 mm/s	Synergistic interaction between HA and lipids to lower the friction	153
	Mica surfaces mounted in a SFA	$\mu \sim 10^{-3}$ for a mixture of 49 µg/mL grafted b-HA, 15 mM DPPC liposomes	up to P ~ 200 atm	This low friction is attributed to the hydration lubrication mechanism born by phosphatidyl choline hydrated heads	128
Phospholipids and Lubricin	Quartz plates mounted in a tribometer	$\mu < 0.005$	at P = 0.3MPa	Lubricin acts as a phospholipids carrier to the cartilage surface. PRG4 is capable of delivering 11.1% of surface-active phospholipids to the articular interface	67
Ions	Hydrophilic PDMS pin on disc tribometer	$\mu = 0.30$ for iodide sodium salt to 0.12 for citrate sodium salt at 1 mM salt concentration	at a load of 2 N	CoF decreased according the Hofmeister series of sodium anions thanks to high hydration, enhanced local viscosity and repulsion of counteranions	155
	Mica surfaces mounted in a SFA	$2.10^{-3} < \mu < 2.10^{-4}$ for 0.1 M NaCl and $NaNO_3$	up to P ~ 1MPa at v = 200 nm/s		21
	Silicon wafer and silica probe AFM	$\mu = 0.33$ for 1 M CsCl, $\mu = 0.24$ for 1 M NaCl and $\mu = 0.09$ for 1 M LiCl, $\mu = 0.17$ for 0.1 M LiCl and $\mu = 0.35$ for 0.01 M LiCl	At aload of 450 nN and v = 2 µm/s	The degree of lubrication follows the capacity of hydration of cations and the concentration of salt	156

1.4.2 Using covalently grafted polymer layers

In order to develop more efficient biolubricant, research teams have taken advantage of the natural lubricant found in joints. A myriad of polymer brushes made of biocompatible materials are now commonly used as surface coatings for biomedical purposes. Inspired from the function of the natural lubricants which attach to the surface to efficiently lubricate under boundary lubrication, using covalently grafted polymer helped the lubricant system to resist high loads and shear. These polymeric materials are studied in view to coat surfaces such as prosthetics or contact lenses because it requires surface chemical modifications to effectively anchor polymers to the substrate (Table 1.2).

1.4.2.1 Polymer brushes properties on lubrication

Polymer brushes are densely grafted polymer chains end-attached to a substrate[162-163]. An interesting review was previously published by Mocny *et al*. concerning the tribological behavior of surface-grafted polymer brushes[86]. Two common ways exist to produce brush layers: the grafting-to technique which consists in the attachment of a polymer chain to a substrate such as a particle or a surface (silicon wafers, glass) *via* a covalent bond and the grafting-from technique which involves the polymerization of monomers from a surface covalently coated with initiators [124, 164-165]. The main differences between both techniques are, for the former, the simple characterization of single chains, but the weak grafting density due to the steric hindrance and, for the latter, a higher grafting density, but an increased difficulty to accurately characterize the resulting macromolecules using common techniques such as gel permeation chromatography (GPC) since the polymers are grafted *in situ* on the substrates. These differences are essential in the friction behavior of polymer brushes. Densely grafted poly(2-methacryloyloxyethyl phosphorylcholine) (PMPC) brushes were synthesized under a lower level of oxygen than usual ATRP in the reaction medium thanks to a longer oxygen evacuation. This lead to a high grafting density of about 2 chains/nm² higher than what was found in the literature according to the authors. This resulted to a very low CoF of $\mu \sim 10^{-4}$ [165] compared to more weakly grafted PMPC in similar saline conditions ($\mu \sim 0.0026$)[83], highlighting the paramount role of the grafting density. In the same view, increasing the molecular weight of poly(N-vinylpyrrolidone) (PVP) brushes from 10 to 1300 kDa lead to a two order of magnitude CoF decrease between polydimethylsiloxane (PDMS) and silicon wafer tribopairs[166]. Thermoresponsive PNIPAM on silicon substrate exhibited a CoF of $\mu = 0.08$ at $T < LCST$ whereas CoF increased one order of magnitude at $T > LCST$ due to the chains dehydration and collapse[167]. Poly(N-isopropylacrylamide) (PNIPAM)-coated carbon nanotubes showed decreasing CoF when PNIPAM chain lengths progressively increased[168] as well as poly[(2-(methacryloyloxy)ethyl) trimethylammonium chloride] (PMETAC) and poly(3-sulfopropylmethacrylate potassium salt) (PSPMA) chains grown on PEEK[169].

1.4.2.2 Charged polymer brushes

Carrillo *et al.* performed molecular dynamics simulations on neutral and charged polymer systems and showed that the CoF was significantly lowered for charged polymers compared to neutral ones, all the other parameters being similar[170]. These results arise from the

hydration shell surrounding the charges generating an additional osmotic pressure and a higher intermolecular repulsive force as long as keeping water molecules mobility[19]. PSPMA successfully lubricated PDMS surfaces up to $\mu \sim 0.02$ at P = 50 kPa at 90 % RH compared to $\mu > 1$ at low RH[171]. The authors developed a switchable lubricating PSMA layer embedding Fe_3O_4 nanoparticles which, upon IR excitation, increased the local temperature and initiated the brush layer dehydration leading to brush height collapse from ~ 200 nm to ~ 70 nm and subsequent friction increase. PSPMA initiated on diamond-like carbon provided CoF as low as $\mu = 0.0062$ at few atmospheres of normal pressure[172]. However, under a saline concentration of 0.15 M NaCl, μ rose to 0.01 as confirmed by numerical simulations which showed that the charge benefits of polyelectrolytes in presence of ions weakened to reach non-charged polymers[173]. In the same view, the addition of oppositely charged surfactants to charged polymer brushes lead to a drastic CoF increase. Cetyl trimethylammonium bromide (CTAB) addition to PSMA or sodium dodecyl sulfate (SDS) addition to PMETAC brushes created a hydrophobic layer which dehydrated the brush layer and lead to an increase of the CoF from $\mu = 10^{-2}$ to $\mu > 0.3$ compared to poly(ethylene glycol methacrylate) (PEGMA) or zwitterionic poly(sulfobetaine methacrylate) (PSBMA) brushes whose tribological behavior did not change upon the addition of both surfactants[174].

1.4.2.3 polyzwitterionic polymer brushes

Polyzwitterionic brushes such as PMPC or PSBMA present an interesting feature for aqueous lubrication since they combine the tribological attributes of charged polymers and a high resistance to electrostatic screening from charged species such as ions or surfactants[83, 174-175]. PMPC brushes were shown to efficiently lubricate substrates as different as mica, silicon wafer, or ultra high molecular weight polyethylene (UHMWPE)[83, 165, 176-179]. Over a wide range of sliding velocities (10^{-5} to 0.1 m/s) and at P = 139 MPa, the CoF of PMPC brushes remained at μ = 0.04-0.14 with the presence of 1 M NaCl at glass/silicon tribopair[177]. In presence of pure water, bovine serum or simulated body fluid at RT or 37 °C, the CoF remained stable at $\mu = 0.02$ at Co-Cr-Mo/UHMWPE tribopairs with an applied pressure of P = 29 MPa[179]. Mica grafted PMPC brushes offered a CoF as low as $\mu \sim 10^{-4}$ at 0.2 M $NaNO_3$ up to P = 150 MPa[165]. Altogether, these promising results with PMPC brushes highlight their potential use in broad medical applications such as prosthetics coatings[179] since the pressures successfully reached in these studies are close or higher than physiological pressures.

Polymer brushes are promising engineering tools to develop molecular switches sensitive to external stimuli such as temperature, pH, salt concentration, or solvent quality by tuning the polymer brush thickness and hydration and thus surface friction[167, 171-172, 175, 180]. Polymer brushes were also employed as particles shells to develop a colloidal system able to lubricate and encapsulate/release drugs[181-182]. PSPMA was grafted on thermoresponsive PNIPAM microgels encapsulating a drug model, namely, aspirin at a PDMS/silicon wafer tribopairs, efficiently providing CoF from 0.005 to 0.015 at a concentration of 0.5 $\%_{wt}$ microgels in aqueous solution and independently of the temperature from 25 to 50 °C[181]. Similarly, PSPMA was grafted on silica nanoparticles loaded with aspirin and provided a CoF of 0.173 up to P = 2.64 GPa[182].

Table 1.2. Tribological properties of covalently-attached polymer brushes

Polymer	Structure	Polymer nature	Substrate and friction tester	CoF	Operative parameters (Pressure or load, sliding rate)	Remarks	References
PVP	mushroom	nonionic	PDMS pin on a silicon wafer in a microtribometer	μ = 0.4 for 10 kDa PVP and μ = 0.007 for 1300 kDa PVP	at v = 0.1 mm/s and P = 80 kPa	At a comparable grafting density, to lower the CoF, a higher Mw was needed	166
PNIPAM	Brush	nonionic	Silica microsphere on polymer initiated on silicon substrates in AFM	μ ~ 0.08 at 25 °C independently of the PNIPAM thickness, μ = 0.5 and 0.9 at 40°C for thin and thick PNIPAM layer, respectively	at v = 1 μm/s up to a load of 60 nN	Beyond LCST, the dehydrated PNIPAM brushes collapsed limiting lateral deformation upon friction, increasing roughness and the CoF	167
PMPC brush	Brush	zwitterionic	PMPC brush grafted from mica surfaces mounted in a SFA	μ = 0.0004 in pure water and μ = 0.0026 in 0.1 M $NaNO_3$	up to 7.5 MPa over v = 10-1000 nm/s	Extremely low CoF due to the high hydration level of the zwitterionic heads. Salting-out effect of the PMPC layers at high saline concentration	83
			PMPC brush grafted from mica surfaces mounted in a SFA	μ ~ 10^{-4} at 0.2 M $NaNO_3$	up to P = 150 MPa and v = 300 nm/s	Lower CoF due to an increase of the PMPC grafting density when decreasing the oxygen species during ATRP PMPC chain growth	165
PSPMA-g-PNIPAAm microgel	Brush on a spherical particle	anionic	PDMS ball on silicon wafer block tribometer	μ = 0.005-0.015 at 0.5 %wt microgels,	v = 100 mm/min at a load of 5 N	Hydration lubrication by the charged brushes. Microgels charged with drug for release in the joints	181
PSPMA-g-silica nanoparticles	Brush on a spherical particle	anionic	steel ball on steel block tribometer	μ = 0.173 at 0.3 %wt nanoparticle	up to P = 2.64 GPa	Combination of drug delivery system with lubrication properties	182
PSPMA	Brush	anionic	PDMS ball on PDMS block tribometer	μ = 0.02 at 90 % relative humidity (RH) and room temperature and μ > 1.0 at low RH or high RH and high	at P ~ 50 kPa	Thermal switch initiated by IR laser exciting Fe_3O_4 nanoparticles embedded in the brush layer which increased the local temperature and initiated the brush layer dehydration (initial brush height : ~ 200 nm, collapsed brush height : ~ 70 nm)	171

				temperature due to Fe_3O_4 nanoparticles excitation			
			PDMS pin on Diamond-like carbon disk tribometer	$\mu = 0.0062$ in pure water and $\mu = 0.01$ in 0.15 M NaCl	at P = 0.28 MPa and v = 0.01 m/s	Brush reversible responsiveness to salt concentration	172
Nonionic PEGMA, anionic PSPMA, cationic PMETAC and zwitterionic PSBMA brushes	Brush		PDMS pin on disk tribometer	$\mu = 0.01$ in pure water and $\mu > 0.3$ when CTAB is added for PSPMA, $\mu = 0.01$ in pure water and $\mu > 1$ when SDS is added for PMETAC, $\mu \sim 0.02$ for PEGMA and $\mu = 0.015$ for PSBMA even upon addition of SDS and CTAB	P = 0.3MPa and v = 2 mm/s	Charged brushes friction was dependent on the amount of oppositely-charged surfactant added contrary to neutral brushes due to the increase of hydrophobicity and brush dehydration	174
Anionic PSPMA and polymethyl acrylic acid sodium (PMAA), cationic PMETAC and zwitterionic PSBMA brushes	Brush		PDMS pin on silicon wafer disk tribometer	$\mu = 0.005$-0.24 for PSPMA following the length of hydrophobic surfactant TBAB < DTAB < CTAB $\mu = 0.006$-1.6 for PMAA following the serie $Na^+ < NH_4^+ <$ TMAB < TEAB < $Cu^{2+} < Fe^{3+}$ $\mu = 0.006$ - 0.83 for PMETAC following the serie $Cl^- < ClO_4^- < PF6^- < TFSI^-$ $\mu = 0.006$ for PMPC whatever the counterions charges	at P = 0.23 MPa and v = 2 mm/s	Charged brushes underwent drastic friction increase in presence of counterions which dehydrated the brush layers. Zwitterionic brushes are stable over pH and salt concentration compared to charged brushes	175
Si-nanowire array modified with PSPMA brushes	Brush		PDMS Pin on coated Si-nanowire disk tribometer	$\mu = 0.04$ under wet state (50 % RH) and $\mu > 1$ under dry state (13 % RH) at P ~ 10 kPa and v = 10 mm/s		Humidity uptake by the polyelectrolyte decreased the CoF whereas under dry condition, dehydration of the brush domain enhanced by the gecko-like surface pattern drastically increased the CoF in a reversible manner	183
PMAA	Brush		PDMS pin on plasma-treated Si wafer tribometer	$\mu = 0.005$-0.01	at P = 0.28 MPa and v = 0.25 - 10 mm/s over 1000 rotation	Thick polymer layer were able to sustain low CoF throughout the experiment contrary to thin layers	184

					cycles for 240 nm thick PMAA layer		
Polyacrylic acid (PAA)	Brush		Silica colloidal probe on silicon wafer AFM	μ hardly exceeded detection limit in presence of 10 mM NaCl and at pH = 3.5 and 7.5 and in presence of 10 mM $CaCl_2$ at pH = 3.5; μ = 0.25 in presence of 10 mM $CaCl_2$ at pH = 7.5	at P = 45 MPa and v = 1 mm/s	Strong reversible bridging interaction between PAA and Ca^{2+} upon loading and shear increased the friction and decreased the layer fluidity	180
cationic PMETAC, anionic PSPMA, zwitterionic PMPC PMETAC-co-PSPMA Crosslinked PMPC	Brush-Gel		Glass ball-on-silicon wafer tribometer	μ = 0.08 for PMETAC, μ = 0.01 for PSPMA up to 450 cycles, μ = 0.015 for PMETAC-co-PSPMA up to 1400 cycles, μ = 0.08 for PMPC up to 60 cycles, μ = 0.13 over 250 cycles for crosslinked PMPC	at P = 139 MPa and v = 1.5 mm/s	Crosslinked brush layers sustained low CoF up to higher friction cycles thanks to a higher polymer layer shear force	176
PHEMA, PMPC	Brush	Nonionic, zwitterionic	Si3N4 probe on polymer grafted on silicon wafer AFM	μ = 0.04-0.12 for PHEMA and μ = 0.04 for PMPC150 brushes	at a load of 0-100 nN and v = 8 μm/s	Higher polymer brush thickness and amount of water in the brush layer were essential to lower CoF	185
linear versus crosslinked PMPC	Brush - Gel	Zwitterionic	Mica surfaces mounted on SFA	μ ~ 10^{-3} - 10^{-4} for both linear and crosslinked brushes	at P = 45 atm and v = 1.5 μm/s	For linear brushes, lubrication was independent of the v whereas for crosslinked brushes, CoF increased with v due to the suppression of the interpenetration of opposing brush layers	178
PSPMA, PMETAC	Brush	anionic, cationic	Steel ball on PEEK surface tribometer	From μ ~ 0.2 to μ ~ 0.01 upon polymerization time from 0 to 90 min	at P = and v = 120 mm/min for both polyeletrolytes	CoF decreased upon polymer chain growing	169
PMPC	Brush	Zwitterionic	Glass ball-on-silicon wafer	μ =0.04- 0.14 in 1 M NaCl	at v = 10^{-5} - 0.1 m/s and P = 139 MPa	PMPC Polyzwitterionic brushes friction properties are independent of saline concentration	177
PMPC	Brush	Zwitterionic	Co-Cr-Mo Ball on UHMWPE plate tribometer	μ = 0.02 in pure water, bovine serum or simulated body fluid at RT or 37 °C	at P = 29 MPa and v = 25 mm/s	Potential in prosthetics coatings	179
PS-b-PAA grafted to OH-activated mica surface	Brush	anionic	Mica surfaces mounted in a SFA	μ ~ 0.1-0.3	up to P = 4 MPa and v = 1 μm/s	Controlled surface density thanks to attachment of PS-b-PAA to a PS monolayer attached to OH-activated mica surface	186
PAM grafted from carbon nanotube	Brush on nanotube	nonionic	Ball on plate tribometer	μ ~ 0.04-0.08	At a load of 392 N and v = 1450 rpm	PAM coating made carbon nanotubes soluble in water CoF decreased with PAM chain length increase	168

1.4.3 Using adsorbed polymer layers

In order to immobilize macromolecules on a substrate without any chemical modifications, one promising alternative is to get inspiration from the anchoring groups of proteoglycanes globular domains[47]. This allows the free non-specific or specific adsorption of the macromolecules to the substrates in view to their direct use in biological media. The major drawback is that the attachment *via* electrostatic interactions, hydrogen bonding, or more specific anchoring groups is generally not as strong as covalently attached polymer layers, but current efforts are focused to overcome this critical point (Table 1.3).

1.4.3.1 Non ionic adsorbed polymer layers

Pr Spencer's lab published several studies about BB polymers based on PLL as main backbone bearing pendant chains in view to electrostatically attach the bottlebrushes to negatively-charged surfaces[104, 187-190]. They showed excellent friction properties of PLL-g-PEG on negatively-charged mica surfaces as well as on ceramic[190], PE[191] or PDMS[188]. For instance, at pH = 12, PLL promoted hydrophobic interaction of the lysine moiety on hydrophobic PDMS surface, and thus decreasing the CoF up to 0.02.[188] PLL backbone can also be modified to bear another pendant chains such as dextran[189]. Compared to poly(allylamine) (PAAm), PLL backbone exhibited better lubrication properties when bearing PEG pendant chains due to the longer spacer in the PLL anchoring groups compared to PAAm. This longer spacer enhanced the number of attachment points and the flexibility of the bottlebrush, thus providing higher PEG density toward the medium, and improving the re-adsorption rate of the polymer upon shear-induced desorption, ensuring better self-healing properties[88]. Many other anchoring groups were designed to attach PEG chains to a surface. Hydrophobic PPO was coupled to PEG in the form of triblock to form polymer loops[192-193]. The studies showed that the longer the PPO chains, the better the lubrication is, due to the formation of a strongly anchored thick hydrated polymer layer providing low CoF of 0.02-0.05 on a Si/Steel tribopair up to ~ 1 GPa[192]. In the same view, PEG brush, bottlebrush or loops were successfully anchored to a variety of surfaces using bioinspired techniques such as thiol-terminated polymers or catechol moities naturally found in mussel's adhesive plaque to provide low friction and wear protection[125, 194-195]. Finally, other nonionic alternatives to PEG were successfully implemented such as PNIPAM or PAM brushes attached via polycationic blocks with an intermediate lubrication behavior up to mild pressures[196-198].

1.4.3.2 Charged adsorbed polymer layer

Charged polymers were also studied as biolubricant with effectively low CoF in pure water or in low salt concentration. Raviv *et al.* tested an anionic poly(methylmethacrylate)-*block*-poly(sodium sulphonated glycidyl methacrylate) copolymer (PMMA-*b*-PSGMA) copolymer and reached a CoF of 0.001 at 3 atm of normal pressure in presence of 10 mM of salt[81]. A cationic polymer of poly[3-(methacryloyl-amino)propyl] trimethylammonium chloride) (PMAPTAC) was also designed and provided low CoF especially in presence of SDS when forming an organized polyelectrolyte-surfactant layer able to sustain loads of 20 MPa with $\mu < 0.05$[199]. The major drawbacks of these polyelectrolytes systems are their propensity to collapse under saline conditions, thus increasing the CoF and decreasing wear resistance at low loads.

1.4.3.3 Polyzwitterionic molecular brushes

Banquy and coworkers designed polyzwitterionic bottlebrush polymers made of PMPC pendant chains able to provide low CoF even in presence of 150 mM NaCl[101-102, 200]. The authors developed mono-, di- and triblock copolymers. Directly bioinspired from LUB or AGG, the monoblock and the central domains of the di- and triblock polymers bear the PMPC pendant chains, micmicking DPPC heads, whereas the di- and triblock bear respectively one and two polycationic/hydrophobic lateral anchoring blocks able to adsorb on negatively-charged surfaces such as mica[201]. They showed CoF of $\mu \sim 0.01$ independently of the polymer structure at pressure in the range of 1.5- 3 to > 14 MPa by using two different anchoring techniques: simple adsorption of the di- and triblock lateral anchoring groups[200-201] or the synergistic interaction *via* entanglements of the monoblock with high molecular weight 1.5 MDa HA at a mass ratio monoblock: HA 1: 10[101, 200].

1.4.3.4 Dendrimers

Like membrane protein architectures, non-covalently adsorbed dendrimers have been successfully used as lubricant in organic solvants. A fifth-generation amino acid-modified poly(propyleneimine) dendrimer was left to adsorb on mica surface and tribo-tested in THF using SFA[202]. A fourth generation carbosilane was experimented on mica surface in toluene[203]. This is an interesting basis to design new and efficient water-soluble architectures for biolubrication.

Table 1.3. Tribological properties of adsorbed polymer

Polymer	Stucture	Polymer nature	Substrate and friction tester	CoF	Operative parameters (Pressure or load, sliding rate)	Remarks	References
PEG-g-PLL	Bottlebrush	Nonionic	Mica surface mounted in SFA	$\mu < 0.001$-0.003 upon changing pure water to 150 mM KCl	P = 10 MPa and v = 0.5-5 µm/s	Resistance to polymer desorption upon salt, load and shear is due to the re-adsorption from the free polymer solution leading to self-healing polymer coating	104
			PDMS surfaces using a pin-on disk tribometer	$\mu \sim 1$ at pH 2 with or without salt, $1 < \mu < 0.02$ at pH 12 with 1 M KCl	with v from 1 to 100 mm/s up to P = 0.53 MPa at 0.25 mg/mL	The hydrophobic part of PLL is able to adsorb under mild conditions on PDMS (low pressure, low salt concentration and high pH to screen amino positive charges	188
			Si_3N_4 and SiC ceramic surfaces using a pin-on disk tribometer	µ dropped from 0.02 to 0.003 when changing HEPES buffer for 0.25 mg/mL PEG-g-PLL solution	v = 120 mm/s and a load of 5 N		190
			PE colloidale sphere versus silica surface in AFM	$\mu \sim 0.08$ for a plat surface and increased up to 0.67 when increasing the roughness of the substrate at 0.25 mg/mL PEG-g-PLL compared to $\mu > 1$ without polymer	up to a load of 120 nN	Flat surfaces ensured a better lubrication than rough surfaces due to PEG brushes which were less stretched and exhibited a lower density grafted brush layer at the rough contact leading to a weaker repulsion force	191
PLL-g-Dextran			Gradient polymer on silicon wafers versus borosilicate colloidal sphere measured in AFM	$\mu \sim 0.1$	for 0.02 mg/mL PLL-g-dextran v = 1 µm/s and P ~ 50 MPa and µ sharply increased for P > 50 MPa	Going from the mushroom state to the brush state by increasing the grafting density, CoF sharply decreased with an increased onset of high friction getting higher when increasing the chain density at low load. A t high load, increasing chain density lead to higher CoF.	189
PMPC mono-, di- and triblock copolymers	Bottlebrush central domain plus none, one or two lateral anchoring groups	zwitterionic	Mica surfaces mounted in a SFA	$\mu \sim 0.02$	P = 3 MPa in pure water and P = 1.5 MPa in 150 mM NaCl with 100 µg/mL PMPC and 1 mg/mL 1.5 MDa HA Up to P > 14 MPa at v = 2.5 µm/s	Salts did not influence the polymer lubrication itself. The critical pressure at which wear initiated increased with the increase of HA Mw due to synergistic entanglements with the PMPC copolymer. The anchoring was enhanced by the strong adsorption on mica surface and the strong intermolecular bridging with HA due to polycationic side groups	101-102, 200-201
PMAPTAC, PMAPTAC-SDS		cationic	Si probe-mica surface AFM	μ = 0.06-0.37 without SDS $\mu < 0.05$	at loads from 0 to 40 nN and v = 2 µm/s	SDS formed a structure surface layer with PMAPTAC brushes ensuring low CoF and high	199

				when SDS was present in solution	without SDS up to a load of 30 nN (P = 20 MPa) with SDS	load bearing capacity	
P(AM-co-MAPTAC)	bottlebrush	nonionic	Silica bead probe on silicon or gold-coated silicon wafer AFM	μ = 0.44-0.67 for Si/Si tribo-pair and μ = 0.22-0.67 for Si/gold tribo-pair for (P(AM 99%-co-MAPTAC 1%))	at a load of 900 nN and v = 0.5-5 µm/s	The polymer -substrate affinity was exchanged from silicon to gold leading to a stronger adsorption and a lower CoF	197-198
PEG-PPO-PEG	Loop	Nonionic	PDMS pin on PDMS disk tribometer	μ = 0.02-0.1at a concentration of 5 mg/mL PEG_{37}-PPO_{56}-PEG_{37},	At a load of 5 N and v = 0.001-0.1 m/s	Adsorption increased and friction decreased with PPO Mw increase	193
PPO-PEG-PPO	loop	Nonionic	Cr-steel ball on silicon wafer or Ti-coated silicon wafer tribometer	μ = 0.02-0.05 (Si/Steel tribopair) and $\mu \sim 0.1$ (Ti/Steel tribopair) for a $6\%_v$ solution PPO_{22}-PEG_{14}-PPO_{22}	at P = 1024 MPa for Si-Steel tribo-pair and at P = 914 MPa for Ti/steel tribo-pair at v = 0.01-0.1 m/s	The polymer with the longest PPO side anchoring blocks provided thick polymer layer and the lowest CoF	192
$((CH_3)_3N^+)$-PEG-NHS		Nonionic	Mica surfaces mounted on SFA	μ = 0.03	up to P = 0.1 atm at v = 300 nm/s	NHS-PEG-NHS did not adsorb on mica contrary to triethyl ammonium end-terminated PEG-NHS which provided low CoF up to low pressures due to interpenetration (low grafting density)	204
Sil-PEG		nonionic	Steel pin on plasma-treated glass disk tribometer	μ = 0.08 at the experiment beginning and reached μ = 0.58 after 50 cycles	at P = 0.51 GPa and v = 5 mm/s	Wear debris and asperities apparition increased the CoF	195
Thiol-terminated (pAA-g-PEG)	bottlebrush	Nonionic	Cartilage-on-glass tribometer	μ = 0.140	at a cartilage compressive strain of 40 % and v = 0.3 mm/s	Lubrication of cartilage depended on the polymer attachment on the surface	125
(PAAm-g-PEG)	bottlebrush	nonionic	Steel ball on plasma-treated glass disk tribometer for sliding tests and mini-traction machine for rolling tests	μ = 0.2-0.3 for a sliding contact and μ = 0.0005-0.001 for a rolling contact	at a load of 2 N and v = 1-19 mm/s	Highlighting the importance of the friction tester. Compared to PLL-g-PEG whose CoF was lower in the same conditions, this highlighted the subtantial role of the anchoring group on lubrication	88
P(EO-co-AGE)-b-PEO-b-P(EO-co-AGE) loop triblock functionalized with silyl-protected	loop	nonionic	Mica surfaces mounted in a SFA	μ = 0.002-0.004	up to P = 3 MPa and v = 2.5 µm/s	Strong anchoring of the polymer to the substrate maintained the loop conformation	194

catechol							
$PEG_{45}MEMA$: METAC Bottle-brush	Bottlebrush	nonionic	Mica silica surfaces in AFM	$\mu = 0.006$	up to P = 30 MPa and v = 4 µm/s	Need to guarantee a high number of side chains to avoid attractive bridging	[205]
			Mica surface and silica probe in AFM	$\mu = 0.04$	up to 60 MPa and v = 2 µm/s	Water content inside the polymer brush layer is > 90 %	[206-207]
PMMA-b-PSGMA		anionic	Hydrophobized mica surfaces mounted in a SFA	$\mu \sim 0.001$	at P = 0.3 MPa and v = 0.5 µm/s with 10 mM salt	Opposed brush chains resisted interpenetration and hydration sheaths generated large osmotic pressure and retaining water fluidity	[81]
Poly(Acryloxyethyl trimethylammonium chloride)-g-$PEO_{45}MEMA$ (AETAC-g-$PEO_{45}MEMA$)	bottlebrush	nonionic	Silica probe on silica surface on AFM	μ = 0.02-0.06	up to P = 35 MPa and v = 4 µm/s		[208]
poly(N-isopropylacrylamide)-block-poly(3-acrylamidopropyl) trimethylammonium chloride), (PNIPAAM-b-PAMPTMA(+))	brush	nonionic	Silica probe on silica surface AFM	μ negligible and drastically increased to 0.5	at T < $LCST_{PNIPAM}$ in 0.1 mM NaCl and drastically increased at a load of 5 nN at v = 4 µm/s	Temperature sensitive lubrication and strong anchoring due to polycationic block	[196]
Poly(glutamic acid-g-hydroxyl benzaldehyde)-g- cyclic poly(2-methyl-2-oxazoline) (PGA-PMOXA-HBA)	Cyclic	nonionic	Degraded cartilage tissues ball on disk tribometer	$\mu = 0.03$ for cyclic polymer with intermediate grafting density compared to $\mu = 0.06$ for the linear polymer	at P = 0.9 MPa and v = 5 mm/s	Cyclic brushes were more lubricous than linear and intermediate lateral chain grafting density was essential to cover the backbone and avoid reduced attachment to the surface	[122]

1.4.4 Using hydrogels

Gel surface structure plays a significant role in lubrication as highlighted by the paramount role of cartilage on joint lubrication firstly presented by McCutchen[82]. Different techniques can be adopted to decrease the friction: decrease the applied stress by increasing the contact area, diminish the adhesion or increase the lubrication of the contact (Table 1.4). Hydrogels, known to possess low coefficient of friction due to their high amount of water and their high deformability, are excellent candidates for tissue engineering[209-210]. The major drawback of gels is their limited resistance to wear upon load and shear. Research teams implemented different technical procedure to decrease the friction of hydrogels.

1.4.4.1 Polyelectrolytes incorporation

To rejoin the previous section, many polyelectrolytes have been successfully incorporated into hydrogel matrix as copolymers to beneficiate from the strong repulsive force arising from the hydration sheaths surrounding the charges. PAM hydrogels friction was significantly

decreased when embedding free PAMPS chains to form a double network (DN) hydrogels or designing a triple network (TN) reaching CoF of $\mu \sim 0.007\text{-}0.02$[211]. Similarly, PAM hydrogels reached CoF from 0.15 to 0.02 when increasing the amount of cationic copolymers of PMETAC[99], from 1 to 0.01 with poly(quaternized *N*-[3-(dimethylamino)propyl]acrylamide) DMAPAA-Q[212] or from 0.1 to 0.01 with anionic copolymer of poly(2-acrylamido-2-methylpropanesulfonic acid sodium salt) PNaAMPS[212]. PAM hydrogel friction was also modified by using different tribopairs going from $\mu < 0.1$ when the hydrogel was sliding over glass surfaces compared to $\mu = 0.06$ when rubbing against another PAM hydrogel[89]. The controlled surface roughness of PAM hydrogels was also assessed in terms of friction. Rough hydrogels ($R_a = 21$ µm) exhibited higher CoF ($\mu = 0.03\text{-}0.09$) compared to flat hydrogels ($R_a = 4$ µm) ($\mu = 0.04\text{-}0.02$) at slow sliding speed, but the rough gel friction drastically decreased at higher sliding speed nearly matching flat hydrogel CoF. These results highlighted the different lubrication modes operating according to the substrate topography[213]. Poly(*N,N*'-dimethyl acrylamide) (PDAM) hydrogels showed significantly different friction behavior when produced on a silicon hydrophilic surface ($\mu = 0.05\text{-}0.5$) or a polystyrene (PS) hydrophobic surface ($\mu = 0.0001\text{-}0.08$) over the studied sliding speed range[214]. The authors proposed that the less crosslinked gel surface in contact with PS surface generated dangling PDAM chains able to decrease the CoF. They demonstrated this hypothesis by embedding PDAM free chains into a PDAM gel made on a hydrophilic substrate which offered similar CoF to the ones prepared on hydrophobic surfaces.

1.4.4.2 Surface texturing

Friction can also be decreased by the surface topography. For instance, vertical pores of 20 µm in diameter and spaced of 20 µm designed at the surface of a PDMS substrate facilitated the water exudation and, thus the creation of a fluid-film lubrication, to the surface when the matrix was deformed due to the applied load resulting in a decrease of the CoF up to $\mu = 0.3$, one order of magnitude lower than pore-free PDMS substrates[215]. Thanks to a similar mechanism, multilayered physical chitosan hydrogels exhibiting a permeable surface made of microchannels of 10 µm in diameter provided lower CoF ($\mu = 0.18$) than surfaces devoid of microchannels ($\mu = 0.38$)[95]. This difference appeared above a critical pressure which triggered the microchannel constriction and pore closure and thus the water exudation to the more permeable side. Similarly, the engineering of alveoli patterns on PAA gels significantly decreased the CoF[216].

1.4.4.3 Layered hydrogels

Layered gels display different CoF depending of the density or the porosity of the surface in contact. The preparation of a softer and more porous hydrogel layer made of a mixture of acrylamides provided a lower CoF compared to a stiffer and denser layer of the same composition by astutely tuning the crosslinking density (from μ = 0.35 to 0.15) [99]. A biphasic PVA hydrogel was obtained using a combination of cast-drying (CD) and freeze-thawing (FT) methods[93]. Interestingly, the CD on FT gel tribopairs exhibited very low CoF (μ = 0.006) compared to monophasic FT or CD or biphasic FT on CD gel tribopairs. Stimuli-responsive hydrogels were also designed to develop surface behaving according to pH such as poly(*N* -(carboxymethyl) -*N*,*N*-dimethyl -2-(methacryloyloxy) ethanaminium) (PCDME) hydrogels with adhesive behavior below pH 8.5 and providing CoF as low as μ = 0.04 at pH = 12.7 [217]. A multiresponsive hydrogel made of poly(*N*-isopropylacrylamide)-poly(sodium methacrylate) (PNIPAM-co-PNaMA) exhibited CoF of μ = 0.05 at RT < LCST and pH = 7 compared to μ > 1 at T = 32 °C > LCST and pH = 2.[218]

Table 1.4. Tribological properties of surface-textured hydrogels

System	Nature	friction tester	CoF and conditions	Operative parameters (Pressure or load, sliding rate)	Remarks	References
PNIPAM-PNaMA	hydrogel	Reciprocating tribometer in a face-to-face contact mode with same hydrogel surfaces	At pH 7 and RT, μ = 0.05 due to PNIPAM and PNaMA swelling, at pH 2 and RT, μ = 0.16 due to PnaMA collapse and μ > 1 at pH 2 and 32 °C due to total chain collapse	at a load of 1 N and v = 200 mm/min	Multiresponsive hydrogels - thermoresponsive PNIPAM and pH-responsive PnaMA. The chain collapse under temperature and pH stimuli can be modulated by the ratio NIPAM: NaMA	218
Biphasic PVA	hydrogel	PVA gel glued on a ball on a glass plate reciprocating tribometer	μ = 0.006 for hybrid CD (cast-drying method, low permeable) on FT (freeze-thawing method, highly permeable) gel, μ = 0.05 for CD gel, μ > 0.1 for FT gel and FT on CD gel	at a load of 2.94 N and v = 4 mm/s	Load support by fluid phase and surface lubricity are key. Friction properties can be modulated by the gel fabrication techniques leading to different nano and microstructural architecture	93
Porous PDMS with pillars of 20 μm in diameter and spaced of 20 μm	gel	Glass ball on PDMS block tribometer	μ ~ 0.25-0.30 for wet and porous gel, μ > 3 for wet and flat gel	At loads of 50- 400 mN and v = 5-1000 μm/s	The creation of pores to a pressurized and sheared surface created fluid exudation able to provide fluid film lubrication	215
Dimpled PAA	hydrogel	Glass ball on hydrogel tribometer	From μ = 0.27 to 0.18 when increasing dimpling area from 0 to 80 % for hard hydrogel (water content 65 %)	At a load of 20 mN and v = 20 μm/s	Lower friction area for highly dimpled hydrogel surface decreased the friction compared to flat hydrogel	216

			From μ = 0.1 to 0.05 when increasing dimpling area from 0 to 80 % for soft hydrogel (water content 90 %)			
poly(AM-*co*-NaAMPS) and poly(AM-*co*-DMAPAA-Q)	hydrogel	Gel on gel Rheometer	μ = 0.1 - 1 for poly(AM-*co*-DMAPAA-Q) when increasing AM content, for poly(AM-*co*-NaAMPS), μ = 0.01 - 0.1 in pure water μ = 0.01 - 0.2 from [NaCl] = 0 to 1 mol/L	At a load of 3 N and v = 0.01 rad/s	CoF decreased with the charge density increase CoF increased with salt concentration	212
P(AMPS-co-AM)	hydrogel	Glass on gel tribometer	μ ~ 0.1 for double network P(AMPS-co-AAm) μ = 0.02 - 0.007 for P(AMPS-coAAm) + PAMPS triple network μ = 0.007-0.003 for P(AMPS-co-AAm) double network + embedded free linear PAMPS	At P = 1-100 kPa and v = 1.7 mm/s	Addition of charges increased osmotic pressure and thus decreased CoF especially when polyelectrolyte chains were highly mobile up to a critical shear rate where linear polymer chains could not follow the sliding velocity	211
PAM	hydrogel	Glass on gel, gel on glass and Gel on gel	μ = 0.3-0.4 for glass on gel, μ = 0.1-0.25 for gel on glass and μ < 0.06 for gel on gel contact	At a P = 1-6 kPa and v = 100 μm/s		89
PAA nanohydrogel array	hydrogel	PDMS ball on gel disk tribometer	μ ~ 0.007 for nanohydrogel array and μ > 0.1 for bulk bulk hydrogel at pH 10	A load of 40 N for nanohydrogel array and a load of 3 N for bulk hydrogel and v = 0.01 m/s	Strongly depended on pH, low pH increased significantly the CoF	219
P(AA-co-SPMA) nanohydrogel array	hydrogel		From μ = 0.34 to 0.01 when increasing SPMA/AA molar ration from 0 to 0.5	At a load of 10 N and v = 0.01 m/s	CoF increased with the presence of NaCl and metal ions	220
PDAM fabricated on hydrophilic and hydophobic substrates	hydrogel	Gel on gel rheometer	μ = 0.05 - 0.5 for gels prepared on hydrophilic silicon, μ = 0.0001 - 0.08 for gels prepared on hydrophobic PS and μ = 0.001-0.08 for gels prepared on hydrophilic substrates + linear polymer chains	At P = 4 kPa and v = 0.01 - 10 rad/s	Hydrophobic substrate generated loosely crosslinked dangling chains at the gel surface dramatically decreasing the CoF	214
Bilayered P(AM-co-AAc-co-METAC)	hydrogel	Steel ball on gel disk tribometer	From μ = 0.35 to 0.11 for the highly crosslinked bulk gel when increasing METAC/AAc content from 0 to	At P = 3.21 mPa and a frequency of 5 Hz	The more lubricious gel surface was due to the more porous structure and the high water trapping ability of METAC	99

			3 $\%_{mol}$ From μ = 0.15 to 0.02 for the weakly crosslinked surface gel when increasing METAC/AAc content from 0 to 2 $\%_{mol}$			
PAM of different surface roughnesses	hydrogel	Gel disk on flat glass rheometer	μ ~ 0.09-0.03 for a rough surface (R_a = 21 µm) μ ~ 0.04-0.02 for a flat surface (R_a = 4 µm)	At P = 11 kPa and v = 0.1 - 1000 µm/s	Friction forces monotonously decreased with velocity on rough surfaces and remained more constant on flat surfaces leading to similar CoF at high sliding velocity	213
PVA-co-PMEDSAH poly([2-(methacryloyloxy) ethyl] dimethyl-(3-sulfopropyl) ammonium hydroxide)	hydrogel	Hydrogel disk and glass rheometer	From μ = 0.14 to μ = 0.02 when increasing PMEDSAH from 0 to 5 $\%_{wt}$	At P = 0.2 MPa and v = 0.065 rad/s		221
PCDME	hydrogel	Hydrogel on glass rheometer	From μ > 1 to 0.04 from pH = 1.9 to 12.7	At P = 2.75 kPa and v = 0.1 - 10 mm/s	Isoelectric point = 8.5. At pH < 8.5, adhesion, at pH > 8.5, lubrication	217
Structured chitosan	hydrogel	Hydrogel on hydrogel tribometer	μ = 0.18 on the more permeable surface exhibiting microchannels and μ = 0.38 on the denser surface	At P = 0.5-100 kPa and v = 5 mm/s	Microchannels closure lead to water exudation and lubrication on the more permeable surface	95

1.5 Bio-inspired wear protection

Wear protection of materials can emerge from the material itself owing highly stiff or organized structure able to sustain the coercions, self-repair *a posteriori*, incorporate additives which increase the mechanical properties of the materials or create a protecting layer at the contact surface.

1.5.1 Wear resistance through natural materials

Naturally-occurring polymers are able to provide wear protection of surfaces as referred in the table 1.5. HA role in biolubrication processes is crucial since it helps LUB and phospholipids to remain in the contact area once anchored at the interface and forms aggregates with AGG, enhancing the mechanical properties of cartilage. Das *et al*. explored this phenomenon to protect mica surfaces using a SFA[79]. The authors compared physisorbed HA and chemically grafted HA in addition with LUB. They showed a higher wear resistance of the surface, with a polymer layer pressure at rupture, P*, increasing from 10 atm to 40 atm, when HA was grafted to the substrate using APTES deposition compared to free HA. Alone, LUB was not able to sustain high loads and shear rates at mica surface. Adsorbed in the loop conformation on hydrophilic mica surfaces, LUB gave rise to CoF of μ = 0.03 up to pressures of P ~ 6 atm, which corresponds to light physical activities physiological pressures in human joints.

However, at higher loads, LUB aggregated and provided a high CoF ($\mu > 0.2$), but ensured a high surface wear protection with no apparent traces of wear on the mica surface[79, 146]. DPPC lipids played also a role on the protection of cartilage plugs when rubbed against a steel ball besides sustaining a low CoF $\mu < 0.05$ up to P = 1 MPa[97].

As well as lubricating in synergy with phospholipids, HA and mucins were found to lubricate in synergy with proteins. Albumin and γ-globulin, two main proteins of synovial fluids, were successfully tested as anti-wear agent for PVA hydrogels. It was shown that γ-globulin and albumin adsorbed on PVA surface providing wear protection[222]. Similar results were obtained with ceramic-on-ceramic tribopairs[223].

To improve the mechanical behavior of cartilage, genipin, a natural crosslinker of collagen was added to cartilage explants. Cross-linking helped the cartilage to increase its wear resistance as analyzed by HYP release by HPLC and apparent wear track[118]. Increasing the genipin concentration from 0 to 10 mM reduced HYP release from 3 µg to 0.3 µg over a stroke of 192 m at 4 mm/s and P = 1.4 MPa at steel/cartilage tribopairs with no apparent wear tracks.

Table 1.5. Wear properties of natural polymers

System	Apparatus	Wear assessment	Experimentation parameters	Remarks	References
polysaccharides		P* = 110 atm for polysaccharides extracted from red alga			100
Physisorbed HA	Mica mounted in SFA	P* = 10 atm for C_{HA} = 3 g/L and C_{PRG4} = 10 mg/mL	μ = 0.23 and v = 3 µm/s	Free HA and PRG4 in solution	79
Grafted HA	Mica coated with APTES mounted in SFA	P* = 2.2 MPa	Independently of HA M_w		103
Grafted HA	Mica coated with APTES mounted in SFA	P* = 40 atm	μ = 0.09 and v = 3 µm/s	Free HA and PRG4 in solution	79
Grafted HA plus PRG4 or BSF	Mica coated with APTES mounted in SFA	P* increased from 4 to 8 MPa in PRG4 and from 15 to 31 MPa in BSF with μ = 0.35		Grafted HA of different molecular weights (40, 500 and 2000 kDa) plus PRG4 or BSF	103
Free PRG4	Mica coated with APTES mounted in SFA	Lubricin thin layer ruptured at P = 6 atm, but mica surface remained intact up to higher loads	μ = 0.03 up to P = 6 atm then $\mu > 0.2$	PRG4 rearrange under shear	146
Free HA, PRG4 and mucin	Glass/cartilage, steel/cartilage, steel/steel, steel/PTFE tribopairs rheometer	Optical profilometer showed that mucin efficiently reduced wear on all tribopairs	P = 0.1 MPa, v = 0.1 mm/s for 1 h	Roughness measurement did not properly report wear	224
Genipin	Steel pin on cartilage disk tribometer	Analysis of Hydroxyproline release from cartilage and No apparent wear tracks for cartilage incubated in 10 mM Genipin and reducing from 3 µg HYP release	P = 1.4 MPa, v = 4 mm/s, l = 192 m and μ ~ 0.2 for control and genipin incubated cartilage at 30 min testing	Collagen cross-linking by Genipin improve wear resistance and chemical degradation in a dose-dependent manner	118

		to half the value at 2 mM and 10 % the value at 10 mM genipin treatment			
Phospholipids	Cartilage pin on steel disk	SEM analysis of cartilage wear showed less wear upon DPPC treatment	P = 1 MPa, v = 0.3 m/s with $\mu < 0.05$		97
Synovial fluid proteins	PVA hydrogels in a reciprocating tester	Lubricant layer fluorescence visualization	P = 0.12 MPa and v = 20 mm/s for albumin and γ-globulin at a concentration 2.1 $\%_{w/w}$ and a ratio 1/2 or 2/1 within a 0.92 MDa HA solution at 0.5 $\%_{w/w}$	At the proper ratio, albumin adsorb on the globulin layer adsorbed on PVA gels protecting the surfaces	222
	Ceramic on Ceramic friction tester	Wear rate is reduced from 0.02 % to 0.007 % when albumin (18 mg/mL) and globulin (13.1 mg/mL) are added to a mucin solution (200 µg/mL) plus wear visualization by SEM	P = 180-255 MPa, μ = 0.15-2 and v = 20 mm/s		223

1.5.2 Wear resistance through synthetic polymer

1.5.2.1 Using covalently grafted polymers

By mimicking the structure of natural brushes found in mucus or synovial joints, molecular brushes were found promising to prevent soft hydrogels and prosthetics wear, to provide antifouling or adhesive properties of biomedical surfaces[194, 225], to design switchable surface functionalities[225-226] or nanoparticles for drug delivery[181, 227] (Table 1.6). Two types of polymer brushes were used in aqueous solutions: nano-micro vectors carrying the brushes or as molecular brushes. PAM grafted from carbon nanotubes significantly decreased wear scratches of steel substrates compared to an aqueous buffer[168]. PSPMA was grafted on silica nanoparticles and drastically decreased the wear volume from 16.96×10^{-4} mm^3 for pure water to 8.02×10^{-4} mm^3 for 0.3 $\%_{wt}$ NPs of a steel substrate[182].

1.5.2.2 Using adsorbed polymers

Molecular brushes were designed to anchor on different substrates from poroelastic hydrogel and cartilage surface to stiff and flat mica surfaces. PAA-g-PEG exhibited a synergistic wear protection of mica surfaces when combined to fibronectin, a naturally-occurring glycoprotein[228]. Similarly, PMPC BB polymers enhanced wear protection of mica as well as chitosan hydrogels disks when used in combination with high molecular weight HA going from few MPa for a monoblock BB without anchoring groups to P* > 14 MPa for a triblock BB polymer with two anchoring groups[101, 200]. The cationic anchoring groups, made of

quaternized poly(2-dimethylaminoethyl methacrylate) (PDMEMA) increased the maintenance of the BB polymer and HA on negatively charged mica surfaces due to macromolecular entanglements and intermolecular interactions. PLL-g-PEG molecular brush made of a polycationic backbone of PLL was able to sustain pressure up to 10 MPa on negatively charged mica[104]. PMMA-g-PSGMA bearing a hydrophobic anchoring group of PMMA sustained a pressure of 0.3 MPa on hydrophobized mica surface at a low sliding velocity of 0.5 µm/s[81]. A molecular cyclic brush composed of poly(glutamic acid-g-hydroxyl benzaldehyde)-g- cyclic poly(2-methyl-2-oxazoline) (PGA-PMOXA-HBA) with HBA attachment groups showed a reduced cartilage degradation thanks to a good lubrication and reduction of degradation enzyme diffusion within cartilage thanks to the formation of an impermeable polymer layer at the cartilage surface[122]. The attachment was provided by HBA which was able to react with amino groups present at the cartilage surface forming Schiff-bases and strongly attached the polymer to the cartilage.

Table 1.6. Wear properties of synthetic polymers

System	Apparatus	Wear assessment	Experimentation parameters	Remarks	References
PAA-g-PEG	Mica surfaces mounted in SFA	Pressure at rupture and FECO fringes showing, P* = 3.4 MPa	$\mu \sim 0.3$ at v ranging from 0.3 to 30 µm/s	Fibronectin had a synergistic effect with the PRG4 mimes to increase pressure at rupture	[228]
PAM grafted from carbon nanotube	Steel ball on plate tribometer	Optical microscopy showed less scratches for a 0.2 %wt coated carbon nanotubes solution than a buffer	At a load of 392 N, $\mu \sim 0.04$-0.08 at v = 1450 rpm		[168]
PSPMA-g-silica nanoparticles	steel ball on steel block tribometer	Wear volume of the steel substrate assessment by a profilometer: 16.96×10^{-4} for pure water, 10.92×10^{-4} for 0.1 $\%_{wt}$ NPs, 8.98×10^{-4} for 0.2 $\%_{wt}$ NPs, and 8.02×10^{-4} mm^3 for 0.3 $\%_{wt}$ NPs	up to P = 2.64 GPa, $\mu = 0.173$ at 2 mm/s	Wear volume decreased with the nanoparticles content and increased with increasing the load	[182]
PGA-PMOXA-HBA	Degraded cartilage tissues ball on disk tribometer	Histological assessment, GAG content assessed by dimetylmethylene blue and safranin-O, resistance to collagenase degradation measured by and Masson Trichrome: cyclic polymer reduced by 50 % cartialge degradation compared to bare cartilage	at P = 0.9 MPa and v = 5 mm/s, μ = 0.03 for cyclic polymer	Anchoring properties due to benzaldehydes able to react with amino groups exposed at cartilgae surface. Antifouling properties for large proteins/enzymes such as Chondroitinase ABC, intermediate antifouling properties to smaller enzymes such as BSA or collagenase due to not sufficient surface coverage	[122]
PMPC	Chitosan disk on	White-light	At P = 50 kPa, and v	Synergistic effect of	[101-102, 200]

bottlebrushes with none (mono-), one (di-) or two (triblock) anchoring groups plus high molecular weight HA	chitosan disk tribometer and mica surfaces mounted in a SFA	interferometry for chitosan gel roughness, FECO fringes deformation and polymer layer thickness for mica surfaces Sa = 1.5 µm for HA, Sa = 0.5 µm for monoblock BB and HA+BB; P * ~ 0.3-0.5 MPa in 150 mM NaCl for monoblock BB and 1.5 MDa HA alone; P* = 1.5 MPa for diblock BB, P* = 8 MPa for triblock BB; P* = 1.5 MPa for HA + monoblock BB, P* = 4 MPa for HA + diblock BB, P* > 14 MPa for HA + triblock BB	= 5 mm/s for chitosan gels, µ = 0.02 for BB and HA+BB and v = 3 µm/s for SFA experiments	HA with BB plus enhancement of wear protection when increasing the number of anchoring groups	
poly(methyl methacrylate)-block-poly(sodium sulphonated glycidyl methacrylate) copolymer (PMMA-b-PSGMA)	Hydrophobized mica surfaces mounted in a SFA	Drastic friction change at P* = 0.3 MPa	µ ~ 0.001 and v = 0.5 µm/s with 10 mM salt	Wear due to polymer peeling off under shear and load	[81]
PLL-g-PEG	Mica surface mounted in SFA	Wear visualization by friction and polymer layer thickness drastic increase, P* = 10 MPa	v = 5 µm/s µ < 0.001- 0.003	Polymer layer rupture when the polymer was not able to re-adsorb fastly	[104]

1.5.3 Wear Resistance using Hydrogels

As hydrogel moduli are typically found in the range of 1-100 kPa, one can easily understand that this promising materials for tissue engineering have a major drawback when used as tissue substitutes to sustain high body coercions. Several research teams have focused their research in designing hydrogels able to sustain *in vivo* coercions which are frequently exceeding several atmospheres or even megapascals such as cartilage (Table 1.7).

1.5.3.1 Using cross-linked networks

Primarily, increasing the crosslinking density or the polymer content of a hydrogel network is a simple way to enhance the mechanical properties of the hydrogels. PHEMA hydrogels exhibited a 60 % wear decrease when cross-linked with 5 mol% ethylene glycol dimethacrylate compared to 2 mol%[114]. A 15 % PVA-PVP blend lost 4.47 % in gel mass after 10^5 cycles at 2.9 MPa and 50 mm/s compared to a 6.05 % mass loss for a 10 % PVA-PVP blend[109]. Similarly, a 4 weeks chondrocyte culture within a potential articular scaffold of PVA

lead to the formation of an ECM composed of collagen and proteoglycans able to provide visible wear protection *via* the presence of stiff ECM clusters like chondrons[96].

1.5.3.2 Using hydrogel composites

The inclusion of inorganic stiff materials to form hydrogel composites is another interesting alternative to enhance the hygrogel mechanical properties. Graphene oxide (GO) was incorporated into PVA gels to drastically increase compressive and tensile stress from 0.35 and 0.7 up to 1 and 1.5 MPa, respectively, from a GO content of 0 to 0.10 wt%[112]. Interestingly, the addition of GO inside PVA matrix increased water content from 80 to 90 % and decreased CoF from $\mu > 0.2$ to a stable Cof of $\mu = 0.07$ over the wear test duration. As a result, final gel roughness was drastically reduced when using 0.10 $\%_{wt}$ GO within PVA gel matrix compared to the totally worn bare PVA gel. Hydroxyapatite was incorporated into freeze-thawed PVA gels and lead to low CoF ($\mu = 0.12$) and low wear when increasing hydroxyapatite content to 3% and freeze-thawing cycle numbers due to the elastic modulus increase from 1 to 14 MPa[229].

1.5.3.3 Using interpenetrated networks(IPN)

IPN is another alternative to provide enhanced wear resistance over single network hydrogel[230-231]. The concept is based on the incorporation of a second - or more - network within an initial polymer network to drastically increase the mechanical behavior of the IPN gel and resulting in a decrease in wear. For instance, a library of DN hydrogels were able to limit final gel roughness at levels similar to UHMWPE stiff substrate (R_a = 9.5, 3.2, 7.8 and 3.3 µm for PAMPS-PAAm, PAMPS-PDAAm and Cellulose-PDAAm and UHMWPE, respectively, at P = 0.1 MPa, 10^6 cycles, and v = 50 mm/s) which is frequently used in commercial prosthesis[113]. Their elastic moduli were found in the range of 0.1-1 MPa whereas they provided low CoF values in the range 0.04-0.12.

Decrease of hydrogel friction and simultaneous reinforcement of mechanical properties are challenging to obtain, but the techniques to reach them separately are well understood. However, the simultaneous enhancement of both gel wear and friction is more difficult since improving wear protection generally leads to friction increase or a friction reduction generally results in an increased wear. Indeed, in the table 1.7, we listed the CoF values for each system deemed to reduce hydrogel wear. Generally, CoF values exceeding 0.1 were obtained even though wear was considerably reduced (Table 1.7). For instance, a more hydrated and

lubricious PAM-PAA-PMETAC upper layer was added to a dense PAM-PAA hydrogel substrate to decrease the CoF to ~ 0.02 but the gel did not sustain wear tests and quickly lead to the upper layer erosion[99].

1.5.3.4 Using sacrificial bonds

Natural materials such as bones, nacre or mollusk's byssus have incredible mechanical strength due to the highly structured natural networks owing a primary stiff network and a weaker network made of biopolymers which easily rupture upon constraints, dissipating a huge amount of energy. As a result, the whole materials requires a higher amount of energy to rupture than its constituents themselves[43, 232]. These "sacrificial bonds" were extended to biomaterials to increase their stiffness via the insertion of weak covalent or non-covalent bonds within their matrices[233]. The principle was introduced by Gong et al. who developed a double-network hydrogel (DN gel) composed of a crosslinked stretchable matrix and a poorly crosslinked brittle network able to reach rubber-like mechanical properties[234-235]. Upon deformation, the brittle network first ruptures and dissipates the fracture energy prior to the whole gel fracture. However, once the covalent bonds of the brittle soft network ruptured, the gel looses mechanical properties over time and repetitions due to the material fatigue. The *in vivo* sustainability of natural materials such as bones are then due to reversible sacrificial bonds based for instance on electrostatic interactions of Ca^{2+} ions between negatively charged collagen fibrils. This concept was successfully expanded to hydrogels using reversible interactions such as ionic bonds, hydrophobic interactions, or H-bonding [236] or molecular diffusion and entanglements[237] leading to self-healing materials[238].

Table 1.7. Wear properties of hydrogels

System		Apparatus	Wear assessment	Experimentation parameters	Remarks	Refe-rences
Bacterial cellulose BC		BC pin-on-cartilage disk tribometer	Carbohydrate wear debris quantification by H_2SO_4 phenol assay and SEM imaging showed little to no wear of the tribopairs	At P = 0.8-2.4 MPa, μ ~ 0.05 and v = 8 mm/s	Carbohydrate only come from BC	119
PHEMA	hydrogel	Steel ball on gel dik tribometer	LVD transformer measuring the linear displacement so the wear depth: 60 % wear depth reducing when increasing crosslinker EGDMA from 2 to 5 mol%, hydrated gel exhibited 130 % wear increase	At a load of 20 N over 30 min, μ = 0.2-0.7	Lubrication and wear resistance are antagonist	114

			compared to non hydrated gel			
PVA-PVP	hydrogel	Co-Cr-Co pin on gel disk	Gravimetric weighting: mass loss of 4.47 % for 15 % PVA-PVP compared to 6.05 % for 10 % PVA-PVP	At P = 2.9 MPa over 10^5 cycles, v = 50 mm/s, μ ~ 0.1 in bovine serum	Higher polymer content correlated with reduced wear	109
PVA-PVP	hydrogel	Gel on cartilage pin on disk tribometer	Profilometer on a replicated gel surface to measure wear volume and white light interferometry: Wear volume loss of 29.8 mm^3 for PVA and 19.0 mm^3 for PVA-PVP 95/5, final gel roughnesses were ~ 1.5-2 nm compared to initial roughness < 0.2 nm	At P = 0.58 MPa l = 1350 m, v = 25 mm/s, μ = 0.12-0.14 for PVA-PVP blends-cartilage tribopairs, μ = 0.03 for cartilage on cartilage tribopairs and μ = 0.46 for steel-cartilage tribopair	Need to reinforce long-term use with IPN	115
PVA	PVA-CD, PVA-FT and PVA-hybrid hydrogels	Co-Cr-Co Alloy or alumina ceramic ball on PVA gel plate or PVA ball on glass plate friction tester	Optical microcopy	At P ~ 0.3 MPa, l = 140 m for alloy and ceramic and P ~ 0.1 MPa, l = 100 m for glass and v = 20 mm/s E_{PVA-FT} = 110 kPA, E_{PVA-CD} = 190 kPa	PVA hybrid showed no wear due to fluid load support	92-93
PHEMA, IPN of PHEMA-PEM and PHEMA-CAB (polyethylmethacrylate and cellulose acetate butyrate)	PHEMA gels on UHMWPE	Stainless steel disk on gel tribometer	SEM	At P = 1 MPa, l = 2500 m and v = 0.34 m/s	Hardness of IPN hydrogels improved wear resistance	94
PHEMA-P(MMA-co-AA) PHEMA-PVP		Gel pin on steel disk	Wear quantified by weight loss and SEM imaging. Wear rate remained between 10^{-6} and 10^{-5} gm^{-1} the lowest was obtained with PHEMA-P(MMA-co-AA) but increased with decreasing sliding speed	P = 2.4-5.5 MPa and v = 0.16 - 0.5 m/s, μ = 0.01-0.09	Most compliant gel suffer from adhesive wear compared to highly crosslinked gel suffereing from abrasion	105
Freeze-dried and self-healing PAAm	hydrogel	ZrO2 ball on gel reciprocating tester	3D laser scanning confocal microscopy, SEM	At a load of 20 mN, 2295 cycles, μ > 0.3 and v = 4 mm/s	After rehydration, the wear tracks disappeared and final roughness reached almost the one of initial gel	239
PMPC grafted on crosslinked PE	hydrogel	Co-Cr-Co ball on gel or alumina ceramic femoral head plate tribometer	Gravimetric analysis: loss of 100 mg of material for bare PE, loss of 20 mg of material for bare CLPE compared to no loss for PMPC-CLPE from 90 nm brush thickness SEM and	At P = 31 MPa, 5.10^6 cycles, v = 50 mm/s and μ = 0.08-0.01 from bare PE to PMPC-PE	Application for prosthesis with reduced wear, and thus inflammation,	106-107

			volumetric wear images			
PVA-FT/annealed	hydrogel	Stainless steel on gel wear test rig	Gravimetric analysis: wear reduction of one order of magnitude wear debris when water content decreased from 85 % to 50 %, 10^4 order when Mw increased from 1800 to 12300 g/mol, 18 % when PVA thickness increased from 2 to 3.6 mm	At a load of 490 N, 10^5 cycles,	PVA with less water content, higher molecular weight and higher polymer thicnkess generated less wear debris	108
PAMPS-PAAm, PAMPS-PDAAm, Cellulose-PDAAm and cellulose-gelatin	DN hydrogel	Alumina ceramic pin on hydrogel plate on a reciprocating tester	Depth and roughness analyzed by confocal laser microscopy: maximun depth (µm) and roughness (µm): 9.5 and 0.23 for PAMPS-PAAm, 3.2 and 0.08 PAMPS-PDAAm, 7.80 and 0.09 for cellulose-PDAAm and 1302 and non measurable for cellulose-Gelatin, 3.3 and 10 for UHMWPE	At P = 0.1 MPa, 10^6 cycles, v = 50 mm/s, µ ~ 0.04 for PAMPS-PAAm, µ ~ 0.12 for PAMPS-PDAAm, µ ~ 0.05 for cellulose-PDAAm, µ ~ 0.3 for cellulose-gelatin	Young modulus (MPa), ultimate stress (MPa), strain at failure (%): 0.33, 17.2 and 92 for PAMPS-PAAm, 0.20, 3.1 and 73 PAMPS-PDAAm, 1.6, 2.9 and 50 for cellulose-PDAAm and 1.7, 3.7 and 37 for cellulose-Gelatin	113
PVA/PLGA microspheres	hydrogel	Steel ball on PVA disk tribometer	SEM imaging: from 10 to 20 % porogen content in PVA gel lead to the appearence of singificative cracks. Culture of chondrocytes for 4 weeks lead to a significant decrease of apparent of hydrogel wear	At P = 0.44 MPa, v = 75 mm/s, l = 135 m, µ = 0.02-0.07	Higher porogen increased porosity and increased wear. extra-cellular matrix secreted from chondrocytes seeded in PVA hydrogels stiffed the gel	96
PVA-Graphene oxide composite	hydrogel	Co-Cr-Co ball on gel disk friction tester	laser confocal microscopy for morphology and roughness: PVA/0.1 %wt GO Ra initial = 6.7 µm, Ra final = 15.5 µm, neat PVA was quickly worn	At loads of 5 N for 90 min, v = 0.08 m/s, from µ ~ 0.1 to 0.07 when increasing GO content from 0 to 0.15 %wt	GO as a filler enhanced the load bearing capacity of PVA hydrogels	112
PVA-GO-PEG nanocomposite	hydrogel	Steel ball on gel disk µ-tribometer	White-light interferometer for morphology and roughness: PVA-PEG Furrow depth F = 149.3 µm, PVA/1.5-2 %wt GO -PEG F ~ 0 µm	At a load of 5 N, v = 60 mm /min, µ > 0.15 for neat PVA up to µ ~ 0.07 for PVA/1.5 %wt GO -PEG	Increasing GO content guaranteed wearless surface	111

PAM-PAA with Fe^{3+} ionic crosslinker	Covalent and ionic crosslinks bilayered structure	Steel ball on gel disk tribometer	SEM imaging: surface micropores vanished but the entire structure remained	At a load of 40 N over 1800 cycles, f = 1 Hz , μ = 0.02-0.06, Elastic modulus increasing from 5 to 50 MPa when increasing AAc-AAm ration from 0.25 to 0.35	Bilayered structure with porous superficial layer due to the presence of saturated and precipitated NaCl during the fabrication process and dense substrate (no NaCl precipitate)	98
Bilayered P(AM-co-AA-co-METAC)	hydrogel	PDMS or steel ball on gel disk tribometer	SEM imaging: Superficial porous structure was removed with hard steel-gel tribopairs and few remained with soft PDMS-gel tribopairs	At P = 1.2 MPa and a frequency of 5 Hz, μ = 0.01-0.03 for PDSM- gel tribopairs and P = 3.21 MPa, μ = 0.03-0.06 for steel- gel tribopairs over 70.10^4 cycles	CoF increasing due to the porous structure removal under shear	99
PVA-hydroxylapatite	Hydrogel composite	PVA hydrogel composite on cartilage micro-tribometer	SEM imaging: Decrease of wear when increasing hydroxylapatite content from 1 to 3 % and when increasing freeze-thawing cycles number	P = 0.58 MPa for 1 h and v = 4 mm/s. μ decreased from ~0.3 to 0.12 when increasing freeze-thawng cycles and hydroxylapatite content	Wear mechanism is plastic flowing and adhesive wear	229

1.6 Conclusion

Bioinspiration of naturally-occurring structures has been proven to be efficient to design aqueous lubricant fluids, lubricated surfaces and self-protecting surfaces. By directly using molecules extracted from joints or mimicking the macromolecular structures and/or chemical functions found in joints, research team were able to reach CoF as low as what can be found in nature without any wear damage up to physiological working conditions. These polymer-based materials can be adapted to plenty of substrates and sustain severe working conditions to replace, supplement or enhance tissues or biomaterials tribological properties.

Problématique

Comme nous l'avons abordé en introduction, il est aujourd'hui nécessaire de développer des traitements contre l'OA moins invasifs que les prothèses afin d'éviter ou, du moins, de différer leur pose. Le traitement de l'OA, caractérisée par une érosion mécanique du cartilage et par un processus inflammatoire, peut être ainsi dirigé soit contre les facteurs biologiques entrainant le catabolisme du cartilage, comme ce qui est généralement étudié[240], ou bien dirigé contre l'abrasion progressive du cartilage. *Ainsi, au regard de cette revue de littérature sur la conception de substituts cartilagineux et synoviaux, garantissant faible friction et résistance à l'usure, que nous manque-t-il pour pouvoir développer des traitements curatifs de l'OA à base de polymère, voire réaliser des articulations artificielles ?*

De manière générale, les systèmes polymériques lubrifiants ne sont généralement pas aptes à résister à toutes les différentes conditions physiologiques des articulations, à savoir, les pressions élevées, la large gamme de vitesses de glissement, la biocompatibilité, la résistance aux milieux physiologiques, notamment la présence des sels et l'immobilisation des macromolécules lubrifiantes sur des surfaces biologiques. Les molécules lubrifiantes naturellement présentes dans les articulations sont sélectivement dégradées lors de processus inflammatoires durant l'OA[241-243]. De plus, la plupart des systèmes polymériques lubrifiants étudiés sont des polymères greffés de manière covalente aux substrats ce qui nécessite des réactions chimiques de greffage *in situ*.

Une alternative innovante est donc de développer un fluide synovial synthétique directement injectable *in situ* capable de réunir toutes les bonnes propriétés tribologiques des articulations synoviales et pallier aux contraintes de l'administration *in vivo*. Pour cela, les brosses moléculaires, conçues comme mimes de la LUB et l'AGG, semblent intéressantes puisqu'elles offrent la possibilité de lubrifier et de s'ancrer sur tout type de surface par simple adsorption. Parmi toutes les brosses moléculaires présentées en introduction, une preuve de concept, présentée par le Pr Banquy, concernant un écouvillon moléculaire polyzwitterionique à base de PMPC a montré de bonnes propriétés lubrifiantes sur des surfaces modèles de mica en présence de sels et sur une large gamme de pressions et de vitesses de cisaillement[201]. Il est néanmoins nécessaire de comprendre comment il est possible d'améliorer l'ancrage et la friction de brosses moléculaires, comprendre leur fonctionnement sous contraintes et fournir une bonne lubrification de surfaces fragiles.

Ainsi, pour tester ces liquides synoviaux synthétiques bioinspirés, il est également nécessaire de concevoir des supports reproductibles ressemblant au cartilage comme le sont les hydrogels. En effet, les hydrogels sont des matériaux prometteurs pour la réparation du cartilage, car ils sont des matériaux viscoélastiques imbibés d'eau pouvant servir d'échafaudage pour la culture cellulaire à l'instar des fibrilles de collagène entourant les chondrocytes et du liquide synovial des articulations[244]. L'équipe Matériaux Polymères à l'Interface avec les Sciences de la Vie du Laboratoire Ingénierie des Matériaux Polymères, spécialisée dans la conception de matériaux polysaccharidiques pour des applications biomédicales, a d'ailleurs publié des études montrant l'ancrage de chondrocytes sur les hydrogels de chitosane et la formation d'agrégats chitosane-ECM-collagène de type II semblable à l'ECM du cartilage[245]. L'équipe a également montré que des techniques de gélification permettaient d'obtenir une structure en multicouches intéressante pour le concept de bioinspiration du cartilage[246-251]. Néanmoins, seules les propriétés mécaniques des hydrogels sont généralement étudiées et celles-ci peinent à atteindre les propriétés mécaniques remarquables du cartilage.

Hypothèse générale de travail et objectifs

Hypothèse générale de travail

En s'inspirant de l'architecture spécifique de l'aggrécane et de la lubricine, macromolécules impliquées dans la réduction du frottement et la protection contre l'usure du cartilage articulaire, il est possible de créer un substitut polymérique synovial possédant des propriétés tribologiques aussi bonnes, voire meilleures que celles des articulations saines.

Objectifs

Notre objectif est donc de concevoir un substitut synovial bioinspiré. Ce fluide permettrait de réduire la friction **et** de protéger contre l'usure soit directement le cartilage soit des supports poroélastiques à base d'hydrogel utiles pour applications biomédicales en créant un revêtement polymérique biocompatible ne nécessitant aucune modification chimique *in situ*.

Pour cela, nous avons défini trois objectifs spécifiques : (i) concevoir une librairie de mimes bioinspirés de l'aggrécane et de la lubricine et caractériser leur pouvoir lubrifiant à l'aide de l'appareil de forces de surface (SFA), (ii) développer un support poroélastique multicouche à base d'hydrogel et déterminer ses propriétés mécaniques, physiques et tribologiques, (iii)

améliorer les propriétés de frottement **et** de résistance à l'usure du substitut poroélastique par l'ajout du fluide synovial bioinspiré.

(i) *Concevoir une librairie de mimes bioinspirés de l'aggrécane et de la lubricine et caractériser leur pouvoir lubrifiant à l'aide d'un appareil de forces de surface.*

Différentes études ont montré que les polymères de type écouvillons moléculaires (ou 'polymères en brosse') possèdent des propriétés lubrifiantes intéressantes dans des gammes de contraintes très variées[201, 207, 252]. À travers cet objectif, l'intérêt est de concevoir une librairie d'écouvillons moléculaires, sans ou avec groupements d'ancrage, lubrifiant et protégeant les surfaces recouvertes sur une large gamme de pression, à différentes vitesses de cisaillement et capable d'opérer en conditions physiologiques (pH 7.4 et force saline de 150 mM). Les propriétés lubrifiantes de nos mimes synoviaux seront évaluées à l'aide du SFA (voir Annexe 1). Nos mimes seront également étudiés en association avec l'Acide Hyaluronique (HA) afin de développer un traitement de viscosupplémentation (administration de HA) combiné à un traitement de "tribosupplémentation" (administration des écouvillons moléculaires), HA et macromolécules lubrifiantes, LUB et AGG, agissant de manière synergique au niveau des articulations.

(ii) *Développer un support poroélastique structuré à base d'hydrogel et déterminer ses propriétés mécaniques, physiques et tribologiques*

Nous allons nous intéresser à comprendre comment la structure des hydrogels influence leurs propriétés mécaniques, physiques et tribologiques. Les aspects tribologiques seront notamment étudiés en utilisant un tribomètre faible charge spécialement conçu pour l'étude au sein du LTDS (École Centrale Lyon, France) (voir Annexe 1). Le choix du chitosane comme matériaux pour nos hydrogels est dû à ses propriétés biomédicales prometteuses en ingénierie tissulaire[41, 250, 253-260] et plus particulièrement en réparation du cartilage[245, 249, 261-263].

(iii) *Améliorer les propriétés de friction **et** de résistance à l'usure du substitut de cartilage par l'ajout du fluide synovial bioinspiré*

Les propriétés tribologiques des substrats hydrogels complètement caractérisés seront étudiées en combinaison avec nos fluides lubrifiants synthétiques. Une étude systématique réalisée à l'aide d'un tribomètre faible charge et d'un interféromètre en distinguant friction et usure. Ceci nous permettra de déterminer la meilleure combinaison pour le développement d'un substitut polymérique articulaire bioinspiré.

Structure de la thèse

En aval de ce chapitre I introductif, ce manuscrit de thèse est composé de trois chapitres de résultats et discussion, d'un chapitre de discussions générales et d'un chapitre de conclusions et perspectives. Les différents chapitres de résultats et discussion seront présentés sous forme de 4 articles publiés et 1 article soumis et permettront de répondre aux objectifs spécifiques listés plus haut. Le chapitre de discussions générales permettra de faire une comparaison de nos résultats avec la littérature. Enfin, des notes complémentaires traitant des techniques expérimentales et des caractérisations *in vitro* et *in vivo* des fluides lubrifiants sont présentées en annexe.

Le chapitre II traite du premier objectif de cette thèse, à savoir la conception d'une librairie de mimes polymériques de l'aggrécane et de la lubricine ainsi que leurs caractérisations, notamment tribologique et conformationnelle, à l'échelle moléculaire à l'aide du SFA. Ce chapitre II est divisé en 3 parties.

La première partie concerne l'étude tribologique d'un écouvillon moléculaire contrôle ne possédant pas de groupement d'ancrage en combinaison ou non avec un élément clé du liquide synovial, l'acide hyaluronique, couramment utilisé en traitement intra-articulaire de viscosupplémentation. Cette étude a fait l'objet d'une publication : Faivre, J., Shrestha, B. R., Burdynska, J., Xie, G., Moldovan, F., Delair, T., Benayoun, S., David, L., Matyjasewski, K. & Banquy, X. (2017). **Wear protection without surface modification using a synergistic mixture of molecular brushes and linear polymers**. *ACS nano*, *11*(2), 1762-1769.

Dans la seconde partie, nous avons étudié les aspects conformationnels du mime polymérique contrôle aux interfaces dans un milieu tamponné à différentes salinités. Nous avons également évalué l'effet de son vieillissement à différentes températures de stockage sur ses propriétés tribologiques. Cette étude a fait l'objet d'une publication : Faivre, J., Shrestha, B. R., Xie, G., Delair, T., David, L., Matyjaszewski, K., & Banquy, X. (2017). **Unraveling the Correlations between Conformation, Lubrication, and Chemical Stability of Bottlebrush Polymers at Interfaces**. *Biomacromolecules*, *18*(12), 4002-4010.

Dans la troisième partie, nous nous sommes intéressés à l'influence de l'architecture des écouvillons moléculaires et notamment de l'influence des groupements d'ancrage sur les paramètres tribologiques de ces polymères. Cette étude a fait l'objet d'une publication : Faivre, J., Shrestha, B. R., Xie, G., Olszewski, M., Adibnia, V., Moldovan, F., Montembault, A., Sudre, G., Delair, T., David, L., Matyjasewski, K. & Banquy, X. (2018) **Intermolecular**

Interactions between Bottlebrush Polymers Boost the Protection of Surfaces against Frictional Wear. *Chemistry of Materials***,** 30(12), 4140-4149.

Le chapitre III s'intéresse à la formulation d'un support poroélastique à base d'hydrogel de structure multicouche permettant de mimer les caractéristiques essentielles du cartilage afin de comprendre l'effet de l'architecture de l'hydrogel sur ses propriétés mécaniques et, de manière originale, sur ses propriétés tribologiques. Cette étude a fait l'objet d'une publication : Faivre, J., Sudre, G., Montembault, A., Benayoun, S., Banquy, X., Delair, T., & David, L. (2018). **Bioinspired microstructures of chitosan hydrogel provide enhanced wear protection**. *Soft Matter*, *14*(11), 2068-2076.

Le chapitre IV s'intéresse à l'amélioration des performances tribologiques des hydrogels par l'ajout un fluide synovial bioinspiré. Cette étude fait l'objet d'une publication : Faivre, J., Montembault, A., Sudre, G., Shrestha, B. R., Matyjaszewski, K., Benayoun, S., Banquy, X., Delair, T., & David, L. (2018). **Lubrication and Wear Protection at Micro-Structured Hydrogels using Bioinspired Fluids**. *Biomacromolecules* (DOI : 10.1021/acs.biomac.8b01311)

Le chapitre V constitue une discussion générale du travail effectué lors de cette thèse. Nos résultats sont discutés, critiqués et comparés à l'état de l'art afin de positionner notre travail vis-à-vis des autres groupes de recherche.

Finalement, le chapitre VI est un chapitre de conclusion. Les perspectives et les applications envisageables pour nos matériaux bio-inspirés sont également exposées.

Deux annexes sont également proposées à la fin de ce manuscrit. La première annexe décrit les deux techniques expérimentales principalement utilisées dans cette thèse, à savoir le SFA et le tribomètre faible charge. La seconde annexe aborde les études *in vitro* et *in vivo* préliminaires qui sont en cours de finalisation.

Références

1. Silberberg, A., Biolubrication. In *Tribology Series*, Georges, J. M., Ed. Elsevier: 1981; Vol. 7, pp 797-809.
2. Kubíček, M.; Florian, Z., Stress strain analysis of knee joint. *Engineering mechanics* **2009,** *16* (5), 315-322.
3. Vornehm, S. I.; Dudhia, J.; von der Mark, K.; Aigner, T., Expression of collagen types IX and XI and other major cartilage matrix components by human fetal chondrocytes in vivo. *Matrix Biology* **1996,** *15* (2), 91-98.
4. Eyre, D., Articular cartilage and changes in Arthritis: Collagen of articular cartilage. *Arthritis Res.* **2002,** *4* (1), 30-35.
5. Furey, M. J.; Burkhardt, B. M., Biotribology: Friction, wear, and lubrication of natural synovial joints. *Lubr. Sci.* **1997,** *9* (3), 255-271.
6. Jahn, S.; Seror, J.; Klein, J., Lubrication of Articular Cartilage. *Annu. Rev. Biomed. Eng.* **2016,** *18* (1), 235-258.
7. Arden, N.; Nevitt, M. C., Osteoarthritis: Epidemiology. *Best Practice & Research Clinical Rheumatology* **2006,** *20* (1), 3-25.
8. Anandacoomarasamy, A.; March, L., Current evidence for osteoarthritis treatments. *Ther. Adv. Musculoskelet. Dis.* **2010,** *2* (1), 17-28.
9. Ammar, T. Y.; Pereira, T. A. P.; Mistura, S. L. L.; Kuhn, A.; Saggin, J. I.; Lopes Júnior, O. V., Viscosupplementation for treating knee osteoarthrosis: review of the literature. *Revista Brasileira de Ortopedia* **2015,** *50* (5), 489-494.
10. Pimentel, R.; Fontes, C.; Àvila, S.; Rios, J.; Magdiel, A.; Fragoso, C.; Cerqueira, I.; Massolino, C. In *Human Factors in Prosthesis of Total Knee Arthroplasty*, Cham, Springer International Publishing: Cham, 2018; pp 508-518.
11. Bayliss, L. E.; Culliford, D.; Monk, A. P.; Glyn-Jones, S.; Prieto-Alhambra, D.; Judge, A.; Cooper, C.; Carr, A. J.; Arden, N. K.; Beard, D. J.; Price, A. J., The effect of patient age at intervention on risk of implant revision after total replacement of the hip or knee: a population-based cohort study. *The Lancet* **2017,** *389* (10077), 1424-1430.
12. Naleway, S. E.; Porter, M. M.; McKittrick, J.; Meyers, M. A., Structural Design Elements in Biological Materials: Application to Bioinspiration. *Adv. Mater.* **2015,** *27* (37), 5455-5476.
13. Benyus, J. M., Biomimicry: Innovation inspired by nature. Morrow New York: 1997.
14. Bronzino, J. D.; Schneck, D. J., *Biomechanics: principles and applications*. CRC press: 2002.
15. Bartenev, G. M.; Lavrentev, V. V.; Payne, D. B.; Lee, L.-H.; Ludema, K. C., Chapter 6 Wear of Polymers. In *Tribology Series*, Bartenev, G. M.; Lavrentev, V. V.; Payne, D. B.; Lee, L.-H.; Ludema, K. C., Eds. Elsevier: 1981; Vol. 6, pp 202-260.
16. Greene, G. W.; Lee, D. W.; Yu, J.; Das, S.; Banquy, X.; Israelachvili, J. N., Lubrication and Wear Protection of Natural (Bio)Systems. In *Polymer Adhesion, Friction, and Lubrication*, John Wiley & Sons, Inc.: 2013; pp 83-133.
17. Authimoolam, S.; Dziubla, T., Biopolymeric Mucin and Synthetic Polymer Analogs: Their Structure, Function and Role in Biomedical Applications. *Polymers* **2016,** *8* (3), 71.
18. Ruoslahti, E., Structure and Biology of Proteoglycans. *Annu. Rev. Cell Biol.* **1988,** *4* (1), 229-255.
19. Klein, J., Hydration lubrication. *Friction* **2013,** *1* (1), 1-23.
20. Jahn, S.; Klein, J., Hydration Lubrication: The Macromolecular Domain. *Macromolecules* **2015,** *48* (15), 5059-5075.
21. Ma, L.; Gaisinskaya-Kipnis, A.; Kampf, N.; Klein, J., Origins of hydration lubrication. *Nature Communications* **2015,** *6*, 6060.
22. Lai, J. H.; del Alamo, J. C.; Rodríguez-Rodríguez, J.; Lasheras, J. C., The mechanics of the adhesive locomotion of terrestrial gastropods. *The Journal of Experimental Biology* **2010,** *213* (22), 3920-3933.
23. Kobayashi, A.; Yamamoto, I.; Aoyama, T., Tribology of a snail (terrestrial gastropod). In *Tribology Series*, Dowson, D.; Priest, M.; Dalmaz, G.; Lubrecht, A. A., Eds. Elsevier: 2003; Vol. 41, pp 429-436.

24. Ewoldt, R. H.; Clasen, C.; Hosoi, A. E.; McKinley, G. H., Rheological fingerprinting of gastropod pedal mucus and synthetic complex fluids for biomimicking adhesive locomotion. *Soft Matter* **2007,** *3* (5), 634-643.
25. Zhang, D.; Chen, Y.; Ma, Y.; Guo, L.; Sun, J.; Tong, J., Earthworm epidermal mucus: Rheological behavior reveals drag-reducing characteristics in soil. *Soil and Tillage Research* **2016,** *158* (Supplement C), 57-66.
26. Li, J.; Liu, Y.; Luo, J.; Liu, P.; Zhang, C., Excellent lubricating behavior of Brasenia schreberi mucilage. *Langmuir* **2012,** *28* (20), 7797-802.
27. Liu, P.; Liu, Y.; Yang, Y.; Chen, Z.; Li, J.; Luo, J., Mechanism of Biological Liquid Superlubricity of Brasenia schreberi Mucilage. *Langmuir* **2014,** *30* (13), 3811-3816.
28. Oh, J. K.; Behmer, S. T.; Marquess, R.; Yegin, C.; Scholar, E. A.; Akbulut, M., Structural, tribological, and mechanical properties of the hind leg joint of a jumping insect: Using katydids to inform bioinspired lubrication systems. *Acta Biomater.* **2017,** *62*, 284-292.
29. Oeffner, J.; Lauder, G. V., The hydrodynamic function of shark skin and two biomimetic applications. *The Journal of Experimental Biology* **2012,** *215* (5), 785-795.
30. Zhang, D.-y.; Luo, Y.-h.; Li, X.; Chen, H.-w., Numerical simulation and experimental study of drag-reducing surface of a real shark skin. *Journal of Hydrodynamics, Ser. B* **2011,** *23* (2), 204-211.
31. Nazanin, M.; Vitaliy, S. R.; Michael, N., Biomimetic approaches for green tribology: from the lotus effect to blood flow control. *Surface Topography: Metrology and Properties* **2015,** *3* (3), 034001.
32. Corfield, A. P., Mucins: A biologically relevant glycan barrier in mucosal protection. *Biochimica et Biophysica Acta (BBA) - General Subjects* **2015,** *1850* (1), 236-252.
33. Sophia Fox, A. J.; Bedi, A.; Rodeo, S. A., The Basic Science of Articular Cartilage: Structure, Composition, and Function. *Sports Health* **2009,** *1* (6), 461-468.
34. Pult, H.; Tosatti, S. G. P.; Spencer, N. D.; Asfour, J.-M.; Ebenhoch, M.; Murphy, P. J., Spontaneous Blinking from a Tribological Viewpoint. *The Ocular Surface* **2015,** *13* (3), 236-249.
35. Button, B.; Cai, L.-H.; Ehre, C.; Kesimer, M.; Hill, D. B.; Sheehan, J. K.; Boucher, R. C.; Rubinstein, M., A Periciliary Brush Promotes the Lung Health by Separating the Mucus Layer from Airway Epithelia. *Science* **2012,** *337* (6097), 937-941.
36. Tabak, L. A., Structure and function of human salivary mucins. *Crit. Rev. Oral Biol. Med.* **1990,** *1* (4), 229-34.
37. Frenkel, E. S.; Ribbeck, K., Salivary mucins in host defense and disease prevention. *J. Oral Microbiol.* **2015,** *7* (1), 29759.
38. Kim, Y. S.; Ho, S. B., Intestinal Goblet Cells and Mucins in Health and Disease: Recent Insights and Progress. *Current Gastroenterology Reports* **2010,** *12* (5), 319-330.
39. Parsons, C. L.; Shrom, S. H.; Hanno, P. M.; Mulholland, S. G., Bladder surface mucin. Examination of possible mechanisms for its antibacterial effect. *Invest. Urol.* **1978,** *16* (3), 196-200.
40. Brockhausen, I.; Schutzbach, J.; Kuhns, W., Glycoproteins and Their Relationship to Human Disease. *Cells Tissues Organs* **1998,** *161* (1-4), 36-78.
41. Kootala, S.; Filho, L.; Srivastava, V.; Linderberg, V.; Moussa, A.; David, L.; Trombotto, S.; Crouzier, T., Reinforcing Mucus Barrier Properties with Low Molar Mass Chitosans. *Biomacromolecules* **2018,** *19* (3), 872-882.
42. Hong-Bin, Y.; Jin, G.; Li-Bo, M.; You-Xian, Y.; Shu-Hong, Y., 25th Anniversary Article: Artificial Carbonate Nanocrystals and Layered Structural Nanocomposites Inspired by Nacre: Synthesis, Fabrication and Applications. *Advanced Materials* **2014,** *26* (1), 163-188.
43. Currey, J., Sacrificial bonds heal bone. *Nature* **2001,** *414*, 699.
44. Fantner, G. E.; Hassenkam, T.; Kindt, J. H.; Weaver, J. C.; Birkedal, H.; Pechenik, L.; Cutroni, J. A.; Cidade, G. A. G.; Stucky, G. D.; Morse, D. E.; Hansma, P. K., Sacrificial bonds and hidden length dissipate energy as mineralized fibrils separate during bone fracture. *Nat Mater* **2005,** *4* (8), 612-616.
45. Thompson, J. B.; Kindt, J. H.; Drake, B.; Hansma, H. G.; Morse, D. E.; Hansma, P. K., Bone indentation recovery time correlates with bond reforming time. *Nature* **2001,** *414*, 773.
46. Amini, S.; Miserez, A., Wear and abrasion resistance selection maps of biological materials. *Acta Biomaterialia* **2013,** *9* (8), 7895-7907.
47. Dedinaite, A., Biomimetic lubrication. *Soft Matter* **2012,** *8* (2), 273-284.

48. Liu, C.; Wang, M.; An, J.; Thormann, E.; Dedinaite, A., Hyaluronan and phospholipids in boundary lubrication. *Soft Matter* **2012,** *8* (40), 10241-10244.
49. Seror, J.; Sorkin, R.; Klein, J., Boundary lubrication by macromolecular layers and its relevance to synovial joints. *Polymers for Advanced Technologies* **2014,** *25* (5), 468-477.
50. Majd, S. E.; Kuijer, R.; Kowitsch, A.; Groth, T.; Schmidt, T. A.; Sharma, P. K., Both Hyaluronan and Collagen Type II Keep Proteoglycan 4 (Lubricin) at the Cartilage Surface in a Condition That Provides Low Friction during Boundary Lubrication. *Langmuir* **2014**, 14566-14572.
51. Pawlak, Z.; Urbaniak, W.; Hagner-Derengowska, M.; Hagner, W., The Probable Explanation for the Low Friction of Natural Joints. *Cell biochemistry and biophysics* **2014**.
52. Dedinaite, A.; Claesson, P. M., Synergies in lubrication. *PCCP* **2017**.
53. Jeffery, A. K.; Blunn, G. W.; Archer, C. W.; Bentley, G., Three-dimensional collagen architecture in bovine articular cartilage. *The Journal of bone and joint surgery. British volume* **1991,** *73* (5), 795-801.
54. Balazs, E. A., The role of hyaluronan in the structure and function of the biomatrix of connective tissues. *Struct. Chem.* **2009,** *20* (2), 233-243.
55. Eggli, P. S.; Herrmann, W.; Hunziker, E. B.; Schenk, R. K., Matrix compartments in the growth plate of the proximal tibia of rats. *Anat. Rec.* **1985,** *211* (3), 246-57.
56. Sobol, E. N.; Baum, O. I.; Shekhter, A. B.; Guller, A.; Baskov, A. V. In *Laser-induced regeneration of cartilage*, SPIE: 2011; p 12.
57. Skioldebrand, E.; Lorenzo, P.; Zunino, L.; Rucklidge, G. J.; Sandgren, B.; Carlsten, J.; Ekman, S., Concentration of collagen, aggrecan and cartilage oligomeric matrix protein (COMP) in synovial fluid from equine middle carpal joints. *Equine Vet. J.* **2001,** *33* (4), 394-402.
58. Lee, H.-Y.; Han, L.; Roughley, P. J.; Grodzinsky, A. J.; Ortiz, C., Age-related nanostructural and nanomechanical changes of individual human cartilage aggrecan monomers and their glycosaminoglycan side chains. *J. Struct. Biol.* **2013,** *181* (3), 264-273.
59. Hughes, L. C.; Archer, C. W.; ap Gwynn, I., The ultrastructure of mouse articular cartilage: collagen orientation and implications for tissue functionality. A polarised light and scanning electron microscope study and review. *European cells & materials* **2005,** *9*, 68-84.
60. ap Gwynn, I.; Wade, S.; Kaab, M. J.; Owen, G. R.; Richards, R. G., Freeze-substitution of rabbit tibial articular cartilage reveals that radial zone collagen fibres are tubules. *J. Microsc.* **2000,** *197* (Pt 2), 159-72.
61. Schmidt, T. A.; Gastelum, N. S.; Nguyen, Q. T.; Schumacher, B. L.; Sah, R. L., Boundary lubrication of articular cartilage: Role of synovial fluid constituents. *Arthritis & Rheumatism* **2007,** *56* (3), 882-891.
62. Jay, G. D.; Waller, K. A., The biology of Lubricin: Near frictionless joint motion. *Matrix Biol.* **2014,** *39*, 17-24.
63. Zappone, B.; Greene, G. W.; Oroudjev, E.; Jay, G. D.; Israelachvili, J. N., Molecular Aspects of Boundary Lubrication by Human Lubricin: Effect of Disulfide Bonds and Enzymatic Digestion. *Langmuir* **2008,** *24* (4), 1495-1508.
64. Jay, G. D.; Torres, J. R.; Warman, M. L.; Laderer, M. C.; Breuer, K. S., The role of lubricin in the mechanical behavior of synovial fluid. *Proc. Natl. Acad. Sci. U.S.A* **2007,** *104* (15), 6194-6199.
65. Estrella, R. P.; Whitelock, J. M.; Packer, N. H.; Karlsson, N. G., The glycosylation of human synovial lubricin: implications for its role in inflammation. *Biochem. J* **2010,** *429* (2), 359-67.
66. Jay, G. D.; Lane, B. P.; Sokoloff, L., Characterization of a bovine synovial fluid lubricating factor. III. The interaction with hyaluronic acid. *Connect. Tissue Res.* **1992,** *28* (4), 245-55.
67. Schwarz, I. M.; Hills, B. A., Surface-active phospholipid as the lubricating component of lubricin. *Rheumatology* **1998,** *37* (1), 21-26.
68. Elsaid, K. A.; Zhang, L.; Waller, K.; Tofte, J.; Teeple, E.; Fleming, B. C.; Jay, G. D., The impact of forced joint exercise on lubricin biosynthesis from articular cartilage following ACL transection and intra-articular lubricin's effect in exercised joints following ACL transection. *Osteoarthritis and cartilage / OARS, Osteoarthritis Research Society* **2012,** *20* (8), 940-8.
69. Teeple, E.; Elsaid, K. A.; Jay, G. D.; Zhang, L.; Badger, G. J.; Akelman, M.; Bliss, T. F.; Fleming, B. C., Effects of supplemental intra-articular lubricin and hyaluronic acid on the progression of posttraumatic arthritis in the anterior cruciate ligament-deficient rat knee. *Am. J. Sports Med.* **2011,** *39* (1), 164-72.

70. Rhee, D. K.; Marcelino, J.; Baker, M.; Gong, Y.; Smits, P.; Lefebvre, V.; Jay, G. D.; Stewart, M.; Wang, H.; Warman, M. L.; Carpten, J. D., The secreted glycoprotein lubricin protects cartilage surfaces and inhibits synovial cell overgrowth. *J. Clin. Invest.* **2005,** *115* (3), 622-31.
71. Sarma, A. V.; Powell, G. L.; LaBerge, M., Phospholipid composition of articular cartilage boundary lubricant. *J. Orthop. Res.* **2001,** *19* (4), 671-6.
72. Kawano, T.; Miura, H.; Mawatari, T.; Moro-Oka, T.; Nakanishi, Y.; Higaki, H.; Iwamoto, Y., Mechanical effects of the intraarticular administration of high molecular weight hyaluronic acid plus phospholipid on synovial joint lubrication and prevention of articular cartilage degeneration in experimental osteoarthritis. *Arthritis and rheumatism* **2003,** *48* (7), 1923-9.
73. Hills, B. A., Identity of the joint lubricant. *The Journal of rheumatology* **2002,** *29* (1), 200-1.
74. Katta, J.; Jin, Z.; Ingham, E.; Fisher, J., Biotribology of articular cartilage—A review of the recent advances. *Medical Engineering & Physics* **2008,** *30* (10), 1349-1363.
75. Forster, H.; Fisher, J., The Influence of Loading Time and Lubricant on the Friction of Articular Cartilage. *Proc. Inst. Mech. Eng., Part H* **1996,** *210* (2), 109-119.
76. Brand, R. A., Joint contact stress: a reasonable surrogate for biological processes? *Iowa Orthop. J.* **2005,** *25*, 82-94.
77. McNary, S. M.; Athanasiou, K. A.; Reddi, A. H., Engineering lubrication in articular cartilage. *Tissue Eng Part B Rev* **2012,** *18* (2), 88-100.
78. Dowson, D., Elastohydrodynamic and micro-elastohydrodynamic lubrication. *Wear* **1995,** *190* (2), 125-138.
79. Das, S.; Banquy, X.; Zappone, B.; Greene, G. W.; Jay, G. D.; Israelachvili, J. N., Synergistic interactions between grafted hyaluronic acid and lubricin provide enhanced wear protection and lubrication. *Biomacromolecules* **2013,** *14* (5), 1669-1677.
80. Lee, D. W.; Banquy, X.; Israelachvili, J. N., Stick-slip friction and wear of articular joints. *Proceedings of the National Academy of Sciences* **2013,** *110* (7), E567-E574.
81. Raviv, U.; Giasson, S.; Kampf, N.; Gohy, J.-F.; Jerome, R.; Klein, J., Lubrication by charged polymers. *Nature* **2003,** *425* (6954), 163-165.
82. McCutchen, C. W., Mechanism of Animal Joints: Sponge-hydrostatic and Weeping Bearings. *Nature* **1959,** *184*, 1284.
83. Chen, M.; Briscoe, W. H.; Armes, S. P.; Klein, J., Lubrication at Physiological Pressures by Polyzwitterionic Brushes. *Science* **2009,** *323* (5922), 1698-1701.
84. Chen, M.; Briscoe, W. H.; Armes, S. P.; Cohen, H.; Klein, J., Polyzwitterionic brushes: Extreme lubrication by design. *European Polymer Journal* **2011,** *47* (4), 511-523.
85. Walker, P. S.; Dowson, D.; Longfield, M. D.; Wright, V., "Boosted lubrication" in synovial joints by fluid entrapment and enrichment. *Ann. Rheum. Dis.* **1968,** *27* (6), 512-20.
86. Mocny, P.; Klok, H.-A., Tribology of surface-grafted polymer brushes. *Molecular Systems Design & Engineering* **2016,** *1* (2), 141-154.
87. McGuiggan, P. M.; Zhang, J.; Hsu, S. M., Comparison of friction measurements using the atomic force microscope and the surface forces apparatus: the issue of scale. *Tribol Lett* **2001,** *10* (4), 217-223.
88. Hartung, W.; Drobek, T.; Lee, S.; Zürcher, S.; Spencer, N. D., The Influence of Anchoring-Group Structure on the Lubricating Properties of Brush-Forming Graft Copolymers in an Aqueous Medium. *Tribol Lett* **2008,** *31* (2), 119-128.
89. Dunn, A. C.; Sawyer, W. G.; Angelini, T. E., Gemini Interfaces in Aqueous Lubrication with Hydrogels. *Tribol Lett* **2014,** *54* (1), 59-66.
90. Tadmor, R.; Chen, N.; Israelachvili, J. N., Thin film rheology and lubricity of hyaluronic acid solutions at a normal physiological concentration. *Journal of biomedical materials research* **2002,** *61* (4), 514-23.
91. Kwiecinski, J. J.; Dorosz, S. G.; Ludwig, T. E.; Abubacker, S.; Cowman, M. K.; Schmidt, T. A., The effect of molecular weight on hyaluronan's cartilage boundary lubricating ability – alone and in combination with proteoglycan 4. *Osteoarthritis and Cartilage* **2011,** *19* (11), 1356-1362.
92. Yarimitsu, S.; Sasaki, S.; Murakami, T.; Suzuki, A., Evaluation of lubrication properties of hydrogel artificial cartilage materials for joint prosthesis. *Biosurface and Biotribology* **2016,** *2* (1), 40-47.

93. Murakami, T.; Yarimitsu, S.; Sakai, N.; Nakashima, K.; Yamaguchi, T.; Sawae, Y.; Suzuki, A., Superior lubrication mechanism in poly(vinyl alcohol) hybrid gel as artificial cartilage. *Proceedings of the Institution of Mechanical Engineers, Part J: Journal of Engineering Tribology* **2017**, 1350650117712881.
94. Bavaresco, V. P.; Zavaglia, C. A. C.; Malmonge, S. M.; Reis, M. C., Viability of pHEMA Hydrogels as Coating in Human Synovial Joint Prosthesis. *Materials Research* **2002,** *5*, 481-484.
95. Faivre, J.; Sudre, G.; Montembault, A.; Benayoun, S.; Banquy, X.; Delair, T.; David, L., Bioinspired Microstructures of Chitosan Hydrogel Provide Enhanced Wear Protection. *Soft Matter* **2018**, 2068-2076.
96. Cao, Y.; Xiong, D.; Wang, K.; Niu, Y., Semi-degradable porous poly (vinyl alcohol) hydrogel scaffold for cartilage repair: Evaluation of the initial and cell-cultured tribological properties. *J. Mech. Behav. Biomed. Mater.* **2017,** *68*, 163-172.
97. Ozturk, H. E.; Stoffel, K. K.; Jones, C. F.; Stachowiak, G. W., The Effect of Surface-Active Phospholipids on the Lubrication of Osteoarthritic Sheep Knee Joints: Friction. *Tribol Lett* **2004,** *16* (4), 283-289.
98. Zhang, R.; Lin, P.; Yang, W.; Cai, M.; Yu, B.; Zhou, F., Simultaneous superior lubrication and high load bearing by the dynamic weak interaction of a lubricant with mechanically strong bilayer porous hydrogels. *Polymer Chemistry* **2017,** *8* (46), 7102-7107.
99. Lin, P.; Zhang, R.; Wang, X.; Cai, M.; Yang, J.; Yu, B.; Zhou, F., Articular Cartilage Inspired Bilayer Tough Hydrogel Prepared by Interfacial Modulated Polymerization Showing Excellent Combination of High Load-Bearing and Low Friction Performance. *ACS Macro Lett.* **2016,** *5* (11), 1191-1195.
100. Gourdon, D.; Lin, Q.; Oroudjev, E.; Hansma, H.; Golan, Y.; Arad, S.; Israelachvili, J., Adhesion and Stable Low Friction Provided by a Subnanometer-Thick Monolayer of a Natural Polysaccharide. *Langmuir* **2008,** *24* (4), 1534-1540.
101. Faivre, J.; Shrestha, B. R.; Burdynska, J.; Xie, G.; Moldovan, F.; Delair, T.; Benayoun, S.; David, L.; Matyjaszewski, K.; Banquy, X., Wear Protection without Surface Modification Using a Synergistic Mixture of Molecular Brushes and Linear Polymers. *ACS Nano* **2017,** *11* (2), 1762-1769.
102. Faivre, J.; Shrestha, B. R.; Xie, G.; Delair, T.; David, L.; Matyjaszewski, K.; Banquy, X., Unraveling the Correlations between Conformation, Lubrication, and Chemical Stability of Bottlebrush Polymers at Interfaces. *Biomacromolecules* **2017**, 4002-4010.
103. Lee, D. W.; Banquy, X.; Das, S.; Cadirov, N.; Jay, G.; Israelachvili, J., Effects of molecular weight of grafted hyaluronic acid on wear initiation. *Acta Biomater.* **2014,** *10* (5), 1817-1823.
104. Drobek, T.; Spencer, N. D., Nanotribology of Surface-Grafted PEG Layers in an Aqueous Environment. *Langmuir* **2008,** *24* (4), 1484-1488.
105. Bavaresco, V. P.; Zavaglia, C. A. C.; Reis, M. C.; Gomes, J. R., Study on the tribological properties of pHEMA hydrogels for use in artificial articular cartilage. *Wear* **2008,** *265* (3), 269-277.
106. Moro, T.; Kawaguchi, H.; Ishihara, K.; Kyomoto, M.; Karita, T.; Ito, H.; Nakamura, K.; Takatori, Y., Wear resistance of artificial hip joints with poly(2-methacryloyloxyethyl phosphorylcholine) grafted polyethylene: Comparisons with the effect of polyethylene cross-linking and ceramic femoral heads. *Biomaterials* **2009,** *30* (16), 2995-3001.
107. Kyomoto, M.; Moro, T.; Takatori, Y.; Kawaguchi, H.; Ishihara, K., Cartilage-mimicking, High-density Brush Structure Improves Wear Resistance of Crosslinked Polyethylene: A Pilot Study. *Clinical Orthopaedics and Related Research* **2011,** *469* (8), 2327-2336.
108. Suciu, A. N.; Iwatsubo, T.; Matsuda, M.; Nishino, T., A Study upon Durability of the Artificial Knee Joint with PVA Hydrogel Cartilage. *JSME International Journal Series C Mechanical Systems, Machine Elements and Manufacturing* **2004,** *47* (1), 199-208.
109. Katta, J. K.; Marcolongo, M.; Lowman, A.; Mansmann, K. A., Friction and wear behavior of poly(vinyl alcohol)/poly(vinyl pyrrolidone) hydrogels for articular cartilage replacement. *Journal of Biomedical Materials Research Part A* **2007,** *83A* (2), 471-479.
110. Baykal, D.; Day, J. S.; Jaekel, D. J.; Katta, J.; Mansmann, K.; Kurtz, S. M., Tribological evaluation of hydrogel articulations for joint arthroplasty applications. *J. Mech. Behav. Biomed. Mater.* **2012,** *14*, 39-47.
111. Meng, Y.; Ye, L.; Coates, P.; Twigg, P., In Situ Cross-Linking of Poly(vinyl alcohol)/Graphene Oxide–Polyethylene Glycol Nanocomposite Hydrogels as Artificial Cartilage

Replacement: Intercalation Structure, Unconfined Compressive Behavior, and Biotribological Behaviors. *The Journal of Physical Chemistry C* **2018**.
112. Shi, Y.; Xiong, D.; Li, J.; Wang, N., The water-locking and cross-linking effects of graphene oxide on the load-bearing capacity of poly(vinyl alcohol) hydrogel. *RSC Advances* **2016,** *6* (86), 82467-82477.
113. Yasuda, K.; Ping Gong, J.; Katsuyama, Y.; Nakayama, A.; Tanabe, Y.; Kondo, E.; Ueno, M.; Osada, Y., Biomechanical properties of high-toughness double network hydrogels. *Biomaterials* **2005,** *26* (21), 4468-4475.
114. Freeman, M. E.; Furey, M. J.; Love, B. J.; Hampton, J. M., Friction, wear, and lubrication of hydrogels as synthetic articular cartilage. *Wear* **2000,** *241* (2), 129-135.
115. Kanca, Y.; Milner, P.; Dini, D.; Amis, A. A., Tribological properties of PVA/PVP blend hydrogels against articular cartilage. *J. Mech. Behav. Biomed. Mater.* **2018,** *78*, 36-45.
116. Park, D. Y.; Min, B. H.; Kim, D. W.; Song, B. R.; Kim, M.; Kim, Y. J., Polyethylene wear particles play a role in development of osteoarthritis via detrimental effects on cartilage, meniscus, and synovium. *Osteoarthritis and Cartilage* **2013,** *21* (12), 2021-2029.
117. Wu, Y. T.; Zhu, L. S.; Tam, K. P. C.; Evans, D. J.; Fleiszig, S. M. J., Pseudomonas aeruginosa Survival at Posterior Contact Lens Surfaces after Daily Wear. *Optometry and vision science : official publication of the American Academy of Optometry* **2015,** *92* (6), 659-664.
118. McGann, M. E.; Bonitsky, C. M.; Jackson, M. L.; Ovaert, T. C.; Trippel, S. B.; Wagner, D. R., Genipin crosslinking of cartilage enhances resistance to biochemical degradation and mechanical wear. *J. Orthop. Res.* **2015,** *33* (11), 1571-1579.
119. Lopes, J. L.; Machado, J. M.; Castanheira, L.; Granja, P. L.; Gama, F. M.; Dourado, F.; Gomes, J. R., Friction and wear behaviour of bacterial cellulose against articular cartilage. *Wear* **2011,** *271* (9), 2328-2333.
120. Thonar, E. J.; Lenz, M. E.; Klintworth, G. K.; Caterson, B.; Pachman, L. M.; Glickman, P.; Katz, R.; Huff, J.; Kuettner, K. E., Quantification of keratan sulfate in blood as a marker of cartilage catabolism. *Arthritis and rheumatism* **1985,** *28* (12), 1367-76.
121. Bartels, E. M.; Christensen, R.; Christensen, P.; Henriksen, M.; Bennett, A.; Gudbergsen, H.; Boesen, M.; Bliddal, H., Effect of a 16 weeks weight loss program on osteoarthritis biomarkers in obese patients with knee osteoarthritis: a prospective cohort study. *Osteoarthritis and Cartilage* **2014,** *22* (11), 1817-1825.
122. Morgese, G.; Cavalli, E.; Rosenboom, J.-G.; Zenobi-Wong, M.; Benetti, E. M., Cyclic Polymer Grafts That Lubricate and Protect Damaged Cartilage. *Angewandte Chemie International Edition* **2017**, n/a-n/a.
123. Bayer, I., Advances in Tribology of Lubricin and Lubricin-Like Synthetic Polymer Nanostructures. *Lubricants* **2018,** *6* (2), 30.
124. Yang, W.; Zhou, F., Polymer brushes for antibiofouling and lubrication. *Biosurface and Biotribology* **2017**.
125. Samaroo, K. J.; Tan, M.; Putnam, D.; Bonassar, L. J., Binding and lubrication of biomimetic boundary lubricants on articular cartilage. *J. Orthop. Res.* **2017,** *35* (3), 548-557.
126. Dedinaite, A.; Claesson, P. M., Synergies in lubrication. *PCCP* **2017,** *19* (35), 23677-23689.
127. Milner, P. E.; Parkes, M.; Puetzer, J. L.; Chapman, R.; Stevens, M. M.; Cann, P.; Jeffers, J. R. T., A low friction, biphasic and boundary lubricating hydrogel for cartilage replacement. *Acta Biomaterialia* **2018,** *65*, 102-111.
128. Seror, J.; Zhu, L.; Goldberg, R.; Day, A. J.; Klein, J., Supramolecular synergy in the boundary lubrication of synovial joints. *Nat. Commun.* **2015,** *6*, 6497.
129. Lindenhayn, K.; Heilmann, H.-H.; Niederhausen, T.; Walther, H.-U.; Pohlenz, K., Elimination of Tritium-Labelled Hyaluronic Acid from Normal and Osteoarthritic Rabbit Knee Joints. In *Clin. Chem. Lab. Med.*, 1997; Vol. 35, p 355.
130. Wobig, M.; Bach, G.; Beks, P.; Dickhut, A.; Runzheimer, J.; Schwieger, G.; Vetter, G.; Balazs, E., The role of elastoviscosity in the efficacy of viscosupplementation for osteoarthritis of the knee: A comparison of Hylan G-F 20 and a lower-molecular-weight hyaluronan. *Clinical Therapeutics 21* (9), 1549-1562.
131. Bailleul, F., Regimens for intra-articular viscosupplementation. Google Patents: 2011.

132. Tadmor, R.; Chen, N.; Israelachvili, J., Normal and Shear Forces between Mica and Model Membrane Surfaces with Adsorbed Hyaluronan. *Macromolecules* **2003,** *36* (25), 9519-9526.
133. Balazs, E. A.; Watson, D.; Duff, I. F.; Roseman, S., Hyaluronic acid in synovial fluid. I. Molecular parameters of hyaluronic acid in normal and arthritic human fluids. *Arthritis & Rheumatism* **1967,** *10* (4), 357-376.
134. Bonnevie, E. D.; Galesso, D.; Secchieri, C.; Cohen, I.; Bonassar, L. J., Elastoviscous Transitions of Articular Cartilage Reveal a Mechanism of Synergy between Lubricin and Hyaluronic Acid. *PLOS ONE* **2015,** *10* (11), e0143415.
135. Singh, A.; Corvelli, M.; Unterman, S. A.; Wepasnick, K. A.; McDonnell, P.; Elisseeff, J. H., Enhanced lubrication on tissue and biomaterial surfaces through peptide-mediated binding of hyaluronic acid. *Nat. Mater.* **2014,** *13* (10), 988-995.
136. Benz, M.; Chen, N.; Israelachvili, J., Lubrication and wear properties of grafted polyelectrolytes, hyaluronan and hylan, measured in the surface forces apparatus. *Journal of biomedical materials research. Part A* **2004,** *71* (1), 6-15.
137. Waller, K. A.; Zhang, L. X.; Fleming, B. C.; Jay, G. D., Preventing friction-induced chondrocyte apoptosis: comparison of human synovial fluid and hylan G-F 20. *The Journal of rheumatology* **2012,** *39* (7), 1473-80.
138. Aduba, D. C.; Yang, H., Polysaccharide Fabrication Platforms and Biocompatibility Assessment as Candidate Wound Dressing Materials. *Bioengineering* **2017,** *4* (1), 1.
139. Brown, T. J.; Laurent, U. B.; Fraser, Turnover of hyaluronan in synovial joints: elimination of labelled hyaluronan from the knee joint of the rabbit. *Exp. Physiol.* **1991,** *76* (1), 125-134.
140. Stokes, J. R.; Macakova, L.; Chojnicka-Paszun, A.; de Kruif, C. G.; de Jongh, H. H., Lubrication, adsorption, and rheology of aqueous polysaccharide solutions. *Langmuir* **2011,** *27* (7), 3474-84.
141. Shi, S.-C.; Lu, F.-I., Biopolymer Green Lubricant for Sustainable Manufacturing. *Materials* **2016,** *9* (5), 338.
142. Kampf, N.; Raviv, U.; Klein, J., Normal and Shear Forces between Adsorbed and Gelled Layers of Chitosan, a Naturally Occurring Cationic Polyelectrolyte. *Macromolecules* **2004,** *37* (3), 1134-1142.
143. Crockett, R., Friction and Adhesion of Polysaccharides. *Tribology Online* **2014,** *9* (4), 154-163.
144. Samsom, M.; Iwabuchi, Y.; Sheardown, H.; Schmidt, T. A., Proteoglycan 4 and hyaluronan as boundary lubricants for model contact lens hydrogels. *J. Biomed. Mater. Res. B Appl. Biomater.* **2017**, 1329-1338.
145. Samsom, M.; Korogiannaki, M.; Subbaraman, L. N.; Sheardown, H.; Schmidt, T. A., Hyaluronan incorporation into model contact lens hydrogels as a built-in lubricant: Effect of hydrogel composition and proteoglycan 4 as a lubricant in solution. *J. Biomed. Mater. Res. B Appl. Biomater.* **2017**.
146. Zappone, B.; Ruths, M.; Greene, G. W.; Jay, G. D.; Israelachvili, J. N., Adsorption, lubrication, and wear of lubricin on model surfaces: polymer brush-like behavior of a glycoprotein. *Biophys. J.* **2007,** *92* (5), 1693-1708.
147. Seror, J.; Merkher, Y.; Kampf, N.; Collinson, L.; Day, A. J.; Maroudas, A.; Klein, J., Articular Cartilage Proteoglycans As Boundary Lubricants: Structure and Frictional Interaction of Surface-Attached Hyaluronan and Hyaluronan–Aggrecan Complexes. *Biomacromolecules* **2011,** *12* (10), 3432-3443.
148. Seror, J.; Merkher, Y.; Kampf, N.; Collinson, L.; Day, A. J.; Maroudas, A.; Klein, J., Normal and Shear Interactions between Hyaluronan–Aggrecan Complexes Mimicking Possible Boundary Lubricants in Articular Cartilage in Synovial Joints. *Biomacromolecules* **2012,** *13* (11), 3823-3832.
149. Goldberg, R.; Schroeder, A.; Silbert, G.; Turjeman, K.; Barenholz, Y.; Klein, J., Boundary lubricants with exceptionally low friction coefficients based on 2D close-packed phosphatidylcholine liposomes. *Adv. Mater.* **2011,** *23* (31), 3517-21.
150. Sivan, S.; Schroeder, A.; Verberne, G.; Merkher, Y.; Diminsky, D.; Priev, A.; Maroudas, A.; Halperin, G.; Nitzan, D.; Etsion, I.; Barenholz, Y., Liposomes act as effective biolubricants for friction reduction in human synovial joints. *Langmuir* **2010,** *26* (2), 1107-16.

151. Goldberg, R.; Klein, J., Liposomes as lubricants: beyond drug delivery. *Chemistry and Physics of Lipids* **2012,** *165* (4), 374-381.
152. Ma, L.; Gaisinskaya-Kipnis, A.; Kampf, N.; Klein, J., Origins of hydration lubrication. *Nat Commun* **2015,** *6*.
153. Forsey, R. W.; Fisher, J.; Thompson, J.; Stone, M. H.; Bell, C.; Ingham, E., The effect of hyaluronic acid and phospholipid based lubricants on friction within a human cartilage damage model. *Biomaterials* **2006,** *27* (26), 4581-90.
154. Raviv, U.; Klein, J., Fluidity of Bound Hydration Layers. *Science* **2002,** *297* (5586), 1540-1543.
155. Garrec, D. A.; Norton, I. T., Boundary lubrication by sodium salts: a Hofmeister series effect. *J. Colloid Interface Sci.* **2012,** *379* (1), 33-40.
156. Donose, B. C.; Vakarelski, I. U.; Higashitani, K., Silica Surfaces Lubrication by Hydrated Cations Adsorption from Electrolyte Solutions. *Langmuir* **2005,** *21* (5), 1834-1839.
157. Pasquali-Ronchetti, I.; Quaglino, D.; Mori, G.; Bacchelli, B.; Ghosh, P., Hyaluronan-phospholipid interactions. *Journal of structural biology* **1997,** *120* (1), 1-10.
158. Gleghorn, J. P.; Jones, A. R.; Flannery, C. R.; Bonassar, L. J., Boundary mode lubrication of articular cartilage by recombinant human lubricin. *J. Orthop. Res.* **2009,** *27* (6), 771-7.
159. An, J.; Dedinaite, A.; Nilsson, A.; Holgersson, J.; Claesson, P. M., Comparison of a brush-with-anchor and a train-of-brushes mucin on poly(methyl methacrylate) surfaces: adsorption, surface forces, and friction. *Biomacromolecules* **2014,** *15* (4), 1515-25.
160. An, J.; Jin, C.; Dédinaité, A.; Holgersson, J.; Karlsson, N. G.; Claesson, P. M., Influence of Glycosylation on Interfacial Properties of Recombinant Mucins: Adsorption, Surface Forces and Friction. *Langmuir* **2017**.
161. Harvey, N. M.; Yakubov, G. E.; Stokes, J. R.; Klein, J., Normal and Shear Forces between Surfaces Bearing Porcine Gastric Mucin, a High-Molecular-Weight Glycoprotein. *Biomacromolecules* **2011,** *12* (4), 1041-1050.
162. Kreer, T., Polymer-brush lubrication: a review of recent theoretical advances. *Soft Matter* **2016,** *12* (15), 3479-3501.
163. Brittain, W. J.; Minko, S., A structural definition of polymer brushes. *Journal of Polymer Science Part A: Polymer Chemistry* **2007,** *45* (16), 3505-3512.
164. Ballauff, M.; Borisov, O., Polyelectrolyte brushes. *Current Opinion in Colloid & Interface Science* **2006,** *11* (6), 316-323.
165. Tairy, O.; Kampf, N.; Driver, M. J.; Armes, S. P.; Klein, J., Dense, Highly Hydrated Polymer Brushes via Modified Atom-Transfer-Radical-Polymerization: Structure, Surface Interactions, and Frictional Dissipation. *Macromolecules* **2015,** *48* (1), 140-151.
166. Sterner, O.; Karageorgaki, C.; Zürcher, M.; Zürcher, S.; Scales, C. W.; Fadli, Z.; Spencer, N. D.; Tosatti, S. G. P., Reducing Friction in the Eye: A Comparative Study of Lubrication by Surface-Anchored Synthetic and Natural Ocular Mucin Analogues. *ACS Applied Materials & Interfaces* **2017**.
167. Ramakrishna, S. N.; Cirelli, M.; Divandari, M.; Benetti, E. M., Effects of Lateral Deformation by Thermoresponsive Polymer Brushes on the Measured Friction Forces. *Langmuir* **2017**.
168. Pei, X.; Hu, L.; Liu, W.; Hao, J., Synthesis of water-soluble carbon nanotubes via surface initiated redox polymerization and their tribological properties as water-based lubricant additive. *European Polymer Journal* **2008,** *44* (8), 2458-2464.
169. Chouwatat, P.; Hirai, T.; Higaki, K.; Higaki, Y.; Sue, H.-J.; Takahara, A., Aqueous lubrication of poly(etheretherketone) via surface-initiated polymerization of electrolyte monomers. *Polymer* **2017,** *116*, 549-555.
170. Carrillo, J.-M. Y.; Russano, D.; Dobrynin, A. V., Friction between Brush Layers of Charged and Neutral Bottle-Brush Macromolecules. Molecular Dynamics Simulations. *Langmuir* **2011,** *27* (23), 14599-14608.
171. Liu, G.; Cai, M.; Feng, Y.; Wang, X.; Zhou, F.; Liu, W., Photothermally actuated interfacial hydration for fast friction switch on hydrophilic polymer brush modified PDMS sheet incorporated with Fe3O4 nanoparticles. *Chemical Communications* **2016,** *52* (18), 3681-3683.
172. Wei, Q.; Pei, X.; Hao, J.; Cai, M.; Zhou, F.; Liu, W., Surface Modification of Diamond-Like Carbon Film with Polymer Brushes Using a Bio-Inspired Catechol Anchor for Excellent Biological Lubrication. *Advanced Materials Interfaces* **2014,** *1* (5), 1400035-n/a.

173. Carrillo, J. M. Y.; Brown, W. M.; Dobrynin, A. V., Explicit Solvent Simulations of Friction between Brush Layers of Charged and Neutral Bottle-Brush Macromolecules. *Macromolecules* **2012,** *45* (21), 8880-8891.
174. Zhang, R.; Ma, S.; Wei, Q.; Ye, Q.; Yu, B.; van der Gucht, J.; Zhou, F., The Weak Interaction of Surfactants with Polymer Brushes and Its Impact on Lubricating Behavior. *Macromolecules* **2015,** *48* (17), 6186-6196.
175. Wei, Q.; Cai, M.; Zhou, F.; Liu, W., Dramatically Tuning Friction Using Responsive Polyelectrolyte Brushes. *Macromolecules* **2013,** *46* (23), 9368-9379.
176. Kobayashi, M.; Terada, M.; Takahara, A., Polyelectrolyte brushes: a novel stable lubrication system in aqueous conditions. *Faraday Discussions* **2012,** *156* (0), 403-412.
177. Kobayashi, M.; Terayama, Y.; Kikuchi, M.; Takahara, A., Chain dimensions and surface characterization of superhydrophilic polymer brushes with zwitterion side groups. *Soft Matter* **2013,** *9* (21), 5138-5148.
178. Iuster, N.; Tairy, O.; Driver, M. J.; Armes, S. P.; Klein, J., Cross-Linking Highly Lubricious Phosphocholinated Polymer Brushes: Effect on Surface Interactions and Frictional Behavior. *Macromolecules* **2017,** *50* (18), 7361-7371.
179. Kyomoto, M.; Moro, T.; Saiga, K.; Hashimoto, M.; Ito, H.; Kawaguchi, H.; Takatori, Y.; Ishihara, K., Biomimetic hydration lubrication with various polyelectrolyte layers on cross-linked polyethylene orthopedic bearing materials. *Biomaterials* **2012,** *33* (18), 4451-4459.
180. Dunér, G.; Thormann, E.; Ramström, O.; Dėdinaitė, A., Letter to the Editor: Friction between Surfaces—Polyacrylic Acid Brush and Silica—Mediated by Calcium Ions. *J. Dispersion Sci. Technol.* **2010,** *31* (10), 1285-1287.
181. Liu, G.; Liu, Z.; Li, N.; Wang, X.; Zhou, F.; Liu, W., Hairy Polyelectrolyte Brushes-Grafted Thermosensitive Microgels as Artificial Synovial Fluid for Simultaneous Biomimetic Lubrication and Arthritis Treatment. *ACS Applied Materials & Interfaces* **2014,** *6* (22), 20452-20463.
182. Liu, G.; Cai, M.; Zhou, F.; Liu, W., Charged Polymer Brushes-Grafted Hollow Silica Nanoparticles as a Novel Promising Material for Simultaneous Joint Lubrication and Treatment. *The Journal of Physical Chemistry B* **2014,** *118* (18), 4920-4931.
183. Ma, S.; Wang, D.; Liang, Y.; Sun, B.; Gorb, S. N.; Zhou, F., Gecko-Inspired but Chemically Switched Friction and Adhesion on Nanofibrillar Surfaces. *Small (Weinheim an der Bergstrasse, Germany)* **2015,** *11* (9-10), 1131-1137.
184. Heeb, R.; Bielecki, R. M.; Lee, S.; Spencer, N. D.; Heeb, R.; Bielecki, R. M.; Lee, S.; Spencer, N. D., Room-temperature, aqueous phase fabrication of PMAA brushes by UV-LED-induced, controlled radical polymerization with high selectivity for surface-bound species. *Macromolecules* **2009,** *42* (22), 9124-9132.
185. Kitano, K.; Inoue, Y.; Matsuno, R.; Takai, M.; Ishihara, K., Nanoscale evaluation of lubricity on well-defined polymer brush surfaces using QCM-D and AFM. *Colloids Surf. B. Biointerfaces* **2009,** *74* (1), 350-357.
186. Liberelle, B.; Giasson, S., Friction and Normal Interaction Forces between Irreversibly Attached Weakly Charged Polymer Brushes. *Langmuir* **2008,** *24* (4), 1550-1559.
187. Morgenthaler, S.; Zink, C.; Stadler, B.; Voros, J.; Lee, S.; Spencer, N. D.; Tosatti, S. G., Poly(L-lysine)-grafted-poly(ethylene glycol)-based surface-chemical gradients. Preparation, characterization, and first applications. *Biointerphases* **2006,** *1* (4), 156-65.
188. Lee, S.; Spencer, N. D., Adsorption Properties of Poly(l-lysine)-graft-poly(ethylene glycol) (PLL-g-PEG) at a Hydrophobic Interface: Influence of Tribological Stress, pH, Salt Concentration, and Polymer Molecular Weight. *Langmuir* **2008,** *24* (17), 9479-9488.
189. Rosenberg, K. J.; Goren, T.; Crockett, R.; Spencer, N. D., Load-Induced Transitions in the Lubricity of Adsorbed Poly(l-lysine)-g-dextran as a Function of Polysaccharide Chain Density. *ACS Appl. Mater. Interfaces* **2011,** *3* (8), 3020-3025.
190. Hartung, W.; Rossi, A.; Lee, S.; Spencer, N. D., Aqueous Lubrication of SiC and Si3N4 Ceramics Aided by a Brush-like Copolymer Additive, Poly(l-lysine)-graft-poly(ethylene glycol). *Tribol Lett* **2009,** *34* (3), 201-210.
191. Ramakrishna, S. N.; Espinosa-Marzal, R. M.; Naik, V. V.; Nalam, P. C.; Spencer, N. D., Adhesion and Friction Properties of Polymer Brushes on Rough Surfaces: A Gradient Approach. *Langmuir* **2013,** *29* (49), 15251-15259.

192. Lin, B.; Tieu, A. K.; Zhu, H.; Kosasih, B.; Novareza, O.; Triani, G., Tribological performance of aqueous copolymer lubricant in loaded contact with Si and coated Ti film. *Wear* **2013,** *302* (1), 1010-1016.
193. Lee, S.; Iten, R.; Müller, M.; Spencer, N. D., Influence of Molecular Architecture on the Adsorption of Poly(ethylene oxide)−Poly(propylene oxide)−Poly(ethylene oxide) on PDMS Surfaces and Implications for Aqueous Lubrication. *Macromolecules* **2004,** *37* (22), 8349-8356.
194. Kang, T.; Banquy, X.; Heo, J.; Lim, C.; Lynd, N. A.; Lundberg, P.; Oh, D. X.; Lee, H. K.; Hong, Y. K.; Hwang, D. S.; Waite, J. H.; Israelachvili, J. N.; Hawker, C. J., Mussel-Inspired Anchoring of Polymer Loops That Provide Superior Surface Lubrication and Antifouling Properties. *ACS Nano* **2016,** *10* (1), 930-7.
195. Lee, S.; Müller, M.; Heeb, R.; Zürcher, S.; Tosatti, S.; Heinrich, M.; Amstad, F.; Pechmann, S.; Spencer, N. D., Self-healing behavior of a polyelectrolyte-based lubricant additive for aqueous lubrication of oxide materials. *Tribol Lett* **2006,** *24* (3), 217.
196. Dedinaite, A.; Thormann, E.; Olanya, G.; Claesson, P. M.; Nystrom, B.; Kjoniksen, A.-L.; Zhu, K., Friction in aqueous media tuned by temperature-responsive polymer layers. *Soft Matter* **2010,** *6* (11), 2489-2498.
197. Plunkett, M. A.; Feiler, A.; Rutland, M. W., Atomic Force Microscopy Measurements of Adsorbed Polyelectrolyte Layers. 2. Effect of Composition and Substrate on Structure, Forces, and Friction. *Langmuir* **2003,** *19* (10), 4180-4187.
198. Feiler, A.; Plunkett, M. A.; Rutland, M. W., Atomic Force Microscopy Measurements of Adsorbed Polyelectrolyte Layers. 1. Dynamics of Forces and Friction. *Langmuir* **2003,** *19* (10), 4173-4179.
199. Dedinaite, A.; Pettersson, T.; Mohanty, B.; Claesson, P. M., Lubrication by organized soft matter. *Soft Matter* **2010,** *6* (7), 1520-1526.
200. Faivre, J.; Shrestha, B. R.; Xie, G.; Olszewski, M.; Adibnia, V.; Moldovan, F.; Montembault, A.; Sudre, G.; Delair, T.; David, L.; Matyjaszewski, K.; Banquy, X., Intermolecular Interactions between Bottlebrush Polymers Boost the Protection of Surfaces against Frictional Wear. *Chem. Mater.* **2018**.
201. Banquy, X.; Burdyńska, J.; Lee, D. W.; Matyjaszewski, K.; Israelachvili, J., Bioinspired Bottle-Brush Polymer Exhibits Low Friction and Amontons-like Behavior. *J. Am. Chem. Soc.* **2014,** *136* (17), 6199-6202.
202. Zhang, X.; Wilhelm, M.; Klein, J.; Pfaadt, M.; Meijer, E. W., Modification of Surface Interactions and Friction by Adsorbed Dendrimers: 1. Low Surface-Energy Fifth-Generation Amino Acid-Modified Poly(propyleneimine) Dendrimers. *Langmuir* **2000,** *16* (8), 3884-3892.
203. Zhang, X.; Klein, J.; Sheiko, S. S.; Muzafarov, A. M., Modification of Surface Interactions and Friction by Adsorbed Dendrimers: 2. High-Surface-Energy −OH-Terminated Carbosilane Dendrimers. *Langmuir* **2000,** *16* (8), 3893-3901.
204. Raviv, U.; Frey, J.; Sak, R.; Laurat, P.; Tadmor, R.; Klein, J., Properties and Interactions of Physigrafted End-Functionalized Poly(ethylene glycol) Layers. *Langmuir* **2002,** *18* (20), 7482-7495.
205. Pettersson, T.; Naderi, A.; Makuska, R.; Claesson, P. M., Lubrication properties of bottle-brush polyelectrolytes: An AFM study on the effect of side chain and charge density. *Langmuir* **2008,** *24* (7), 3336-3347.
206. Liu, X.; Dedinaite, A.; Rutland, M.; Thormann, E.; Visnevskij, C.; Makuska, R.; Claesson, P. M., Electrostatically Anchored Branched Brush Layers. *Langmuir* **2012,** *28* (44), 15537-15547.
207. Liu, X.; Thormann, E.; Dedinaite, A.; Rutland, M.; Visnevskij, C.; Makuska, R.; Claesson, P. M., Low friction and high load bearing capacity layers formed by cationic-block-non-ionic bottle-brush copolymers in aqueous media. *Soft Matter* **2013,** *9* (22), 5361-5371.
208. Krivorotova, T.; Makuska, R.; Naderi, A.; Claesson, P. M.; Dedinaite, A., Synthesis and interfacial properties of novel cationic polyelectrolytes with brush-on-brush structure of poly(ethylene oxide) side chains. *European Polymer Journal* **2010,** *46* (2), 171-180.
209. Spiller, K. L.; Maher, S. A.; Lowman, A. M., Hydrogels for the Repair of Articular Cartilage Defects. *Tissue Eng., Part B* **2011,** *17* (4), 281-299.
210. Caló, E.; Khutoryanskiy, V. V., Biomedical applications of hydrogels: A review of patents and commercial products. *European Polymer Journal* **2015,** *65*, 252-267.

211. Kaneko, D.; Tada, T.; Kurokawa, T.; Gong, J. P.; Osada, Y., Mechanically Strong Hydrogels with Ultra-Low Frictional Coefficients. *Advanced Materials* **2005,** *17* (5), 535-538.
212. Gong, J. P.; Kagata, G.; Osada, Y., Friction of Gels. 4. Friction on Charged Gels. *The Journal of Physical Chemistry B* **1999,** *103* (29), 6007-6014.
213. Yashima, S.; Takase, N.; Kurokawa, T.; Gong, J. P., Friction of hydrogels with controlled surface roughness on solid flat substrates. *Soft Matter* **2014,** *10* (18), 3192-3199.
214. Kurokawa, T.; Gong, J. P.; Osada, Y., Substrate Effect on Topographical, Elastic, and Frictional Properties of Hydrogels. *Macromolecules* **2002,** *35* (21), 8161-8166.
215. Khosla, T.; Cremaldi, J.; Erickson, J. S.; Pesika, N. S., Load-Induced Hydrodynamic Lubrication of Porous Films. *ACS Appl. Mater. Interfaces* **2015,** *7* (32), 17587-17591.
216. Liu, X.; Nanao, H.; Li, T.; Mori, S., A study on the friction properties of PAAc hydrogel under low loads in air and water. *Wear* **2004,** *257* (7), 665-670.
217. Ahmed, J.; Guo, H.; Yamamoto, T.; Kurokawa, T.; Takahata, M.; Nakajima, T.; Gong, J. P., Sliding Friction of Zwitterionic Hydrogel and Its Electrostatic Origin. *Macromolecules* **2014,** *47* (9), 3101-3107.
218. Wu, Y.; Pei, X.; Wang, X.; Liang, Y.; Liu, W.; Zhou, F., Biomimicking lubrication superior to fish skin using responsive hydrogels. *Npg Asia Materials* **2014,** *6*, e136.
219. Ma, S.; Scaraggi, M.; Wang, D.; Wang, X.; Liang, Y.; Liu, W.; Dini, D.; Zhou, F., Nanoporous Substrate-Infiltrated Hydrogels: a Bioinspired Regenerable Surface for High Load Bearing and Tunable Friction. *Advanced Functional Materials* **2015,** *25* (47), 7366-7374.
220. Zhang, R.; Feng, Y.; Ma, S.; Cai, M.; Yang, J.; Yu, B.; Zhou, F., Tuning the Hydration and Lubrication of the Embedded Load-Bearing Hydrogel Fibers. *Langmuir* **2017,** *33* (9), 2069-2075.
221. Osaheni, A. O.; Finkelstein, E. B.; Mather, P. T.; Blum, M. M., Synthesis and characterization of a zwitterionic hydrogel blend with low coefficient of friction. *Acta Biomaterialia* **2016,** *46*, 245-255.
222. Nakashima, K.; Sawae, Y.; Murakami, T., Study on Wear Reduction Mechanisms of Artificial Cartilage by Synergistic Protein Boundary Film Formation. *JSME International Journal Series C Mechanical Systems, Machine Elements and Manufacturing* **2005,** *48* (4), 555-561.
223. Ghosh, S.; Choudhury, D.; Roy, T.; Moradi, A.; Masjuki, H. H.; Pingguan-Murphy, B., Tribological performance of the biological components of synovial fluid in artificial joint implants. *Science and Technology of Advanced Materials* **2015,** *16* (4), 045002.
224. Boettcher, K.; Winkeljann, B.; Schmidt, T. A.; Lieleg, O., Quantification of cartilage wear morphologies in unidirectional sliding experiments: Influence of different macromolecular lubricants. *Biotribology* **2017,** *12*, 43-51.
225. Xu, G.; Liu, X.; Liu, P.; Pranantyo, D.; Neoh, K. G.; Kang, E.-T., Arginine-based Polymer Brush Coatings with Hydrolysis-Triggered Switchable Functionalities from Antimicrobial (Cationic) to Antifouling (Zwitterionic). *Langmuir* **2017**.
226. Demirci, S.; Kinali-Demirci, S.; Jiang, S., A switchable polymer brush system for antifouling and controlled detection. *Chemical Communications* **2017,** *53* (26), 3713-3716.
227. Rabanel, J.-M.; Faivre, J.; Paka, G. D.; Ramassamy, C.; Hildgen, P.; Banquy, X., Effect of polymer architecture on curcumin encapsulation and release from PEGylated polymer nanoparticles: Toward a drug delivery nano-platform to the CNS. *European Journal of Pharmaceutics and Biopharmaceutics* **2015,** *96*, 409-420.
228. Andresen Eguiluz, R. C.; Cook, S. G.; Tan, M.; Brown, C. N.; Pacifici, N. J.; Samak, M. S.; Bonassar, L. J.; Putnam, D.; Gourdon, D., Synergistic Interactions of a Synthetic Lubricin-Mimetic with Fibronectin for Enhanced Wear Protection. *Front. Bioeng. Biotechnol.* **2017,** *5* (36).
229. Zhang, D.; Shen, Y.; Ge, S., Research on the friction and wear mechanism of Poly(vinyl alcohol)/hydroxylapatite composite hydrogel. *Science in China Series E: Technological Sciences* **2009,** *52* (8), 2474-2480.
230. Matricardi, P.; Di Meo, C.; Coviello, T.; Hennink, W. E.; Alhaique, F., Interpenetrating Polymer Networks polysaccharide hydrogels for drug delivery and tissue engineering. *Advanced Drug Delivery Reviews* **2013,** *65* (9), 1172-1187.
231. Myung, D.; Waters, D.; Wiseman, M.; Duhamel, P.-E.; Noolandi, J.; Ta, C. N.; Frank, C. W., Progress in the development of interpenetrating polymer network hydrogels. *Polymers for Advanced Technologies* **2008,** *19* (6), 647-657.

232. Zhou, X.; Guo, B.; Zhang, L.; Hu, G.-H., Progress in bio-inspired sacrificial bonds in artificial polymeric materials. *Chem. Soc. Rev.* **2017,** *46* (20), 6301-6329.
233. Nakajima, T., Generalization of the sacrificial bond principle for gel and elastomer toughening. *Polym. J.* **2017,** *49* (6), 477-485.
234. Gong, J. P., Why are double network hydrogels so tough? *Soft Matter* **2010,** *6* (12), 2583-2590.
235. Gong, J. P.; Katsuyama, Y.; Kurokawa, T.; Osada, Y., Double-Network Hydrogels with Extremely High Mechanical Strength. *Advanced Materials* **2003,** *15* (14), 1155-1158.
236. Tang, Z.; Kotov, N. A.; Magonov, S.; Ozturk, B., Nanostructured artificial nacre. *Nat Mater* **2003,** *2* (6), 413-8.
237. Zhang, H.; Xia, H.; Zhao, Y., Poly(vinyl alcohol) Hydrogel Can Autonomously Self-Heal. *ACS Macro Letters* **2012,** *1* (11), 1233-1236.
238. Taylor, D. L.; in het Panhuis, M., Self-Healing Hydrogels. *Advanced Materials* **2016,** *28* (41), 9060-9093.
239. Kim, C.-L.; Kim, D.-E., Durability and Self-healing Effects of Hydrogel Coatings with respect to Contact Condition. *Scientific Reports* **2017,** *7* (1), 6896.
240. Maudens, P.; Jordan, O.; Allemann, E., Recent advances in intra-articular drug delivery systems for osteoarthritis therapy. *Drug Discov. Today* **2018**.
241. Huang, K.; Wu, L. D., Aggrecanase and aggrecan degradation in osteoarthritis: a review. *J. Int. Med. Res.* **2008,** *36* (6), 1149-60.
242. Szychlinska, M. A.; Leonardi, R.; Al-Qahtani, M.; Mobasheri, A.; Musumeci, G., Altered joint tribology in osteoarthritis: Reduced lubricin synthesis due to the inflammatory process. New horizons for therapeutic approaches. *Ann. Phys. Rehabil. Med.* **2016,** *59* (3), 149-156.
243. Kogan, G.; Šoltés, L.; Stern, R.; Gemeiner, P., Hyaluronic acid: a natural biopolymer with a broad range of biomedical and industrial applications. *Biotechnol. Lett* **2007,** *29* (1), 17-25.
244. Liu, M.; Zeng, X.; Ma, C.; Yi, H.; Ali, Z.; Mou, X.; Li, S.; Deng, Y.; He, N., Injectable hydrogels for cartilage and bone tissue engineering. *Bone Research* **2017,** *5*, 17014.
245. Montembault, A.; Tahiri, K.; Korwin-Zmijowska, C.; Chevalier, X.; Corvol, M. T.; Domard, A., A material decoy of biological media based on chitosan physical hydrogels: application to cartilage tissue engineering. *Biochimie* **2006,** *88* (5), 551-564.
246. Montembault, A.; Viton, C.; Domard, A., Physico-chemical studies of the gelation of chitosan in a hydroalcoholic medium. *Biomaterials* **2005,** *26* (8), 933-943.
247. David, L.; Domard, A.; Popa-Nita, S.; Boucard, N.; Montembault, A.; Ladet, S.; Viton, C., New chitosan hydrogels: Mechanical properties and multiscale microstructure. *Abstracts of Papers of the American Chemical Society* **2006,** *231*.
248. Rivas-Araiza, R.; Alcouffe, P.; Rochas, C.; Montembault, A.; David, L., Micron Range Morphology of Physical Chitosan Hydrogels. *Langmuir* **2010,** *26* (22), 17495-17504.
249. Ladet, S. G.; Tahiri, K.; Montembault, A. S.; Domard, A. J.; Corvol, M. T. M., Multi-membrane chitosan hydrogels as chondrocytic cell bioreactors. *Biomaterials* **2011,** *32* (23), 5354-5364.
250. Malaise, S.; Rami, L.; Montembault, A.; Alcouffe, P.; Burdin, B.; Bordenave, L.; Delmond, S.; David, L., Bioresorption mechanisms of chitosan physical hydrogels: A scanning electron microscopy study. *Materials Science & Engineering C-Materials for Biological Applications* **2014,** *42*, 374-384.
251. Sereni, N.; Enache, A.; Sudre, G.; Montembault, A.; Rochas, C.; Durand, P.; Perrard, M. H.; Bozga, G.; Puaux, J. P.; Delair, T.; David, L., Dynamic Structuration of Physical Chitosan Hydrogels. *Langmuir* **2017,** *33* (44), 12697-12707.
252. Li, X.; Prukop, S. L.; Biswal, S. L.; Verduzco, R., Surface Properties of Bottlebrush Polymer Thin Films. *Macromolecules* **2012,** *45* (17), 7118-7127.
253. Mao, J.; Zhao, L.; De Yao, K.; Shang, Q.; Yang, G.; Cao, Y., Study of novel chitosan-gelatin artificial skin in vitro. *Journal of biomedical materials research. Part A* **2003,** *64* (2), 301-8.
254. Kim, T. H.; Park, I. K.; Nah, J. W.; Choi, Y. J.; Cho, C. S., Galactosylated chitosan/DNA nanoparticles prepared using water-soluble chitosan as a gene carrier. *Biomaterials* **2004,** *25* (17), 3783-3792.

255. Rinaudo, M., Chitin and chitosan: Properties and applications. *Progress in Polymer Science* **2006,** *31* (7), 603-632.
256. Zhou, Y.; Liedberg, B.; Gorochovceva, N.; Makuska, R.; Dedinaite, A.; Claesson, P. M., Chitosan-N-poly(ethylene oxide) brush polymers for reduced nonspecific protein adsorption. *Journal of Colloid and Interface Science* **2007,** *305* (1), 62-71.
257. Xu, J.-P.; Wang, X.-L.; Fan, D.-Z.; Ji, J.; Shen, J.-C., Construction of phospholipid anti-biofouling multilayer on biomedical PET surfaces. *Applied Surface Science* **2008,** *255* (2), 538-540.
258. Croisier, F.; Jérôme, C., Chitosan-based biomaterials for tissue engineering. *European Polymer Journal* **2013,** *49* (4), 780-792.
259. Pickenhahn, V. D.; Darras, V.; Dziopa, F.; Biniecki, K.; De Crescenzo, G.; Lavertu, M.; Buschmann, M. D., Regioselective thioacetylation of chitosan end-groups for nanoparticle gene delivery systems. *Chemical Science* **2015,** *6* (8), 4650-4664.
260. Fiamingo, A.; Montembault, A.; Boitard, S.-E.; Naemetalla, H.; Agbulut, O.; Delair, T.; Campana-Filho, S. P.; Menasché, P.; David, L., Chitosan Hydrogels for the Regeneration of Infarcted Myocardium: Preparation, Physicochemical Characterization, and Biological Evaluation. *Biomacromolecules* **2016,** *17* (5), 1662-1672.
261. Jin, R.; Moreira Teixeira, L. S.; Dijkstra, P. J.; Karperien, M.; van Blitterswijk, C. A.; Zhong, Z. Y.; Feijen, J., Injectable chitosan-based hydrogels for cartilage tissue engineering. *Biomaterials* **2009,** *30* (13), 2544-2551.
262. Kaderli, S.; Boulocher, C.; Pillet, E.; Watrelot-Virieux, D.; Rougemont, A. L.; Roger, T.; Viguier, E.; Gurny, R.; Scapozza, L.; Jordan, O., A novel biocompatible hyaluronic acid-chitosan hybrid hydrogel for osteoarthrosis therapy. *International journal of pharmaceutics* **2015,** *483* (1-2), 158-68.
263. Mohan, N.; Mohanan, P. V.; Sabareeswaran, A.; Nair, P., Chitosan-hyaluronic acid hydrogel for cartilage repair. *Int. J. Biol. Macromol.* **2017**.

CHAPITRE II - Conception d'une librairie de mimes bioinspirés de l'aggrécane et de la lubricine et caractérisation de leurs propriétés tribologiques

- Chapitre II-

Conception d'une librairie de mimes bioinspirés de l'aggrécane et de la lubricine et caractérisation de leurs propriétés tribologiques

Introduction générale du chapitre II

Les articulations synoviales sont des systèmes tribologiques exceptionnels, car elles garantissent la mobilité du squelette tout au long de la vie. Généralement, leur efficacité est caractérisée par un coefficient de friction (CoF) très faible et aucune usure des surfaces jusqu'à des pressions de plusieurs mégapascals et des vitesses de glissement allant jusqu'à 10^{6-7} s^{-1}.[1] Néanmoins, peu de dispositifs médicaux ou bancs de simulation ne sont capables de reproduire totalement les mécanismes complexes de la friction et de la résistance à l'usure des articulations. De plus, aucun traitement curatif n'existe à ce jour permettant de stopper ou même ralentir la dégénérescence du cartilage qui est le résultat de pathologies comme l'OA.

Dans l'optique de développer un fluide lubrifiant permettant de pallier la dégradation des molécules jouant un rôle prépondérant sur la lubrification des articulations lors de l'OA, nous nous sommes intéressés au traitement intra-articulaire de viscosupplémentation qui consiste en l'injection de l'acide Hyaluronique (HA), un glycosaminoglycane (GAG), principale molécule du fluide synovial (SF) et longtemps considéré comme la macromolécule responsable de cette lubrification. En effet, durant l'avancement de l'OA, HA, ainsi que d'autres macromolécules sont sélectivement dégradés par des enzymes, d'où l'idée de réintroduire du HA de haut poids moléculaire et à concentration naturelle de l'ordre de quelques milligrammes par millilitre. De plus, HA possède des propriétés anti-inflammatoires[2]. Généralement, ce traitement est constitué d'une seringue de ~ 2 mL comportant du HA de haut poids moléculaire solubilisé à ~ 10 mg/mL dans un tampon isotonique et est commercialisé sous les noms de SYNVISC®, SINOVIAL®, SYNOCROM®, STRUCTOVIAL®, SINOVIAL®, OSTENIL®, GO-ON®, EUFLEXXA®, DUROLANE®, ARTHRUM®, ADANT® en tant que dispositifs médicaux tandis que l'injection HYALGAN® est classée comme un médicament. Néanmoins, il est maintenant reconnu que HA ne joue pas un rôle direct majeur sur la lubrification, mais permet de

maintenir par enchevêtrements et autoassemblage les glycoprotéines et phospholipides lubrifiants dans les zones de contact entre les deux surfaces cartilagineuses[3-4].

Jusqu'à présent, plusieurs stratégies ont été étudiées pour lubrifier et protéger les surfaces articulaires. L'extraction des molécules du fluide synovial et leur utilisation a posteriori n'ont pas permis de retrouver les mêmes propriétés tribologiques que celles rencontrées dans les articulations saines du fait de la complexité de leur mode d'action, résultat de mécanismes synergiques entre les différentes molécules du SF et la structure du cartilage[3]. Le greffage de brosses de polymères biocompatibles , inspirée de la structure de la lubricine ou l'aggrécane adsorbée sur des surfaces articulaires, a permis d'obtenir des revêtements très lubrifiants jusqu'à des pressions de plusieurs dizaines de mégapascals[5-7]. Ce concept de lubrification requiert cependant une modification chimique des surfaces, ce qui n'est pas envisageable in vivo, mais est très pertinent pour la fonctionnalisation de surface de prothèse pour les rendre davantage biofonctionnelles et limiter leur usure. Finalement, certains groupes de recherche se sont intéressés au développement d'écouvillons moléculaires, en tant que mimes polymériques de la lubricine ou de l'aggrécane, capables de s'adsorber sur les surfaces et de garantir une bonne lubrification[8-9]. Ces mimes polymériques sont une des thématiques d'étude du Laboratoire Biomatériaux et Interfaces Structurées du Pr Xavier Banquy à l'Université de Montréal. Une preuve de concept prometteuse a d'ailleurs été présentée[10] en étudiant le comportement aux interfaces d'un écouvillon moléculaire capable de fournir un CoF aussi faible que μ =0.0115 (Fig. 2.1) à une pression de 2.1 MPa.

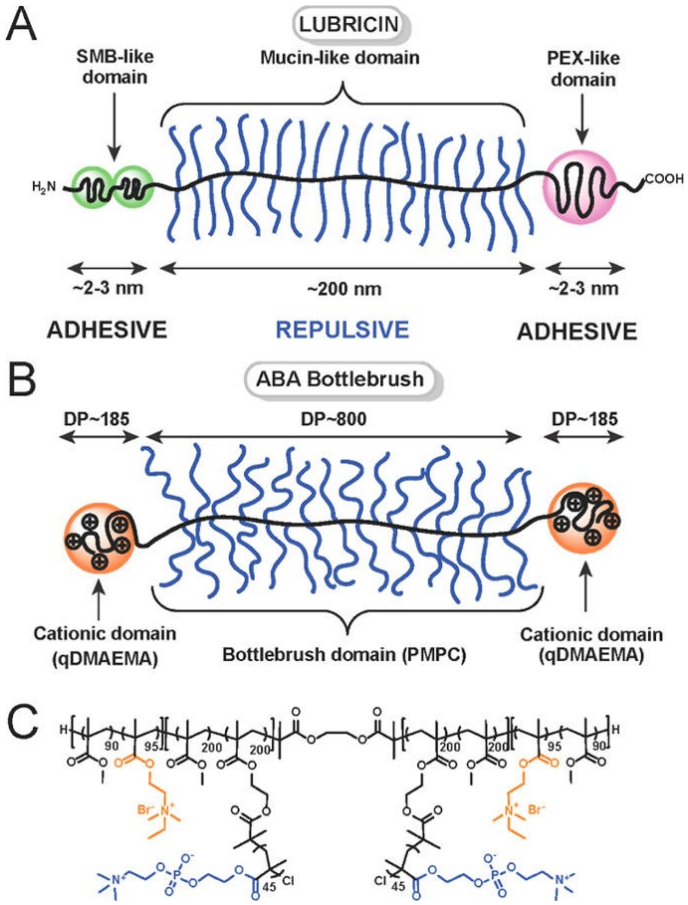

Figure 2.1. *Représentations schématiques (A) du PG Lubricine et (B) de l'écouvillon moléculaire mime tribloc de la Lubricine. (C) Structure chimique du mime polymérique*[10].

À travers ce chapitre, nous souhaitons développer un SF synthétique pour la tribosupplémentation articulaire capable de lubrifier avec des CoF dans la gamme physiologique et résister à des pressions de plusieurs dizaines d'atmosphères. Ce SF est constitué d'un polymère, structuré en écouvillon moléculaire, mime des macromolécules lubrifiantes en combinaison avec du HA directement injectable dans l'articulation.

Introduction de la partie 1

Les macromolécules que l'on retrouve dans les articulations synoviales remplissent des rôles cruciaux dans la lubrification de nos articulations[11]. La lubricine, se retrouve à la surface du cartilage et peut, grâce à des groupements d'ancrage spécifiques (Fig. 2.2), s'auto-assembler et former une couche lubrifiante et protectrice en surface du cartilage avec l'HA. Au contraire, l'aggrécane forme des complexes très hydratés emprisonnés au sein de la matrice extracellulaire du cartilage[1, 12]. Sa fonction est d'augmenter les propriétés mécaniques du cartilage sous contrainte grâce à la pression osmotique générée (Fig. 2.2). Dans les deux cas, ces macromolécules possèdent un domaine central en peigne avec des chaines latérales hydrophiles et négativement chargées, constituées principalement de motifs sucrés pour la lubricine et de GAG chondroïtine sulfate et de kératane sulfate pour l'aggrécane (Fig. 2.2). Ce domaine central est couplé à des domaines globulaires qui permettent l'ancrage spécifique sur des surfaces physiologiques et leur assemblage sous contrainte. Les chaines latérales pendantes très hydrophiles sont responsables de l'excellente lubrification, car elles empêchent l'interpénétration des macromolécules entre elles en raison de la gêne stérique engendrée par une grande densité de greffage et aux forces d'hydratation répulsives générées par les têtes hydrophiles très hydratées.

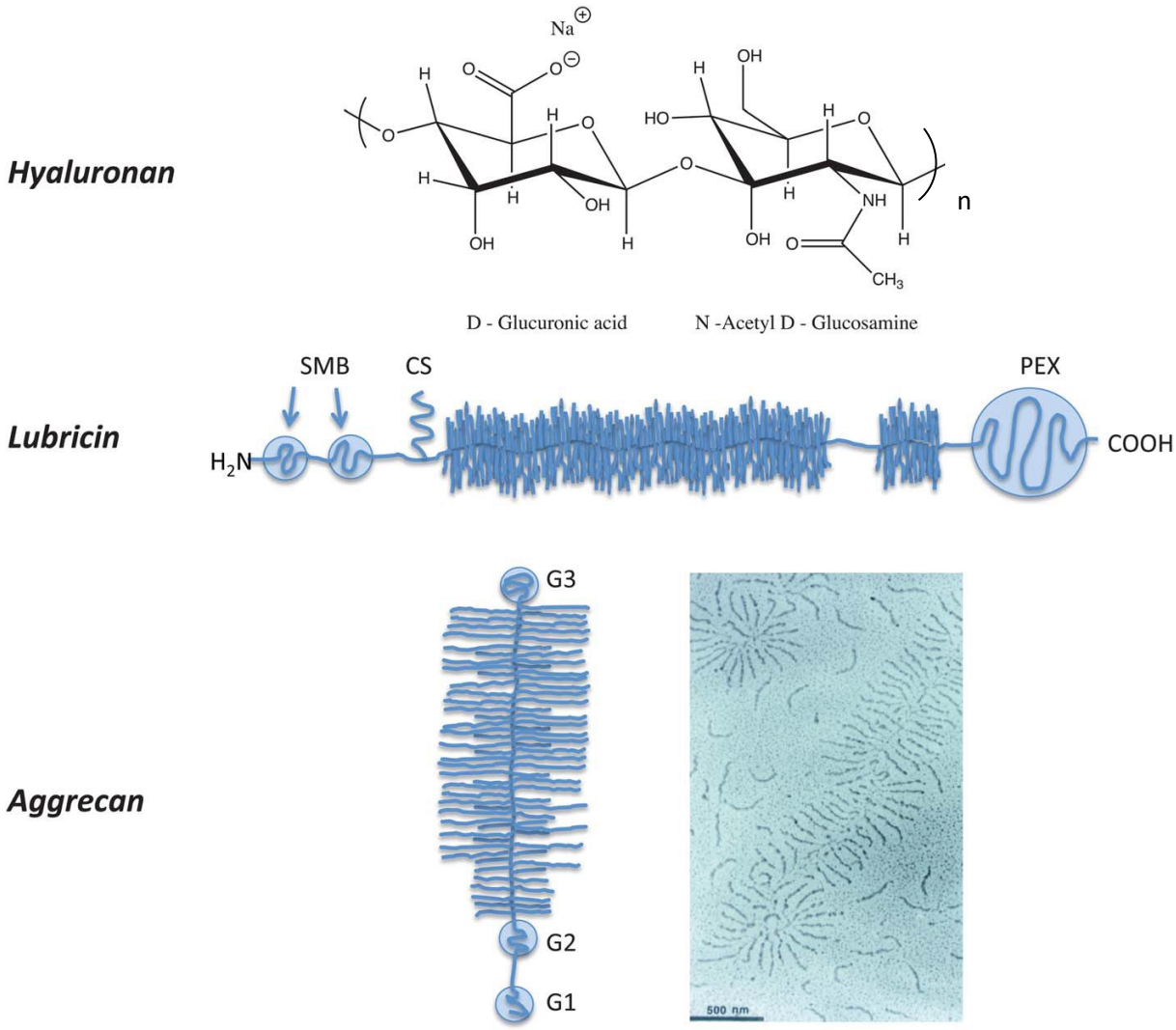

Figure 2.2. *Structure des macromolécules impliquées dans la lubrification articulaire.* ***Hyaluronan*** *: le motif disaccharide constitutif de l'acide hyaluronique,* ***Lubricin*** *: le domaine central en peigne est fortement glycosylé et comporte quelques chaines de GAG (chondroïtine sulfate). Latéralement sont disposés des domaines globulaires 2-somatomedin B (SMB) (du coté mine terminale) et haemopexin (PEX) (du coté acide carboxylique terminal). Le domaine du côté amine terminal créé des liaisons disulphide entre deux lubricines pour son autoassociation*[13]*. Aggrecan : à gauche, le domaine central en peigne est constitué de chaines de GAG, chondroïtine sulfate pour les plus longues et kératane sulfate pour les plus courtes. Latéralement, trois domaines globulaires (G) jouent des rôles différents. Le domaine G1 est notamment impliqué dans la liaison à l'HA. À droite, une image de SEM d'un complexe HA-Aggrécane composé d'un squelette central d'HA et de chaines latérales d'aggrécane (barre d'échelle 500 nm). Extrait de la référence*[11]*.*

L'hypothèse centrale de ce travail est que la structure peigne (domaine central fortement greffé et groupements latéraux facilitant l'ancrage) ainsi que la nature chimique des composants des molécules lubrifiantes (domaines fortement hydratés) sont les principales causes de l'excellente lubrification articulaire.

Dans cette partie, nous avons conçu un mime bioinspiré de ces macromolécules, ne possédant pas de groupement d'ancrage, afin de déterminer sa capacité à induire une résistance à l'usure et à réduire le coefficient de frottement. Le domaine central en peigne a été constitué avec des motifs polyzwitterioniques très hydrophiles et biocompatibles de phosphoryle choline, motif omniprésent dans les fluides articulaires grâce à la présence des phospholipides. Ce mime a été synthétisé par ATRP qui est une technique de polymérisation qui permet d'obtenir des architectures complexes avec une très faible dispersité[14-15]. Ce polymère a été testé tribologiquement à l'échelle moléculaire en utilisant le SFA et à l'échelle macroscopique en utilisant un tribomètre, spécialement conçu pour l'étude. Les surfaces utilisées pour caractériser l'usure ont été d'une part, le mica qui est une surface non poreuse, dure et négativement chargée en milieu aqueux et d'autre part, des hydrogels qui sont des surfaces poroélastiques neutres à pH 7.4[16]. Dans les deux cas, ces surfaces s'usent très rapidement si le lubrifiant ne joue plus son rôle protecteur. Cela permet donc une mesure directe *in vitro* de l'efficacité du mime polymérique par caractérisation *a posteriori* de l'état de surface du substrat. Finalement, afin de ressembler encore plus au SF et de se comparer aux solutions de viscosupplémentation commerciales, des HA de différentes masses molaires ont été caractérisés tribologiquement avec ou sans notre mime polymérique[17]. Les différentes masses molaires ont été choisies pour mimer l'avancement de l'OA qui se caractérise également par une dégradation progressive du HA.

Cette étude fait l'objet d'une publication parue dans le Journal de l'American Chemical Society, *ACS Nano*, publiée le 2 janvier 2017[18] et intitulée : *Wear Protection Without Surface Modification Using a Synergistic Mixture of Molecular Brushes and Linear Polymers*. Le polymère a été conçu conjointement par le laboratoire Biomatériaux et Interfaces Structurées du Pr Xavier Banquy, et le laboratoire Matyjaszewski Polymer Group du Pr Krzysztof Matyjaszewski. La synthèse a été effectuée par les Dr Joanna Burdynska et Dr Guojun Xie du laboratoire du Pr Matyjaszewski. Les expériences de tribologie ont été effectuées par le Dr Buddha R. Shrestha (étude SFA) et moi-même (étude SFA, tribomètre et interféromètre) au sein des laboratoires du Pr Xavier Banquy pour le SFA et le Laboratoire de Tribologie et de Dynamique des Systèmes du Pr Stéphane Benayoun pour le tribomètre. Les hydrogels ont été

fabriqués et caractérisés dans l'équipe Matériaux Polymères à l'Interface avec les Sciences de la Vie du Laboratoire Ingénierie des Matériaux Polymères (groupe animé par Pr Laurent David et Pr Thierry Delair).

Wear Protection Without Surface Modification Using a Synergistic Mixture of Molecular Brushes and Linear Polymers

Jimmy Faivre[1,3], Buddha R. Shrestha[1], Joanna Burdynska[2], Guojun Xie,[2] Florina Moldovan[3], Thierry Delair[4],Stéphane Benayoun,[5] Laurent David[4], Krzysztof Matyjaszewski[2*], Xavier Banquy[1*]

[1]*Canadian Research Chair in Bioinspired materials, Faculty of Pharmacy, Université de Montréal, Montréal, Qc, Canada*

[2]*Center for Macromolecular Engineering, Department of Chemistry, Carnegie Mellon University, Pittsburgh, PA, USA*

[3]*CHU Sainte Justine Research Center and Department of Stomatology, Faculty of Dentistry*

[4]*Université de Lyon, Université Claude Bernard Lyon 1, CNRS, Ingénierie des Matériaux Polymères (IMP-UMR 5223), 15 Boulevard Latarjet, 69622 Villeurbanne Cedex, France*

[5]*Laboratoire de Tribologie et Dynamique des Systèmes, UMR 5513 CNRS, Ecole Centrale de Lyon, 36 Avenue Guy de Collongue, 69134 Ecully Cedex, France*

Abstract.

We describe the design of lubricating and wear protecting fluids based on mixtures of bottlebrushes (BB) and linear polymers solutions. To illustrate this concept we used hyaluronic acid (HA) - a naturally occurring linear polyelectrolyte, and a water soluble synthetic BB polymer. Individually, these two polymers exhibit poor wear protecting capabilities compared to saline solutions. Mixture of the two polymers in pure water or in saline allows to drastically increase wear protection of surfaces over a wide range of shearing conditions. We demonstrate that this synergy between the BB and HA polymers emerges from a strong cohesion between the two components forming the boundary film due to entanglements between both polymers. We show that this concept can be applied to other types of linear polymers and surfaces and is independent of the chemical and mechanical properties of the surfaces.

Keywords.

Biolubrication, wear resistance, bottle-brush polymer, surface forces, hyaluronic acid

Table of Contents

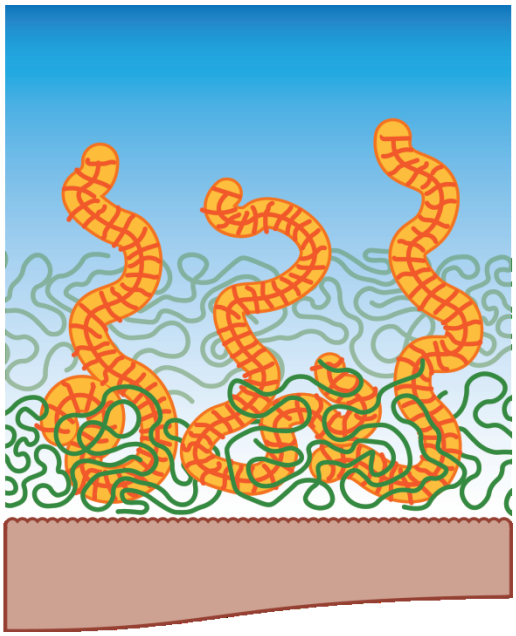

2.1 Introduction

With the ever-increasing need of more efficient and long lasting machinery and devices, certain issues such as control of wear and fatigue of machine parts have become extremely challenging.[19] The design of lubricating fluids able to protect surfaces against wear and high friction has been one the several tools used by engineers to improve machines' life time.[20]

It is generally assumed that damage caused during sliding, commonly known as "abrasive friction", is due to a high friction force and, therefore, a large coefficient of friction. Accordingly, to prevent surface damage or wear one should aim to reduce the coefficient of friction, which has been the traditional focus of basic research into many bio and non-biolubrication systems. However, many biological and non-biological systems (especially involving soft polymeric surfaces) exhibit very complex behavior where the coefficient of friction and wear (abrasion) are not simply related, and sometimes even have an inverse relationship. Therefore, other factors, such as the surface structure, the lubricant distribution and conformation, and the lubricant-surface interaction are certainly more important than the coefficient of friction in determining the onset of wear.

Recent advances have suggested that using inspiration from nature, lubricating fluids or coatings could provide enhanced wear protection without any loss of lubrication.[21-22] The exceptional wear resistance and unparalleled lubricating properties of articular joints have motivated a lot of research aimed to unravel the molecular mechanism at the origin of joints tribological properties. Several design strategies aimed to enhance wear protection have emerged involving polymer brushes either in their molecular form as BB polymers,[23-26] or grafted on surfaces as polymer brush coatings.[27-31] Polymer brushes are known to provide excellent lubrication to surfaces *via* low interpenetration of polymer chains under compression.[32-33] Other mechanisms involving linear polymers mechanically trapped at the interface have also been suggested as a mechanism used by nature to maintain high wear resistance even under high compressive stress. All these strategies require the lubricating or wear protecting molecules to be strongly anchored to the surfaces in order to avoid close contact between the surfaces. Strong anchoring of molecules on surfaces requires a good knowledge of the chemistry and structure of the surface which complicates dramatically the translation of these technologies towards industrial settings.

In this study we show that it is possible to design lubricating fluids able to provide excellent wear protection without any chemical modification of the surfaces. The fluids use two

components, BB polymers shown in Figure 2.3A containing zwitterionic pendant chains synthesized by atom transfer radical polymerization, ATRP [14, 34] and a natural linear polymer, sodium hyaluronate (HA, Figure 2.3B). Both components are soluble in pure water or saline conditions.

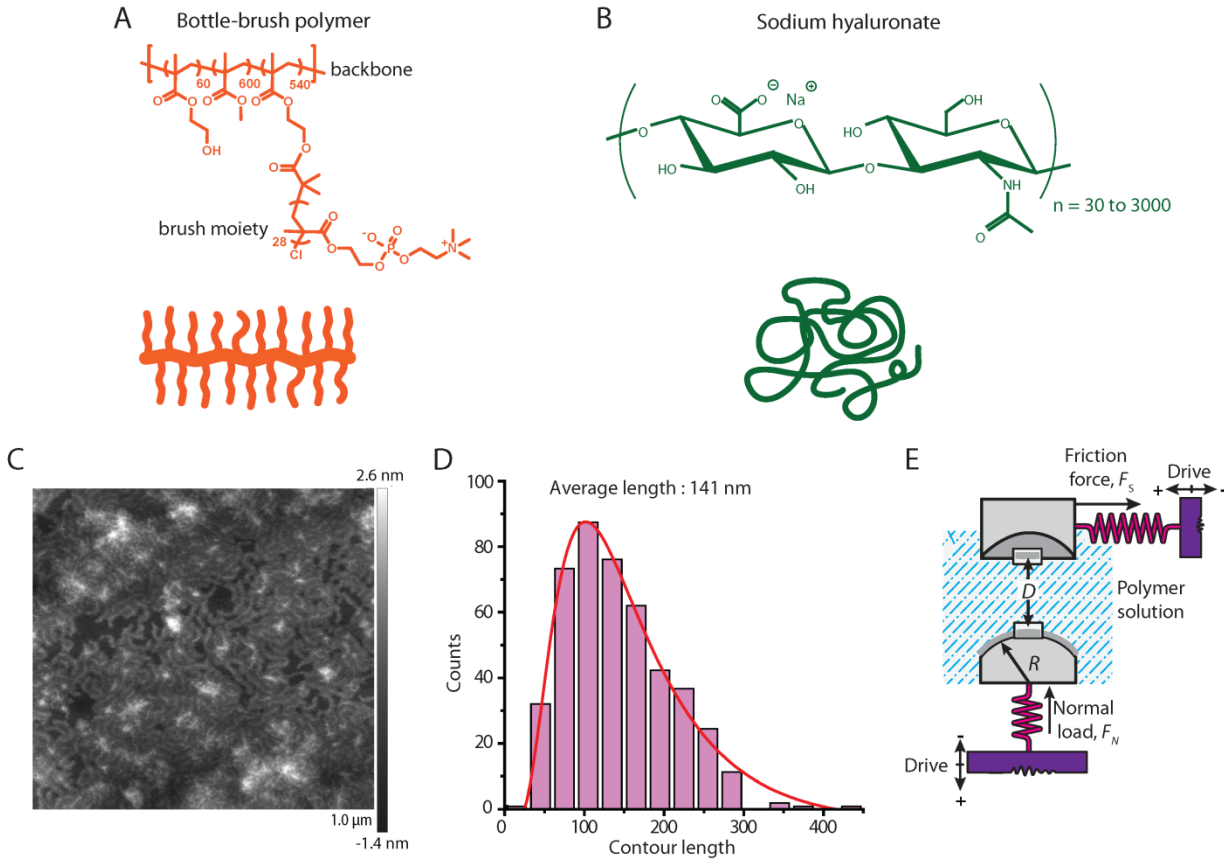

Figure 2.3. *(A) Schematic representation of the BB polymer and (B) the sodium hyaluronate polymers used in the present study; (C) Atomic force microscope image in air of the BB polymer deposited on mica and (D) its contour length distribution; (E) Mechanical equivalent of the experimental set up of the Surface Forces Apparatus in the used configuration.*

We used the surface force apparatus (SFA) to characterize the wear protection capacity and the lubricating properties of the fluids (see Figure 2.3E and materials and methods for procedures). The SFA allows measuring frictional forces over a wide range of pressure and sliding speeds while monitoring the separation distance between the surfaces at ± 0.5 Å resolution as well as the shape of the contact. Muscovite mica is the substrate of choice in SFA experiments mostly because of its optical transparency and atomic flatness. In our particular study, mica was used due to its extreme propensity to suffer damage under

moderate shearing conditions in water and saline conditions which makes it the perfect substrate to test wear protection.

2.2 Materials and methods

2.2.1 Materials

Methyl methacrylate (MMA, purity = 99%, Sigma-Aldrich, USA) and 2-(trimethylsilyloxy)ethyl methacrylate (HEMA-TMS, purity > 96%, Scientific Polymer Products Inc., USA) were passed through a column filled with basic alumina prior to use. 2-Methacryloyloxyethyl phosphorylcholine (MPC, purity ≥ 97%, Sigma-Aldrich, USA) was recrystallized from acetonitrile and dried under vacuum overnight at room temperature before polymerization. Tetrahydrofuran (THF) was used after it was purified by tapping off from a solvent purification column right. Ethyl α-bromoisobutyrate (EBiB, purity ≥ 98%, Sigma-Aldrich, USA), copper(I) chloride ($Cu^{I}Cl$, purity ≥ 99.995% trace metals basis, Sigma-Aldrich, USA), copper(II) chloride ($Cu^{II}Cl_2$, purity ≥ 99.995% trace metals basis, anhydrous, Sigma-Aldrich, USA), 2,2′-bipyridine (bpy, purity ≥ 99%, Sigma-Aldrich, USA), 4,4′-dinonyl-2,2′-bipyridine (dNbpy, purity ≥ 97%, Sigma-Aldrich, USA), potassium fluoride (KF, purity ≥ 99%, spray-dried, Sigma-Aldrich, USA), tetrabutylammonium fluoride (TBAF, 1M solution in THF, Sigma-Aldrich, USA) and α-bromoisobutyryl bromide (purity = 98%, Sigma-Aldrich, USA were used without any additional purification. Ruby mica-sheets were purchased from S&J Trading Inc. (Glen Oaks, NY, USA). Milli-Q quality water was obtained from a Millipore Gradient A10 S10 purification system (resistance = 18.2 MΩ.cm, TOC ≤ 4 ppb). Phosphate buffer saline (10mM Phosphate, 150mM NaCl and pH 7.4) was prepared in our laboratory. Hyaluronic acids of different molecular weights were obtained from Lifecore biomedical (Minneapolis, USA). Solvents were purchased from Aldrich and used as received without further purification.

2.2.2 Equipment and Analysis

Proton nuclear magnetic resonance (^{1}H NMR) spectroscopy was performed using Bruker 300 MHz spectrometer. In all cases deuterated chloroform ($CDCl_3$) was used as a solvent, except for bottle-brush polymer which was analyzed using deuterated methanol (CD_3OD). ^{1}H chemical shifts are reported in parts per million (ppm) downfield from tetramethylsilane (TMS). Apparent molecular weights and molecular weight distributions measurements of polymers except bottle-brush and hyaluronic acid polymers were measured by size exclusion chromatography (SEC) using Polymer Standards Services (PSS) columns (guar 10^5, 10^3, and 500 Å), with THF or DMF as eluent at 35°C at a constant flow rate of 1.00 mL/min, and

differential refractive index (RI) detector (Waters). The apparent number-average molecular weights (M_n) and molecular weight distributions (M_w/M_n) were determined with a calibration based on linear poly(methyl methacrylate) (PMMA) standards and diphenyl ether as an internal standard.

The properties of the different HA samples used in this study are summarized in the Table 2.1. Hyaluronic acid molecular weight and dispersity were assessed by aqueous SEC in 10mM PBS, pH 7.4, 150mM NaCl buffer using TSKgel columns (TSKgel G6000PW, particle size 17µm, and TSKgel G2500PW, particle size 12µm, Tosoh Bioscience LLC) at a constant flow rate of 0.5 mL/min, Multi-Angle static Light Scattering (DAWN HELEOS-II, Wyatt), and Refractometer (Optilab T-rEX, Wyatt). The absolute number-averaged molecular weights (M_n) and molecular weight dispersity (M_w/M_n) were determined with a dn/dc set at 0.16 mL/g.

Table 2.1: Properties of the different HA polymers used in this study

	M_w [g/mol]	Dispersity	R_g [nm][a]	
			10 mM[b]	150 mM
10kDa HA	1.16×10^4	1.26	-	16 ± 2
60kDa HA	5.97×10^4	1.43	-	33 ± 1
300kDa HA	3.25×10^5	1.54	71	69 ± 4
1.5MDa HA	1.32×10^6	1.44	220	154 ± 12

[a]Measured by static light scattering

[b]from ref. [35-36]

2.2.3 Bottlebrush polymer synthesis

A molecular bottlebrush with 50% grafting density of hydrophilic (phosphorylcholine-, **PMPC B2**) grafts was prepared *via* 'grafting from' approach (scheme 1). The backbone for the brush was synthesized through equimolar copolymerization of HEMA-TMS and MMA, resulting in the polymer (**B2**) with DP~1200. GPC characterization of **B2** showed the signal with M_n=132,000 and low dispersity M_w/M_n=1.16 (Figure 2.5, black). The subsequent functionalization of **B2** with ATRP functionalities yielded the macroinitiator (**B2 MI**) with M_n=163,000 and low dispersity M_w/M_n=1.15 (Figure 2.5, red). ^{1}H NMR analysis of **B2 MI** was used to determine the ratio of MMA and HEMA-TMS incorporated into the polymer (Figure 2.4), confirming incorporation of 50 mol % of HEMA-TMS into the backbone. The spectra showed incomplete functionalization of HEMA-TMS resulting in 40 mol % of ATRP

initiator sites in **B2 MI**. **B2 MI** was later used to graft hydrophilic side chains *via* ATRP, as shown on Scheme 2.1.

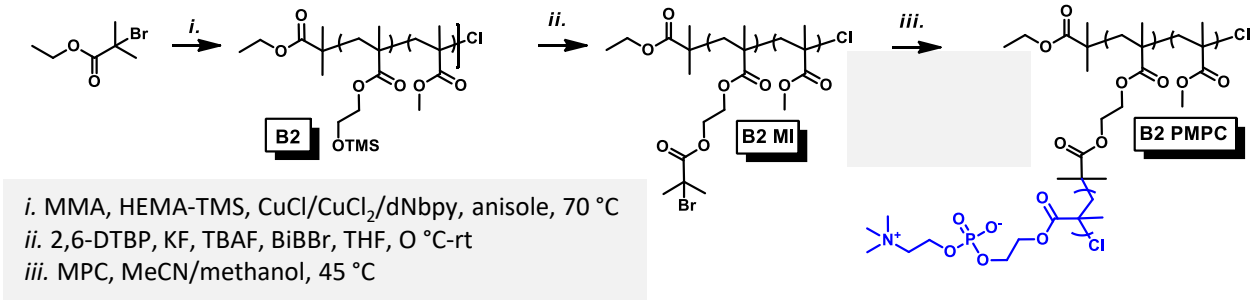

Scheme 2.1. *Synthetic pathways for the preparation of ABA bottlebrush copolymers with PMPC (**PMPC B2**) side chains.*

The grafting of hydrophilic PMPC side chains (**PMPC B2**) was performed in methanol/acetonitrile mixture (70/30, v./v. %) at 45 °C, yielding **PMPC B2** brush with the composition of (PBiBEM$_{540}$-*g*-PMPC$_{28}$)-*stat*-PHEMA$_{60}$-*stat*-PMMA$_{600}$.

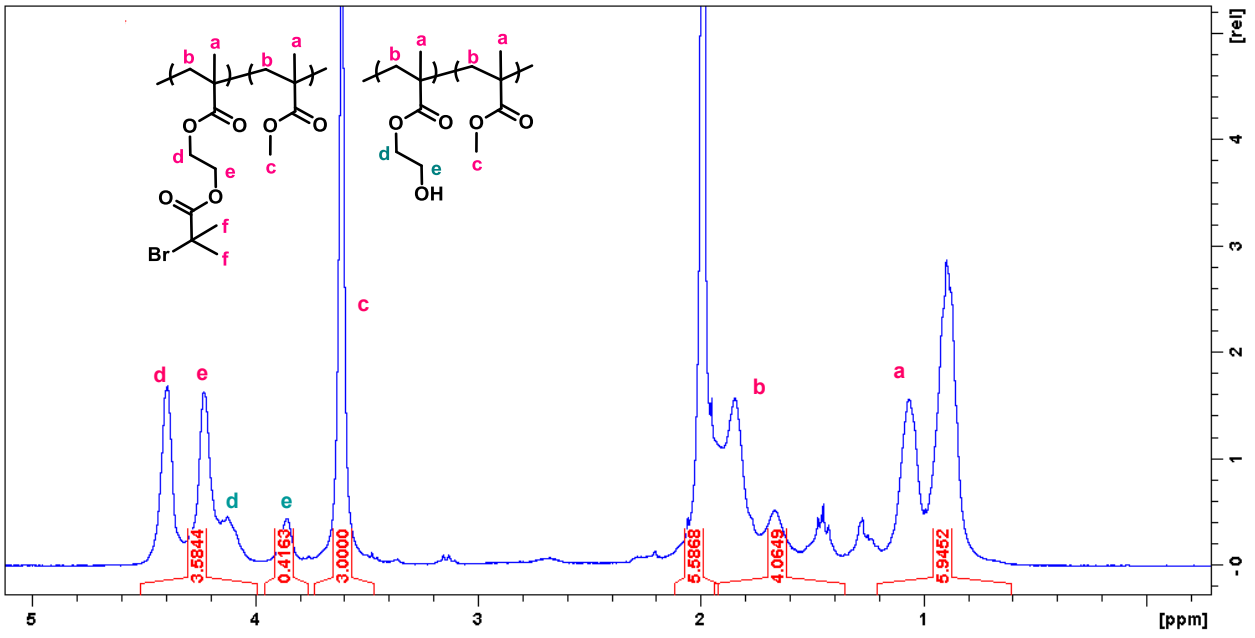

Figure 2.4. *^{1}H NMR spectra of PMMA$_{540}$-stat-PHEMA$_{60}$-stat-PBiBEM$_{600}$ (**B2 MI**).*

Synthesis of P(HEMA-TMS)$_{600}$-*stat*-MMA$_{600}$ (B2). A dry 25 mL Schlenk flask was charged with ethyl α-bromoisobutyrate (EBiB) (5.8 mg, 4.4 µL 0.030 mmol), $Cu^{II}Cl_2$ (3.1 mg, 0.023 mmol), dNbpy (0.113g, 0.276 mmol), HEMA-TMS (9.28g, 10.0 mL, 45.9 mmol), MMA

(4.59 g, 4.9 mL, 45.9 mmol) and anisole (3.2 mL). The solution was degassed by three freeze-pump-thaw cycles. During the final cycle, the flask was filled with nitrogen and $Cu^{I}Cl$ (11.4 mg, 0.115 mmol) was quickly added to the frozen reaction mixture. The flask was sealed, evacuated and back-filled with nitrogen five times, and then immersed in an oil bath at 70 °C. Reaction was stopped after 67 h *via* exposure to air, reaching the degree of polymerization 1200 for the final polymer. The monomers consumption was calculated by the integration of MMA and HEMA-TMS vinyl groups signal (C*H*H=C-CH_3, 6.11 ppm or 5.56 ppm) against the internal standard (anisole, *o*,*p*-Ar-H, 6.91 ppm). The product was purified by three precipitations from hexanes, dried under vacuum for 16 h at room temperature, and analyzed by ^{1}H NMR spectroscopy. The ratio of PMMA (*s*, broad, CO-O-C*H*$_3$, 3.54-3.68 ppm) to P(HEMA-TMS) (*s*, broad, OCO-*CH*$_2$-, 3.90-4.17 ppm) peaks resulted in the polymer composition: P(HEMA-TMS)$_{600}$-*stat*-PMMA$_{600}$. Apparent molecular weights were determined using PMMA standards in THF GPC: M_n = 132,000 and M_w/M_n = 1.16 (black, Figure 2.5).

Synthesis of PBiBEM$_{540}$-*stat*-PHEMA$_{60}$-*stat*-PMMA$_{600}$ (B2 MI). The polymer, **B2**, (3.00 g, 0.017 mmol of polymer; 9.90 mmol of HEMA-TMS units), potassium fluoride (0.701 g, 11.9 mmol) and 2,6-di-*tert*-butylphenol (0.204 g, 0.99 mmol) were placed in a 100 ml round bottom flask. The flask was sealed, flushed with nitrogen, and then dry THF (30 mL) was added. The mixture was cooled in an ice bath to 0 °C, tetrabutylammonium fluoride solution in THF (1M, 0.05 mL, 0.05 mmol) was injected into the flask, followed by the drop-wise addition of *α*-bromoisobutyryl bromide (2.73 g, 1.50 mL, 11.9 mmol). After the addition the reaction mixture was allowed to reach room temperature and stirring was continued for 16 h. Next, triethylamine (1.0 mL) and another portion of *α*-bromoisobutyryl bromide (0.4 mL) were added, and the mixture was stirred for another hour. The solids were filtered off, and the solution was precipitated into methanol:water (70:30, v/v%). The precipitate was re-dissolved in chloroform and passed through a short column filled with basic alumina. The filtrate was re-precipitated three times from chloroform into hexanes and dried under vacuum overnight at room temperature. Apparent molecular weights were determined using PMMA standards in THF SEC: M_n=163,000 and M_w/M_n=1.15 (red, Figure 2.5).

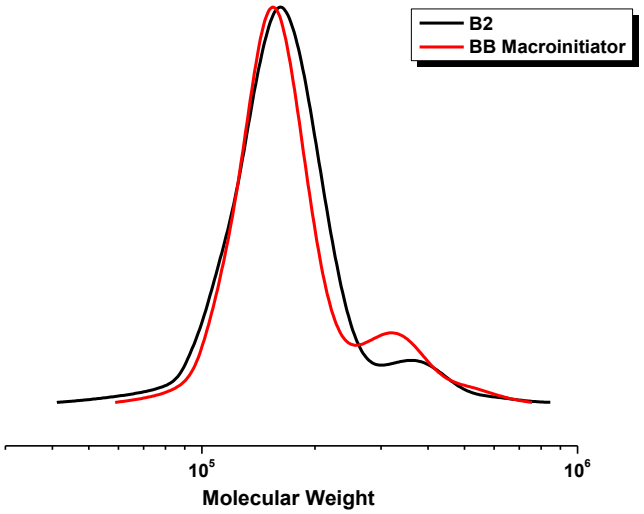

Figure 2.5. *GPC traces recorded for (black)* ***B2*** *and (red)* ***B2 MI****.*

Synthesis of (PBiBEM$_{540}$-*g*-PMPC$_{28}$)-*stat*-PHEMA$_{60}$-*stat*-PMMA$_{600}$ (PMPC B2). A dry 10 mL Schlenk flask was charged with polymer macroinitiator (**B2 MI**) (0.0059, 0.0124 mmol of BiBEM groups), 2-methacryloyloxyethyl phosphorylcholine (MPC) (1.10 g, 3.73 mmol), bpy (0.0066 g, 0.0422 mmol), $Cu^{II}Cl_2$ (0.33 mg, 2.5 µmol), and acetonitrile/methanol (1.0 mL/2.5 mL). The solution was degassed by three freeze-pump-thaw cycles. The flask was sealed, evacuated and back-filled with nitrogen and then immersed in an oil bath thermostated 45 °C Then the degassed $Cu^{I}Cl$ solution in methanol (18.4 mg, 18.6µmol in 1.0 mL methanol) was added to the reaction mixture. The polymerization was stopped after 1.25 h by expositing the solution to air, achieving the brush with DP~28 of PMPC side chains as determined by ^{1}H NMR. The brush was purified by dialysis against methanol using a 25,000 MWCO membrane. **PMPC B2** brush was obtained as white powder. GPC characterization was not performed due to the unavailability of water GPC system. PMPC B2 brush was obtained as white powder.

2.2.4 Surface Forces Measurements

Formulation of polymer mixtures: 10.0 mg of different molecular weight HA were dissolved with magnetic stirring in 10 mL Milli-Q water or 10 mM PBS pH 7.4 in a glass vial. The solution was kept at 4°C for 24 h prior to use. 1 mg/mL solution of BB polymer was prepared in the same buffers. 50 µL of the polymeric solution was added to 450 µL of HA solution

corresponding to a solution of BB polymer at 100 µg/mL and HA at 0.9 mg/mL and was homogenized with a vortex for 1 min. The solution was centrifuged at 14,000 rpm during 10 min to remove aggregates or particles if any. For each SFA analysis, 50 µL of fluid was injected between the surfaces. Surfaces were then let to equilibrate for 1h prior to the measurements.

Normal Interaction Forces: Measurements of the normal interaction forces between two opposing surfaces as a function of the separation distance were carried out using a Surface Forces Apparatus. The normal interaction force F_N is determined by measuring the deflection of the spring cantilever (spring constant of 482 N/m) supported by the lower surface. The distance between the surfaces is measured using Multiple Beam Interferometry. The two disks were mounted in the SFA chamber in cross cylinder geometry and brought into mica-mica adhesive contact in dry air in order to determine the reference position. Afterward, the cylindrical disks were separated by roughly 1 mm and the polymer solution was injected between the surfaces. Immediately after injection, the bottom of the SFA chamber was filled with water in order to saturate the surrounding vapors and to limit evaporation of the injected liquid. The normal interaction forces between the two polymer coated surfaces as a function of surface separation were determined on approaching (compression) and separating (decompression) the surfaces. For each test, all force runs (in and out) were performed at least in triplicate with the motor or the piezoelectric tube at a speed range of 0.4 to 1.6 nm/s. Each experiments were reproduced two to six times.

Friction Force Measurements: The friction force F_s was measured by moving the lower surface horizontally and measured the response of the upper surface. Before measuring the friction forces, three cycles of normal compression/decompression were performed on the same contact position. For friction tests, a piezo bimorph drove the lower surface in a back and forth motion at a constant sliding frequency of 50 mHz controlled by a function generator. The friction force transmitted to the upper surface was detected by semi conductive strain gauges, and digitally recorded. Acquired data were processed using Origin® software. Separation distance and surface deformation were continuously recorded during the experiment using the FECO fringes analysis.

2.2.5 Chitosan gels and tribotesting.

A 2.5%w/w chitosan solution (M_w $6.04.10^5$, Mw/Mn 1.64, DA 4.3%) was prepared by dissolving the polymer in an aqueous acetic acid solution. Air bubbles were removed by

centrifugation and the highly viscous solution was compression-molded to obtain a slab of constant thickness. The chitosan solution was then placed in a 1 M NaOH coagulation bath to complete gelation. Gel disks of 11 and 21 mm in diameter were obtained using biopsy punchers and neutralized in pure water until use. For the tribo-testing experiments, the 11 mm diameter gel disk was glued on the top mobile part of a custom-made tribometer. The larger gel disk was glued on a metallic immobile bath filled with the tested polymer solution and left to incubate for 1h prior to experimentation. Normal and tangential forces were recorded and analyzed with a home-made routine programmed in labview®. Roughness of the gels was quantified after performing tribo-testing using an interferometric microscope.

2.2.6 Microcalorimetry experiments

Isothermal titration calorimetry of the BB polymer in different polymer solutions was performed using a VP ITC from MicroCal. running on Origin(R) 7. In the syringe, a buffered BB polymer solution was loaded at a concentration of 0.6 mg/mL and in the receptor cell, a buffered solution of HA or PVP at 1 mg/mL was loaded. All solutions have an ionic strength of 150 mM and were degased prior use. Experiments consisted in 25 injections of 10 uL each in the receptor cell (1.42 mL) at an injection speed of 2 uL/s and agitation speed of 300 rpm.
As a control, the BB polymer solution was also titrated in buffered saline to obtain the dilution heat of the polymer.

2.3 Results and Discussion

2.3.1 Interaction profiles

We first measured the normal interaction forces, F_N, between two facing mica surfaces of curvature R, in presence of the different components of the lubricating fluids, first individually and then mixed together (Fig. 2.6). To cover a wide range of conditions, we tested different HA molecular weights, M_w, in pure water and in phosphate buffer salines (PBS 150 mM for low ionic strength, and 1500 mM NaCl for high ionic strength, both at pH = 7.4). The interaction forces were recorded as a function of the separation distance, D, between the surfaces starting from several hundreds of nanometers (zero interaction regime) down to a few angstroms (strong interaction regime) in order to capture the full interaction force profile (force law) of the system.

In Figures 2.6A and 2.7 are shown the force profiles measured in HA solutions in pure water and in saline buffers. HA being negatively charged under all tested conditions, it is expected

to adsorb as a random coil on negatively charged mica surfaces through the formation of hydrogen bonds. As shown in Figure 2.6A, force profiles present two distinctive trends, depending on the ionic strength of the medium. In pure water, the onset of the interaction forces was located between 20 and 30 nm independently of the molecular weight of HA (Fig. 2.7). Such weak dependence on the molecular weight suggests that during the time window of the experiment, only low molecular weight chains could adsorb on the surfaces (a case similar to the Vroman effect). Low molecular weight molecules are expected to adsorb first on mica surfaces, since they are more mobile. Later, larger molecules which have higher affinity for the surface, are expected to displace them. In saline, the interaction forces exhibited shorter range forces starting between 5 to 10 nm. These short range interaction forces systematically presented periodic instabilities indicating the presence of a layered structure at the surfaces (see inset of Fig. 2.6A). The characteristic size ΔD of these instabilities was ΔD = 0.2-0.3 nm in agreement with the size of a water molecule. Adhesive forces were systematically measured upon separation of the surfaces independently of the medium (pure water or saline).

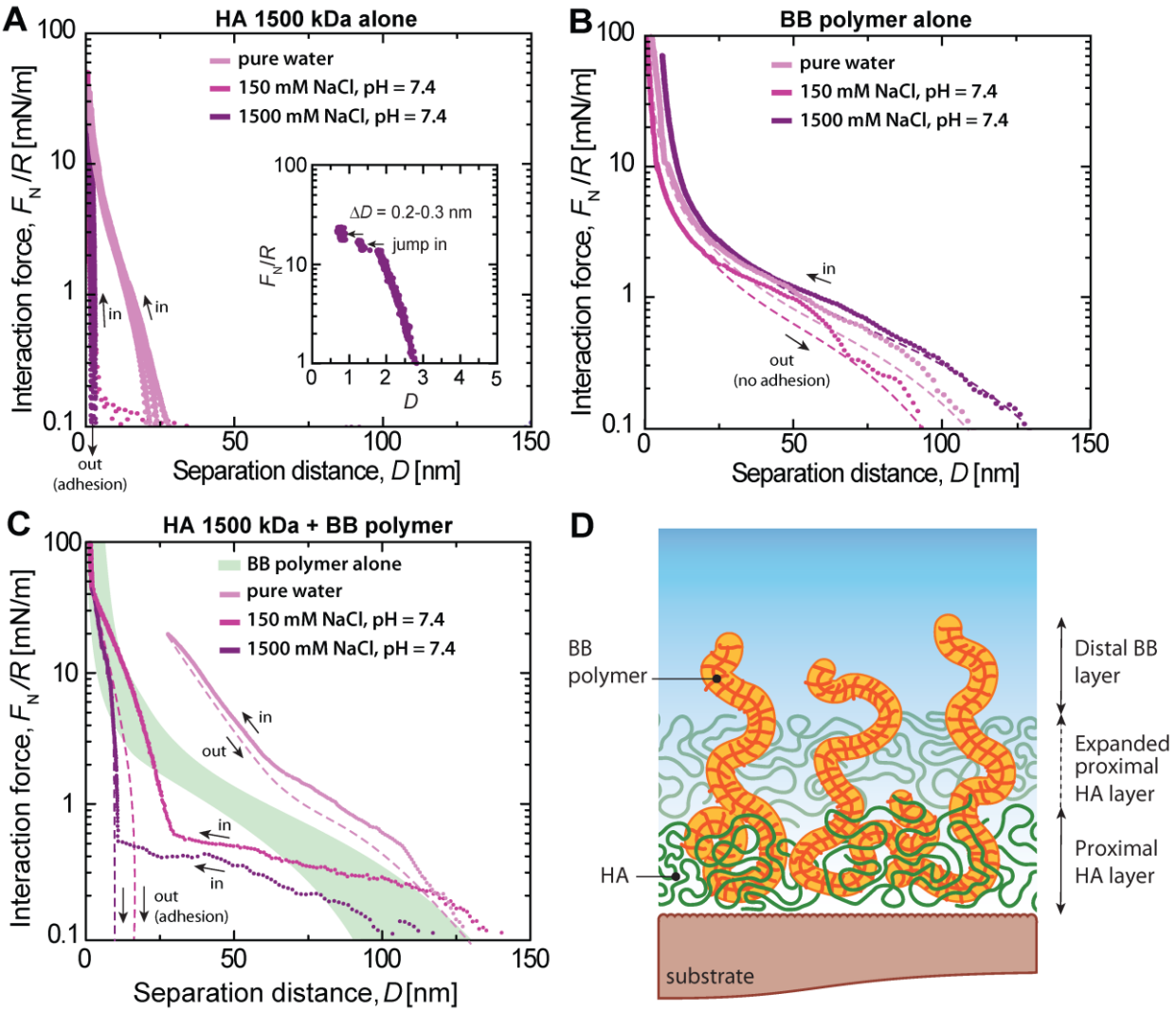

Figure 2.6. *Interaction force profiles measured across (A) HA solution (1mg/mL) at increasing ionic strength. Inset is an expanded view of the force profile at 1500 mM NaCl showing characteristic step-like instabilities in the interaction forces indicating the presence of a layered structure in the confined space; (B) BB polymer solution (0.1 mg/mL) at increasing ionic strength; (C) Mixture of BB polymer and HA 1500 kDa at different ionic strength. (D) Schematic representation of the interfacial polymer layer in presence of HA and BB polymers.*

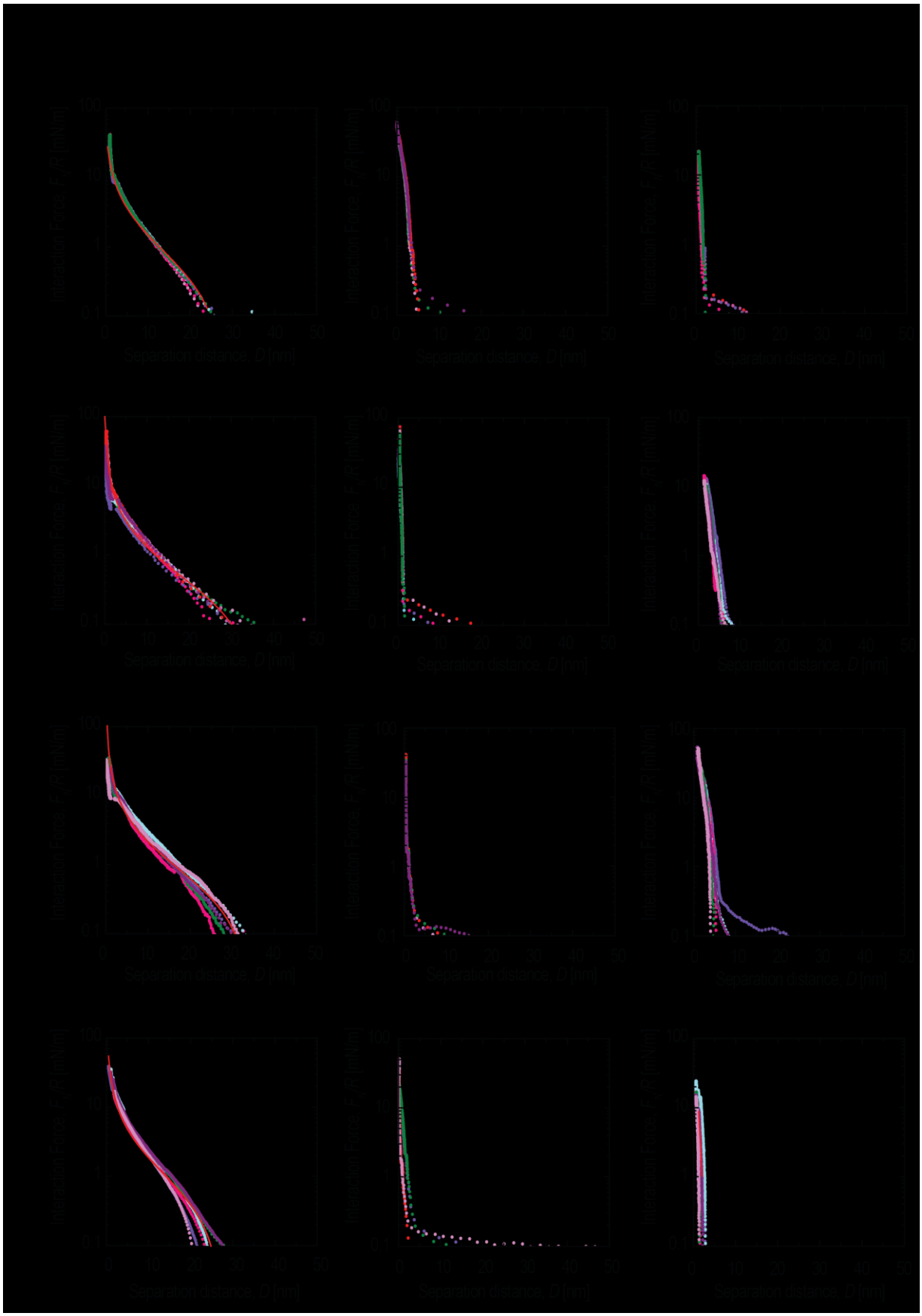
Interaction Force, F/R [mN/m]
Separation distance, D [nm]

Figure 2.7. *Interaction forces measured in presence of HA (1 mg/mL) in different media. Out run (forces measured upon separation) are not represented for clarity but presented systematically weak adhesion.*

These observations demonstrate that under the present experimental conditions, HA does not strongly bound to the mica surfaces in saline due to the presence of a 2 to 3 nm thick hydration layer strongly interacting with the surface, while in pure water, the polymer can adsorb strongly and form a stable soft layer.

Interaction forces in presence of the BB polymer alone were strikingly different from HA polymer alone (Fig. 2.6B). Repulsive forces were measured on approach and separation of the surfaces, independently of the ionic strength of the medium. More interestingly, the force profiles were insensitive to the ionic strength of the medium. Interestingly, the conformation of linear polymer chains of MPC has been reported to be insensitive to the ionic strength in solution[5], and at surfaces.[37] The onset of the interaction forces (determined at F_N/R = 0.01 mN/m) was found to vary between 100 nm and 125 nm, independently of the medium ionic strength (Fig. 2.6B). Given that the contour length of the polymer, assessed by AFM imaging in air (Fig. 2.3D), is ~140 nm, a significant part of the BB polymer is expected to be extending towards the medium.

Interaction forces under high confinement (D < 10 nm) did not present any layering transition or any evidence of hydration forces which confirms that the BB polymer interacts strongly with the hydrated surface layer, strongly enough to displace the water molecules present at the surface. Such observations echoes some reports showing that charged amine head groups adjacent to H-bonding donors groups can efficiently remove bound water from a hydrated surface and facilitate H- bonding.[38-39] No adhesive forces were measured upon separation of the surfaces.

Interaction forces across HA-BB polymer mixtures in saline presented similar features to BB polymer alone (Fig 2.3C and 2.8). Exception made of the mixture containing HA 10 kDa, the onset of the interaction forces measured for the different polymer mixtures ranged between 120 nm and 180 nm depending on the medium, which is similar to the onset measured with the BB polymer alone and at least twice the value measured for any of the tested HA alone solutions. Below a separation distance $D \approx 50$ nm, a steep increase in the interaction forces was systematically observed suggesting the presence of a dense/stiff layer of polymer at the

surfaces. The thickness of this dense (proximal) polymer layer, was found to be highly sensitive to the ionic strength of the medium. Based on the force profiles, the thickness of the proximal layer can vary from approximately 20 nm at 150 mM NaCl to 5 nm at 1500 mM NaCl. No adhesive forces were measured if the surfaces were separated at D > 50 nm (in the distal region of the interaction profile) while weak adhesive forces were systematically observed when separating the surfaces at D < 50 nm. These observations confirmed that the proximal layer contains mainly HA.

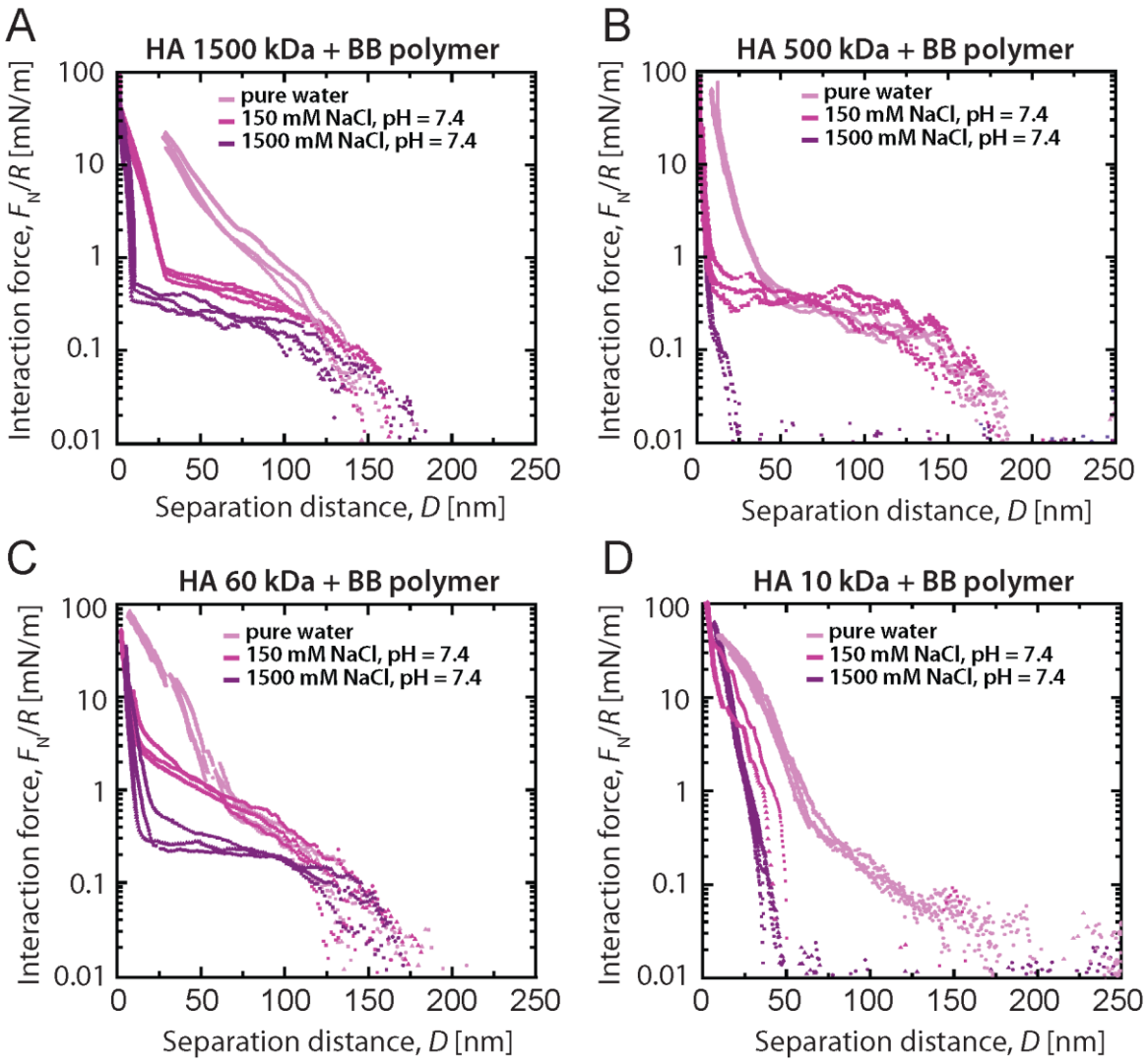

Figure 2.8. *(A-D) Interaction forces between mica surfaces across mixtures of HA and BB polymer and fitting of the long and short range forces with a two layers (proximal-blue and distal-red) model.*

These force profiles demonstrate that the polymer mixtures form an interpenetrated layered thin film as represented in Figure 6D. The proximal layer of such film contains most of the

HA molecules adsorbed at the surface and portions of BB polymer chains while the distal layer is composed solely of BB polymer molecules extending in the medium.

In pure water, the force profiles of the different mixtures did not exhibit any marked transition between the HA-rich proximal layer and the BB polymer distal layer. Instead, the force profiles show a continuous increase, consistent with an extended proximal layer fully overlapping with the distal layer.

2.3.2 Lubrication properties

After measuring the normal interaction forces in the different media, we characterized the tribological properties of the different polymer mixtures. In a first series of experiments, we measured the friction force, F_S, as a function of the applied normal force F_N (Fig. 2.9). For all the tested conditions, the friction force, F_S, was found to increase linearly with F_N until damage of the surfaces occurred (Fig. 2.9A). We therefore defined the friction coefficient of our system as $\mu = F_S/F_N$. In saline only (no polymer added), frictional forces were very weak (not shown), giving a friction coefficient of $\mu = 0.002 \pm 0.001$ (Fig. 2.9B), in good agreement with previous reports.[40] Using optical interferometry,[41] we measured the critical pressure, P^*, at which the onset of surface damage was triggered. Onset of damage appeared as sudden cracks formation and propagation along the direction of shearing. We found a value of $P^* = 0.73 \pm 0.03$ MPa for both saline conditions. We also found that μ increased two orders of magnitude after damage occurred and ranged between 0.2 and 0.7, as shown in Figure 2.9B. On the other hand, in pure water, damage of the surfaces occurred almost immediately after a few shearing cycles indicating that $P^* \approx 0$ MPa. The present results echo recent studies demonstrating that, in saline medium, surface adsorbed ions facilitate the formation of a lubricating water layer able to sustain a significant amount of normal pressure under shear and therefore protecting the surfaces from damage.[42-43]

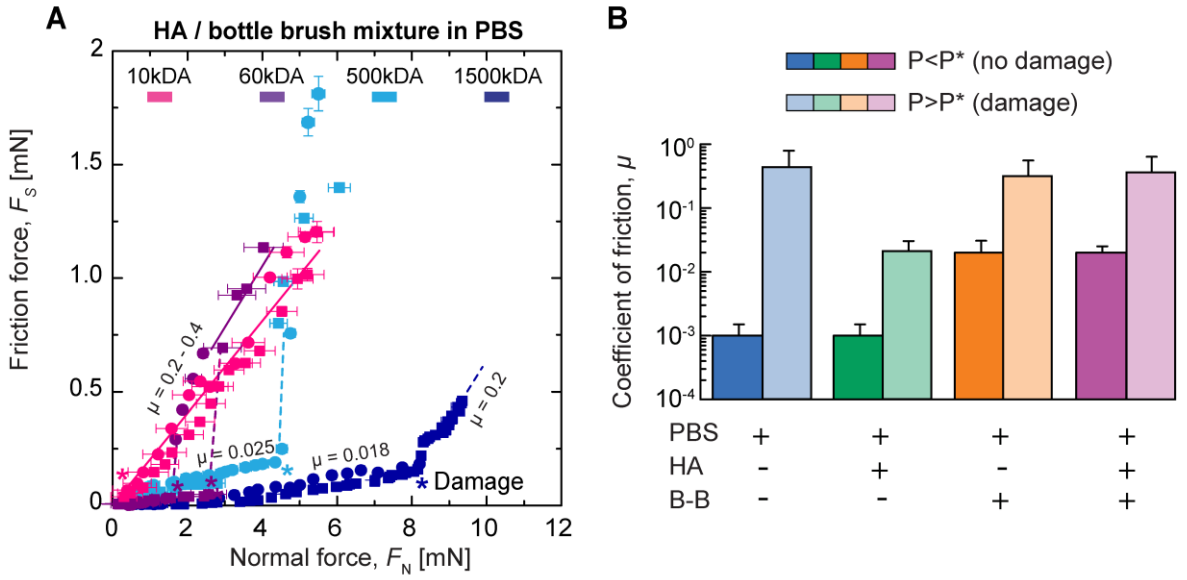

Figure 2.9. *(A) Tribological testing of the BB (0.1 mg/mL) and HA (1mg/mL) polymer mixtures in PBS (150 mM NaCl) performed at a sliding speed of 3 µm/s. (B) Measured friction coefficients in saline (150 mM and 1500 mM NaCl) before and after damage in presence of BB and HA polymers, alone and mixed together. Onset of damage is indicated by * symbol.*

In presence of HA, the measured values of µ in saline before damage ($P < P^*$) were found to be independent of the molecular weight of the polymer (Fig. 2.9B) and close to the values found in saline only ($\mu_{PBS} \approx 10^{-3}$). Measurements of the thickness and refractive index of the confined film before damage shows that the contact area is quickly depleted of polymer leaving only adsorbed ions and water molecules at the interface (Fig. 2.10). As the applied pressure increases with time the film thickness decreases and concomitantly the refractive index of the confined film increases slightly from 1.33 (bulk water) up to ~1.47. Experiments performed in PBS and in buffered HA present the same trend suggesting that HA is quickly depleted from the contact as the normal pressure is applied.

The value of P^* for HA was $P^* \approx 0.7$ MPa independently of its molecular weight, which is identical to the value encountered in saline only and consistent with the previous observation of HA being depleted from the contact before damage occurs. In pure water, HA solutions demonstrated very poor stability and systematically lead to the formation of polymer aggregates in the shearing contact. These polymer aggregates lead to focal pressure increase throughout the contact area and eventually triggered crack formation. As a consequence, the

measured value of $P^* \approx 0$ MPa even though $\mu = 0.02$ for all the M_w tested after damage occurred.

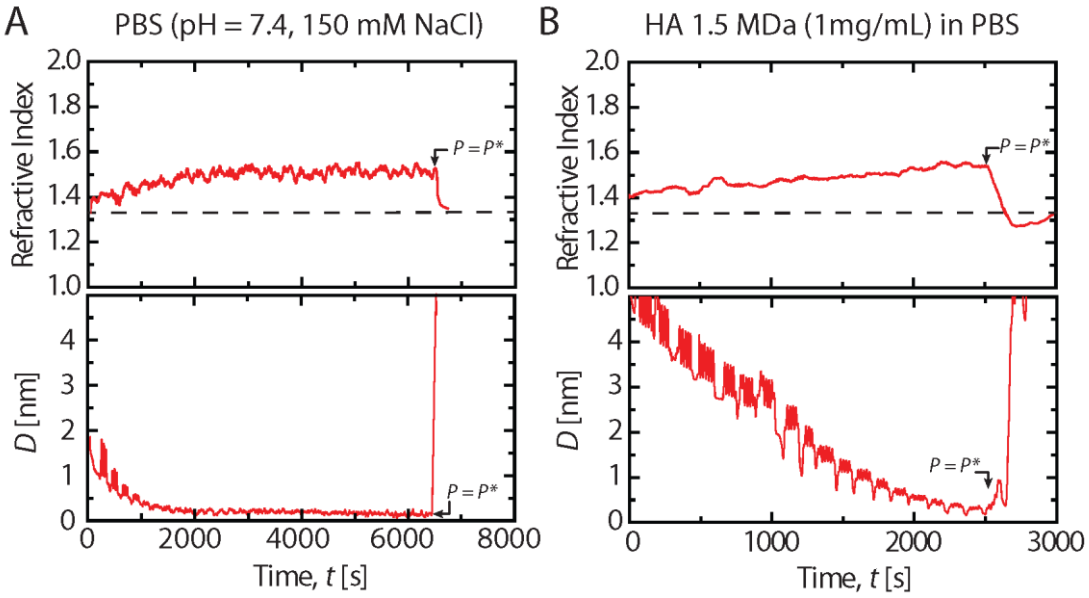

Figure 2.10. *Measurement of the film thickness and refractive index during shear (v_s = 3 µm/s). The film thickness D decreases gradually due to the increase of the normal pressure/load during the course of the experiment. When P = P*, damage of the surfaces occurs abruptly as shown by the rapid increase in D. Shearing speed v_s = 3 µm/s*

Frictional properties of the BB polymer alone in pure water and saline were drastically different from HA or saline alone (Fig. 2.9B). The measured friction coefficient µ before damage was one order of magnitude higher than HA or saline alone and was equal to $\mu = 0.03 \pm 0.01$, independently of the ionic strength of the medium. This result is consistent with the previous observation from the normal force profiles showing that BB polymer adsorption and conformation on mica was independent of the ionic strength. In saline and pure water, the measured values of P^* were 0.25 ± 0.02 and 0.56 ± 0.04 respectively, which is lower than HA and saline alone under similar conditions.

As shown in Figure 2.9A and B, mixing HA and the BB polymer did not improve significantly the lubricating properties of the surfaces. The measured friction coefficient of the different mixtures before damage ($P < P^*$) was independent of HA molecular weight and equal to $\mu = 0.02 \pm 0.01$, independently of the medium's ionic strength. This observation

suggests that the friction coefficient of the mixture is solely controlled by the presence of the BB polymer when $P < P^*$.

Most interestingly, the value of P^*, which relates to the wear protection capacity of the polymer mixture, was highly sensitive to HA molecular weight. As can be seen in Figure 11A, for mixtures of final concentration 100 µg/mL of BB polymer and 1 mg/mL of HA (1:10 mass ratio), P^* increased significantly with HA molecular weight as $P^* \propto \log(M_w)$. In pure water, the HA - BB polymer mixture lead systematically to a significant increase in wear protection, especially at high HA molecular weight, with P* increasing from 0 MPa in absence of BB polymer to 3.2 MPa in presence of BB polymer. A similar trend was observed in saline solutions, with a two fold increase of P^* at the highest HA molecular weight in presence of the BB polymer.

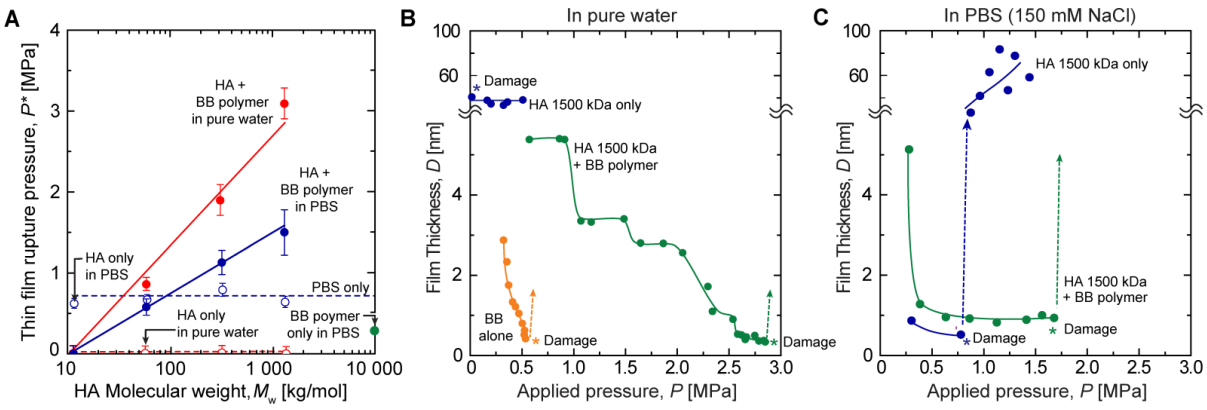

Figure 2.11. *Synergistic enhancement of wear protection using HA and BB polymer mixtures. (A) The thin film rupture pressure P* was measured in presence of 1mg/mL HA solution mixed with a 0.1 mg/mL BB polymer solution at a sliding speed of 3 µm/s. The value of P* for each of the component alone was below the value of pure PBS independently of HA molecular weight, while the mixtures presented significantly higher value of P*, especially at high HA M_w. (B-C) Measurements of the thin film thickness during shear in pure water and in PBS shows that the polymer mixtures are able to sustain significantly more pressure compared to the polymers alone and in a M_w-dependent manner.*

To obtain more insights into the mechanism underlying such phenomenon, we monitored the evolution with shearing time of the film thickness under different shearing conditions. Figure 11B shows that, as the normal pressure P is increased, the film thickness, D, increases dramatically when the medium contains HA only in pure water, indicating the immediate

aggregation of the polymer and the triggering of surface wear. In saline (Fig. 2.11C and 2.10), the data show that HA is quickly depleted from the contact leading to a rapid decrease of *D* down to 0.5 nm before damage occurs at $P = P^*$.

In presence of BB polymers alone, the film thickness at $P = P^*$ was 1 nm for both saline conditions which is thicker than the previously mentioned value obtained for HA solutions. Such high value of the film thickness indicates that BB polymer chains are still present in the contact at the onset of wear. Similar observations were confirmed with the different polymer mixtures, although the values of P^* were significantly higher than BB or HA alone (Fig. 2.11B and C). The significant increase of P^* in the case of the polymer mixtures correlates with the higher film thickness at the onset of damage which indicates the existence of strong intermolecular interactions between HA and the BB polymer. Such interactions maintain a strong cohesion between the different polymer chains under shearing conditions and allows the confined film to sustain significantly more normal pressure.

2.3.3 Mechanisms and proof of concept

To elucidate the nature of the interactions responsible of such strong intermolecular cohesion, we performed a series of isothermal titration calorimetry experiments (Fig. 2.12). No thermal signature was measured during mixing of the polymers indicating that no detectable interaction (electrostatic or hydrophobic) exists between the two polymers. Therefore, the important role played by HA molecular weight in tuning the cohesive strength of the film demonstrate that chain entanglements are the main factor responsible for the polymer film cohesion (Figure 2.13).

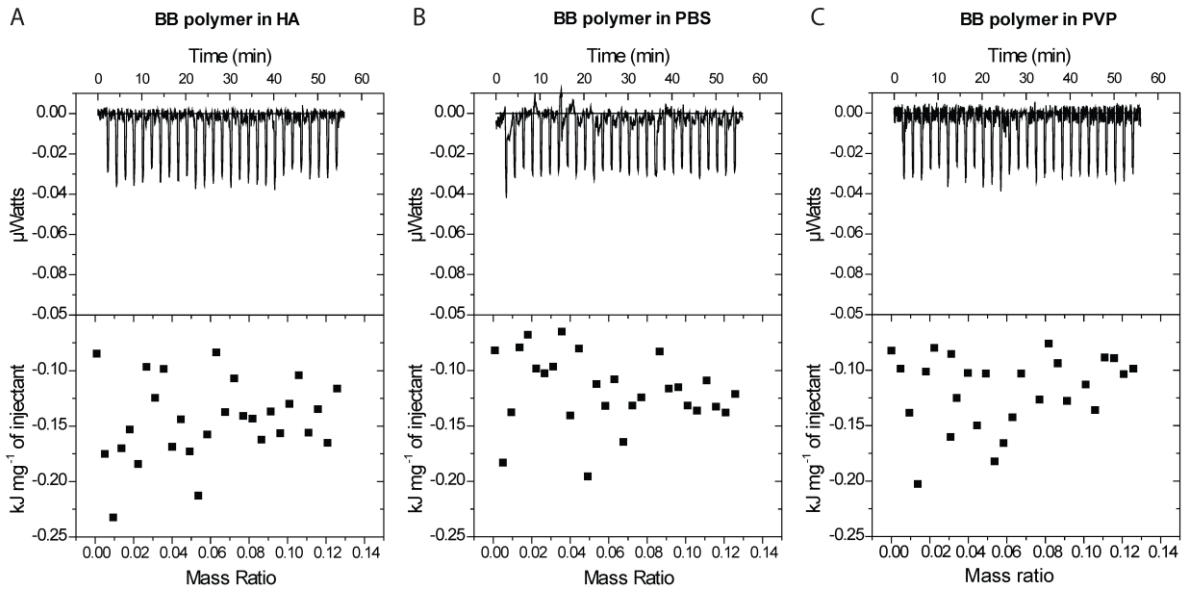

Figure 2.12. *Differential power (top panel) and integrated released heat (lower panel) recorded during the titration of BB polymer into A) HA in buffered saline; B) buffered saline; C) PVP in buffered saline.*

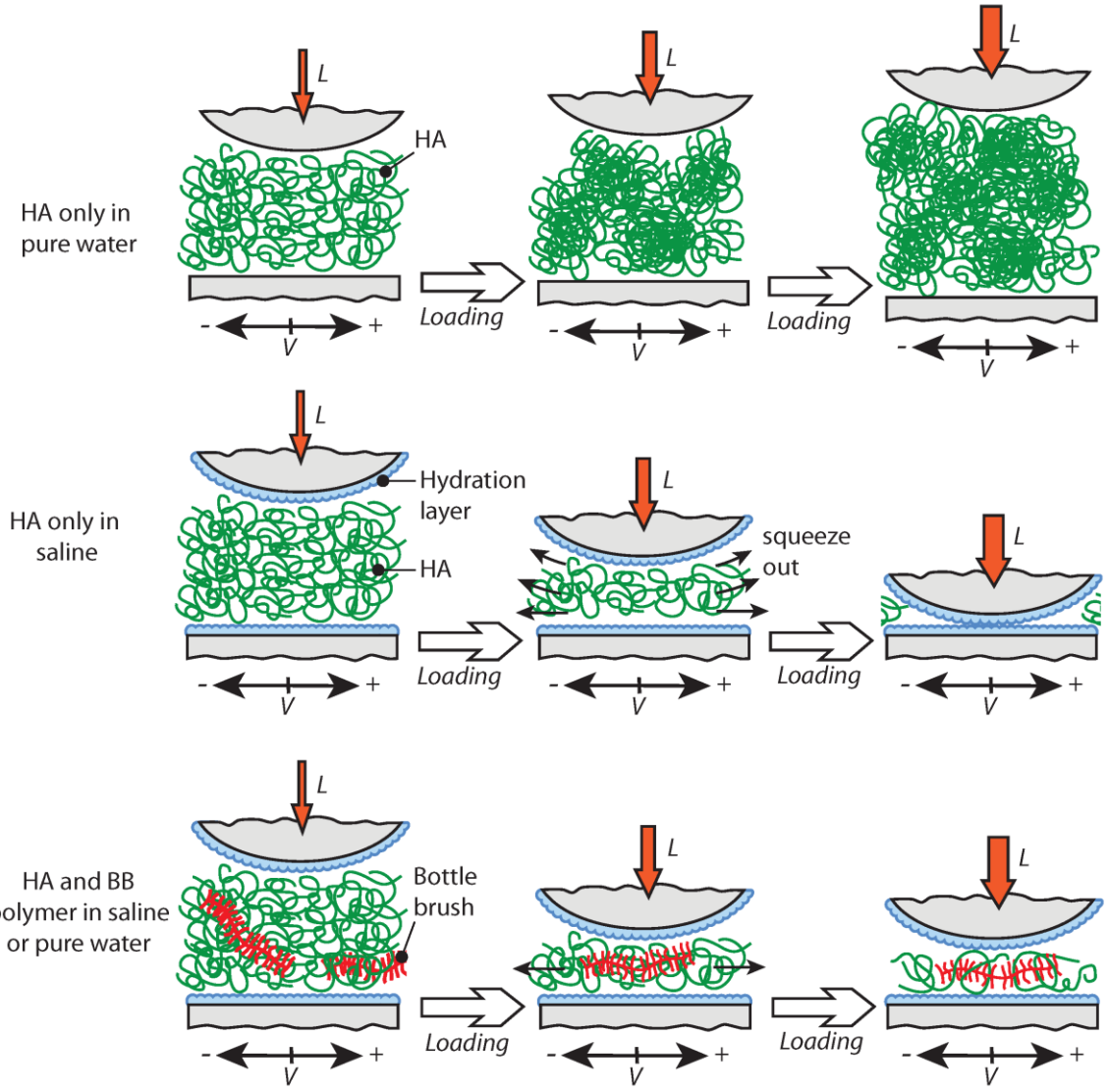

Figure 2.13. *Schematic representation of the wear protection mechanism observed in presence of the mixture of HA and BB polymers in pure water and in saline.*

In order to demonstrate the generality of the mechanism and its broad application, we performed a second series of tribological tests to establish the impact of shearing speed, BB:HA polymer ratio, polymer chemical structure and surface chemistry (Fig. 2.14). As shown in figure 2.14A, varying the sliding speed over three decades, between 0.01 and 10 µm/s at $P < P^*$, did not trigger any damage of the surfaces indicating a weak dependence, if any, of P^* on the sliding speed. In figure 2.14B, we show that P^* depends strongly on BB:HA

ratio and is optimum at a ratio of BB:HA = 1:10 (mg/mg). Above this optimum ratio, the value of P^* is equal to the value of HA alone indicating that HA has displaced the BB polymer from the surface. Below the optimal ratio, the value of P^* is equal to the value obtained for BB alone indicating that BB polymer is the sole component in the confined film. A similar synergistic behavior between BB polymer and HA was also observed when replacing HA by poly(N-vinylpyrrolidone) (PVP), a neutral, water soluble polymer (M_w = 40 kDa). Figure 2.14C shows that the value of P^* in saline (150 mM, pH = 7.4) exhibits a 2 fold increase with a 1:10 mixture ratio of BB:PVP compared to PVP alone. Similarly to HA, PVP did not show any direct interaction with the BB polymer by ITC (Fig. 2.12). The HA - BB polymer mixture was tested against mica-gold tribo-pair as well. Gold being a ductile metal, its tribological properties are very poor in terms of wear resistance (Fig. 2.14D). For the tribo-pair mica / gold, P^* was inferior to 1 MPa in presence of HA or BB polymer alone. As shown in Figure 14D, the polymer mixture was once again significantly more efficient in protecting the surfaces compared to the single components alone.

In all the tested conditions, the value of P^* associated to the polymer mixture is systematically superior to the sum of the value associated to the polymers alone indicating a true synergistic interaction between both components in terms of wear protection.

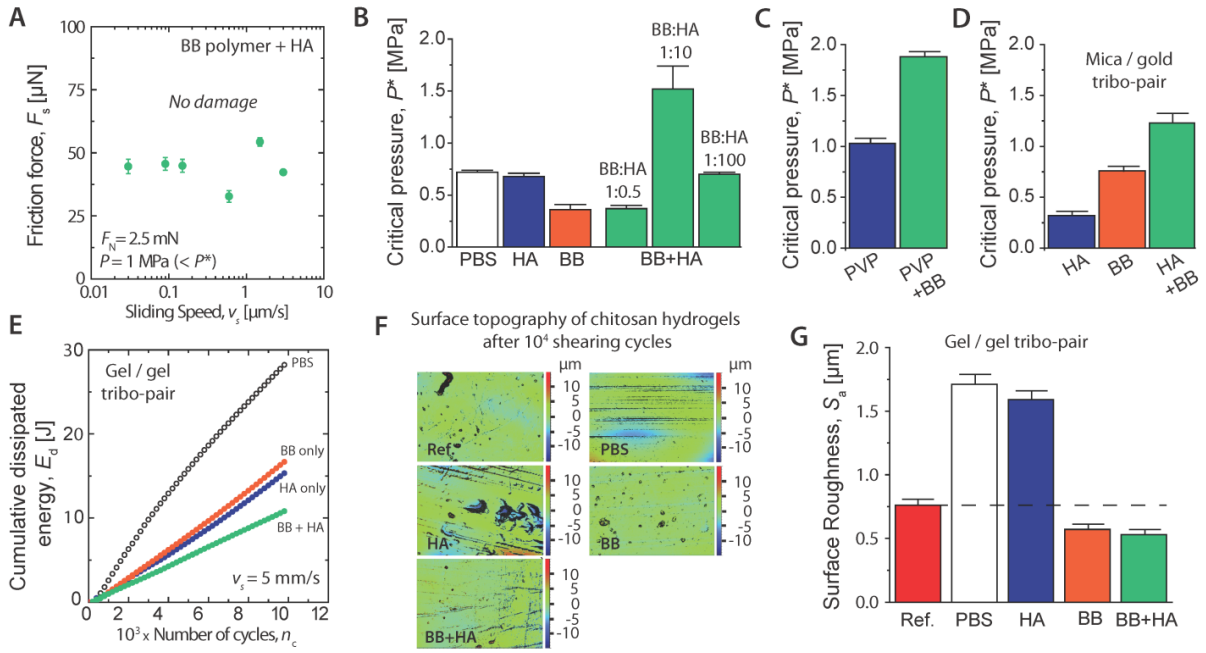

Figure 2.14. *A) The wear protection imparted by the BB polymer - HA mixture was not affected by the sliding speed of the surfaces. At a pressure of 0.5P*, no damage of the surfaces was observed even when varying the sliding speed by three orders of magnitude; B)*

The BB:HA (1.5 MDa) ratio has a significant impact on P and was found to be optimum at 1:10; C) HA can be replaced by PVP to obtain similar synergistic wear protection when mixed with the BB polymer; D) The BB polymer - HA mixture was tested with mica-gold tribo-pair demonstrating similar wear protection enhancement compared to mica-mica. E) Cumulative dissipated energy generated during shearing of two 2.5 w% chitosan hydrogel plugs, lubricated with different polymer solutions. F and G) Interferometric micrographs and associated surface roughness of the hydrogel plugs after 10^4 shearing cycles at 5 mm/s (shearing amplitude of 5 mm, applied pressure P = 50 kPa).*

We finally tested the lubricating fluids between macroscopic hydrogel plugs of chitosan as model soft polymeric surfaces (Fig. 2.14E-G). Chitosan hydrogels have been extensively tested as cellular scaffolds for tissue engineering applications but their poor resistance against abrasive wear has hampered their translation to clinical settings. Tribo-testing of the hydrogels (2.5 w%) have shown that the cumulated dissipated energy, E_d, which is directly related to the wear volume, W_v,[44] is strongly diminished in presence of the HA - BB mixture compared to each component alone. Concomitantly, the surfaces' roughness, S_a, was found to significantly decrease in presence of the mixture compared to all other conditions due to surface polishing and restructuring.

2.4 Conclusion

The results shown in this study allow to confidently anticipate a large range of applications for such fluids. The polymers tested are known to be biocompatible and suitable for intra-articular injection which suggests a potential use as biolubricants. Other applications requiring wear protection of soft or ductile materials such as plastics (e.g. medical devices) or metals (e.g. articular implants) can be envisioned as well. The present strategy should be applicable to non-aqueous systems as well by simply adapting the chemical functionalities of the BB polymer and the linear polymer counterpart. On a more fundamental level, the lubricating system described in this study demonstrates that it is possible to control lubrication (i.e. the coefficient of friction μ) and wear protection (P^*) independently by tuning the properties of each component.

Acknowledgements.

XB acknowledges the financial support from CIHR (950-228948 and ONM-143062) and NSERC (RGPIN-2014-06316). JF is grateful to the Arthritis Society (Award TGP-16-183) and the French Embassy (Frontenac) for financial supports. BRS thanks the financial support of GRUM. We are also indebted to Matthieu Guibert (LTDS) for the tribometer design and fabrication and Thomas Malhomme (LTDS) for wear assessment of the gels. KM and GX acknowledge support from NSF (DMR 1436219).

Conclusions de la partie 1

À travers cette étude, nous avons retenu plusieurs enseignements concernant la biolubrification à partir de mimes polymériques. Tout d'abord, le domaine polymérique en brosse est responsable de la lubrification puisque l'emploi de cette structure a permis d'obtenir un CoF dans la gamme physiologique et indépendant de la force ionique. Ensuite, l'absence de groupements d'ancrage donne lieu a une faible résistance à l'usure puisque le film de polymère rompt a une faible pression. De plus, l'utilisation de HA seul n'a démontré aucune propriété lubrifiante. Finalement, la combinaison au bon ratio de mime polymérique et de HA de haut poids moléculaire a permis d'aboutir a une résistance à l'usure fortement améliorée grâce à des enchevêtrements entre les deux types de macromolécules. Ce concept innovant a permis de mettre en évidence une nouvelle technique d'adhésion d'un film polymérique sur des surfaces sans modification chimique et peut être utilisé pour une large gamme d'applications tout en imaginant d'autres groupes chimiques pour interagir avec les surfaces. La biocompatibilité de nos matériaux a d'ailleurs été vérifiée sur des cellules d'un patient atteint d'OA (voir Annexe 2). En plus de l'application en viscosupplémentation articulaire, d'autres applications sont possibles comme le revêtement de lentille cornéenne[45] ou de surfaces aux propriétés antimicrobienne[46] capables de lubrifier et limiter l'adhésion de protéines et de microorganismes tout en résistant aux contraintes (battements des paupières, désorption et diffusion). Ce travail a aussi fait l'objet d'une demande de brevet (Compositions polymères en goupillon, liquide lubrifiant, matériaux poreux comprenant lesdites compositions, et surface portant lesdites compositions WO 2017181274 A1)

Références

1. Jahn, S.; Seror, J.; Klein, J., Lubrication of Articular Cartilage. *Annu. Rev. Biomed. Eng.* **2016,** *18* (1), 235-258.
2. Masuko, K.; Murata, M.; Yudoh, K.; Kato, T.; Nakamura, H., Anti-inflammatory effects of hyaluronan in arthritis therapy: Not just for viscosity. *Int. J. Gen. Med.* **2009,** *2*, 77-81.
3. Das, S.; Banquy, X.; Zappone, B.; Greene, G. W.; Jay, G. D.; Israelachvili, J. N., Synergistic interactions between grafted hyaluronic acid and lubricin provide enhanced wear protection and lubrication. *Biomacromolecules* **2013,** *14* (5), 1669-1677.
4. Seror, J.; Sorkin, R.; Klein, J., Boundary lubrication by macromolecular layers and its relevance to synovial joints. *Polymers for Advanced Technologies* **2014,** *25* (5), 468-477.
5. Kobayashi, M.; Terayama, Y.; Kikuchi, M.; Takahara, A., Chain dimensions and surface characterization of superhydrophilic polymer brushes with zwitterion side groups. *Soft Matter* **2013,** *9* (21), 5138-5148.
6. Ramakrishna, S. N.; Espinosa-Marzal, R. M.; Naik, V. V.; Nalam, P. C.; Spencer, N. D., Adhesion and Friction Properties of Polymer Brushes on Rough Surfaces: A Gradient Approach. *Langmuir* **2013,** *29* (49), 15251-15259.
7. Zhulina, E. B.; Rubinstein, M., Lubrication by Polyelectrolyte Brushes. *Macromolecules* **2014,** *47* (16), 5825-5838.
8. Lee, S.; Spencer, N. D., Adsorption Properties of Poly(l-lysine)-graft-poly(ethylene glycol) (PLL-g-PEG) at a Hydrophobic Interface: Influence of Tribological Stress, pH, Salt Concentration, and Polymer Molecular Weight. *Langmuir* **2008,** *24* (17), 9479-9488.
9. Rosenberg, K. J.; Goren, T.; Crockett, R.; Spencer, N. D., Load-Induced Transitions in the Lubricity of Adsorbed Poly(l-lysine)-g-dextran as a Function of Polysaccharide Chain Density. *ACS Appl. Mater. Interfaces* **2011,** *3* (8), 3020-3025.
10. Banquy, X.; Burdyńska, J.; Lee, D. W.; Matyjaszewski, K.; Israelachvili, J., Bioinspired Bottle-Brush Polymer Exhibits Low Friction and Amontons-like Behavior. *J. Am. Chem. Soc.* **2014,** *136* (17), 6199-6202.
11. Dedinaite, A., Biomimetic lubrication. *Soft Matter* **2012,** *8* (2), 273-284.
12. Sophia Fox, A. J.; Bedi, A.; Rodeo, S. A., The Basic Science of Articular Cartilage: Structure, Composition, and Function. *Sports Health* **2009,** *1* (6), 461-468.
13. Jay, G. D.; Waller, K. A., The biology of Lubricin: Near frictionless joint motion. *Matrix Biol.* **2014,** *39*, 17-24.
14. Sheiko, S. S.; Sumerlin, B. S.; Matyjaszewski, K., Cylindrical molecular brushes: Synthesis, characterization, and properties. *Prog Polym Sci* **2008,** *33* (7), 759-785.
15. Matyjaszewski, K., Atom Transfer Radical Polymerization (ATRP): Current Status and Future Perspectives. *Macromolecules* **2012,** *45* (10), 4015-4039.
16. Nie, J.; Lu, W.; Ma, J.; Yang, L.; Wang, Z.; Qin, A.; Hu, Q., Orientation in multi-layer chitosan hydrogel: morphology, mechanism, and design principle. *Sci. Rep.* **2015,** *5*, 7635.
17. Lee, D. W.; Banquy, X.; Das, S.; Cadirov, N.; Jay, G.; Israelachvili, J., Effects of molecular weight of grafted hyaluronic acid on wear initiation. *Acta Biomater.* **2014,** *10* (5), 1817-1823.
18. Faivre, J.; Shrestha, B. R.; Burdynska, J.; Xie, G.; Moldovan, F.; Delair, T.; Benayoun, S.; David, L.; Matyjaszewski, K.; Banquy, X., Wear Protection without Surface Modification Using a Synergistic Mixture of Molecular Brushes and Linear Polymers. *ACS Nano* **2017,** *11* (2), 1762-1769.
19. Holmberg, K.; Andersson, P.; Erdemir, A., Global energy consumption due to friction in passenger cars. *Tribol Int* **2012,** *47*, 221-234.
20. Tzanakis, I.; Hadfield, M.; Thomas, B.; Noya, S. M.; Henshaw, I.; Austen, S., Future perspectives on sustainable tribology. *Renew Sust Energ Rev* **2012,** *16* (6), 4126-4140.
21. Moro, T.; Takatori, Y.; Ishihara, K.; Konno, T.; Takigawa, Y.; Matsushita, T.; Chung, U.-i.; Nakamura, K.; Kawaguchi, H., Surface grafting of artificial joints with a biocompatible polymer for preventing periprosthetic osteolysis. *Nature materials* **2004,** *3* (11), 829-836.
22. Klein, J., Chemistry. Repair or replacement--a joint perspective. *Science* **2009,** *323* (5910), 47-8.

23. Liu, X.; Dedinaite, A.; Rutland, M.; Thormann, E.; Visnevskij, C.; Makuska, R.; Claesson, P. M., Electrostatically anchored branched brush layers. *Langmuir* **2012,** *28* (44), 15537-47.
24. Pettersson, T.; Naderi, A.; Makuska, R.; Claesson, P. M., Lubrication properties of bottle-brush polyelectrolytes: An AFM study on the effect of side chain and charge density. *Langmuir* **2008,** *24* (7), 3336-3347.
25. Liu, X.; Thormann, E.; Dedinaite, A.; Rutland, M.; Visnevskij, C.; Makuska, R.; Claesson, P. M., Low friction and high load bearing capacity layers formed by cationic-block-non-ionic bottle-brush copolymers in aqueous media. *Soft Matter* **2013,** *9* (22), 5361-5371.
26. Chen, M.; Briscoe, W. H.; Armes, S. P.; Cohen, H.; Klein, J., Polyzwitterionic brushes: Extreme lubrication by design. *European Polymer Journal* **2011,** *47* (4), 511-523.
27. Ohsedo, Y.; Takashina, R.; Gong, J. P.; Osada, Y., Surface friction of hydrogels with well-defined polyelectrolyte brushes. *Langmuir* **2004,** *20* (16), 6549-6555.
28. Raviv, U.; Giasson, S.; Kampf, N.; Gohy, J. F.; Jerome, R.; Klein, J., Lubrication by charged polymers. *Nature* **2003,** *425* (6954), 163-165.
29. Tairy, O.; Kampf, N.; Driver, M. J.; Armes, S. P.; Klein, J., Dense, Highly Hydrated Polymer Brushes via Modified Atom-Transfer-Radical-Polymerization: Structure, Surface Interactions, and Frictional Dissipation. *Macromolecules* **2015,** *48* (1), 140-151.
30. Kobayashi, M.; Tanaka, H.; Minn, M.; Sugimura, J.; Takahara, A., Interferometry Study of Aqueous Lubrication on the Surface of Polyelectrolyte Brush. *Acs Applied Materials & Interfaces* **2014,** *6* (22), 20365-20371.
31. Morse, A. J.; Edmondson, S.; Dupin, D.; Armes, S. P.; Zhang, Z.; Leggett, G. J.; Thompson, R. L.; Lewis, A. L., Biocompatible polymer brushes grown from model quartz fibres: synthesis, characterisation and in situ determination of frictional coefficient. *Soft Matter* **2010,** *6* (7), 1571-1579.
32. Klein, J.; Kumacheva, E.; Mahalu, D.; Perahia, D.; Fetters, L. J., Reduction of Frictional Forces between Solid-Surfaces Bearing Polymer Brushes. *Nature* **1994,** *370* (6491), 634-636.
33. Klein, J., Shear, friction, and lubrication forces between polymer-bearing surfaces. *Annu Rev Mater Sci* **1996,** *26*, 581-612.
34. Banquy, X.; Burdynska, J.; Lee, D. W.; Matyjaszewski, K.; Israelachvili, J., Bioinspired Bottle-Brush Polymer Exhibits Low Friction and Amontons-like Behavior. *Journal of the American Chemical Society* **2014,** *136* (17), 6199-6202.
35. Terbojevich, M.; Cosani, A.; Palumbo, M.; Pregnolato, F., Structural properties of hyaluronic acid in moderately concentrated solutions. *Carbohydrate Research* **1986,** *149* (2), 363-377.
36. Terbojevich, M.; Carraro, C.; Cosani, A.; Marsano, E., Solution studies of the chitin-lithium chloride-N,N-di-methylacetamide system. *Carbohydrate Research* **1988,** *180* (1), 73-86.
37. Chen, M.; Briscoe, W. H.; Armes, S. P.; Klein, J., Lubrication at Physiological Pressures by Polyzwitterionic Brushes. *Science* **2009,** *323* (5922), 1698-1701.
38. Maier, G. P.; Rapp, M. V.; Waite, J. H.; Israelachvili, J. N.; Butler, A., BIOLOGICAL ADHESIVES. Adaptive synergy between catechol and lysine promotes wet adhesion by surface salt displacement. *Science* **2015,** *349* (6248), 628-32.
39. Petrone, L.; Kumar, A.; Sutanto, C. N.; Patil, N. J.; Kannan, S.; Palaniappan, A.; Amini, S.; Zappone, B.; Verma, C.; Miserez, A., Mussel adhesion is dictated by time-regulated secretion and molecular conformation of mussel adhesive proteins. *Nature Communications* **2015,** *6*.
40. Ma, L.; Gaisinskaya-Kipnis, A.; Kampf, N.; Klein, J., Origins of hydration lubrication. *Nat Commun* **2015,** *6*, 6060.
41. Heuberger, M.; Luengo, G.; Israelachvili, J., Topographic Information from Multiple Beam Interferometry in the Surface Forces Apparatus. *Langmuir* **1997,** *13* (14), 3839-3848.
42. Perkin, S.; Goldberg, R.; Chai, L.; Kampf, N.; Klein, J., Dynamic properties of confined hydration layers. *Faraday Discuss* **2009,** *141*, 399-413; discussion 443-65.
43. Raviv, U.; Perkin, S.; Laurat, P.; Klein, J., Fluidity of water confined down to subnanometer films. *Langmuir* **2004,** *20* (13), 5322-32.
44. Fouvry, S.; Liskiewicz, T.; Kapsa, P.; Hannel, S.; Sauger, E., An energy description of wear mechanisms and its applications to oscillating sliding contacts. *Wear* **2003,** *255*, 287-298.
45. Sterner, O.; Karageorgaki, C.; Zürcher, M.; Zürcher, S.; Scales, C. W.; Fadli, Z.; Spencer, N. D.; Tosatti, S. G. P., Reducing Friction in the Eye: A Comparative Study of Lubrication by Surface-Anchored Synthetic and Natural Ocular Mucin Analogues. *ACS Applied Materials & Interfaces* **2017**.

46. Higaki, Y.; Kobayashi, M.; Murakami, D.; Takahara, A., Anti-fouling behavior of polymer brush immobilized surfaces. *Polym. J.* **2016,** *48* (4), 325-331.

Introduction de la partie 2

La viscosupplémentation est un traitement symptomatique intra-articulaire des patients atteints d'OA qui consiste généralement en trois injections de hyaluronate de sodium de 2 mL à 8-10 mg/mL espacées d'une semaine. Les bienfaits ressentis par le patient après une telle injection peuvent durer plusieurs mois voire plusieurs années, même si l'HA lui-même est rapidement éliminé de la synovie [1-2] et dégradé par des enzymes spécialisées (hyaluronidases), notamment dans les articulations touchées par l'OA[3]. Ainsi, la première question qui est soulevée concerne la stabilité des molécules écouvillon synthétisées et injectées dans l'espace intra-articulaire.

Ainsi, nous avons caractérisé la stabilité de l'écouvillon moléculaire dans un milieu tamponné salin adapté pour l'injection intra-articulaire à différentes températures. Le SFA a permis de caractériser à la fois la lubrification (CoF) et l'usure de notre écouvillon moléculaire en milieu tamponné. Les profils de force ont également été obtenus au cours du temps et en fonction de la température de stockage afin de visualiser le vieillissement en solution. Enfin, un modèle théorique a été développé afin de comprendre le comportement de notre écouvillon moléculaire aux interfaces et au cours du temps (conformation et impact du vieillissement hydrolytique).

Cette étude a fait l'objet d'une publication dans le journal de l'American Chemical Society, *Biomacromolecules*, publiée le 29 septembre 2017[4] et intitulée : *Unraveling the Correlations between Conformation, Lubrication and Chemical Stability of Bottlebrush Polymers at Interfaces*. Le polymère est le même qu'utilisé dans la partie précédente synthétisé au sein du laboratoire du Pr Matyjaszewski. Les profils d'interaction et l'étude tribologique à l'aide du SFA ont été effectués par Dr Buddha R. Shrestha et moi-même au sein du laboratoire du Pr Xavier Banquy. Enfin, les expérimentations GPC ont été menées dans le laboratoire des Pr Laurent David et Thierry Delair, sur la plateforme de chromatographie de l'ICL (dont la responsable est Agnès Crépet).

Unraveling the Correlations between Conformation, Lubrication and Chemical Stability of Bottlebrush Polymers at Interfaces

Jimmy Faivre[1,3], Buddha Ratna Shrestha[1], Guojun Xie,[2] Thierry Delair[3], Laurent David[3], Krzysztof Matyjaszewski[2*], Xavier Banquy[1*]

[1]*Canada Research Chair in Bioinspired materials, Faculty of Pharmacy, Université de Montréal, Montréal, Qc, Canada*

[2]*Center for Macromolecular Engineering, Department of Chemistry, Carnegie Mellon University, Pittsburgh, PA, USA*

[3]*Université de Lyon, Université Claude Bernard Lyon 1, CNRS, Ingénierie des Matériaux Polymères (IMP-UMR 5223), 15 Boulevard Latarjet, 69622 Villeurbanne Cedex, France*

Abstract

In the present study, we monitored the conformation and chemical stability of a hydrophilic bottlebrush (BB) polymer in pure water and buffered saline solutions. We correlated these parameters to lubricating and wear protecting properties. Using the Surface Forces Apparatus (SFA), we show that the BB polymer partially adsorbs on mica surfaces and extends half its contour length toward the aqueous media. This conformation gives rise to a strong repulsive interaction force when surfaces bearing BB polymer chains are pressed against each other. Analysis of these repulsive forces demonstrated that the adsorbed polymer chains could be described as end-attached elastic rods. After 2 months of aging at temperatures ranging from 4 to 37 °C, partial scission of the BB polymer's lateral chains was observed by Gel Permeation Chromatography with a half-life time of the polymer of at least two years. The thickness of the BB polymer layer assessed by SFA appeared to quickly decrease with aging time and temperature which was mainly caused by the adsorption to the substrate of the released lateral chains. The gradual loss of the BB polymer lateral chains did not impact significantly the tribological properties of the BB polymer solution nor its wear protection capacity. The friction coefficient between mica surfaces immersed in the BB polymer solution was μ = 0.031 ± 0.002, and was independent of the aging conditions and remained constant up to an applied pressure P = 0.2-0.25 MPa. Altogether, this study demonstrates that besides the gradual loss of lateral chains, the BB polymer is still able to perform adequately as a lubricant and wear protecting agent over a time period suitable for *in vivo* administration.

Keywords: Bottlebrush polymer, stability, wear protection, polymer conformation

Table of Contents

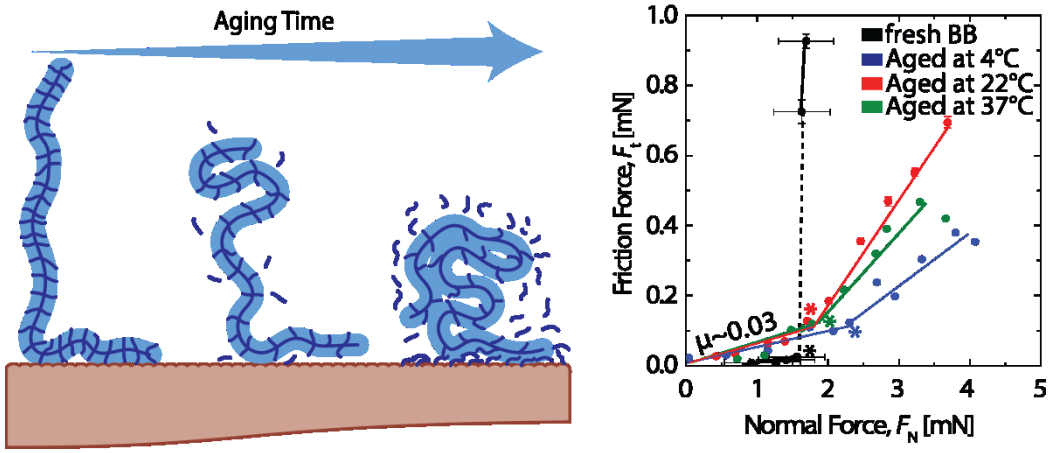

2.5 Introduction

Bottlebrush (BB) polymers are composed of a linear macromolecular backbone to which are densely grafted side chains[5]. The strong steric repulsion between side chains leads to the backbone extension resulting in a worm-like conformation of the polymer which can be modulated by side-chain grafting density and length[5-6]. BB polymers have attracted a growing interest in many application fields ranging from materials to biomedical engineering[7]. Indeed, grafted or adsorbed BB polymers exhibit exceptional antifouling[8], viscoelastic[9], lubrication[10], surface coating[11] and photonic[12] properties. BB polymers combined with contrast agents have also demonstrated exceptional properties as diagnostic tools for MRI and fluorescence imaging[13]. Recent reports are now suggesting the use of BB polymers as drug delivery systems[14]. Contrarily to spherical polymeric particles which have been extensively studied, cylindrical polymer brushes have demonstrated longer blood circulation time[15-16] and improved biodistribution[17], revealing them as promising drug carriers. The BB architecture is abundantly present in nature, in particular in proteins such as mucins and proteoglycans found in articular joints or in the gastro intestinal tract. First reported in natural systems including the protein lubricin[18-23] or agrecans[24-26] and later in synthetic systems [10, 27-31], the BB architecture is well known to provide excellent friction reduction capabilities to lubricating polymers.

Three main synthetic routes exist to prepare polymeric molecular brushes: the "grafting to" polymerization *via* the coupling reaction of an end-functionalized side-branch to a polymeric backbone; the "grafting through" polymerization of macromonomers bearing the pendant chains and the "grafting from" polymerization of monomers from a macroinitiator[7]. These techniques can be implemented to grow polymer chains on surfaces or in solution. This allows to obtain a rich variety of brushes besides the fact that these strategies are challenging to implement due to the steric hindrance between lateral chains and the stress it creates on the BB polymer backbone.

BB polymers chemical stability at surfaces or in solution have been studied extensively[32-34]. Different mechanisms leading to BB chemical degradation have been identified. Sheiko *et al*. reported carbon-carbon bond scissions at the backbone of hydrophobic BB polymers deposited on flat surfaces[33]. The authors attributed this phenomenon to an increased backbone tension originated by the spreading of the densely grafted side chains on the substrate. Xia *et al.* observed the same phenomenon with ultrahigh molecular weight cyclic BB polymer deposited on graphite[34]. Chen *et al.* reported that end-grafted polystyrene (PS) chains in the

brush conformation can also suffer chain scission[35]. The authors explained their results invoking intermolecular transfer reactions which occurred at higher rates for PS brushes compared to free PS chains due to their close packing. Higher degradation rates were also reported for grafted poly(lactic acid) (PLA) brushes compared to bulk PLA[36]. In this case, the degradation mechanism was mediated by intramolecular transesterification and ester hydrolysis[36]. Naturally occurring BB macromolecules such as proteoglycans have been reported to undergo degradation as well *via* proteolysis. This is particularly the case in adult articular joints where the aggrecan, a densely grafted proteoglycan acting as a joint lubricant, suffers from fragmentation by enzymatic chain scission[37]. This phenomenon can be accelerated in an inflamed environment such as arthritic articular joints where specific enzymes degrade chondroitin and keratan sulfates glycosaminoglycans side chains.

So far, only a few studies have investigated the changes in BB polymers interfacial properties along with their time-dependent structural changes. In this manuscript, we intent to relate the interfacial properties (normal interaction forces and lubrication forces) of BB polymers to their chemical stability. We used a BB polymer known to exhibit excellent lubricating properties (friction coefficient $\mu \sim 0.02$) anti-wear properties (pressure at onset of damage > 3 MPa) when combined with high molecular weight hyaluronic acid (HA)[38]. We first used the surface forces apparatus (SFA) to characterize the interfacial properties of the BB polymer. The wear protection capacity and the lubricating properties of BB polymer solutions as well as the interaction forces between mica surfaces across such solutions were monitored under different aging conditions and correlated to the chemical stability of the polymer. The chemical stability of the BB polymer was assessed by estimating the side chains grafting density using the SFA, the BB backbone contour length by atomic force microscopy (AFM) and the molecular weight of the BB polymer using GPC.

2.6 Materials and methods

2.6.1 Polymer synthesis and Formulation.

The synthesis of the zwitterionic BB polymer was performed as previously reported[38]. The polymer was synthesized by atom transfer radical polymerization (ATRP)[39-40], purified by dialysis in pure water prior to recovery. For all stability studies, the BB polymer (white powder) was dissolved at 100 µg/mL in phosphate buffered saline (PBS, 150 mM NaCl, pH = 7.4) and left in solution in a dark container at 4°C, 22°C or 37°C.

2.6.2 AFM imaging.

At different time points, aliquots of BB polymer solutions were diluted with pure water up to a concentration of 50 to 5 µg/mL and deposited on freshly cleaved mica. The BB polymer was left to adsorb for 20 min then exceeding solution was removed using a kimwipe and the surface was washed several times with water to completely remove remaining salt cristals. The surface was air dried prior to imaging. For imaging, a Multimode Dimension 3100 AFM equipped with nanoscope VIII controller (Digital instruments) was used in the peak force QNM mode. Scanasyst-air silicon tips were used for imaging. The contour length of the BB polymer was obtained by analysing AFM images using WormTracker plug-in for ImageJ[41].

2.6.3 Interaction forces.

A Surface Forces Apparatus (SFA 2000, SurForce LLC, USA) was used to measure the interaction force profiles between mica surfaces across BB solutions. Briefly, back-silvered mica sheets were glued (epoxy glue Epon 1004F) on glass cylindrical disks with a curvature, R, of 2 cm under a laminar flow hood. The disks were then mounted in the SFA chamber in a cross configuration. The SFA chamber was then purged with dry argon and the surfaces were brought into adhesive contact to quantify the mica surfaces' thickness. The surfaces were then separated again and 50 µL of BB polymer solution were injected between the surfaces. To avoid evaporation of the solution during experiment, pure water was deposited at the bottom of the chamber to saturate the closed atmosphere. The setup was left to equilibrate for 1 h before measurements were started. The separation distance between the two opposing mica surfaces was determined by multiple beam interferometry. The wavelength of the Fringes of Equal Chromatic Order (FECO) was measured with a spectrometer and converted into separation distance using the three layer interferometer model[42]. The normal interaction forces, F_N, were recorded as a function of separation distance, D, for in (compression) and out (separation) runs at a speed of 1 nm/s. The fringes were analyzed using a in-house Matlab® routine. Experiments were performed at least three times at different contact positions.

2.6.4 Tribological experiments.

The friction forces, F_t, as a function of normal force, F_N, were measured using the friction device and bimorph slider[43]. As in the interaction forces section, 50 µL BB polymer solution were injected between the surfaces and a small amount of pure water was added in the chamber to limit evaporation. The setup was left to equilibrate for 1 h before experimentation. To ensure reproducible BB polymer surface coverage, normal force profiles measurements were carried out right before tribotesting. The normal force was monitored using semi-conductive strain gauges mounted on the double cantilever of the bimorph slider. Friction and normal forces were recorded on a digital recorder (Soltec TA220-2300A). The sliding velocity was fixed at 2.5 µm/s using a Function/Arbitrary waveform generator (Agilent 33250A). The amplitude of the sliding motion was set to 50 µm. The separation distance, *D*, wear initiation and surface contact area were simultaneously monitored during tribological experiments by continuously recording the FECO using a CCD camera[44].

2.6.5 Gel Permeation Chromatography (GPC).

Monitoring of the molecular weight and dispersity of the BB polymer was assessed by GPC with an eluting phase of 10mM phosphate aqueous buffer at pH 7.4. The GPC was equipped with a light scattering HELEOS (Wyatt), refractive index detector rEX, Wyatt QELS+ and UV detectors and a PL aquagel OH M 8 micro and H 8 micro columns. The flow rate was set at 0.5mL/min and the system was systematically equilibrated at 25°C for all measurements. The value of the BB polymer refractive index increment, dn/dc, was set to 0.142 mL/g [45].

2.7 Results and Discussion

The chemical composition of the BB polymer was **(**PBiBEM$_{459}$-*g*-PMPC$_{35}$)-*stat*-PMMA$_{370}$ (Fig. 2.15A). A similar polymer was recently shown to have excellent lubricating properties with a friction coefficient close to 10^{-2} under a normal pressure of 15 atm when used in combination with high molecular weight hyaluronic acid in buffered saline.[38] These properties make this polymer a promising candidate for biomedical applications such as viscosuplementation of osteoarthritic joints to re-establish wear protection and possibly decelerate cartilage erosion. The architecture of the BB polymer used in this study, shown in figure 2.15A and B, mimics the lubricating proteins encountered in synovial joints[10, 46] such as lubricin and aggrecans. The contour length of the BB polymer, measured by AFM imaging, was found to be 141 ± 25 nm. Figure 2.15C represents a perpendicular cross-sectional profile of the BB polymer deposited on a mica substrate. The hydrophilic side-side chains of the polymer appeared to spread on the surface suggesting a favorable affinity towards the surface.

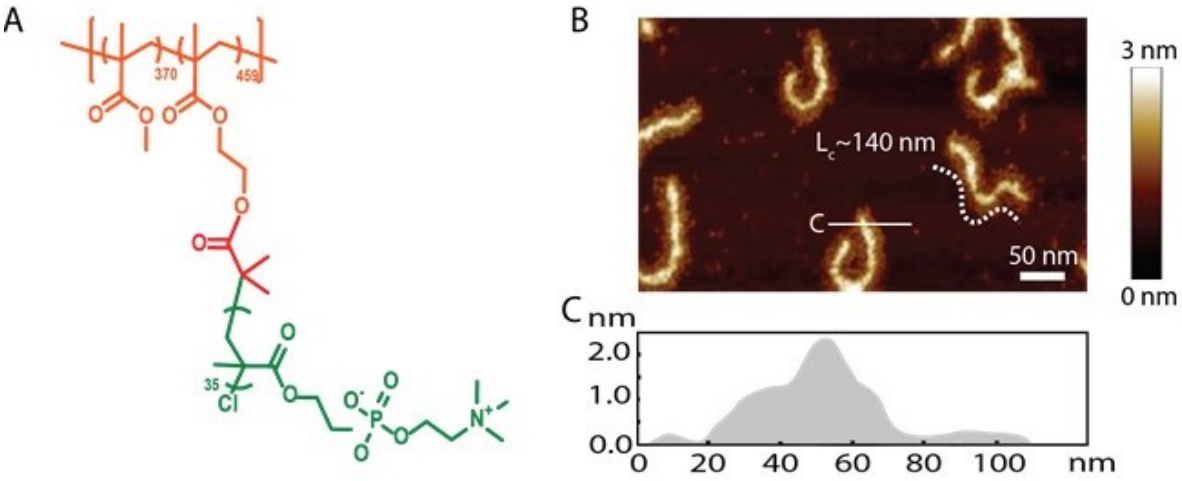

Figure 2.15. *(A) Chemical structure of the bottle-brush polymer used in the study. (B) AFM picture of BB polymer deposited on mica surfaces from a 10 µg/mL polymer solution. (C) BB height profile of a perpendicular cross-section indicated with the white line in fig. 1B showing the contour of the polymer.*

2.7.1 Interaction forces across BB polymer solutions

We used the SFA to measure the interaction profiles across BB polymer solutions in water or in saline solutions (Fig. 2.16A). As can be seen in Fig. 2.16B, repulsive forces were recorded

during the in (surfaces approach) and out (surfaces separate) runs. At a fixed BB polymer concentration of 100 µg/mL, the profiles were identical, independently of the ionic strength of the medium, as previously observed for polyzwitterionic brushes.[38, 47-48] The onset of the interaction forces, given by the separation distance at which adsorbed BB chains facing each other start interacting (D_{onset}, determined at F_N/R = 0.01 mN/m), ranged between 125 to 150 nm. The onset of interaction being equal to twice the adsorbed polymer layer thickness, L (L= 62-75 nm, no interdigitation hypothesis, see schematic Fig. 2.16C) and the average contour length of the polymer L_c being equal to ~ 140 ± 20 nm (assessed by AFM), we can conclude that adsorbed BB polymer chains extend on average half their contour length toward the medium. Under high pressure, the BB polymer film is about 5 nm thick, indicating the presence of at least one molecular layer of polymer.

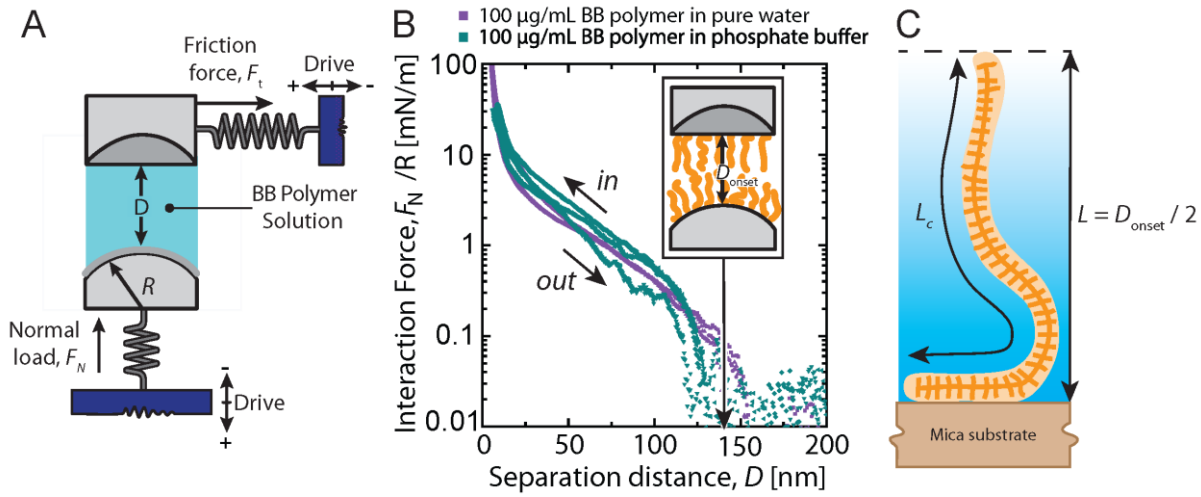

Figure 2.16. *(A) SFA experimental setup used for normal force profiles and tribology experiments. (B) Interaction force profiles across BB solution at 100 µg/mL in pure water and in a phosphate buffer at 150 mM NaCL and pH 7.4. C) Schematic representation of the BB polymer conformation on the mica substrate with its characteristic dimensions.*

In order to determine the conformation and interfacial properties of the polymer, we performed measurements of interaction forces between mica surfaces across solutions of BB polymer at two different concentrations (10 and 100 µg/mL) and two different saline conditions (pure water and PBS). The measured interaction forces shown in Figure 2.17A present features common to all tested conditions. The force profiles (F_N/R vs D) were once again purely repulsive even at 10 µg/mL where the surfaces were not fully covered (Figure 2.15B) which could have facilitated polymer bridging. Another interesting common feature is the constant onset of interaction forces for all polymer concentrations or saline conditions

tested. Such behavior is quite unusual since the conformation, and therefore the polymer layer thickness, of randomly adsorbed or end-grafted linear polymer chains' conformation is known to depend on chain surface density.[49]

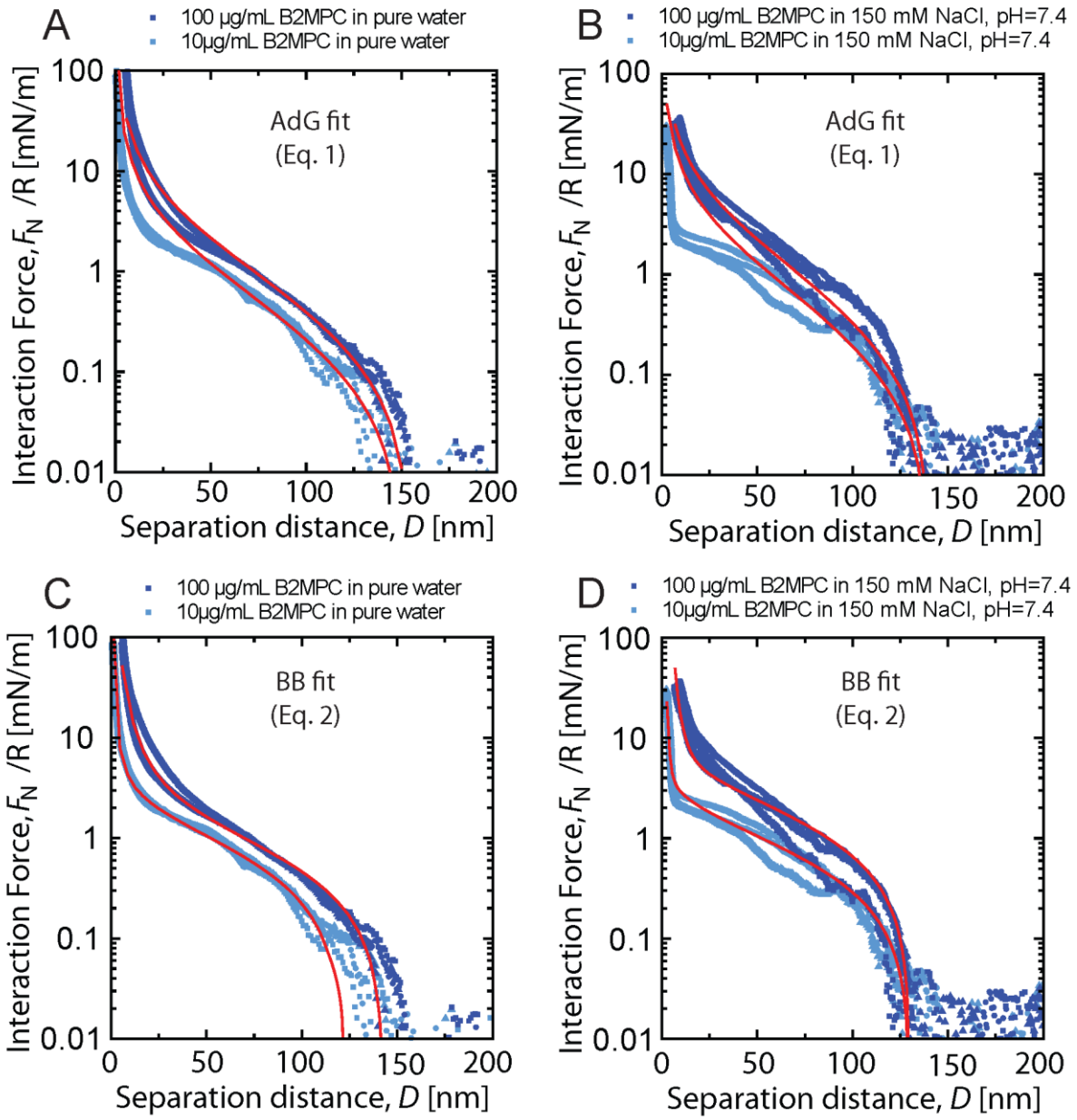

Figure 2.17. *(A) Interaction force profile between mica surfaces across a solution of BB polymer in pure water (A and C) and in buffered saline (B and D). The red lines are the best fitted curves using Eq. 1 (AdG fit) and Eq. 2 (in the manuscript, BB fit).*

Reports on interaction forces between BB polymer coated surfaces are scarce, therefore analysis of the present experimental force profiles needs particular attention. In order to

analyse the interaction profiles, we used two different theories: the Alexander-de Gennes (AdG) brush theory[50] (Eq. 1) and a theory based on the entropy and bending energies of BB polymers (BB model, Eq. 2).

In the AdG brush theory, the interaction energy between two flat surfaces bearing polymer brushes, W, which is related to the interaction force via the Derjaguin approximation ($F_N = 2\pi R W$) has two main contributions: an osmotic contribution that increases as separation distance between the surfaces decreases due to concentration of polymer segments, and an elastic contribution that decreases with the separation distance. The resulting force law reads:

$$\frac{F_N}{R} = \frac{16\pi k_B T L}{35 s^3}\left[7\left(\frac{2L}{D}\right)^{5/4} + 5\left(\frac{D}{2L}\right)^{7/4} - 12\right] \quad \text{(Eq. 1)}$$

where $s = 1/\sqrt{\pi\Gamma}$.

The AdG model has been shown to apply to many different systems, not only to end grafted brushes. Studies have demonstrated that the AdG model describes correctly the density profile and interaction profiles between end-adsorbed diblock polymers[51]. It also described fairly well the density profile of polymer loops and their interaction forces[52]. Interaction forces between surfaces bearing lubricin followed the AdG model as well.[18] Therefore we can assume that the same model could apply to the present system. The tests performed at different polymer concentrations demonstrated that the AdG model was not able to fit satisfactorily the data in the whole range of concentration studied (Fig. 2.17A and B). Indeed, from the data provided in Table 2.2, we can immediately see that AdG model does not fit satisfactorily the experimental data at low polymer concentration. The force profiles also demonstrate that the onset of interaction is insensitive to the polymer solution concentration (and therefore to the surface density as well) which is inconsistent with the AdG brush model. Indeed, the AdG theory predicts that the brush height L is given by $L \sim N\Gamma^{1/3}$ where N is the number of segments per chain and Γ the grafting density.

Table 2.2: Brush layer thickness and grafting density obtained from AdG model (Eq. 1)

	PBS			Pure water		
	Γ [nm]$^{-2}$	L [nm]	R^2	Γ [nm]$^{-2}$	L [nm]	R^2
10 mg/mL	1.5×10^{-3}	71	0.62	2.2×10^{-3}	77	0.51

100 mg/mL	2.1×10^{-3}	70	0.95	3.4×10^{-3}	75	0.94

Recent simulation studies have proposed that grafted BB polymers behave as elastic rods.[53] AFM images confirmed that the persistence length of the polymer adsorbed on mica surfaces was similar to the contour length of the polymer (Figure 2.15B) therefore supporting this assumption. In this framework, the expected contributions to the total interaction energy between BB polymer coated surfaces are the bending energy of the rod[53] and its conformational entropy.[54] Considering these two contributions, the interaction forces can be written as:

$$\frac{F_N}{R} \approx \mathrm{Ak_B}T\frac{\Gamma^2}{D^4} + \mathrm{Bk_B}T\Gamma\ln\left(\frac{2L}{D}\right) \qquad D < L \quad \text{(Eq. 2)}$$

The first left-hand term in Eq. 2 represents the bending contribution of the BB polymer at the anchoring point (A being a prefactor depending on the brush architecture and Γ the grafting density)[53] and the second term, the entropic contribution of the non-adsorbed portion of the BB polymer (L being the height of the BB polymer layer and B being a prefactor close to unity). At low grafting density, Eq. 2 predicts that the entropic contribution is the main contribution to the long range forces. Therefore, under such conditions, the onset of the interaction forces is expected to depend weakly on the grafting density as observed experimentally (Fig 2.17). In table 2.3 we show the fitted parameters using Eq. 2 (parameters for the entropic term only are shown for comparison purposes). As can be seen in figure 2.17C and D and Table 2.3, equation 2 shows excellent agreement with the experimental data independently of the ionic strength of the medium or the polymer concentration.

Table 2.3: Brush layer thickness and grafting density obtained from Eq. 2

	PBS			Pure water		
	Γ [nm]$^{-2}$	L [nm]	R^2	Γ [nm]$^{-2}$	L [nm]	R^2
10 mg/mL	4.2×10^{-2}	65	0.95	4.4×10^{-2}	60	0.91
100 mg/mL	7.8×10^{-2}	67	0.97	8.0×10^{-2}	67	0.97

2.7.2 Impact of aging on the BB polymer conformation at interfaces

Using the framework of the rod-like behavior described by Eq. 2, we performed measurements of interactions forces between surfaces across aged BB polymer solutions. In this study, we used PBS as the solution medium and stored the polymer solutions at three different temperatures for a period of several weeks. Figure 2.18 presents the evolution of the measured interaction forces with the storage time at 4 °C, 22 °C and 37 °C. We can notice a systematic decrease of the onset of interaction, $D_{onset,}$= $2L$, with the storage time. The decrease of the onset of interaction increased significantly from low to high storage temperature. At high normal forces, the film thickness remained almost constant at ~ 5nm independently of the storage conditions. As shown in Figure 2.18, the force profiles were adequately described by Eq. 2 allowing to determine accurately the BB polymer layer thickness, L, reported in Figure 2.19.

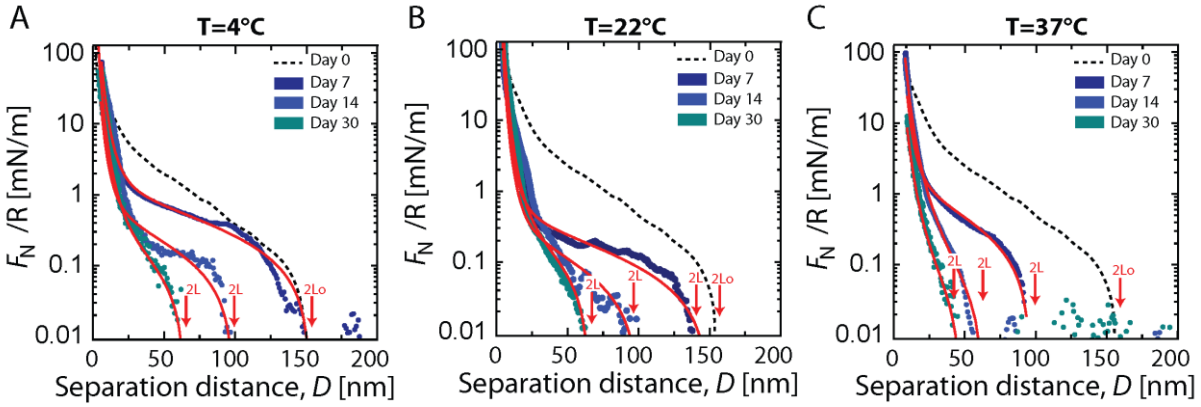

Figure 2.18. *Interaction force profile between mica surfaces across a solution of 100 µg/mL BB polymer stored during 7, 14 and 30 days in buffered saline at (A) 4°C, (B) 22°C, and (C) 37°C. Dashed line is day 0 BB interaction forces profiles extracted from figure 2. Red lines are fittings obtained from equation 2.*

The decay of the onset of interaction L shown in Fig. 2.19 suggests a gradual change of the BB polymer size or a transition from a rigid to a more flexible BB polymer. Changes in the length of the BB polymer could be the result of a scission of the polymer backbone due to strong steric hindrance generated by the grafted side chains. On the other hand, a transition towards a more flexible BB polymer could be the product of the cleavage of lateral chains over time. Indeed, mean field theory[5] predicts that the mean square size of a BB polymer chain, $<R^2>$, which is, as a first order approximation, related to the onset of interaction L ($L^2 \sim <R^2>$) measured by SFA, is proportional to the side chain grafting density z, i.e. $<R^2> \propto z^{\alpha}$ with α being close to unity. The decay of L^2 (normalized by the onset of interaction at t = 0,

L_0) was accurately fitted with a first order kinetic law at all temperatures except 37 °C At this temperature, a second distinct (much slower) kinetic process appears at incubation time longer than 15 days. From these data, the rate constant k of the fast process only was estimated at the different temperatures tested and the corresponding half-life time of the fast process, $t_{1/2}$ was estimated to vary between 10 and 30 days depending on the storage temperature.

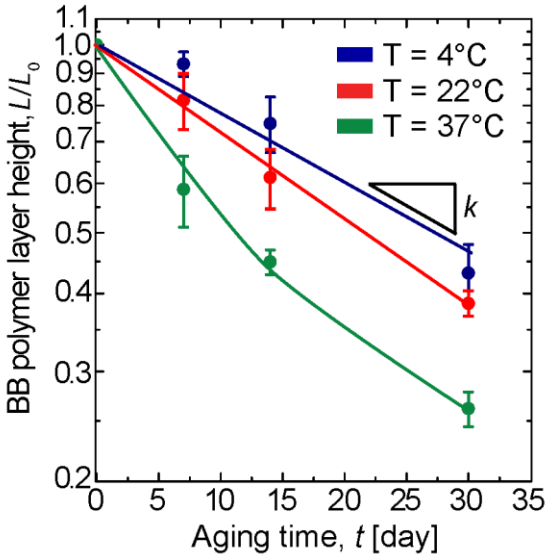

Figure 2.19. *(A) Evolution of BB polymer length using SFA interaction onset and BB fitting as a function of time at 4, 22 and 37°C. Solid lines are guide for the eyes.*

In order to confirm the origin of the observed conformational changes of the BB polymers, we first measured the contour length of the BB polymer aged at 22 °C for 60 days by AFM imaging (Fig. 2.20A). No significant variation in the contour length, L_c, could be observed from the analysis of the AFM images (Fig. 2.20A and B). Some evidence of side-chains degrafting was obtained by aqueous GPC (in PBS) of the BB polymer solutions stored at different temperatures. The analysis revealed the appearance of a small population of low molecular weight chains at long storage time (peak 2 in Fig. 2.20C) alongside with a strong and constant peak corresponding to the BB polymer (peak 1). Peak 1 presents a small shoulder that appears at all incubation times and temperatures which was already present in the macroinitiator GPC trace (data not shown). The molecular weight of peak 2 obtained by GPC was close to the expected molecular mass of pMPC lateral chain, M_w ~ 20 000 g/mol, and was independent of the storage temperature. This last observation confirmed that degrafting of the lateral chains indeed occurs and happens predominantly at the junction

between the pendant chain and the BB polymer backbone. It could potentially be related to hydrolysis of the ester bonds linking side chains to the backbone. A similar observation was reported for brushes covalently linked to solid wafers in aqueous media.[55] The areas of peak 2 allow to estimate a fraction of degrafted chains of less than 4 % for all tested conditions after two months of storage. These results suggest that the half-life time of the BB polymer is at least 2 years. GPC results can be compared to previous SFA observations. For example, GPC data show a degrafting ratio of 3.5% after one month of aging at 4 °C which corresponds to a grafting ratio z = 0.55 - 0.04 = 0.51. The expected value of the corresponding BB polymer layer L/L_0 is 0.96 which is significantly larger than the value of 0.43 obtained by SFA under the same aging conditions.

The differences between the SFA and GPC kinetic results could originate from small chains released from the BB polymer adsorbing preferentially on the surfaces therefore modifying the affinity / conformation of the BB polymer to the substrate.

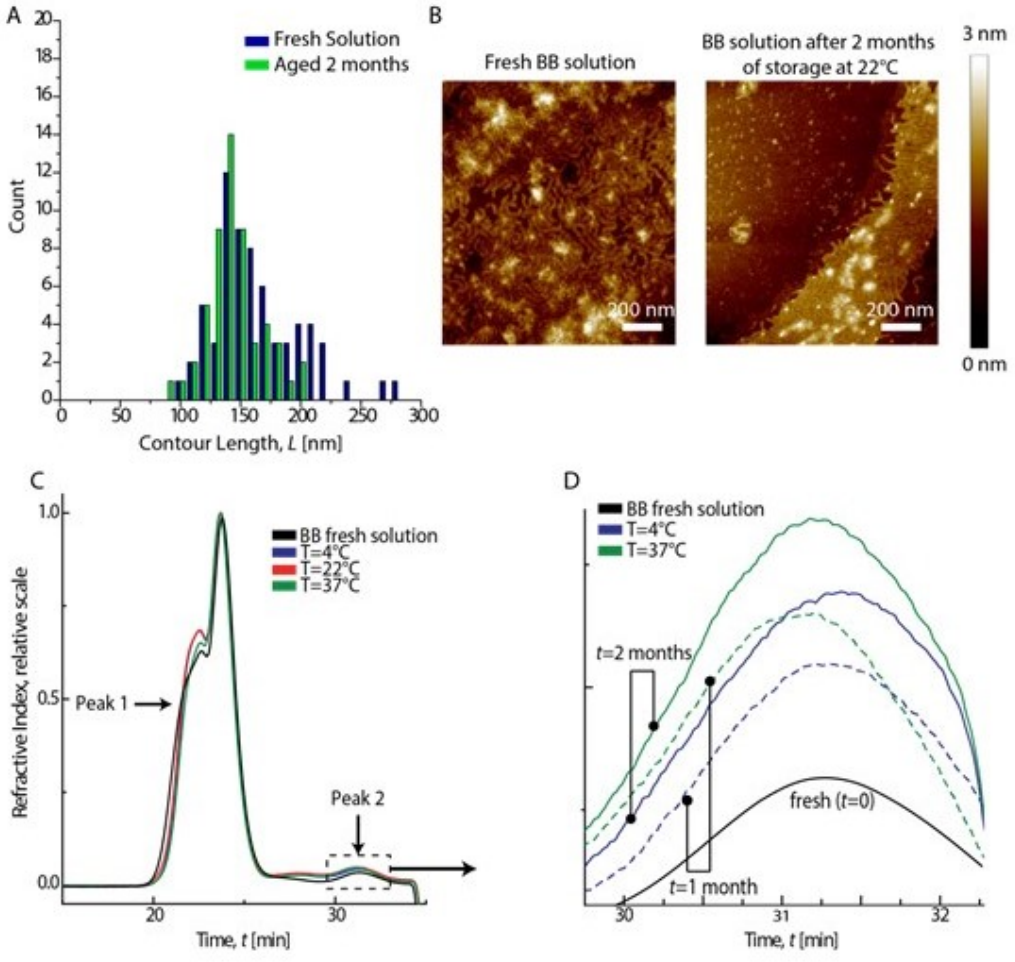

Figure 2.20. *(A) BB polymer contour length distribution in PBS solution at 22°C measured immediately after dissolution and after 2 months of storage analyzed by AFM imaging, (B) Film of BB polymer chains dried on mica immediately after dissolution and after 2 months of storage. A 35 µg/mL BB polymer solution was used to generate the adsorbed films; (C) GPC traces of aged BB polymer in phosphate buffer, pH = 7.4, at 4, 22 and 37°C compared to a fresh solution; (D) zoom-in of the elution chromatogram of peak 2 region showing the slight increase of the peak with storage time and temperature.*

2.7.3 Lubrication and wear protection by aged BB polymers

Finally, we characterized the impact of the structural changes affecting the BB polymer on its frictional properties. Frictional properties of BB polymer fresh saline solution and stored 3 months at different temperatures were recorded using the SFA equipped with a bimorph slider designed for tribotesting. After storage, the solutions were placed in the SFA and friction forces, F_t, were recorded at different applied normal forces F_N and constant sliding velocity. As shown in Fig. 2.21A, a linear relationship between the friction force and the normal force was observed for all samples tested. Such behavior was already reported in a previous report with a BB polymer with a triblock architecture designed to strongly adsorb on the substrate[10]. The linear relationship between F_t and F_N , which is reminiscent of the peculiar rheological properties of the polymer under confinement, allows to extract the friction coefficient (CoF) defined as $\mu = F_t / F_N$.

The measured CoF of the different solutions of BB polymer before and after the occurrence of damage were μ = 0.031 ± 0.002 and μ = 0.605 ± 0.040, respectively (Fig. 2.21B). Surprisingly, the CoF values before damage were independent of the storage temperature or storage time.

The wear initiation, characterized by the critical pressure of lubricating film rupture, P^*, was obtained through the analysis of the contact shape and separation between the surfaces assessed by multiple beam interferometry[42]. The measured values were P^* = 0.25 ± 0.02 MPa for BB fresh solution and P^* = 0.21 ± 0.06 for the BB solutions stored 3 months at different temperatures (Fig. 2.21C).

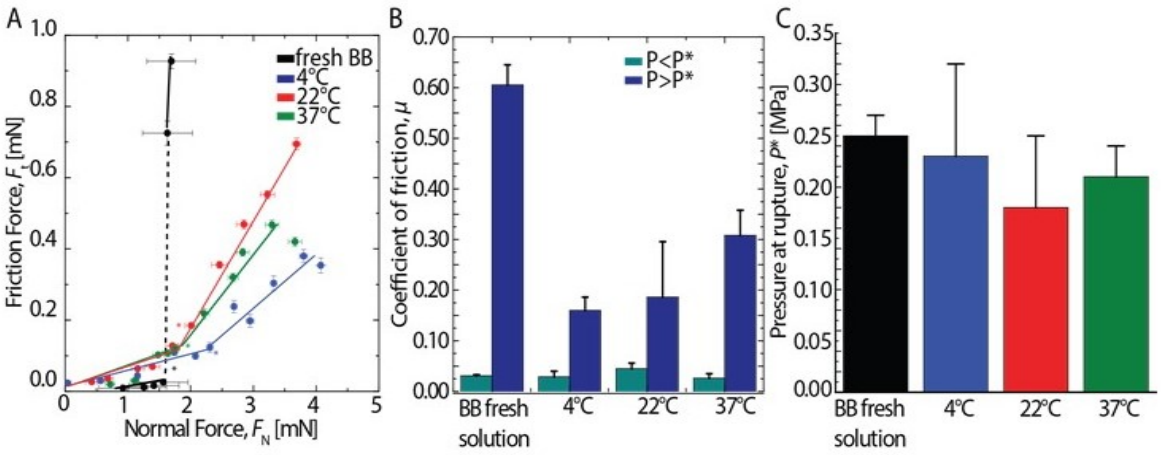

Figure 2.21. *Tribology testing of BB polymer solutions after 3 months of storage in a phosphate buffer, pH 7.4 and 150 mM NaCl, at 4, 22 and 37°C are compared to a BB fresh solution: (A) frictional forces, F_t, as a function of normal force, F_N, (B) Friction coefficient, μ,before (P < P*) and after (P > P*) wear initiation, (C) Evolution of the critical pressure at thin film rupture, P*, hallmark of wear initiation, with the different storage conditions.*

This series of experiments demonstrated that the tribological properties of the BB polymer solution did not present any significant changes after 3 months of storage even if the polymer suffered detectable changes in its structure such as degrafting of lateral chains. We also noticed that the degrafting of the lateral chains of the BB polymer was associated to a less dramatic transition from smooth contact (no damage) to strongly damaged surfaces. A closer look of the evolution of the contact topography, assessed by the FECO shape, revealed that for the fresh BB solution, the wear initiation is not gradual but rather abrupt (Fig 2.22A a-c and B), due to the sudden formation of aggregates at the edge of the contact (highlighted by a white arrow in figure 2.22A-c). In contrast, the transition to wear was smoother for aged BB polymer solutions (Fig 2.22A d-f and B). A gradual accumulation of material inside the contact zone lead to an increase in separation distance before damage of mica occurred. Such smoother transition towards damage can be associated to the presence of degrafted pMPC chains covering the mica surface as previously suggested. The presence of these small and more mobile chains favors the accumulation of material in the contact instead of at the edge.

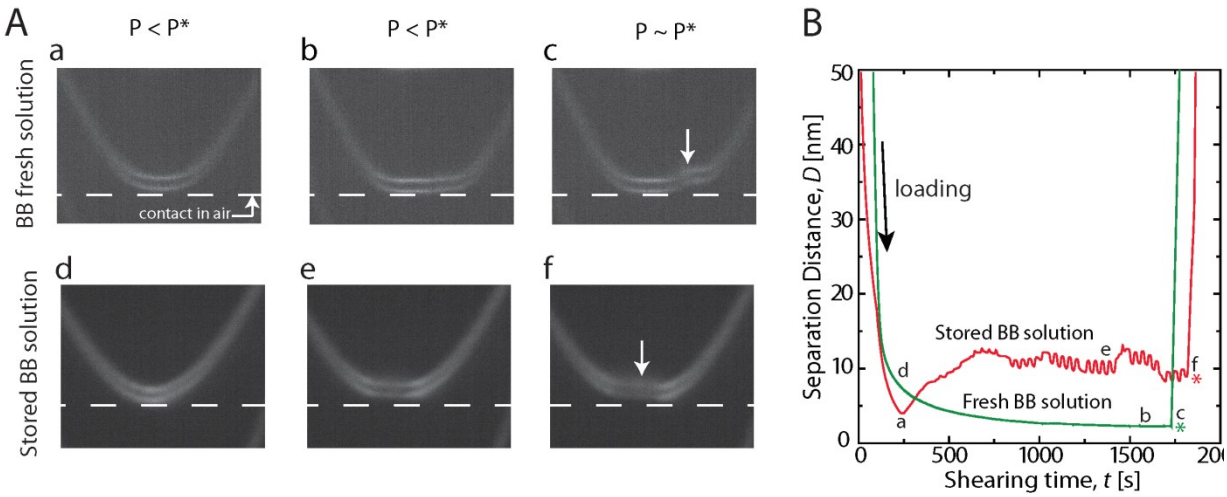

Figure 2.22. *Evolution of FECO fringe shape with pressure for (A) BB polymer fresh solution (a-c), and 3 months aged at 22°C BB polymer solution (d-f) White arrows, in A-c and f, highlight the region of wear initiation; (B) Separation distance as a function of time for fresh and stored BB polymer solutions. Initiation of wear is indicated by an asterisk.*

2.8 Conclusions

The present study has shown that BB polymers conformation at surfaces can evolve slowly with time and temperature. Careful experiments with the SFA allowed to quantify the dynamics of such gradual conformational changes and to correlate it with the adsorption of lateral chains on the substrate. These chains were slowly released from the BB polymer via hydrolysis of the linker functional group. The presence of these small chains on the surface did not have any impact on the tribological properties of the BB polymer. We observed no significant difference in the friction of coefficient or the critical pressure at onset of damage between all tested storage conditions. Altogether, the present study demonstrates that the BB polymer is stable enough in PBS to be considered as a potential injectable biolubricant for biomedical applications.

Acknowledgements

XB acknowledges the financial support from CIHR (CRC and Bridge grants) and NSERC (Discovery grant). JF is grateful to the Arthritis Society and the French Embassy (Frontenac scholarship) for financial support. BRS thanks the financial support of GRUM. KM acknowledges support from NSF (DMR 1501324 and DMR 1436219). We thank Agnes Crepet for her help with GPC experiments.

Conclusions de la partie 2

Cette étude nous a permis d'évaluer la conformation et la stabilité de notre écouvillon moléculaire en milieu tamponné. Nous avons démontré que notre écouvillon moléculaire se comporte comme un cylindre déformable exerçant une force purement répulsive due à l'encombrement stérique des chaines opposées et à la pression osmotique générée par la force d'hydratation des chaines polyzwitterioniques. Nous avons pu également observer que la gène stérique de ce polymère génère le dégreffage partiel des chaines latérales qui sont portées par des liaisons esters réversibles. Cependant, ce vieillissement n'altère pas ses propriétés lubrifiantes. Avec un temps de demi-vie de deux ans, notre écouvillon polymère peut être stocké pour injection ultérieure, après stérilisation par filtration à 0.4 μm. En perspectives à cette étude, il serait opportun d'étudier la stabilité et le temps de résidence de ce polymère *in vivo*, en d'autres termes, la pharmacocinétique, en utilisant par exemple une technique d'imagerie et un écouvillon moléculaire marqué avec un fluorophore ou un radiotraceur. En effet, durant des périodes inflammatoires, les conditions plus acides et des enzymes comme des estérases peuvent augmenter la vitesse de dégradation de notre polymère. De plus, le drainage lymphatique du SF pourrait permettre l'élimination plus rapide de notre mime comme c'est le cas avec HA, même si notre écouvillon est conçu pour s'adsorber efficacement sur la surface articulaire.

Références

1. Lindenhayn, K.; Heilmann, H.-H.; Niederhausen, T.; Walther, H.-U.; Pohlenz, K., Elimination of Tritium-Labelled Hyaluronic Acid from Normal and Osteoarthritic Rabbit Knee Joints. In *Clin. Chem. Lab. Med.*, 1997; Vol. 35, p 355.
2. Brown, T. J.; Laurent, U. B.; Fraser, Turnover of hyaluronan in synovial joints: elimination of labelled hyaluronan from the knee joint of the rabbit. *Exp. Physiol.* **1991,** *76* (1), 125-134.
3. Tehranzadeh, J.; Booya, F.; Root, J., Cartilage metabolism in osteoarthritis and the influence of viscosupplementation and steroid: a review. *Acta Radiol.* **2005,** *46* (3), 288-96.
4. Faivre, J.; Shrestha, B. R.; Xie, G.; Delair, T.; David, L.; Matyjaszewski, K.; Banquy, X., Unraveling the Correlations between Conformation, Lubrication and Chemical Stability of Bottlebrush Polymers at Interfaces. *Biomacromolecules* **2017**.
5. Paturej, J.; Sheiko, S. S.; Panyukov, S.; Rubinstein, M., Molecular structure of bottlebrush polymers in melts. *Sci. Adv.* **2016,** *2* (11).
6. Denesyuk, N. A., Conformational properties of bottle-brush polymers. *Phys. Rev. E: Stat. Nonlinear Soft Matter Phys.* **2003,** *67* (5 Pt 1), 051803.
7. Sheiko, S. S.; Sumerlin, B. S.; Matyjaszewski, K., Cylindrical molecular brushes: Synthesis, characterization, and properties. *Prog. Polym. Sci.* **2008,** *33* (7), 759-785.
8. Zheng, X.; Zhang, C.; Bai, L.; Liu, S.; Tan, L.; Wang, Y., Antifouling property of monothiol-terminated bottle-brush poly(methylacrylic acid)-graft-poly(2-methyl-2-oxazoline) copolymer on gold surfaces. *J. Mater. Chem. B* **2015,** *3* (9), 1921-1930.
9. Daniel, W. F. M.; Burdynska, J.; Vatankhah-Varnoosfaderani, M.; Matyjaszewski, K.; Paturej, J.; Rubinstein, M.; Dobrynin, A. V.; Sheiko, S. S., Solvent-free, supersoft and superelastic bottlebrush melts and networks. *Nat. Mater.* **2016,** *15* (2), 183-189.
10. Banquy, X.; Burdyńska, J.; Lee, D. W.; Matyjaszewski, K.; Israelachvili, J., Bioinspired Bottle-Brush Polymer Exhibits Low Friction and Amontons-like Behavior. *J. Am. Chem. Soc.* **2014,** *136* (17), 6199-6202.
11. Li, X.; Prukop, S. L.; Biswal, S. L.; Verduzco, R., Surface Properties of Bottlebrush Polymer Thin Films. *Macromolecules* **2012,** *45* (17), 7118-7127.
12. Sveinbjörnsson, B. R.; Weitekamp, R. A.; Miyake, G. M.; Xia, Y.; Atwater, H. A.; Grubbs, R. H., Rapid self-assembly of brush block copolymers to photonic crystals. *Proc. Natl. Acad. Sci. U.S.A* **2012,** *109* (36), 14332-14336.
13. Sowers, M. A.; McCombs, J. R.; Wang, Y.; Paletta, J. T.; Morton, S. W.; Dreaden, E. C.; Boska, M. D.; Ottaviani, M. F.; Hammond, P. T.; Rajca, A.; Johnson, J. A., Redox-responsive branched-bottlebrush polymers for in vivo MRI and fluorescence imaging. *Nat. Commun.* **2014,** *5*, 5460.
14. Johnson, J. A.; Lu, Y. Y.; Burts, A. O.; Xia, Y.; Durrell, A. C.; Tirrell, D. A.; Grubbs, R. H., Drug-Loaded, Bivalent-Bottle-Brush Polymers by Graft-through ROMP. *Macromolecules* **2010,** *43* (24), 10326-10335.
15. Venkataraman, S.; Hedrick, J. L.; Ong, Z. Y.; Yang, C.; Ee, P. L. R.; Hammond, P. T.; Yang, Y. Y., The effects of polymeric nanostructure shape on drug delivery. *Adv. Drug Delivery Rev.* **2011,** *63* (14–15), 1228-1246.
16. Müllner, M.; Dodds, S. J.; Nguyen, T.-H.; Senyschyn, D.; Porter, C. J. H.; Boyd, B. J.; Caruso, F., Size and Rigidity of Cylindrical Polymer Brushes Dictate Long Circulating Properties In Vivo. *ACS Nano* **2015,** *9* (2), 1294-1304.
17. Devarajan, P. V.; Jindal, A. B.; Patil, R. R.; Mulla, F.; Gaikwad, R. V.; Samad, A., Particle Shape: A New Design Parameter for Passive Targeting In Splenotropic Drug Delivery. *J. Pharm. Sci.* **2010,** *99* (6), 2576-2581.
18. Zappone, B.; Ruths, M.; Greene, G. W.; Jay, G. D.; Israelachvili, J. N., Adsorption, lubrication, and wear of lubricin on model surfaces: polymer brush-like behavior of a glycoprotein. *Biophys. J.* **2007,** *92* (5), 1693-1708.
19. Jay, G. D.; Torres, J. R.; Warman, M. L.; Laderer, M. C.; Breuer, K. S., The role of lubricin in the mechanical behavior of synovial fluid. *Proc. Natl. Acad. Sci. U.S.A* **2007,** *104* (15), 6194-6199.

20. Chang, D. P.; Abu-Lail, N. I.; Guilak, F.; Jay, G. D.; Zauscher, S., Conformational Mechanics, Adsorption, and Normal Force Interactions of Lubricin and Hyaluronic Acid on Model Surfaces. *Langmuir* **2008,** *24* (4), 1183-1193.
21. Coles, J. M.; Chang, D. P.; Zauscher, S., Molecular mechanisms of aqueous boundary lubrication by mucinous glycoproteins. *Curr. Opin. Colloid Interface Sci.* **2010,** *15* (6), 406-416.
22. Das, S.; Banquy, X.; Zappone, B.; Greene, G. W.; Jay, G. D.; Israelachvili, J. N., Synergistic interactions between grafted hyaluronic acid and lubricin provide enhanced wear protection and lubrication. *Biomacromolecules* **2013,** *14* (5), 1669-1677.
23. Majd, S. E.; Kuijer, R.; Kowitsch, A.; Groth, T.; Schmidt, T. A.; Sharma, P. K., Both Hyaluronan and Collagen Type II Keep Proteoglycan 4 (Lubricin) at the Cartilage Surface in a Condition That Provides Low Friction during Boundary Lubrication. *Langmuir* **2014**, 14566-14572.
24. Han, L.; Dean, D.; Ortiz, C.; Grodzinsky, A. J., Lateral Nanomechanics of Cartilage Aggrecan Macromolecules. *Biophys. J.* **2007,** *92* (4), 1384-1398.
25. Seror, J.; Merkher, Y.; Kampf, N.; Collinson, L.; Day, A. J.; Maroudas, A.; Klein, J., Articular Cartilage Proteoglycans As Boundary Lubricants: Structure and Frictional Interaction of Surface-Attached Hyaluronan and Hyaluronan–Aggrecan Complexes. *Biomacromolecules* **2011,** *12* (10), 3432-3443.
26. Roughley, P.; Mort, J., The role of aggrecan in normal and osteoarthritic cartilage. *J. Exp. Orthop.* **2014,** *1* (1), 1-11.
27. Pettersson, T.; Naderi, A.; Makuska, R.; Claesson, P. M., Lubrication properties of bottle-brush polyelectrolytes: An AFM study on the effect of side chain and charge density. *Langmuir* **2008,** *24* (7), 3336-3347.
28. Russano, D.; Carrillo, J. M. Y.; Dobrynin, A. V., Interaction between Brush Layers of Bottle-Brush Polyelectrolytes: Molecular Dynamics Simulations. *Langmuir* **2011,** *27* (17), 11044-11051.
29. Liu, X.; Dedinaite, A.; Rutland, M.; Thormann, E.; Visnevskij, C.; Makuska, R.; Claesson, P. M., Electrostatically Anchored Branched Brush Layers. *Langmuir* **2012,** *28* (44), 15537-15547.
30. Liu, X.; Thormann, E.; Dedinaite, A.; Rutland, M.; Visnevskij, C.; Makuska, R.; Claesson, P. M., Low friction and high load bearing capacity layers formed by cationic-block-non-ionic bottle-brush copolymers in aqueous media. *Soft Matter* **2013,** *9* (22), 5361-5371.
31. Singh, M. K.; Ilg, P.; Espinosa-Marzal, R. M.; Kroeger, M.; Spencer, N. D., Polymer Brushes under Shear: Molecular Dynamics Simulations Compared to Experiments. *Langmuir* **2015,** *31* (16), 4798-4805.
32. Milchev, A.; Paturej, J.; Rostiashvili, V. G.; Vilgis, T. A., Thermal Degradation of Adsorbed Bottle-Brush Macromolecules: A Molecular Dynamics Simulation. *Macromolecules* **2011,** *44* (10), 3981-3987.
33. Sheiko, S. S.; Sun, F. C.; Randall, A.; Shirvanyants, D.; Rubinstein, M.; Lee, H.-i.; Matyjaszewski, K., Adsorption-induced scission of carbon-carbon bonds. *Nature* **2006,** *440* (7081), 191-194.
34. Xia, Y.; Boydston, A. J.; Grubbs, R. H., Synthesis and Direct Imaging of Ultrahigh Molecular Weight Cyclic Brush Polymers. *Angew. Chem. Int. Ed.* **2011,** *50* (26), 5882-5885.
35. Chen, K.; Susner, M. A.; Vyazovkin, S., Effect of the Brush Structure on the Degradation Mechanism of Polystyrene–Clay Nanocomposites. *Macromol. Rapid Commun.* **2005,** *26* (9), 690-695.
36. Xu, L.; Crawford, K.; Gorman, C. B., Effects of Temperature and pH on the Degradation of Poly(lactic acid) Brushes. *Macromolecules* **2011,** *44* (12), 4777-4782.
37. Lee, H. Y.; Han, L.; Roughley, P. J.; Grodzinsky, A. J.; Ortiz, C., Age-related nanostructural and nanomechanical changes of individual human cartilage aggrecan monomers and their glycosaminoglycan side chains. *Journal of structural biology* **2013,** *181* (3), 264-73.
38. Faivre, J.; Shrestha, B. R.; Burdynska, J.; Xie, G.; Moldovan, F.; Delair, T.; Benayoun, S.; David, L.; Matyjaszewski, K.; Banquy, X., Wear Protection without Surface Modification Using a Synergistic Mixture of Molecular Brushes and Linear Polymers. *ACS Nano* **2017,** *11* (2), 1762-1769.
39. Wang, J.-S.; Matyjaszewski, K., Controlled/"living" radical polymerization. atom transfer radical polymerization in the presence of transition-metal complexes. *J. Am. Chem. Soc.* **1995,** *117* (20), 5614-5615.
40. Matyjaszewski, K., Atom Transfer Radical Polymerization (ATRP): Current Status and Future Perspectives. *Macromolecules* **2012,** *45* (10), 4015-4039.

41. Nussbaum-Krammer, C. I.; Neto, M.; aacute; rio, F.; Brielmann, R.; e, M.; Pedersen, J. S.; Morimoto, R. I., Investigating the Spreading and Toxicity of Prion-like Proteins Using the Metazoan Model Organism C. elegans. *J. Vis. Exp.* **2015,** (95).
42. Israelachvili, J. N., Thin film studies using multiple-beam interferometry. *J. Colloid Interface Sci.* **1973,** *44* (2), 259-272.
43. Israelachvili, J.; Min, Y.; Akbulut, M.; Alig, A.; Carver, G.; Greene, W.; Kristiansen, K.; Meyer, E.; Pesika, N.; Rosenberg, K.; Zeng, H., Recent advances in the surface forces apparatus (SFA) technique. *Rep. Prog. Phys.* **2010,** *73* (3).
44. Banquy, X.; Lee, D. W.; Das, S.; Hogan, J.; Israelachvili, J. N., Shear-Induced Aggregation of Mammalian Synovial Fluid Components under Boundary Lubrication Conditions. *Adv. Funct. Mater.* **2014,** *24* (21), 3152-3161.
45. Lewis, A.; Tang, Y.; Brocchini, S.; Choi, J. W.; Godwin, A., Poly(2-methacryloyloxyethyl phosphorylcholine) for protein conjugation. *Bioconjug. Chem.* **2008,** *19* (11), 2144-55.
46. Dedinaite, A., Biomimetic lubrication. *Soft Matter* **2012,** *8* (2), 273-284.
47. Chen, M.; Briscoe, W. H.; Armes, S. P.; Klein, J., Lubrication at Physiological Pressures by Polyzwitterionic Brushes. *Science* **2009,** *323* (5922), 1698-1701.
48. Kobayashi, M.; Terayama, Y.; Kikuchi, M.; Takahara, A., Chain dimensions and surface characterization of superhydrophilic polymer brushes with zwitterion side groups. *Soft Matter* **2013,** *9* (21), 5138-5148.
49. Fleer, G.; Stuart, M. C.; Scheutjens, J.; Cosgrove, T.; Vincent, B., *Polymers at interfaces*. Springer Science & Business Media: 1993.
50. Degennes, P. G., Polymers at an Interface - a Simplified View. *Adv Colloid Interfac* **1987,** *27* (3-4), 189-209.
51. Tirrell, M.; Patel, S.; Hadziioannou, G., Polymeric amphiphiles at solid-fluid interfaces: Forces between layers of adsorbed block copolymers. *Proc. Natl. Acad. Sci. U.S.A* **1987,** *84* (14), 4725-4728.
52. Marzolin, C.; Auroy, P.; Deruelle, M.; Folkers, J. P.; Léger, L.; Menelle, A., Neutron Reflectometry Study of the Segment-Density Profiles in End-Grafted and Irreversibly Adsorbed Layers of Polymer in Good Solvents. *Macromolecules* **2001,** *34* (25), 8694-8700.
53. Russano, D.; Carrillo, J. M.; Dobrynin, A. V., Interaction between brush layers of bottle-brush polyelectrolytes: molecular dynamics simulations. *Langmuir* **2011,** *27* (17), 11044-51.
54. Brangbour, C.; du Roure, O.; Helfer, E.; Demoulin, D.; Mazurier, A.; Fermigier, M.; Carlier, M. F.; Bibette, J.; Baudry, J., Force-velocity measurements of a few growing actin filaments. *PLoS Biol* **2011,** *9* (4), e1000613.
55. Tugulu, S.; Klok, H.-A., Stability and nonfouling properties of poly (poly (ethylene glycol) methacrylate) brushes under cell culture conditions. *Biomacromolecules* **2008,** *9* (3), 906-912.

Introduction de la partie 3

À travers ces deux premières parties, nous avons synthétisé et caractérisé un écouvillon moléculaire sans groupement d'ancrage avec de bonnes propriétés lubrifiantes, mais ayant une faible résistance aux pressions et cisaillement appliqués dans un contact mica-mica. Ce polymère est capable de conserver ces propriétés lubrifiantes sur une longue période de temps en milieu tamponné salin et interagit de manière synergique avec l'HA de haut poids moléculaire afin de résister à des pressions qui restent inférieures aux pressions que peut subir une articulation synoviale humaine[1]. L'objectif de cette partie est donc de concevoir une librairie de polymères résistants à de plus fortes pressions (de l'ordre de 10 MPa) tout en conservant les propriétés de lubrification en les munissant de groupements d'ancrage adaptés à la surface d'étude. Avec une collaboration avec le laboratoire du Pr Matyjaszewski, nous avons mis au point des écouvillons moléculaires possédant un ou deux groupements d'ancrage polycationiques en plus de notre contrôle sans groupement d'ancrage (témoin). Dans toute cette partie 3, ces différents polymères sont nommés mono (pas de groupement d'ancrage, un bloc en peigne), di (un groupement d'ancrage et un domaine en peigne) et tribloc (deux groupements d'ancrage et un domaine central en peigne) en référence aux nombres de blocs constituant chaque polymère. Ces polymères, conçus pour s'ancrer sur des surfaces anioniques, s'adsorbent sur le mica[2] permettant l'analyse tribologique à l'aide du SFA.

Cette étude a fait l'objet d'un article dans le journal de l'American Chemical Society, *Chemistry of Materials*, publié le 30 mai 2018 et intitulé : *Intermolecular Interactions between Bottlebrush Polymers Boost the Protection of Surfaces against Frictional Wear*. Les polymères mono et tribloc ont été synthétisés au sein du laboratoire du Pr Matyjaszewski tandis que le dibloc a été synthétisé par mes soins. Les profils d'interaction et la tribologie à l'aide du SFA ont été effectués par Dr Buddha R. Shrestha et moi-même au sein du laboratoire du Pr Xavier Banquy. La caractérisation par AFM des structures des polymères a été réalisée par le Pr Xavier Banquy et moi-même. Enfin, les expérimentations GPC ont été menées dans le laboratoire des Pr Laurent David et Thierry Delair.

Intermolecular Interactions between Bottlebrush Polymers Boost the Protection of Surfaces against Frictional Wear

Jimmy Faivre[1,4], Buddha Ratna Shrestha[1], Guojun Xie,[2] Mateusz Olszewski,[2] Vahid Adibnia[1], Florina Moldovan[3], Alexandra Montembault[4], Guillaume Sudre[4], Thierry Delair[4], Laurent David[4], Krzysztof Matyjaszewski[2*], Xavier Banquy[1*]

[1]*Canadian Research Chair in Bioinspired Materials, Faculty of Pharmacy, Université de Montréal, Montréal, Qc, Canada*

[2]*Center for Macromolecular Engineering, Department of Chemistry, Carnegie Mellon University, Pittsburgh, PA, USA*

[3]*Department of Stomatology, Faculty of Dentistry, CHU Sainte Justine Research Center, Montréal QC H3T 1C5, Canada*

[4]*Université de Lyon, Université Claude Bernard Lyon 1, CNRS UMR 5223, Ingénierie des Matériaux Polymères (IMP), 15 Boulevard Latarjet, 69622 Villeurbanne Cedex, France*

Abstract

Polymers exhibiting the bottlebrush (BB) architecture have excellent lubricating properties. However, in order to motivate their use in real life systems, they must also protect surfaces against frictional damage. In this article, we synthesized a library of polyzwiterrionic bottlebrush polymers of different architectures to explore the effect of intermolecular interactions on their conformation at interfaces and their tribological properties. Using the surface forces apparatus, we show that increasing the number of adhesives blocks on the BB polymers does not impact the friction coefficient on mica surfaces, μ, which remained close to μ = 0.02 but drastically increased the threshold pressure, P^*, at which wear initiates from P^* = 0.4 ± 0.1 MPa up to P^* = 8.0 ± 0.8 MPa. In mixtures of high molecular weight hyaluronic acid (HA) and BB polymers, a synergistic interaction between polymers occurred leading to a significant increase of P^*, independently of the BB polymer tested and even reaching super-protection for strongly interacting polymers (up to P^* > 14 MPa). Overall, these results show that strong intermolecular interaction between BB polymers and high molecular weight linear polymers is a promising strategy to create highly-protective lubricants.

Keywords: lubrication, bottlebrush polymer, wear resistance, bio-inspired polymer, SFA

Table of Contents

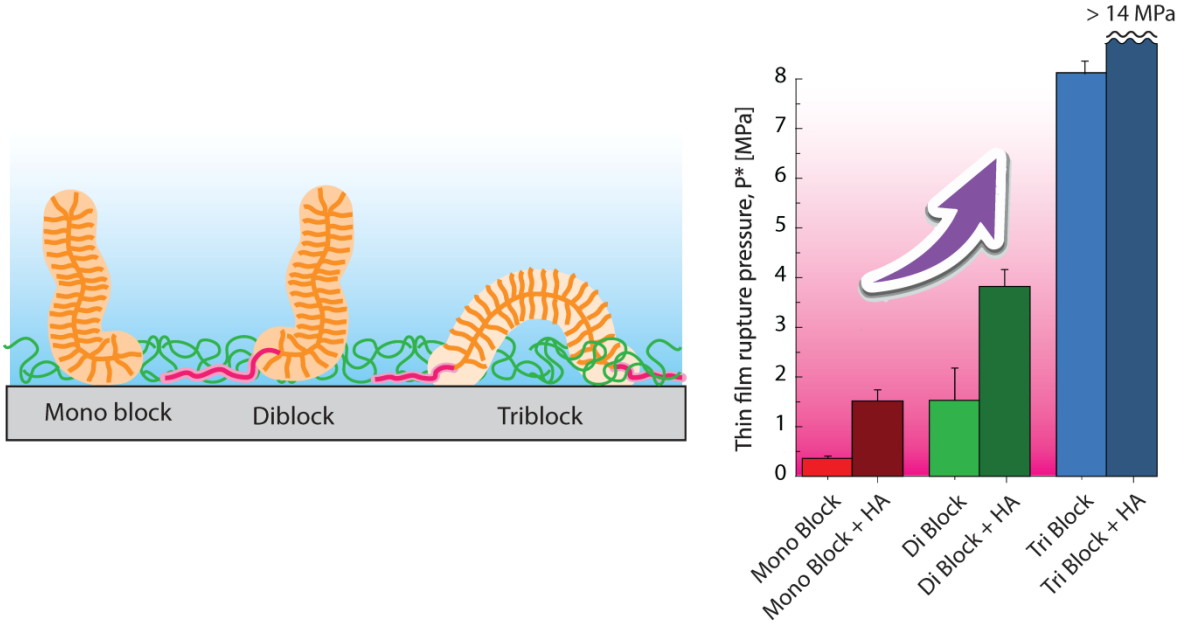

2.9 Introduction

Using inspiration from nature, new materials able to perform under severe working conditions have been designed and tested successfully. Bioinspiration mimicks naturally-occurring nano, micro and macroscale structures which are remarkably efficient in resisting specific environmental stresses[3].This concept has been applied to a myriad of materials[3-5] with the aim to significantly enhance their mechanical, biological, physical or chemical properties. Bioinspiration has fostered a breadth of new technologies in many different fields. To name only a few, we can cite the development of superhydrophobic coatings inspired from the lotus leaf[6], bioadhesive coatings or surfaces inspired from the Gecko's feet or the mussel's adhesive foot proteins, antifouling coatings making use of anti-adhesive proteoglycans-mimicking polymers[2, 7-8], antireflective coatings mimicking the Moth's eyes structure[9-10], optically active surfaces inspired from the beetle scales structure[11] , advanced robotic devices able to evolve in complex environments using animal-like locomotion[12], drug-delivery systems mimicking bacteria or immune cells[13-14], vaccines technologies using virus-like particles[15] and biomaterial scaffolds mimicking bone or cartilage structure[16-17] .

Among all these examples of bioinspired materials, bottlebrush (BB) polymers, or macromolecular brushes,[18-19]are promising materials for lubrication applications. Their architecture mimicks mucin-like proteoglycans found in synovial joints such as lubricin and aggrecans. These proteins are known to play a key role in the biolubrication and wear resistance of articular cartilage, and using a biomimetic approach, researchers have been able to design artificial lubricants displaying extremely low coefficients of friction (CoF) and high wear protection of fragile soft surfaces.[2, 20-24] The structure of lubricin includes a highly hydrated central domain and two adhesive side domains[25-32]. The central domain consists of a polypeptide backbone bearing heavily glycosylated side chains composed of a significant amount of anionic carbohydrate units such as N- acetylneuraminic acid for lubricin and chondroitin and keratan sulfate moieties for aggrecan[26, 33]. This central domain is known to impart excellent anti-adhesive properties to lubricin mostly due to strongly repulsive steric and hydration forces. On the other hand, adhesive domains are essential under severe working conditions. In the case of lubricin, the formation of the lubricant protective layer at the cartilage surface is provided by means of its affinity to fibronectin, type-II collagen or cartilage oligomeric matric protein[34]. For aggrecans, their attachment at one extremity to hyaluronic acid (HA) is mediated *via* the link protein which allows them to remain inside the cartilage matrix in order to increase its osmotic pressure.[35-36]

BB polymers mimic the branched architecture of these proteins with pendant chains grafted to a backbone[2, 37] and often exceed 1 MDa in molecular weight and 100 nm in contour length. Anchoring groups have also been incorporated at the extremities of these polymers[2], or distributed along the polymer backbone[38-40] in order to improve their adhesion to different substrates. To ensure lubrication under severe working conditions such as boundary lubrication condition, anchoring groups must be designed to interact strongly with the surface they are meant to protect. Different types of anchoring groups have been probed making use of a large variety of molecular interactions such as electrostatic interactions using poly(L-Lysine)[41], 2-methacryloyloxyethyl trimethyl ammonium chloride[42-43] or quaternized 2-(dimethylaminoethyl) methacrylate[2], as well as hydrophobic interactions[39], or covalent bounding.[8]

Many structural parameters of BB polymers can be varied to optimize their lubricating properties. A variety of bottle-brush domains have been reported using either uncharged pendant chains (poly(ethylene glycol), dextran)[23, 39, 41], charged anionic[44] or cationic[45] pendant chains and zwitterionic (2-methacryloyloxyethyl phosphorylcholine)[2] pendant chains, all leading to a low CoF over several decades of applied normal forces and shear rates. Carillo *et al*. demonstrated that charged BB polymers exhibited a lower CoF compared to neutral polymers due to the additional osmotic pressure originated from their charges and surrounding counter-ions, a phenomenon that could be decreased with the ionic strength increase[46] but not for polyzwitterionic polymers[47]. The length of the pendant chains as well as the backbone chain seem to also impact the lubrication of surfaces *in vitro* in a non trivial way.[8]

We recently showed that mixtures of BB polymers and hydrophilic, high molecular weight, and linear polymers exhibit synergistic wear protection properties.[47] The synergy arises from strong, yet transient, intermolecular entanglements appearing during high compression/confinement. This synergy was observed with a monoblock BB polymer, designed to interact with the hydrophilic linear polymer only *via* physical entanglements and not *via* electrostatic, hydrophobic or any specific interactions. The aim of the present study is to explore the effect of the intermolecular interactions between linear and BB polymers on their lubricating and wear protecting capacity. We synthesized a series of BB polymers exhibiting adhesive blocks designed to interact strongly with polyanionic electrolytes such as hyaluronic acid. We characterized the tribological properties of the polymer mixtures with the

surface forces apparatus in order to elucidate the interaction forces creating the synergistic effect and rationalize its properties.

2.10 Materials and methods

2.10.1 Materials

Methyl methacrylate (MMA, purity = 99%, Sigma-Aldrich, USA) and 2-(trimethylsilyloxy)ethyl methacrylate (HEMA-TMS, purity > 96%, Scientific Polymer Products Inc., USA), 2-(dimethylamino)ethyl methacrylate (DMAEMA, 98%, Sigma-Aldrich, USA) were passed through a column filled with basic alumina prior to use. 2-Methacryloyloxyethyl phosphorylcholine (MPC, purity ≥ 97%, Sigma-Aldrich, USA) was recrystallized from acetonitrile and dried under vacuum overnight at room temperature before polymerization. Tetrahydrofuran (THF) was used after it was purified by tapping off from a solvent purification column right. Ethyl α-bromoisobutyrate (EBiB, purity ≥ 98%, Sigma-Aldrich, USA), α-Bromoisobutyryl bromide 98% (BiBB, purity ≥ 98%, Sigma-Aldrich, USA) copper(I) chloride ($Cu^{I}Cl$, purity ≥ 99.995% trace metals basis, Sigma-Aldrich, USA), copper(II) chloride ($Cu^{II}Cl_2$, purity ≥ 99.995% trace metals basis, anhydrous, Sigma-Aldrich, USA), 2,2′-bipyridyl (bpy, purity ≥ 99%, Sigma-Aldrich, USA), 4,4′-Dinonyl-2,2′-dipyridyl (dNbpy, purity ≥ 97%, Sigma-Aldrich, USA), potassium fluoride (KF, purity ≥ 99%, spray-dried, Sigma-Aldrich, USA), tetrabutylamonium fluoride (TBAF, 1M solution in THF, Sigma-Aldrich, USA) and α-bromoisobutyryl bromide (purity = 98%, Sigma-Aldrich, USA were used without any additional purification. Ethylene bis(2-bromoisobutyrate) (2f-BiB) was synthesized according to procedures reported in the literature[48]. Ruby mica-sheets were purchased from S&J Trading Inc. (Glen Oaks, NY, USA). Milli-Q quality water was obtained from a Millipore Gradient A10 S10 purification system (resistance = 18.2 MΩ.cm, TOC ≤ 4 ppb). Phosphate buffer saline (10mM Phosphate, 150mM NaCl and pH 7.4) was prepared in our laboratory. 1.5 MDa sodium hyaluronate was obtained from lifecore biomedical (Minneapolis, USA).

2.10.2 BB polymers characterizations

Proton nuclear magnetic resonance (^{1}H NMR) spectroscopy was performed using Variant 400 MHz spectrometer. In all cases deuterated chloroform ($CDCl_3$) was used as a solvent, except for bottle-brush polymer which was analyzed using deuterated methanol (CD_3OD). ^{1}H chemical shifts are reported in parts per million (ppm) downfield from tetramethylsilane (TMS). Apparent molecular weights and molecular weight distributions measurements of

polymers except bottle-brush polymer were measured by size exclusion chromatography (SEC) using Polymer Standards Services (PSS) columns (SDV: guard, 10^5, 10^3, and 500 Å; GRAM: guard, 10^5, 10^3, and 10^2 Å), with THF or DMF as eluent at 35°C or 50 °C at a constant flow rate of 1.00 mL/min, and differential refractive index (RI) detector (Waters and Wyatt). The apparent number-average molecular weights (M_n) and molecular weight distribution (M_w/M_n) were determined with a calibration based on linear poly(methyl methacrylate) (PMMA) standards and diphenyl ether as an internal standard. Hyaluronic acid apparent molecular weights and distributions measurements were assessed by aqueous SEC in 10mM PBS, pH 7.4, 150mM NaCl buffer using TSKgel columns (TSKgel G6000PW, particle size 12µm, and TSKgel G2500PW, particle size 12µm) at a constant flow rate of 1.00 mL/min, and differential refractive index (RI) detector (Waters). The apparent number-average molecular weights (M_n) and molecular weight distribution (M_w/M_n) were determined with a dn/dc set at 0.16 mL/mg.

2.10.3 BB polymers syntheses

2.10.3.1 Monoblock bottlebrush polymer synthesis (Fig. 2.23)

Synthesis of poly(HEMA-TMS)$_{459}$-co-PMMA$_{370}$ (A block). A dry 25 mL Schlenk flask was charged with bis(2-bromoisobutyrate) (2f-BiB, 25.8 mg, 0.0718 mmol), $Cu^{II}Cl_2$ (7.8 mg, 0.057 mmol), dNbpy (0.294 g, 0.718 mmol), HEMA-TMS (23.2 g, 25.0 mL, 115 mmol), MMA (11.5 g, 12.3 mL, 115 mmol) and anisole (4.1 mL). The solution was degassed by three freeze-pump-thaw cycles. During the final cycle, the flask was filled with nitrogen and $Cu^{I}Cl$ (28.4 mg, 0.287 mmol) was quickly added to the frozen reaction mixture. The flask was sealed, evacuated and back-filled with nitrogen five times, and then immersed in an oil bath at 70 °C. Reaction was stopped when the monomer conversion reached 25.9%. The monomers consumption was calculated by the integration of MMA and HEMA-TMS vinyl groups signal (C*H*H=C-CH_3, 6.11 ppm or 5.56 ppm) against the internal standard (anisole, *o*,*p*-Ar-H, 6.91 ppm). The A block was purified by three precipitations from hexane, dried under vacuum for 16 h at room temperature, and analyzed by ^{1}H NMR spectroscopy. The ratio of PMMA (*s*, broad, CO-O-C*H*$_3$, 3.54-3.68 ppm) to P(HEMA-TMS) (*s*, broad, O-C*H*$_2$-CH_2-O, 3.72-3.85 ppm) peaks resulted in the polymer composition, P(HEMA-TMS)$_{459}$-co-PMMA$_{370}$. Apparent molecular weights were determined using THF SEC: M_n = 82,200, M_w/M_n = 1.16.

Synthesis of polyBiBEM$_{459}$-co-PMMA$_{370}$ (A Block macroinitiator, A MI). The polymer, **A block** (0.687 g, containing 2.42 mmol of HEMA-TMS units), potassium fluoride (0.171 g,

2.90 mmol) and 2,6-di-*tert*-butylphenol (49.8 mg, 0.242 mmol) were placed in a 50 ml round bottom flask. The flask was sealed, flushed with nitrogen, and dry THF (20 mL) was added. The mixture was cooled in an ice bath to 0 °C, tetrabutylammonium fluoride solution in THF (1M, 0.02 mL, 0.02 mmol) was injected to the flask, followed by the drop-wise addition of 2-bromoisobutyryl bromide (0.36 mL, 2.9 mmol). After the addition the reaction mixture was allowed to reach room temperature and stirring was continued for 24 h. The solids were filtered off, and the solution was precipitated into methanol:water (70:30, v/v%). The precipitate was re-dissolved in chloroform and passed through a short column filled with basic alumina. The filtrate was re-precipitated three times from chloroform into hexanes and dried under vacuum overnight at room temperature.

Synthesis of poly[(BiBEM$_{400}$-*g*-MPC$_{41}$)-*stat*-MMA$_{400}$] (Monoblock BB polymer). A dry 5 mL Schlenk flask was charged with polymer **A MI** (10.2 mg, 2.8 μmol of BiBEM), 2-methacryloyloxyethyl phosphorylcholine (2.5 g, 8.5 mmol), 2,2'-bipyridyl (15.0 mg, 0.0960 μmol), $Cu^{II}Cl_2$ (as a stock solution, 0.76 mg, 0.056 mmol), acetonitrile (3.0 mL) and methanol (7.0 mL). The solution was degassed by three freeze-pump-thaw cycles. After the final cycle $Cu^{I}Cl$ (4.2 mg, 0.042 μmol) was added followed by thawing reaction mixture under nitrogen atmosphere, and the flask was immersed in an oil bath thermostated at 50 °C. The reaction was stopped by exposing the solution to air when the monomer conversion reached 13.8%, achieving the monoblock BB polymer. The brush was purified by dialysis against MeOH for 48 h using tubes with a pore size molar mass cut off 10,000 kDa. The Monomer conversion was calculated by ^{1}H NMR analysis, resulting in the average degree of polymerization of the side chains, DP~41.

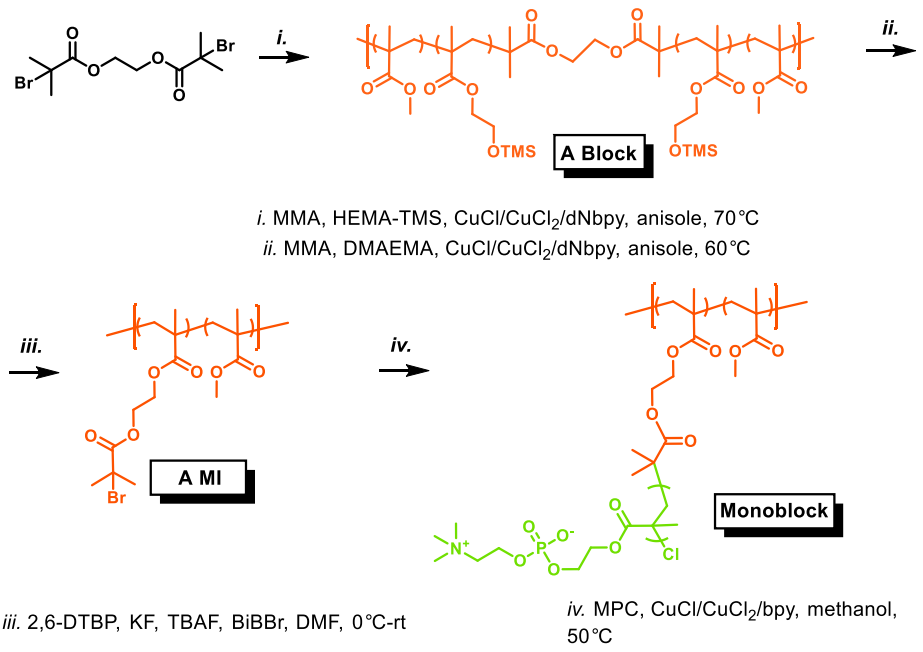

Figure 2.23. *Synthesis of the monoblock BB polymer*

2.10.3.2 Triblock BB polymer synthesis (Fig. 2.24)

Synthesis of poly[(DMAEMA$_{98}$-*stat*-MMA$_{65}$)-*b*-(HEMA-TMS$_{459}$-*stat*-MMA$_{370}$)-*b*-(DMAEMA$_{98}$-*stat*-MMA$_{65}$)] (BAB). A dry 10 mL Schlenk flask was charged with **the previous A block** (1.02 g, 0.0081 mmol), $Cu^{II}Cl_2$ (as a stock solution, 0.54 mg, 4.0 µmol), dNbpy (0.0330 g, 0.0808 mmol), DMAEMA (2.03 g, 2.17 mL, 12.9 mmol), MMA (1.29 g, 1.38 mL, 12.9 mmol) and anisole (3.6 mL). The solution was degassed by three freeze-pump-thaw cycles. During the final cycle, the flask was filled with nitrogen and $Cu^{I}Cl$ (0.0034 g, 0.035 mmol) was quickly added to the frozen reaction mixture. The flask was sealed, evacuated and back-filled with nitrogen five times, and then immersed in an oil bath at 60 °C. Reaction was stopped via exposure to air when the monomer conversion reached 15.3%. The product was precipitated from hexanes (twice) and water, re-dissolved in chloroform and passed through neutral alumina. The solvent was removed and the purified product was dried overnight under vacuum at room temperature. The ^{1}H NMR spectra of a pure **BAB** was used to evaluate its final composition, giving poly[(DMAEMA$_{98}$-*stat*-MMA$_{65}$)-*b*-(HEMA-TMS$_{459}$-*stat*-MMA$_{370}$)-*b*-(DMAEMA$_{98}$-*stat*-MMA$_{65}$)] (**BAB**). The structure of the polymer was determined from the ratio of selected polymer signals: PMMA (*s*, broad, CO-O-C*H*$_3$, 3.54-3.68 ppm), P(HEMA-TMS) (*s*, broad, O-C*H*$_2$-CH$_2$-O, 3.72-3.85 ppm) and PDMAEMA (*m*, C*H*$_2$-NMe$_2$, 2.55-2.65 ppm). Apparent molecular weights were obtained using THF SEC: M_n = 110,000, M_w/M_n = 1.33.

Synthesis of poly[(qDMAEMA$_{98}$-*stat*-MMA$_{65}$)-*b*-(HEMA-TMS$_{459}$-*stat*-MMA$_{370}$)-*b*-(qDMAEMA$_{98}$-*stat*-MMA$_{65}$)] (quaternized BAB, qBAB). BAB (0.8962 g, containing 1.16 mmol DMAEMA units) was placed in 50 mL flask and dissolved in acetone (25 mL). The solution was cooled in an ice bath to 0 °C, followed by a slow addition of bromoethane (0.48 g, 0.33mL, 4.4 mmol). The reaction was stirred at room temperature for the next 48 h. The solvent was removed and the product was dried under vacuum at room temperature. ^{1}H NMR spectra of the product, **qBAB**, showed the quantitative quaternization of -NMe$_2$ groups, as confirmed by the disappearance of signals corresponding to methylene (C*H*$_2$-NMe$_2$, 2.55-2.65 ppm) and methyl groups (*m*, CH$_2$-N(C*H*$_3$)$_2$, 2.27-2.35) of PDMAEMA.

Synthesis of poly[(qDMAEMA$_{95}$-*stat*-MMA$_{90}$)-*b*-(BiBEM$_{400}$-*stat*-MMA$_{400}$)-*b*-(DMAEMA$_{95}$-*stat*-MMA$_{90}$)] (qBAB macroinitiator, qBAB MI). The polymer, **qBAB** (2.38 g, containing 1.96 mmol of HEMA-TMS units), potassium fluoride (0.139 g, 2.35 mmol) and 2,6-di-*tert*-butylphenol (40.4 mg, 0.196 mmol) were placed in a 100 ml round bottom flask. The flask was sealed, flushed with nitrogen, and dry DMF (30 mL) was added. The mixture was cooled in an ice bath to 0 °C, tetrabutylammonium fluoride solution in THF (1M, 0.02 mL, 0.02 mmol) was injected to the flask, followed by the drop-wise addition of 2-bromoisobutyryl bromide (0.29 mL, 2.35 mmol). After the addition the reaction mixture was allowed to reach room temperature and stirring was continued for 24 h. The product was purified by dialysis against DMF using dialysis tubes with a pore size molar mass cut off 10 kDa..

Synthesis of poly[(qDMAEMA$_{98}$-*stat*-MMA$_{65}$)-*b*-((BiBEM-g-poly(MPC)$_{35}$)$_{459}$-*stat*-MMA$_{370}$)-*b*-(qDMAEMA$_{98}$-*stat*-MMA$_{65}$)] (triblock BB polymer). A dry 50 mL Schlenk flask was charged with polymer **qBAB MI** (32.6 mg in 3 wt% DMF stock solution, containing 0.056 μmol of BiBEM), 2-methacryloyloxyethyl phosphorylcholine (5.00 g, 17.0 mmol), 2,2'-bipyridyl (30.0 mg, 0.192 mmol), Cu^{II}Cl$_2$ (1.5 mg, 0.011 mmol), and methanol (22.0 mL). The solution was degassed by three freeze-pump-thaw cycles. After the final cycle, Cu^{I}Cl (8.4 mg, 0.085 mmol) was added followed by thawing reaction mixture under nitrogen atmosphere, and the flask was immersed in an oil bath thermostated at 45 °C. The reaction was stopped when monomer conversion reached 11.8%. The resulting brush was purified by dialysis against MeOH for 48 h using dialysis tubes with a pore size molar mass cut off 10 kDa. The Monomer conversion was calculated by ^{1}H NMR analysis, resulting in the average degree of polymerization of the side chains, DP~35.

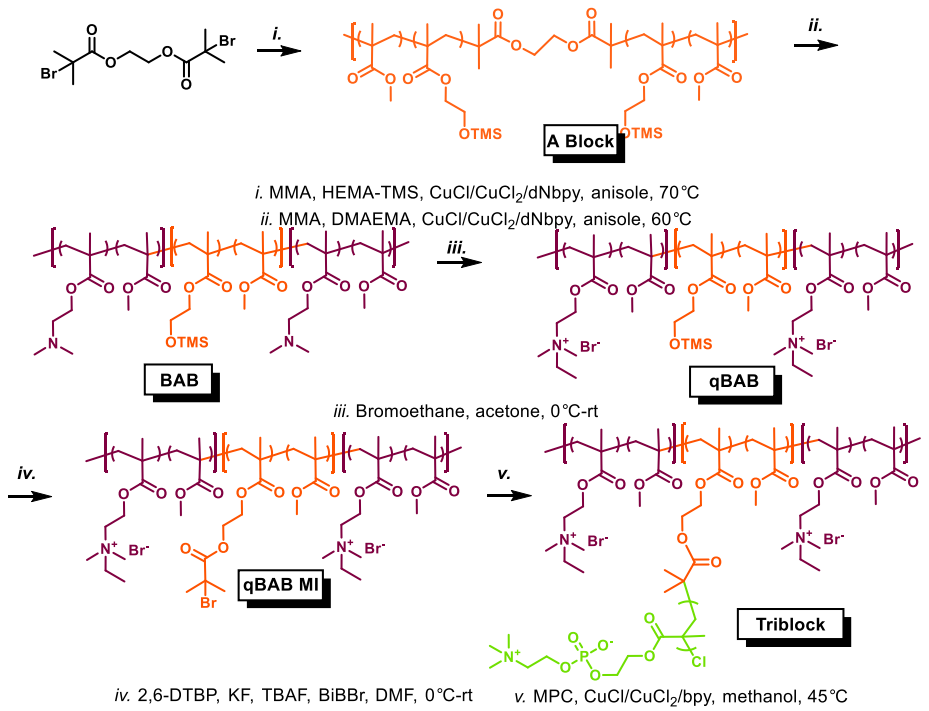

Figure 2.24. *Synthesis of the triblock BB polymer*

2.10.3.3 Diblock BB polymer synthesis (Fig. 2.25)

Synthesis of poly(HEMA-TMS)$_{551}$-co-PMMA$_{338}$ (A block).: A dried round bottom flask was charged with BBiB (3.4 µL, 0.023 mmol), dNbpy (112.8 mg, 0.276 mmol), HEMA-TMS (10.0 mL, 45.9 mmol), MMA (4.9 mL, 45.9 mmol) and anisole (3.0 mL). The solution was bubbled with argon for 30'. $Cu^{I}Br$ (0.0158 g, 0.110 mmol), and $Cu^{II}Br_2$ (0.0061 g, 0.028 mmol) were charged in a dried 50 mL round bottom flask and 3 argon-vacuum cycles were performed to remove oxygen. The flask was sealed, and then immersed in an oil bath at 40 °C. After bubbling, the monomer solution was injected into the catalyst solution. Reaction was stopped after 14 h via exposure to air, reaching the degree of polymerization of the product 500. The monomers consumption was calculated by the integration of MMA and HEMA-TMS vinyl groups signal (C*H*H=C-CH$_3$, 6.11 ppm or 5.56 ppm) against the internal standard (anisole, *o*,*p*-Ar-H, 6.91 ppm). The product **A** was purified by three precipitations from methanol, dried under vacuum overnight at room temperature, and analyzed by GPC and ^{1}H NMR spectroscopy. The ratio of PMMA (*s*, broad, CO-O-C*H*$_3$, 3.54-3.68 ppm) to P(HEMA-TMS) (*s*, broad, OCO-C*H*$_2$, 3.90-4.17 ppm) signals gave the polymer composition.

Synthesis of (PDMAEMA$_{94}$-*stat*-PMMA$_{153}$)-*b*-[P(HEMA-TMS$_{551}$-*stat*-PMMA$_{338}$] (BA): A dried round bottom flask was charged with **A block** (1.0 g, 0.0094 mmol), dNbpy (70 mg, 0.17 mmol), DMAEMA (1.2 mL, 7.0mmol), MMA (0.75 mL, 7.0 mmol) and anisole (4.0

mL). The solution was bubbled with argon for 30'. $Cu^{I}Cl$ (0.0074 g, 0.0752 mmol), and $Cu^{II}Cl_2$ (0.0010 g, 7.46 µmol) were charged in a dried 25 mL round bottom flask and 3 argon-vacuum cycles were performed to remove oxygen. The flask was sealed, and then immersed in an oil bath at 60 °C. After bubbling, the monomer solution was injected into the catalyst solution. Reaction was stopped after 48 h via exposure to air. The product was diluted in dichloromethane, passed through a neutral alumina column, concentrated under vacuum and precipitated twice from hexanes and water. The solvent was removed under vacuum and the product was dried overnight under vacuum at room temperature. The structure of the polymer was determined from the ratio of selected polymer signals: PMMA (*s*, broad, CO-O-CH_3, 3.54-3.68 ppm),P(HEMA-TMS) (*s*, broad, O-Si(CH_3)$_3$, 0.11-0.21 ppm) and PDMAEMA (*m*, CH_2-NMe_2, 2.55-2.65 ppm).

Synthesis of [PBiBEM-*stat*-PMMA]-*b*-(PDMAEMA-*stat*-PMMA) (BA macroinitiator, BA MI): BA (0.1840 g), potassium fluoride (0.030 g, 0.52 mmol) and 2,6-di-*tert*-butylphenol (0.0090 g, 0.0439 mmol) were placed in a 20 ml round bottom flask. The flask was sealed, flushed with argon, and finally anhydrous THF (7 mL) was added. The mixture was cooled in an ice bath to 0 °C, tetrabutylammonium fluoride solution in THF (1M, 0.44 mL, 0.44mmol) was injected to the flask, followed by a drop-wise addition of 2-bromoisobutyryl bromide (0.121 g, 65 µL, 0.526mmol). After the addition the reaction mixture was allowed to reach room temperature and stirring was continued for 24 h. The solution was passed through a short column filled with basic alumina, precipitated into hexanes and then methanol:water (70:30, v/v%) three times. The filtrate was dried under vacuum overnight at room temperature.

Synthesis of [(PBiBEM-*g*-PMPC)-*stat*-MMA]-*b*-(PDMAEMA-*stat*-PMMA) (BAC): A dry 10 mL round bottom flask was charged with polymer **BA MI** (2mg), 2-methacryloyloxyethyl phosphorylcholine (MPC)(0.2540 g, 0.860mmol), 2,2'-bipyridyl (bpy) (22 mg, 14.23 µmol), $Cu^{I}Cl$ (6 mg, 60 µmol), and copper (II) chloride ($Cu^{II}Cl_2$) (1 mg, 7.40 µmol). A dry 10 mL round bottom flask was charged with methanol (3.0 mL) and anisole (500 µL). The solution was bubbled with argon for 15'. The flask was sealed, and then immersed in an oil bath at 50 °C. After bubbling, the solvent solution was injected into the catalyst/monomer solution. Time of reaction was determine thanks to MPC conversion measurement by 1HNMR to reach a DP of 35. Reaction was then stopped via exposure to air achieving PMPC diblock brush. The resulting brush was purified by ultrafiltration against MeOH under pressure using regenerated cellulose membrane (Milli Pore) with a pore size molar mass cut off 30,000 Da.

Synthesis of [(PBiBEM-*g*-PMPC)-*stat*-MMA]-*b*-(PqDMAEMA-*stat*-PMMA) (diblock BB polymer) was placed in 20 mL vial and dissolved in Methanol (10 mL). The solution was cooled in an ice bath to 0 °C, followed by a slow addition of bromoethane (0.5mL, 6.7 mmol). The reaction was stirred at room temperature for the next 48 h. The solvent and the unreacted reagent were evaporated under gentle pressure and solvent was exchanged for water by ultrafiltration. The polymer was freeze-dried and stored at -20°C in a dark container. The quantitative quaternization of -NMe_2 groups of **diblock BB polymer** was determined by ^1H NMR.

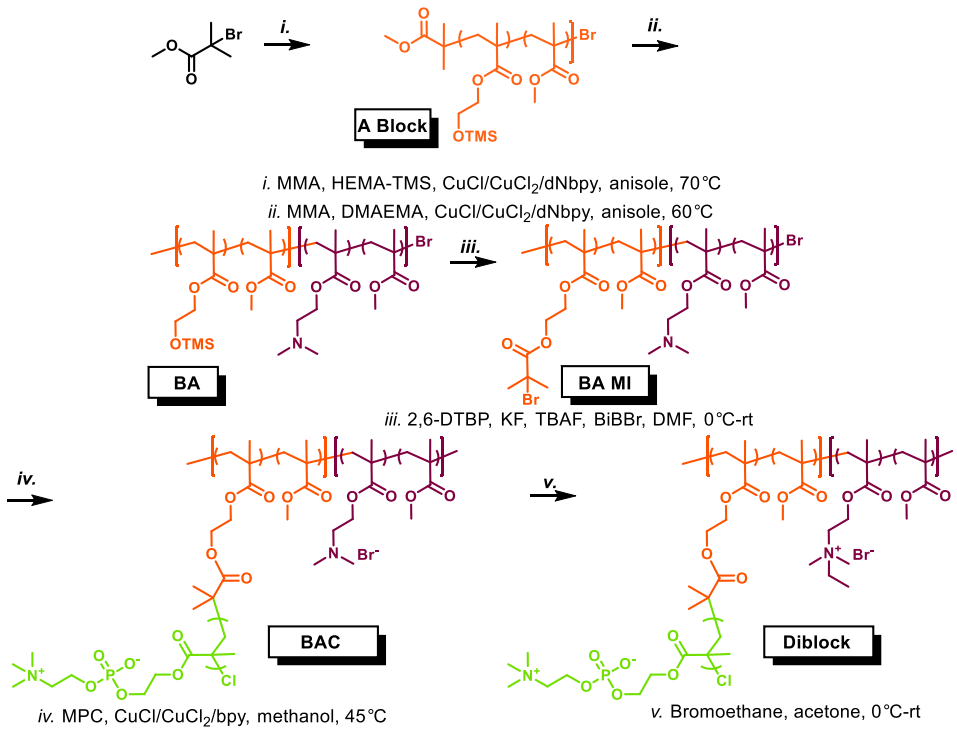

Figure 2.25. *Synthesis of the diblock BB polymer*

2.10.4 AFM imaging

The mono, di and triblock BB polymers were imaged by atomic force microscopy (Multimode Dimension 3100 AFM). The polymers were dissolved at a concentration of 15 µg/mL and deposited on a freshly cleaved mica surface. The BB polymers were left to adsorb and the supernatant was rinsed three times to isolate polymer single chains. The surface was nitrogen-dried prior to AFM measurements. The AFM equipped with nanoscope VIII controller (Digital instruments) was set on the peak force QNM mode. The Scanasyst-air tips were used for AFM imaging.

2.10.5 Synthetic synovial fluid formulation

For all the next experimentations, the BB polymers were dissolved at a concentration of 100 µg/mL in a phosphate buffered saline (10 mM PBS, 150 mM NaCl, pH 7.4). 1.5 MDa HA was added to the BB polymer solutions at a concentration of 1 mg/mL leading synthetic synovial fluids (SSF). SSF were left in solution in a dark container at 4 °C.

2.10.6 SFA normal forces profiles

A Surface Forces Apparatus was used to measure the normal interaction forces, F_N, as a function of the separation distance, D, between two opposing and atomically flat mica surfaces covered with BB polymer (SFA 2000, SurForce LLC, USA). F_N was determined by measuring the deflection of the spring cantilever with a spring constant of 482 N/m. The distance between the surfaces was assessed using the fringes of equal chromatic order (FECO) *via* multiple beam interferometry (MBI) calibrated with mica/mica air contact. The two mica surfaces were glued on glass cylinder with a curvature of 2 cm, degassed for 1 h with nitrogen. 50 µL of SSF were injected between the surfaces and left to adsorb for 1 h. Water was added at the bottom of the SFA chamber to saturate the chamber and limit the SSF evaporation. In and out runs were recorded in triplicate with the motor set a constant speed at 1 nm/s. The fringes were analyzed using a in-house Matlab® routine.

2.10.7 SFA friction forces measurement

The friction forces, F_t, were measured as a function of the normal forces, F_N, using the SFA. A piezo bimorph drove the lower surface in a back and forth motion at a constant sliding frequency of 50 mHz controlled by a function generator. The friction forces transmitted to the upper surface were detected by semi conductive strain gauges. Acquired data were recorded and processed using Origin® software. The separation distance and surface wear initiation were continuously recorded during the experiment using the FECO fringes position and shape.

2.11 Results and discussion

2.11.1 Polymers Design

We developed a library of BB polymers with a central brush block composed of poly(2-methacryloyloxyethyl phosphoryl choline) (PMPC) pendant chains and an adhesive block made of quaternized poly(2-dimethyalminoethyl methacrylate)-co-poly(methyl methacrylate) (Fig. 2.26)[2, 47, 49]. PMPC was chosen because of its excellent biocompatibility[50-51] and tribological properties[19, 52]. The adhesive block was designed to interact strongly with polyanionic electrolytes *via* electrostatic interactions between quaternized amine groups and negatively charged functional groups such as carboxylates. Three polymers were synthesized: a monoblock possessing only the bottle-brush central block, a diblock polymer exhibiting one lateral adhesive block and a triblock polymer exhibiting two lateral adhesive blocks.

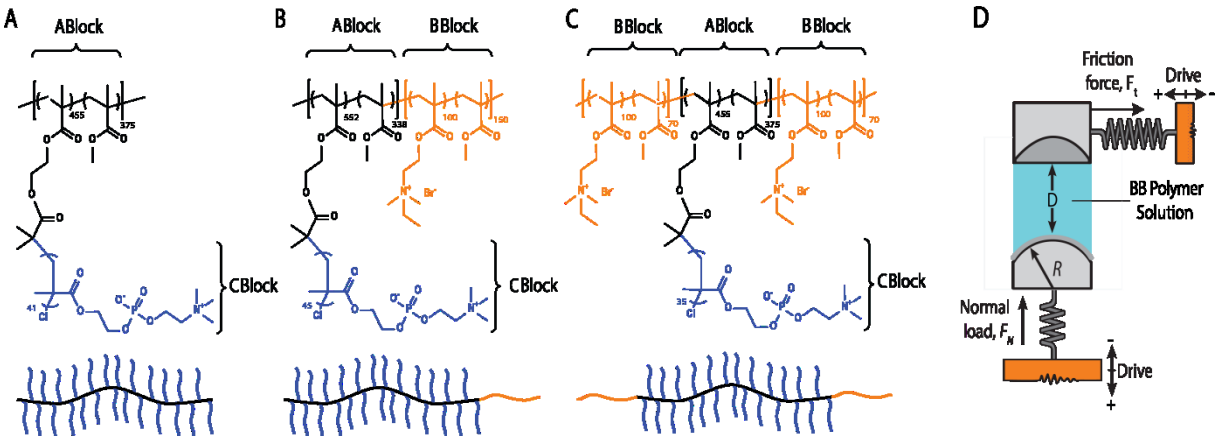

Figure 2.26. *Chemical structure and schematic of the (A) mono, (B) di, and (C) triblock BB polymers. (D) Schematics of the SFA setup. For each BB polymer, the A block is the backbone bearing the densely grafted C block. The pendant chains are represented by the block C. For BB polymers bearing anchoring groups (di and tri-block BB polymer), the B block represents the anchoring groups.*

These polymers were dissolved at a concentration of 100 µg/mL in a PBS. The BB polymer solution was then injected in the SFA chamber prior to normal forces profiles measurement and tribotesting. High molecular mass HA (M_w = 1.5 MDa) at 1 mg/mL was also mixed to the BB polymers to characterize the possible synergy and interactions between the two polymers[47].

Mono and triblock BB polymers were synthesized by atom-transfer radical polymerization (ATRP) using the same bifunctional initiator ethylene bis(2-bromoisobutyrate) whereas the diblock BB polymer was initiated using the monofunctional ethyl α-bromoisobutyrate[53-54](Scheme 2.2). Both methyl methacrylate (MMA) and 2-(trimethylsilyloxy)ethyl methacrylate (HEMA-TMS) were copolymerized using the similar ratio of initiator/MMA/HEMA-TMS to lead to almost the same backbone length (Table 2.4). HEMA-TMS was used as initiator precursor and constituted about 50 mol% of the backbone repeat unit (Table 2.4). This ratio was chosen to decrease the steric hindrance rising between pendant chain[55] which can potentially lead to backbone chain scission.

Scheme 2.2. *Schematic representation of the synthesis of mono, di and triblock BB polymers (For further details, see experimental section and Table 2.4)*

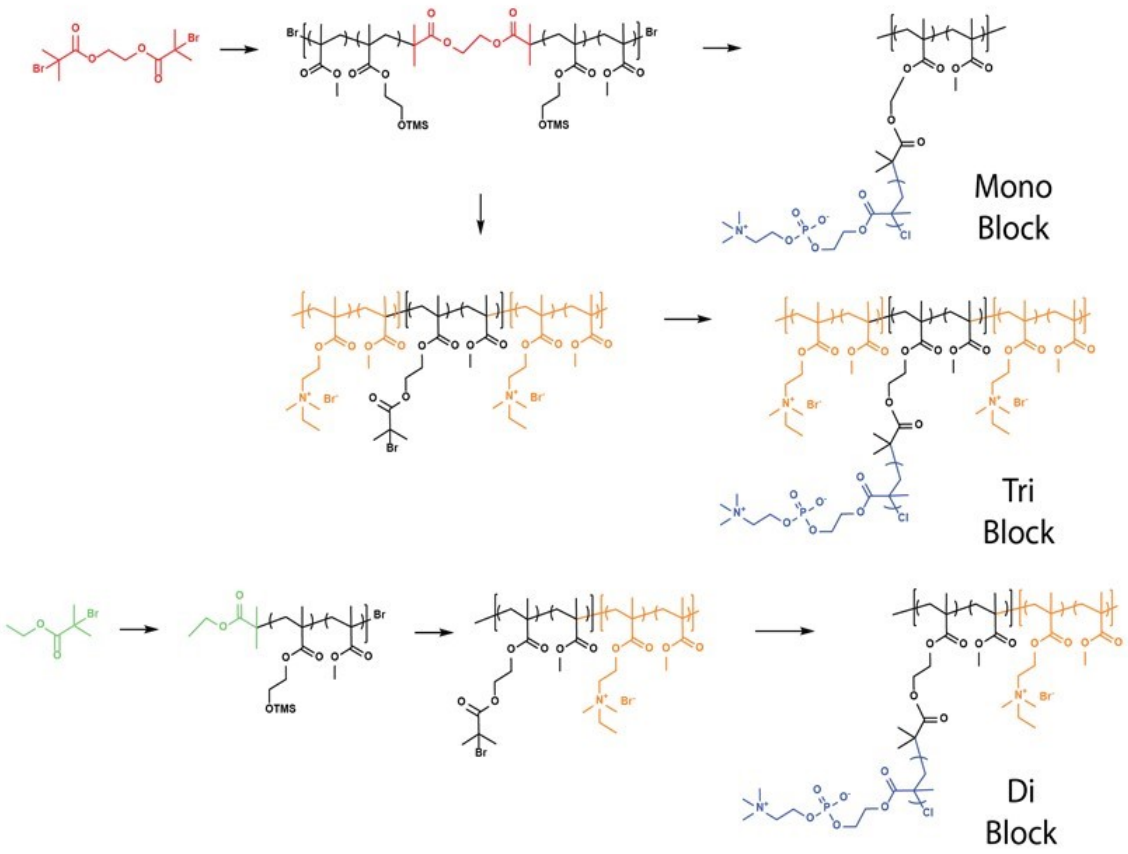

From the copolymer backbone, the reactive living ends were either left free for the monoblock BB polymer or used as initiators for the adhesive blocks composed of copolymer of MMA and 2-(dimethylamino)ethyl methacrylate (DMAEMA) with ratios of DMAEMA/MMA = 1/1 for the diblock and triblock polymers. DMAEMA was then quaternized to obtain a

polycationic attachment group able to non-specifically bound to polyanionic electrolyte hyaluronic acid. The post modifications of the BB polymers backbone consisted of the removal of the protecting TMS groups and the addition of BiBB followed by the polymerization of the lateral chains of MPC. To ensure the same degree of polymerization (DP) of pendant chains in all polymers, the amount of MPC was adjusted to the number of initiating sites on the backbone. The DP of the MPC chains was monitored by the conversion of the MPC monomer and set at DP ~ 40 (Table 2.4).

Table 2.4. Summary of the BB polymers composition

BB Polymer	DP central block A[a,b]	Ratio MMA/HEMA-TMS[a]	Molecular mass Central block A M_n (kg/mol) (M_w/M_n) [a,b]	DP of Lateral block B[a]	Ratio MMA/DMAEMA[a]	Molecular mass of the lateral block B M_n (kg/mol)[a]	DP block C[a]
Monoblock	830	45 %	132 (1.16)	n/a	-	n/a	41
Diblock	890	38 %	145 (1.31)	250	60 %	40	45
Triblock	830	45 %	132 (1.16)	170 × 2	40 %	32 × 2	35

[a] determined by ^{1}H NMR, [b] measured by GPC

The BB polymer structure was assessed by AFM imaging (Fig. 2.27). Each polymer exhibited the characteristic linear structure of BB polymers with almost identical contour lengths (≈ 140 nm).

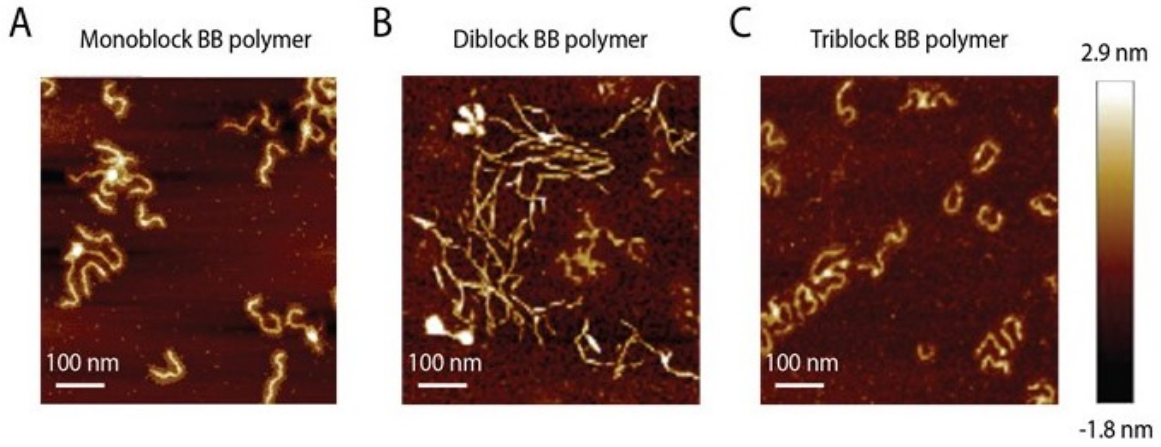

Figure 2.27. *AFM pictures of the (A) monoblock, (B) di and (C) triblock BB polymers deposited on freshly cleaved mica surfaces at a concentration of 15 µg/mL.*

2.11.2 Normal force profiles

Normal forces profiles, F_N/R, as a function of the separation distance, D, between two mica surfaces immersed in a BB polymer solution at 100 µg/mL in PBS were then recorded and compared to forces profiles in presence of HA (M_w = 1.5 MDa at 1 mg/mL). In each experiment, the polymer mixture was let free to adsorb on the mica surfaces for 1 h prior to force measurements. For each BB polymer tested with or without HA, the approach and separation speeds of the surfaces were set at ~ 1 nm/s. As can be seen in Fig. 2.28, the interaction profiles measured with all three BB polymers (no HA) was repulsive on approach as well as on separation (separation profiles are not shown for clarity). The onset of the interaction forces, i.e. the separation distance, D_{onset}, at which the interaction force intensity is above the noise level, varies between 125 and 150 nm for the mono block and diblock polymers and was around 50 nm for the triblock polymer. As previously shown, [47, 56] the interaction forces rising from the monoblock polymer are reminiscent from the particular conformation of the polymer at the surface. The monoblock polymer adsorbed at one extremity of its backbone, leaving the other extremity free to move in the medium. Given the higher rigidity of the BB polymer compared to a linear random coil chain, the interaction force law between surfaces bearing end adsorbed BB polymers can be derived assuming that the polymer behaves as a rigid rod, end attached to the surface.[57] In that formalism, the interaction forces can be described by the following equation:[56]

$$\frac{F_N}{R} \approx k_B T \Gamma \ln\left(\frac{D_{onset}}{D}\right) \qquad D < D_{onset} \qquad (1)$$

where μ is the effective density of adsorbed BB polymer and k_B the Boltzmann constant.

The rigid rod model predicts that the onset of interaction is independent of the grafting density of the polymer as previously confirmed experimentally.[56] The similarity between the force profiles shown in Figures 2.28A and B strongly suggest that the diblock polymer conformation is identical to the monoblock polymer. The onset of interaction, D_{onset} (obtained using Eq. 1), being on average equal to twice the thickness of the polymer layer adsorbed on the surfaces (no interdigitation approximation), we can estimate a thickness of 65-75 nm for both monoblock and diblock polymer layers. Given that the contour length of the polymer is around 140 nm for both polymers, we can conclude that half of the polymer length is in contact with the mica surface while the other half is extending towards the medium.

For the triblock polymer, D_{onset} = 42 nm which is significantly shorter than the other two polymers and in good agreement with previous measurements reported in PBS for a similar triblock polymer.[58] A shorter onset of interactions, corresponding to a polymer layer thickness of 21 nm, indicates a drastically different conformation compared to the other two polymers. As shown previously,[58] the conformation of the triblock polymer is close to a loop conformation, which is consistent with a shorter onset of interaction since the two adhesives blocks are expected to be strongly anchored onto the surface.

The mixtures of HA and the BB polymers presented marked differences compared to the BB polymers alone. Again, from Figure 2.28A and B, we can see that the monoblock and the diblock behave very similarly. The interaction force profile presents a long range portion with a D_{onset} very similar to the BB polymer alone suggesting that this interaction regime is largely dominated by the interaction between BB polymer chain ends extending in the medium (distal layer interaction, as shown in the schematics). In this regime, the interaction forces are weaker compared to the BB polymer alone due to a lower concentration of adsorbed polymer at the mica/liquid interface. Using Eq. 1, we estimated the effective surface concentration of the monoblock and diblock BB polymer and found that their concentration decreased 40 to 70 % when mixed with HA. A simple explanation for this behavior is the competitive adsorptions of BB polymer and HA on mica surfaces.

As the surfaces are brought closer together, a second interaction regime develops abruptly at a separation distance of $2L_s$. The value of L_s was estimated by extrapolating the interaction forces to zero force using a decaying power law and was 5 nm and 9 nm for the monoblock and the diblock respectively (dashed line in Figure 2.28). As previously reported,[47] the value

of L_s decreases with increasing the ionic strength of the medium which indicates the presence of HA in this layer.

For the triblock polymer / HA mixture, the force profile was markedly different. The long range portion of the interaction forces observed for the previous two polymers was not present. The onset of interaction was much shorter and similar to the triblock BB polymer alone with L_s = 42 nm but significantly more repulsive than the triblock alone. These observations suggest that the polymer layer on the surface is composed of triblock polymer in the loop conformation mixed with HA macromolecules (see schematic).

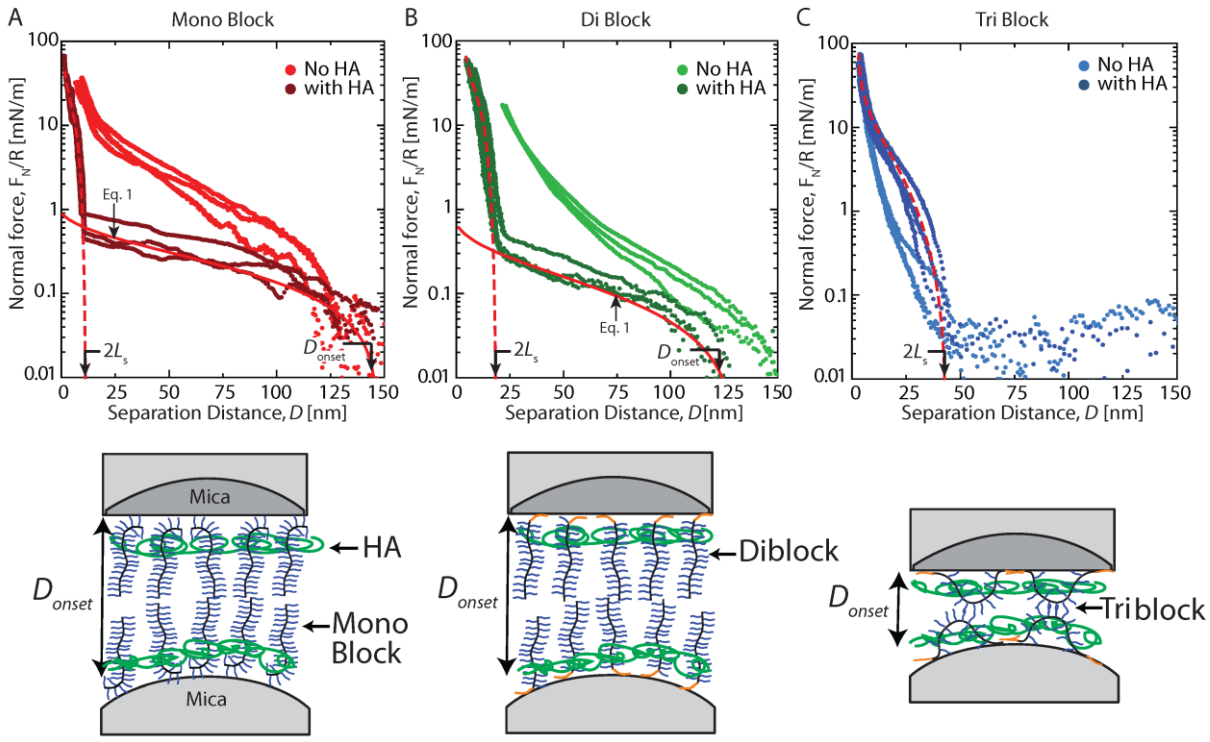

Figure 2.28. *Normal force profiles of (A) mono-, (B) di-, and (C) tri-block BB polymers at 100 µg/mL in presence or absence of 1.5 MDa HA at 1mg/mL between mica surfaces using the SFA. Data in panel A were adapted from* [47].

2.11.3 Tribological properties

In order to quantify the impact of the molecular architecture of the BB polymer as well as its capacity to bind to HA on the tribological properties of the polymer mixture, a series of tests to assess the friction coefficient and threshold pressure at the onset of damage under shearing conditions was performed.

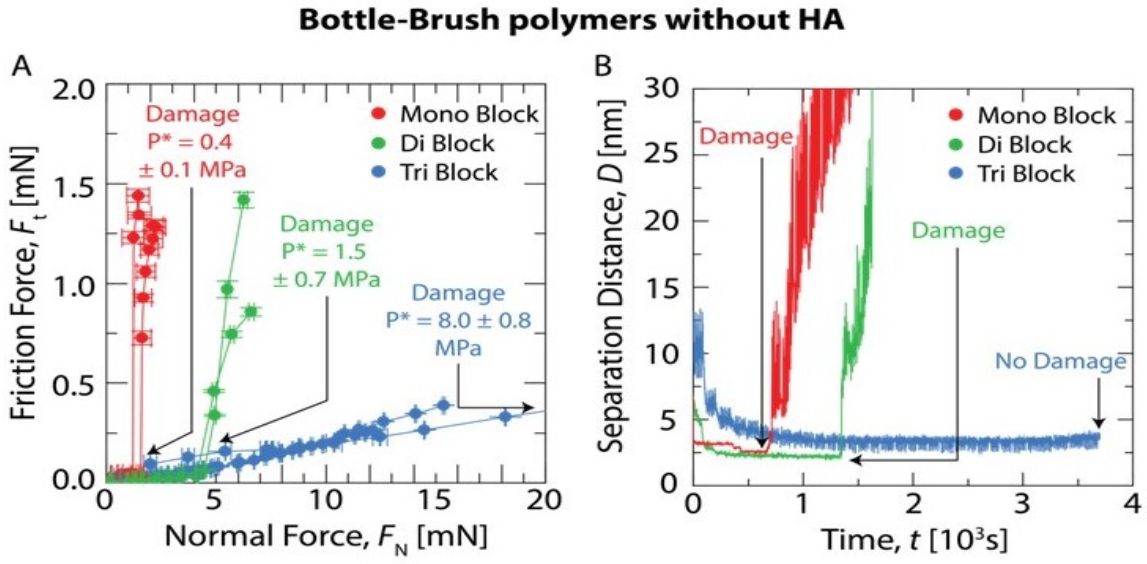

Figure 2.29. *(A) Friction as a function of normal force for the mono, di and tri-blocks BB polymers at 100 µg/mL using the SFA. (B) Separation distance of the polymeric layer thickness as the function of time during tribotesting measured by the FECO fringes.*

The friction force, F_t, as a function of the normal applied force, F_N, of the BB polymer solutions without HA in between atomically flat mica surfaces were first recorded (Fig. 2.29A). The results showed a linear relationship between the friction force and the normal force for all polymer solutions tested, which allowed to determine the coefficient of friction, μ, defined as the ratio $\mu = F_S/F_N$. [2, 47] The measured value of the friction coefficient was $\mu \sim 0.013$ for the monoblock and diblock polymers and increased slightly for the triblock to 0.021 demonstrating that the lubrication properties of the BB polymers are entirely governed by the BB domain of the polymer rather than its lateral blocks. In contrast, the architecture of the polymer seems to have a much more pronounced effect on the onset of wear damage. Damage of mica surfaces by frictional wear can be easily detected in the SFA using multiple beam interferometry in order to monitor any sudden or gradual change in the shape of the Fringes of Equal Chromatic Order (FECO)[49]. As shown in Figure 2.29A, the pressure onset of wear damage, P^*, increases with the number of adhesives blocks present in the polymer. We found that $P^* = 0.4 \pm 0.1$ MPa for the monoblock, $P^* = 1.5 \pm 0.7$ MPa for the diblock and $P^* = 8.0 \pm 0.8$ MPa for the triblock. As a comparison, PBS alone has a $P^* = 0.7$ MPa.[47] Monitoring of the polymer layer thickness with time allows to gain more insights on the origin of lubrication failure. As shown in Figure 2.29B, the thickness of the BB polymer lubricating film remained

almost constant during the tribotest (before damage) and was equal to 2.5 nm for the monoblock and diblock and 3.5 nm for the triblock polymer. At $P = P^*$, the separation distance drastically increased due to surface damage and debris accumulation at the contact point. In the case of the mono and diblock polymers, the ultimate film thickness before damage is consistent with a monomolecular thin film of polymer while for the triblock polymer, the film thickness is more consistent with two polymer layers. Interestingly, in the case of the monoblock and diblock polymers, damage of the surfaces occurs when the surfaces are still separated by a polymer film. The rupture of the polymer film creates polymer particles at the point of contact which locally increases the pressure and deformation of the mica surface and triggers its fracture. As it will be shown, this mechanism does not occur in presence of HA.

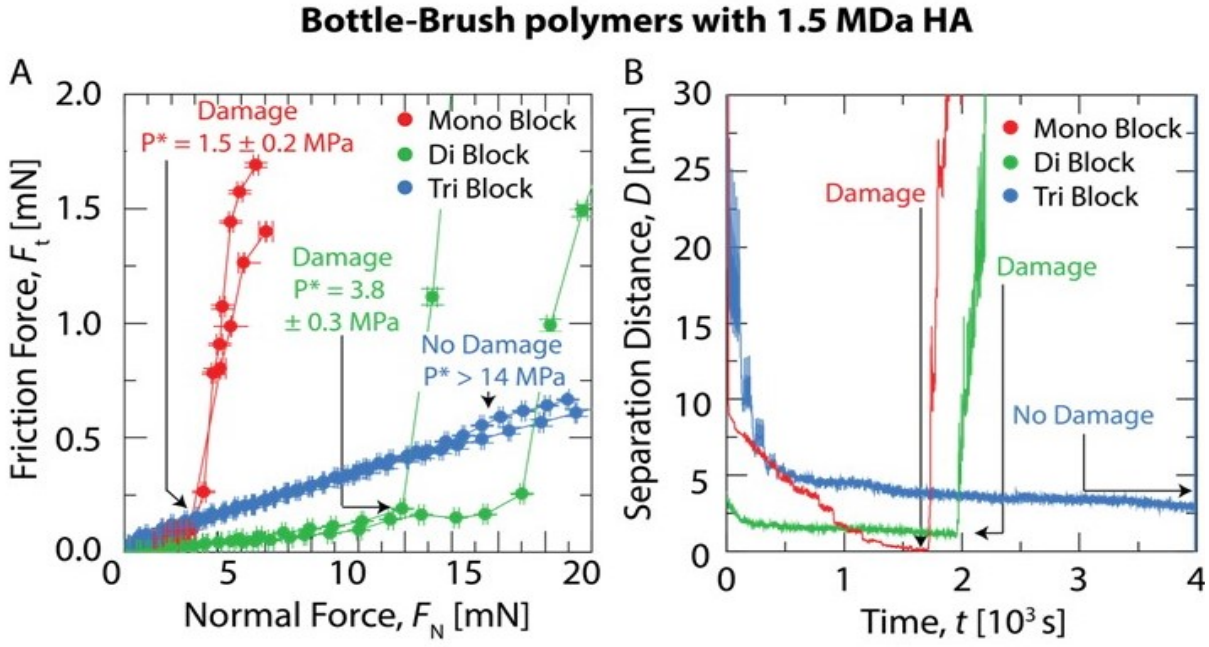

Figure 2.30. *(A) Friction as a function of normal force for the mono, di and tri-blocks BB polymers at 100 µg/mL with 1.5 MDa HA at 1 mg/mL using the SFA. (B) Separation distance of the polymeric layer thickness as function of time during tribotesting. Each stepwise decrement of the separation distance corresponds to an increase of the applied load.*

The mixtures of HA and BB polymers were tested following the same protocol. Again, the friction forces increased linearly with the applied load for all three polymers but the corresponding friction coefficients were slightly different. For the monoblock and triblock

polymers, μ = 0.03 and 0.035 respectively while for the diblock, μ = 0.015 (Fig. 2.30A). These values are slightly higher than the measured values for the BB polymers alone which can be due to a concomitant decrease of BB polymer at the interface and an increase of HA concentration. This explanation is consistent with the observations from the normal force profiles where the presence of HA in the proximal layer was confirmed together with a smaller concentration of the BB polymer. The friction coefficient of grafted HA layers ($\mu \approx 0.5$)[59] is significantly higher than the BB polymers which rules out the possibility of total depletion of the BB polymers from the contact.

Differences between the polymer mixtures were again more apparent when comparing their wear protection capacity. For the HA / monoblock polymer mixture, initiation of wear was recorded at P^* = 1.5 ± 0.2 MPa, and it increased to P^* = 3.8 ± 0.3 MPa for the diblock whereas the triblock polymer mixture did not present any lubrication failure up to P = 14 MPa, which was the pressure limit reached by our setup. For the diblock and the triblock polymers, the thickness of the lubricating film remained constant at 1-1.5 nm and 2.5-3 nm respectively while it decreased continuously as the normal load was increased for the monoblock BB polymer / HA mixture until reaching the value of 0.3 nm at $P = P^*$ which corresponds to the thickness of a monolayer of water molecules (Fig. 2.30B).

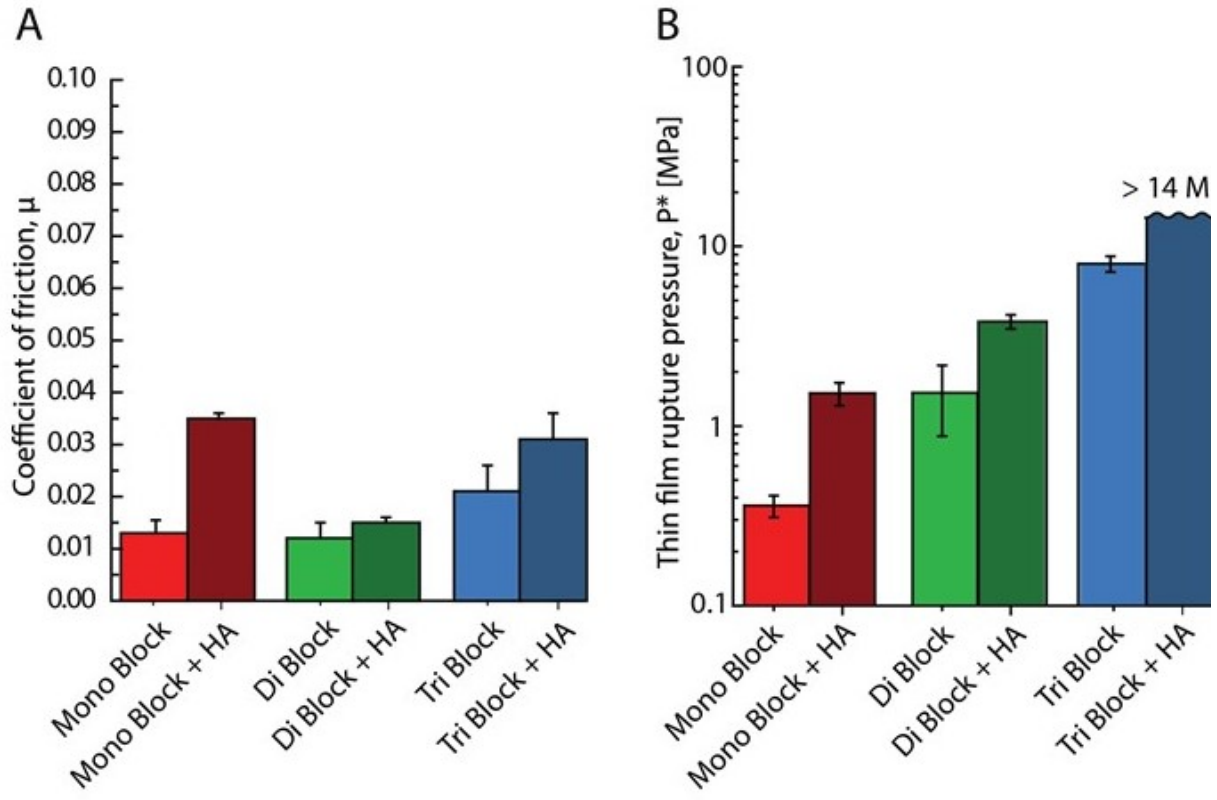

Figure 2.31. *Histograms of the tribological results of the bioinspired fluid made of 100 µg/mL of BB polymer in presence or absence of 1.5 MDa HA at 1 mg/mL. (A) CoF as a function of the lubricant system and (B) the lubricating film rupture pressure, P*, of the different lubricating systems.*

These tribostests allowed to draw some consistent trends differentiating the BB polymers alone and mixed with HA. When used alone, the BB polymers exhibit a low friction coefficient which value depends weakly on the architecture of the polymer. All three polymers had a friction coefficient between 0.01 and 0.03 (Fig. 2.31A), which is below the value of lubricin (μ = 0.038)[60] and also much smaller than synovial fluid (μ = 0.2)[61]. The friction coefficient of HA solutions measured in the SFA was recently reported[47] and was found to be identical to the friction coefficient of PBS ($\mu \approx 0.002$). As previously reported,[62] HA does not adsorb strongly on mica surfaces and is easily removed from the mica surface if not grafted physically of chemically[59] explaining why its tribological properties are similar to PBS. The BB polymer architecture seemed to control significantly the wear resistance, measured *via* the critical pressure of damage onset, *P**. As shown in Figure 2.31B, the values

of P^* increases with the number of adhesive blocks in the polymer non-linearly. This observation suggests that besides the differences in surface conformations observed between the different BB polymers, P^* is solely controlled be the BB polymer interaction with the surface.

In presence of HA, the friction coefficient of the mixtures was systematically higher than the BB polymer alone, although differences were rather small (between 0.01 and 0.03). The largest difference was observed between the monoblock polymer alone and when mixed with HA. The monoblock BB polymer is expected to have the weakest interaction with the mica surface and was found to be strongly depleted from the surface when mixed with HA. Normal force runs confirmed the presence of HA close to the surface, probably adsorbed on the mica surface *via* the formation of an intermolecular complex with the BB polymer. Friction coefficient of strongly adsorbed HA layers has been reported to be close to synovial fluid (μ = 0.2), much higher to the values measured in our study. Therefore, the increase of the friction coefficient measured for the HA/BB polymer mixtures is expected to be due to the presence of HA and depletion of the BB polymer from the surface. For the diblock and triblock polymers, their interaction with HA is expected to be stronger *via* the positively charged groups present on the adhesive lateral blocks and the anionic carboxylic functions of HA. This electrostatic intermolecular interaction increases the cohesive strength of the interfacial polymer film and therefore its resistance to shear damage. The measured values of P^* for the polymer mixtures were always higher than the values of the BB polymer alone and HA alone taken together ($P^*_{HA} + P^*_{BB}$) indicating that a positive synergy is at play between the polymers. We can quantify such synergy *via* the synergy factor SF defined as:

$$SF = \frac{P^*_{mixture}}{P^*_{HA}+P^*_{BB}} \quad (2)$$

For the mono and diblock polymers, we found that SF = 1.4. As we already reported,[47] the observed synergy is due to entanglements between the BB polymer and HA which transiently increases the cohesion between the two polymers under confinement. The presence of an adhesive polycationic block in the diblock BB polymer does not improve the synergy, certainly because parts the adhesive block adsorbs on the mica surface and therefore does not contribute efficiently to strengthen the cohesion of the lubricant film.

Interestingly, the synergy factor increased for the triblock polymer / HA mixture. Considering that for this mixture, the highest applied pressure without any sign of damage was equal to P

= 14 MPa, we can estimate a lower value of SF = 1.7, which is significantly higher than the other two BB polymer mixtures. This analysis shows that the synergy between the BB polymers and HA is greatly enhanced by the intermolecular bridges between HA and the triblock polymer.

Amongst all the identified contributions to the wear protection capacity of the polymer mixtures, intermolecular bridges seem to be far more important than the interaction between the BB polymer and the surface or even entanglements and intermolecular complexation between the polymers. This result suggest interesting new routes to design surface protecting lubricating fluids based on interacting polymer mixtures that could be tailored on demand to adapt to ambient conditions.

2.12 Conclusions

In summary, this study demonstrates the crucial role of intermolecular interactions between molecular brushes and HA on controlling the lubrication and wear resistance of surfaces. Indeed, although the bottlebrush block was shown to control the coefficient of friction, the adhesive blocks appear to tune the range of working conditions of the molecular brushes. The use of a non-specific anchoring group made of polycationic chain can be used to interact strongly with negatively charged polymers and surfaces to provide high wear resistance up to pressures much higher than those usually at work in biological systems (10 MPa or less). This work anticipates that other types of interaction could be used to tune even more finely the wear protection capacity of the polymer mixtures, for example using stimuli responsive adhesive groups, therefore opening a new dimension in the formulation of lubricating fluids.

Acknowledgements

XB acknowledges the financial support from CIHR (CRC and Bridge grants) and NSERC (Discovery grant). JF is grateful to the Arthritis Society, the French Embassy (Frontenac scholarship) and the Faculté des études supérieures et postdoctorales from the Université de Montréal for financial supports. BRS thanks the financial support of GRUM. GS and XB are grateful to the FRQNT for the Samuel de Champlain France-Quebec cooperation grant. KM acknowledges support from the NSF (DMR 1501324). This work has benefited from the facilities and expertise of the *Liquid Chromatography* Platform (Agnès Crépet, Institut de Chimie de Lyon) for the characterization of polymers.

Conclusions de la partie 3

À travers cette étude, nous avons mis en relief l'influence de la structure des écouvillons moléculaires sur la biolubrification. Nous avons montré que le domaine central était responsable de la faible friction, mais ne permettait pas de la garantir sur de larges gammes de pression sans l'aide de groupements d'ancrage. Ainsi, l'ancrage de ces macromolécules est un point crucial pour garantir une lubrification pour tout type d'applications et de contraintes. Dans cette étude, les ancrages polycationiques sont conçus pour s'adsorber sur des surfaces anioniques comme le mica de manière non spécifique. De plus, ces groupements sont obtenus en peu d'étapes de synthèse et avec des produits commerciaux peu chers. L'architecture finale du polymère dibloc peut s'apparenter à la structure de l'aggrécane possédant un groupement d'ancrage à l'HA tandis que le polymère tribloc forme des boucles sur la surface comme peut le faire la lubricine. Ces macromolécules peuvent également s'adapter à des surfaces physiologiques comme la matrice extracellulaire du cartilage qui est fortement anionique. Ainsi ces polymères peuvent être utilisés de manière polyvalente pour diverses applications biomédicales en utilisant l'eau comme solvant. Pour obtenir une adsorption plus efficace entre le cartilage et ces mimes, la synthèse de groupes d'ancrage spécialisés semble également prometteuse, comme la synthèse de groupements thiolés [8] permettant l'établissement de ponts disulfures, ou l'utilisation de peptide interagissant de manière spécifique avec le collagène ou le HA. Ainsi, ces polymères possèderaient *a priori* une plus grande résistance aux contraintes mécaniques des articulations et également un meilleur ciblage de zones d'intérêt. Cependant, ces polymères nécessitent des modifications chimiques sans connaitre les effets secondaires (ponts disulfures) ou encore l'emploi de peptides plus couteux, ce qui rend leur utilisation plus difficile.

Conclusion générale du chapitre II

Les mimes polymériques des protéoglycanes semblent prometteurs pour le rétablissement des propriétés lubrifiantes et de résistance à l'usure des articulations en remplaçant les macromolécules naturellement dégradées lors de l'OA. Ceux-ci peuvent être synthétisés par ATRP et leurs groupements d'ancrage peuvent être également modifiés pour s'adsorber sur différents types de surface. Le domaine en peigne polyzwitterionique garanti, quant à lui, des CoF de l'ordre de 10^{-2} en mimant les têtes hydrophiles des phospholipides présents dans la synovie d'une articulation saine. Il permet également au polymère de rester étiré dans sa conformation brosse, quelque soit la force saline du milieu contrairement à de nombreux autres écouvillons moléculaires purement anioniques ou cationiques[63]. Un polymère linéaire, hydrophile et de haut poids moléculaire, type HA, peut être ajouté pour permettre l'enchevêtrement des écouvillons moléculaires et améliorer les propriétés de lubrification. D'autres alternatives à base de monomères zwitterioniques permettraient également de bénéficier des mêmes propriétés lubrifiantes comme des monomères de la famille des bétaïnes[64].

Références

1. Seror, J.; Merkher, Y.; Kampf, N.; Collinson, L.; Day, A. J.; Maroudas, A.; Klein, J., Articular Cartilage Proteoglycans As Boundary Lubricants: Structure and Frictional Interaction of Surface-Attached Hyaluronan and Hyaluronan–Aggrecan Complexes. *Biomacromolecules* **2011,** *12* (10), 3432-3443.
2. Banquy, X.; Burdyńska, J.; Lee, D. W.; Matyjaszewski, K.; Israelachvili, J., Bioinspired Bottle-Brush Polymer Exhibits Low Friction and Amontons-like Behavior. *J. Am. Chem. Soc.* **2014,** *136* (17), 6199-6202.
3. Naleway, S. E.; Porter, M. M.; McKittrick, J.; Meyers, M. A., Structural Design Elements in Biological Materials: Application to Bioinspiration. *Adv. Mater.* **2015,** *27* (37), 5455-5476.
4. Hwang, J.; Jeong, Y.; Park, J. M.; Lee, K. H.; Hong, J. W.; Choi, J., Biomimetics: forecasting the future of science, engineering, and medicine. *Int. J. Nanomed.* **2015,** *10*, 5701-5713.
5. Green, J. J.; Elisseeff, J. H., Mimicking biological functionality with polymers for biomedical applications. *Nature* **2016,** *540* (7633), 386-394.
6. Li, Y.; Li, L.; Sun, J., Bioinspired Self-Healing Superhydrophobic Coatings. *Angew. Chem.* **2010,** *122* (35), 6265-6269.
7. Lawrence, A.; Xu, X.; Bible, M. D.; Calve, S.; Neu, C. P.; Panitch, A., Synthesis and characterization of a lubricin mimic (mLub) to reduce friction and adhesion on the articular cartilage surface. *Biomaterials* **2015,** *73* (Supplement C), 42-50.
8. Samaroo, K. J.; Tan, M.; Andresen Eguiluz, R. C.; Gourdon, D.; Putnam, D.; Bonassar, L. J., Tunable Lubricin-mimetics for Boundary Lubrication of Cartilage. *Biotribology* **2017,** *9* (Supplement C), 18-23.
9. Sun, C.-H.; Jiang, P.; Jiang, B., Broadband moth-eye antireflection coatings on silicon. *Appl. Phys. Lett.* **2008,** *92* (6), 061112.
10. Wilson, S. J.; Hutley, M. C., The Optical Properties of 'Moth Eye' Antireflection Surfaces. *J. Mod. Opt.* **1982,** *29* (7), 993-1009.
11. Simonis, P.; Vigneron, J. P., Structural color produced by a three-dimensional photonic polycrystal in the scales of a longhorn beetle: Pseudomyagrus waterhousei (Coleoptera: Cerambicidae). *Phys. Rev. E* **2011,** *83* (1), 011908.
12. Kim, S.; Laschi, C.; Trimmer, B., Soft robotics: a bioinspired evolution in robotics. *Trends Biotechnol.* **2013,** *31* (5), 287-294.
13. Parodi, A.; Quattrocchi, N.; van de Ven, A. L.; Chiappini, C.; Evangelopoulos, M.; Martinez, J. O.; Brown, B. S.; Khaled, S. Z.; Yazdi, I. K.; Enzo, M. V.; Isenhart, L.; Ferrari, M.; Tasciotti, E., Synthetic nanoparticles functionalized with biomimetic leukocyte membranes possess cell-like functions. *Nat. Nanotechnol.* **2013,** *8* (1), 61-68.
14. Yoo, J.-W.; Irvine, D. J.; Discher, D. E.; Mitragotri, S., Bio-inspired, bioengineered and biomimetic drug delivery carriers. *Nat. Rev. Drug Discov.* **2011,** *10* (7), 521-535.
15. Zhang, P.; Chen, Y.; Zeng, Y.; Shen, C.; Li, R.; Guo, Z.; Li, S.; Zheng, Q.; Chu, C.; Wang, Z.; Zheng, Z.; Tian, R.; Ge, S.; Zhang, X.; Xia, N.-S.; Liu, G.; Chen, X., Virus-mimetic nanovesicles as a versatile antigen-delivery system. *Proc. Natl. Acad. Sci. U. S. A.* **2015,** *112* (45), 6129-6138.
16. A, A.; Menon, D.; T. B, S.; Koyakutty, M.; Mohan, C. C.; Nair, S. V.; Nair, M. B., Bioinspired Composite Matrix Containing Hydroxyapatite–Silica Core–Shell Nanorods for Bone Tissue Engineering. *ACS Appl. Mater. Interfaces* **2017,** *9* (32), 26707-26718.
17. Tatman, P. D.; Gerull, W.; Sweeney-Easter, S.; Davis, J. I.; Gee, A. O.; Kim, D.-H., Multiscale Biofabrication of Articular Cartilage: Bioinspired and Biomimetic Approaches. *Tissue Eng., Part B* **2015,** *21* (6), 543-559.
18. Lee, H.-i.; Pietrasik, J.; Sheiko, S. S.; Matyjaszewski, K., Stimuli-responsive molecular brushes. *Prog. Polym. Sci.* **2010,** *35* (1), 24-44.
19. Kobayashi, M.; Terayama, Y.; Kikuchi, M.; Takahara, A., Chain dimensions and surface characterization of superhydrophilic polymer brushes with zwitterion side groups. *Soft Matter* **2013,** *9* (21), 5138-5148.

20. Pettersson, T.; Naderi, A.; Makuska, R.; Claesson, P. M., Lubrication properties of bottle-brush polyelectrolytes: An AFM study on the effect of side chain and charge density. *Langmuir* **2008,** *24* (7), 3336-3347.
21. Russano, D.; Carrillo, J. M. Y.; Dobrynin, A. V., Interaction between Brush Layers of Bottle-Brush Polyelectrolytes: Molecular Dynamics Simulations. *Langmuir* **2011,** *27* (17), 11044-11051.
22. Carrillo, J.-M. Y.; Brown, W. M.; Dobrynin, A. V., Explicit Solvent Simulations of Friction between Brush Layers of Charged and Neutral Bottle-Brush Macromolecules. *Macromolecules* **2012,** *45* (21), 8880-8891.
23. Liu, X.; Thormann, E.; Dedinaite, A.; Rutland, M.; Visnevskij, C.; Makuska, R.; Claesson, P. M., Low friction and high load bearing capacity layers formed by cationic-block-non-ionic bottle-brush copolymers in aqueous media. *Soft Matter* **2013,** *9* (22), 5361-5371.
24. Andresen Eguiluz, R. C.; Cook, S. G.; Tan, M.; Brown, C. N.; Pacifici, N. J.; Samak, M. S.; Bonassar, L. J.; Putnam, D.; Gourdon, D., Synergistic Interactions of a Synthetic Lubricin-Mimetic with Fibronectin for Enhanced Wear Protection. *Front. Bioeng. Biotechnol.* **2017,** *5* (36).
25. Jay, G. D.; Torres, J. R.; Warman, M. L.; Laderer, M. C.; Breuer, K. S., The role of lubricin in the mechanical behavior of synovial fluid. *Proc. Natl. Acad. Sci. U.S.A* **2007,** *104* (15), 6194-6199.
26. Jay, G. D.; Waller, K. A., The biology of Lubricin: Near frictionless joint motion. *Matrix Biol.* **2014,** *39*, 17-24.
27. Zappone, B.; Ruths, M.; Greene, G. W.; Jay, G. D.; Israelachvili, J. N., Adsorption, lubrication, and wear of lubricin on model surfaces: polymer brush-like behavior of a glycoprotein. *Biophys. J.* **2007,** *92* (5), 1693-1708.
28. Coles, J. M.; Chang, D. P.; Zauscher, S., Molecular mechanisms of aqueous boundary lubrication by mucinous glycoproteins. *Curr. Opin. Colloid Interface Sci.* **2010,** *15* (6), 406-416.
29. Majd, S. E.; Kuijer, R.; Kowitsch, A.; Groth, T.; Schmidt, T. A.; Sharma, P. K., Both Hyaluronan and Collagen Type II Keep Proteoglycan 4 (Lubricin) at the Cartilage Surface in a Condition That Provides Low Friction during Boundary Lubrication. *Langmuir* **2014**, 14566-14572.
30. Seror, J.; Zhu, L.; Goldberg, R.; Day, A. J.; Klein, J., Supramolecular synergy in the boundary lubrication of synovial joints. *Nat. Commun.* **2015,** *6*, 6497.
31. Samsom, M.; Iwabuchi, Y.; Sheardown, H.; Schmidt, T. A., Proteoglycan 4 and hyaluronan as boundary lubricants for model contact lens hydrogels. *J. Biomed. Mater. Res. B Appl. Biomater.* **2017**, 1329-1338.
32. Swann, D. A.; Hendren, R. B.; Radin, E. L.; Sotman, S. L.; Duda, E. A., The lubricating activity of synovial fluid glycoproteins. *Arthritis Rheum.* **1981,** *24* (1), 22-30.
33. Dedinaite, A., Biomimetic lubrication. *Soft Matter* **2012,** *8* (2), 273-284.
34. Raj, A.; Wang, M.; Liu, C.; Ali, L.; Karlsson, N. G.; Claesson, P. M.; Dėdinaitė, A., Molecular synergy in biolubrication: The role of cartilage oligomeric matrix protein (COMP) in surface-structuring of lubricin. *J. Colloid Interface Sci.* **2017,** *495*, 200-206.
35. Roughley, P.; Mort, J., The role of aggrecan in normal and osteoarthritic cartilage. *J. Exp. Orthop.* **2014,** *1* (1), 1-11.
36. Kiani, C.; Chen, L.; Wu, Y. J.; Yee, A. J.; Yang, B. B., Structure and function of aggrecan. *Cell Res.* **2002,** *12* (1), 19-32.
37. Bolton, J.; Bailey, T. S.; Rzayev, J., Large Pore Size Nanoporous Materials from the Self-Assembly of Asymmetric Bottlebrush Block Copolymers. *Nano Lett.* **2011,** *11* (3), 998-1001.
38. Ramakrishna, S. N.; Espinosa-Marzal, R. M.; Naik, V. V.; Nalam, P. C.; Spencer, N. D., Adhesion and Friction Properties of Polymer Brushes on Rough Surfaces: A Gradient Approach. *Langmuir* **2013,** *29* (49), 15251-15259.
39. Lee, S.; Spencer, N. D., Adsorption Properties of Poly(l-lysine)-graft-poly(ethylene glycol) (PLL-g-PEG) at a Hydrophobic Interface: Influence of Tribological Stress, pH, Salt Concentration, and Polymer Molecular Weight. *Langmuir* **2008,** *24* (17), 9479-9488.
40. Olanya, G.; Iruthayaraj, J.; Poptoshev, E.; Makuska, R.; Vareikis, A.; Claesson, P. M., Adsorption Characteristics of Bottle-Brush Polymers on Silica: Effect of Side Chain and Charge Density. *Langmuir* **2008,** *24* (10), 5341-5349.
41. Rosenberg, K. J.; Goren, T.; Crockett, R.; Spencer, N. D., Load-Induced Transitions in the Lubricity of Adsorbed Poly(l-lysine)-g-dextran as a Function of Polysaccharide Chain Density. *ACS Appl. Mater. Interfaces* **2011,** *3* (8), 3020-3025.

42. Claesson, P. M.; Makuska, R.; Varga, I.; Meszaros, R.; Titmuss, S.; Linse, P.; Pedersen, J. S.; Stubenrauch, C., Bottle-brush polymers: Adsorption at surfaces and interactions with surfactants. *Adv. Colloid Interface Sci.* **2010,** *155* (1), 50-57.
43. Liu, X.; Dedinaite, A.; Rutland, M.; Thormann, E.; Visnevskij, C.; Makuska, R.; Claesson, P. M., Electrostatically Anchored Branched Brush Layers. *Langmuir* **2012,** *28* (44), 15537-15547.
44. Raviv, U.; Giasson, S.; Kampf, N.; Gohy, J.-F.; Jerome, R.; Klein, J., Lubrication by charged polymers. *Nature* **2003,** *425* (6954), 163-165.
45. Dedinaite, A.; Pettersson, T.; Mohanty, B.; Claesson, P. M., Lubrication by organized soft matter. *Soft Matter* **2010,** *6* (7), 1520-1526.
46. Carrillo, J.-M. Y.; Russano, D.; Dobrynin, A. V., Friction between Brush Layers of Charged and Neutral Bottle-Brush Macromolecules. Molecular Dynamics Simulations. *Langmuir* **2011,** *27* (23), 14599-14608.
47. Faivre, J.; Shrestha, B. R.; Burdynska, J.; Xie, G.; Moldovan, F.; Delair, T.; Benayoun, S.; David, L.; Matyjaszewski, K.; Banquy, X., Wear Protection without Surface Modification Using a Synergistic Mixture of Molecular Brushes and Linear Polymers. *Acs Nano* **2017,** *11* (2), 1762-1769.
48. Qin, S.; Matyjaszewski, K.; Xu, H.; Sheiko, S. S., Synthesis and Visualization of Densely Grafted Molecular Brushes with Crystallizable Poly(octadecyl methacrylate) Block Segments. *Macromolecules* **2003,** *36* (3), 605-612.
49. Faivre, J.; Shrestha, B. R.; Xie, G.; Delair, T.; David, L.; Matyjaszewski, K.; Banquy, X., Unraveling the Correlations between Conformation, Lubrication and Chemical Stability of Bottlebrush Polymers at Interfaces. *Biomacromolecules* **2017**.
50. Nowak, T.; Nishida, K.; Shimoda, S.; Konno, Y.; Ichinose, K.; Sakakida, M.; Shichiri, M.; Nakabayashi, N.; Ishihara, K., Biocompatibility of MPC: in vivo evaluation for clinical application. *J. Artificial Organs* **2000,** *3* (1), 39-46.
51. Yusa, S.-i.; Fukuda, K.; Yamamoto, T.; Ishihara, K.; Morishima, Y., Synthesis of Well-Defined Amphiphilic Block Copolymers Having Phospholipid Polymer Sequences as a Novel Biocompatible Polymer Micelle Reagent. *Biomacromolecules* **2005,** *6* (2), 663-670.
52. Moro, T.; Takatori, Y.; Kyomoto, M.; Ishihara, K.; Kawaguchi, H.; Hashimoto, M.; Tanaka, T.; Oshima, H.; Tanaka, S., Wear resistance of the biocompatible phospholipid polymer-grafted highly cross-linked polyethylene liner against larger femoral head. *J. Orthop. Res.* **2015,** *33* (7), 1103-1110.
53. Sheiko, S. S.; Sumerlin, B. S.; Matyjaszewski, K., Cylindrical molecular brushes: Synthesis, characterization, and properties. *Prog. Polym. Sci.* **2008,** *33* (7), 759-785.
54. Matyjaszewski, K., Atom Transfer Radical Polymerization (ATRP): Current Status and Future Perspectives. *Macromolecules* **2012,** *45* (10), 4015-4039.
55. Faivre, J.; Shrestha, B. R.; Xie, G.; Delair, T.; David, L.; Matyjaszewski, K.; Banquy, X., Unraveling the Correlations between Conformation, Lubrication, and Chemical Stability of Bottlebrush Polymers at Interfaces. *Biomacromolecules* **2017**, 4002-4010.
56. Faivre, J.; Shrestha, B. R.; Xie, G.; Delair, T.; David, L.; Matyjaszewski, K.; Banquy, X., Unraveling the Correlations between Conformation, Lubrication, and Chemical Stability of Bottlebrush Polymers at Interfaces. *Biomacromolecules* **2017,** *18* (12), 4002-4010.
57. Brangbour, C.; du Roure, O.; Helfer, E.; Demoulin, D.; Mazurier, A.; Fermigier, M.; Carlier, M. F.; Bibette, J.; Baudry, J., Force-Velocity Measurements of a Few Growing Actin Filaments. *Plos Biol* **2011,** *9* (4).
58. Banquy, X.; Burdynska, J.; Lee, D. W.; Matyjaszewski, K.; Israelachvili, J., Bioinspired Bottle-Brush Polymer Exhibits Low Friction and Amontons-like Behavior. *J Am Chem Soc* **2014,** *136* (17), 6199-6202.
59. Yu, J.; Banquy, X.; Greene, G. W.; Lowrey, D. D.; Israelachvili, J. N., The Boundary Lubrication of Chemically Grafted and Cross-Linked Hyaluronic Acid in Phosphate Buffered Saline and Lipid Solutions Measured by the Surface Forces Apparatus. *Langmuir* **2012,** *28* (4), 2244-2250.
60. Zappone, B.; Ruths, M.; Greene, G. W.; Jay, G. D.; Israelachvili, J. N., Adsorption, lubrication, and wear of lubricin on model surfaces: Polymer brush-like behavior of a glycoprotein. *Biophys J* **2007,** *92* (5), 1693-1708.
61. Banquy, X.; Lee, D. W.; Das, S.; Hogan, J.; Israelachvili, J. N., Shear-Induced Aggregation of Mammalian Synovial Fluid Components under Boundary Lubrication Conditions. *Adv Funct Mater* **2014,** *24* (21), 3152-3161.

62. Benz, M.; Chen, N. H.; Jay, G.; Israelachvili, J. I., Static forces, structure and flow properties of complex fluids in highly confined geometries. *Ann Biomed Eng* **2005,** *33* (1), 39-51.
63. Yao, K.; Chen, Y.; Zhang, J.; Bunyard, C.; Tang, C., Cationic salt-responsive bottle-brush polymers. *Macromol. Rapid Commun.* **2013,** *34* (8), 645-51.
64. Wei, Q.; Cai, M.; Zhou, F.; Liu, W., Dramatically Tuning Friction Using Responsive Polyelectrolyte Brushes. *Macromolecules* **2013,** *46* (23), 9368-9379.

Chapitre III - Développement d'hydrogels de chitosane multicouches et caractérisations structurales, physiques, mécaniques et tribologiques

-Chapitre III-

Développement d'hydrogels de chitosane multicouches et caractérisations structurales, physiques, mécaniques et tribologiques

Introduction générale du chapitre III

De nombreux biomatériaux développés pour la réparation articulaire utilisent, seuls ou en combinaison, des hydrogels[1]. En effet, les hydrogels, composés d'une matrice polymérique gonflée par l'eau, reprennent les caractéristiques physiques du cartilage, à savoir un matériau viscoélastique, propice à la survie cellulaire en conditions plutôt hypoxiques. Néanmoins, les propriétés mécaniques en compression et/ou en cisaillement des hydrogels sont généralement inférieures à celles du cartilage qui sont de l'ordre de quelques MPa. Des alternatives prometteuses comme les réseaux interpénétrés permettent d'atteindre des modules élastiques comparables[2]. Cependant, très peu d'études se sont intéressées aux propriétés tribologiques des substituts articulaires. Les plus significatives sont celles du groupe du Pr Gong qui a développé les hydrogels interpénétrés et également fortement contribué à l'étude de la friction des hydrogels en développant des modèles tribologiques[3-9]. L'usure des hydrogels est un phénomène encore moins étudié, même si l'intégrité des biomatériaux *in vivo* est primordiale pour la mise en place de substituts qui doivent assurer 'une tenue en service'. À travers ce chapitre, nous avons conçu une librairie d'hydrogels de chitosane, un polysaccharide largement utilisé comme biomatériau[10-14] notamment dans la réparation articulaire[15-19], possédant une microstructure particulière rejoignant la structure microscopique du cartilage[20-21]. Comprendre les effets de ces structurations est intéressant dans l'optique de concevoir un substitut à la fois lubrifiant et limitant l'usure. La structuration des gels a été vérifiée par microscopie électronique à balayage et microscopie confocale. Les propriétés mécaniques, de transport de fluide sous contraintes et les propriétés tribologiques ont été évaluées par analyse mécanique dynamique, redistribution de la fluorescence après photoblanchiment (FRAP) et par un tribomètre faible-charge assisté d'un interféromètre, respectivement. Le tribomètre a été spécialement adapté à notre étude au sein du laboratoire LTDS grâce au Pr Stéphane Benayoun et Matthieu Guibert.

Cette étude a fait l'objet d'un article dans le journal de la Royal Chemical Society, *Soft Matter*, publié le 16 février 2018[22] et intitulé : *Bioinspired microstructures of chitosan hydrogel provide enhanced wear protection*. La fabrication des hydrogels et leurs caractérisations structurales, mécaniques et physiques ont été réalisées par mes soins au sein du laboratoire IMP avec l'aide du Dr Guillaume Sudre et du Dr Alexandra Montembault. Les analyses par microscopique électronique et microscopie confocale ont été effectuées au centre technologique des microstructures de l'Université Claude Bernard Lyon 1 avec l'aide du Dr Béatrice Burdin et Pierre Alcouffe. Les aspects tribologiques ont été menés au LTDS avec l'aide de Matthieu Guibert (tribomètre), Thomas Malhomme (interféromètre) et du Pr Stéphane Benayoun.

Bioinspired Microstructures of Chitosan Hydrogel Provide Enhanced Wear Protection

Jimmy Faivre[1,3], Guillaume Sudre[1], Alexandra Montembault[1], Stéphane Benayoun[2], Xavier Banquy[3*], Thierry Delair[1], Laurent David[1*]

[1]*Université de Lyon, Université Claude Bernard Lyon 1, CNRS UMR 5223, Ingénierie des Matériaux Polymères (IMP), 15 Boulevard Latarjet, 69622 Villeurbanne Cedex, France*

[2]*Laboratoire de Tribologie et Dynamique des Systèmes, UMR 5513 CNRS, Ecole Centrale de Lyon, 36 Avenue Guy de Collongue, 69134 Ecully Cedex, France*

[3]*Canadian Research Chair in Bioinspired Materials, Faculty of Pharmacy, Université de Montréal, Montréal, Qc, Canada*

Abstract

We describe the fabrication of physical chitosan hydrogels exhibiting a layered structure. This bilayered structure, as shown by SEM and confocal microscopy, is composed of a thin dense superficial zone (SZ), covering a deeper zone (DZ) containing microchannels orientated perpendicularly to the SZ. We show that such structure favors diffusion of macromolecules within the hydrogel matrix up to a critical pressure, σ_c, above which channels were constricted. Moreover, we found that the SZ provided a higher wear resistance than the DZ which was severely damaged at a pressure equal to the elastic modulus of the gel. The coefficient of friction (CoF) of the SZ remained independent of the applied load with μ_{SZ} = 0.38 ± 0.02, while CoF measured at DZ exhibited two regimes: an initial CoF close to the value found on the SZ, and a CoF that decreased to μ_{DZ} = 0.18 ± 0.01 at pressures higher than the critical pressure σ_c. Overall, our results show that internal structuring is a promising avenue in controlling and improving the wear resistance of soft materials such as hydrogels.

Keywords: hydrogel microstructure, gel-gel friction, lubrication, wear resistance, chitosan

Table of Contents

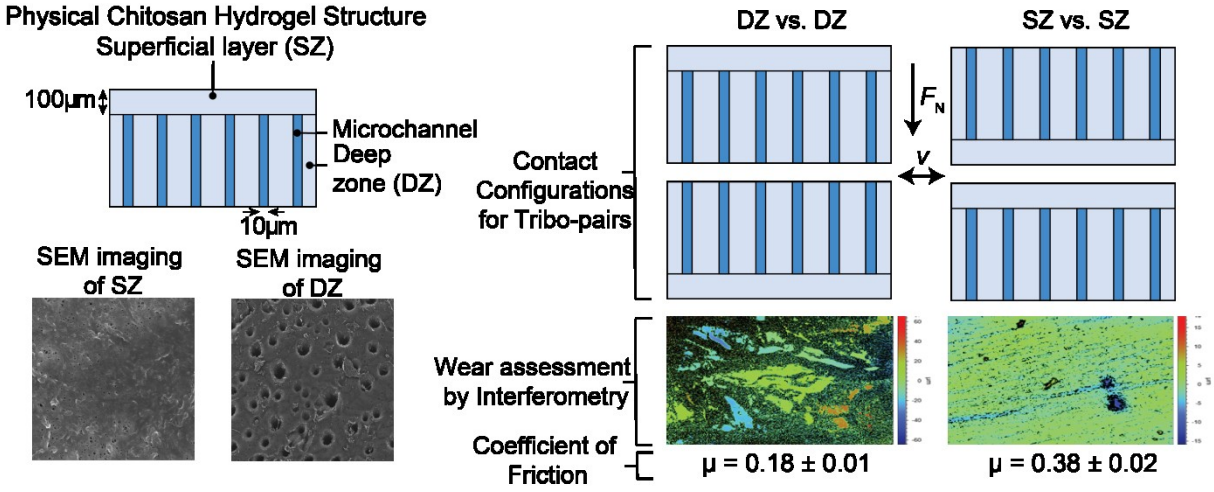

3.1 Introduction

Hydrogels scaffolds are receiving a growing interest in tissue engineering since they can advantageously combine cytocompatible polymers with a high amount of water, therefore, mimicking living tissues[23]. These materials have been used as scaffolds for cartilage[13, 24], bone[25], or nervous tissue repair[26]. In addition, they can be used as artificial skin[10, 16], or as carriers for drug delivery of active molecules[27-29]. These applications emerge from their tunable chemical properties, their multi-scale microstructure (porosity, crystallinity, macromolecular network topology), and their adjustable mechanical and physical properties (viscoelasticity, toughness, permeability[1, 30]).

The design of tissue-mimicking hydrogels for a specific application depends on the choice of raw material (natural polymers or biocompatible synthetic polymers) and the gelation technique. A useful concept for hydrogel design is bio-inspiration: to take advantage of naturally-occurring chemical and physical architectures for manipulating physical, mechanical and biological behaviors[31-32]. This material development strategy leads to the concept of hydrogel materials as “decoys for biological media”[24]. The methods used to induce structuring within hydrogels at different length scales are themselves of great interest. The common structuring methods include freeze or vacuum-casting, layer-by-layer deposition, templating, 3D-printing, and self-assembly, which are used depending on the polymer nature and/or the solvent[31, 33]. Despite the significant number of reports demonstrating the intimate relationship between hydrogels microstructure and macroscopic properties, very few reports have focused on the control of the tribological properties, especially wear resistance. This lack of fundamental knowledge has hampered the use of structured hydrogels in many biomedical applications such as joint replacement. In the present study, we demonstrate that the generation of bioinspired microstructures in physical chitosan hydrogels dramatically allows to control their lubrication and wear resistance. Chitosan hydrogels are especially suitable for cartilage repair since they are excellent for 3D-chondrocyte growth and proliferation[13, 17, 24], and for cartilage substitutes[18, 34]. In this paper, we focus on the impact of the hydrogel structuring on their transport and mechanical properties and more specifically on hydrogel/hydrogel tribological properties to understand and rationalize the effects of the multi-scale structure on wear resistance.

3.2 Materials and methods

3.2.1 Materials

Chitosan (M_w 6.04 10^5 g/mol, M_w/M_n 1.64, DA 4.3%, from squid pen chitin) was purchased from Mahtani Chitosan Pvt. Ltd. Acetic acid, ammonium hydroxide, HEPES and FITC-modified dextran probes (4.0 10^4 g/mol, 5.00 10^5 g/mol, and 2.00 10^6 g/mol) were supplied from Sigma-Aldrich. NaOH pellets, NaCl, and absolute anhydrous ethanol were obtained from Carlo Erba Reagents.

3.2.2 Chitosan Purification

Chitosan was purified on filtration columns with Millipore membranes. A 0.5 $\%_{w/w}$ acidic chitosan aqueous solution was prepared by adding a stoechiometric amount of acetic acid to glucosamine units. The solution was passed though filtration columns with a pressure kept constant at 3 bars with membrane porosities of successively 3, 0.8, and 0.45 µm. Chitosan was precipitated by adding a small amount of ammonium hydroxide to get a pH of 9 and thoroughly washed with distilled water using a centrifuge (10 min at 10000 rpm). Supernatant was removed and replaced by pure water and the procedure was repeated up to distilled water pH. Finally, chitosan was freeze-dried to obtain a purified powder.

3.2.3 Polymer Characterizations

The molar mass, dispersity, and radius of gyration of chitosan and dextran fluorescent probes were analyzed using aqueous Gel Permeation Chromatography (Wyatt Technology). Refractive Index (rEX), UV (DAWN HELEOS), and QELS (Wyatt QELS+) detectors were used for the experiments. GPC parameters for chitosan analysis were: flow rate 0.5 mL/min, *dn/dc*(chitosan) 0.198 mL/g, , TSK6000 and TSK2500 columns (Tosoh Bioscience LLC.), column temperature 25 °C, laser wavelength 664 nm. Samples were dissolved at 0.5 mg/mL in filtered acetic acid buffer (pH 4.5, filtered at 0.1 µm using CME membrane) and filtered at 0.45 µm on CME membrane. For dextran-FITC analysis, parameters were: flow rate 0.5 mL/min, dn/dc (DexFITC) 0.152 mL/g, , TSK6000 and TSK2500 columns, column temperature 25 °C, laser wavelength 664 nm. Samples were dissolved at 0.5 mg/mL in filtered Phosphate Buffered Saline buffer (PBS) (pH 7.4, 10 mM PBS, 0.15 M NaCl, filtered at 0.1 µm using CME membrane) and filtered at 0.45 µm on CME membrane.

The degree of acetylation of chitosan was assessed using ^{1}H-NMR spectroscopy (Bruker 400 MHz). The DA was calculated according to the method of Hirai et al.,[35] from the ratio the

integration of acetyl group protons (δ: 2.4-1.7 ppm) by the integration of glucosamine unit protons (δ: 4.3-2.7 ppm). Chitosan was dissolved in D_2O with 5 µL of 37 % HCl solution for 12 h at room temperature.

3.2.4 Chitosan hydrogel disks

A chitosan solution was prepared by dissolving purified chitosan powder into water at the polymer concentrations 1.5, 2.5 and 5 $\%_{w/w}$ with a stoechiometric amount of glacial acetic acid to ensure the protonation of every amino groups using the following equation:

$$m_{chitosan} = \frac{m_{chitosan} \times (1 - DA) \times (1 - \frac{m_{water}}{100}) \times M_{acetic\ acid}}{M_{chitosan}} \quad \text{Eq. 6}$$

m being the mass (g), M is the molar weight (g/mol) and $M_{chitosan}$ is defined by $M_{chitosan} = 42 \times DA + 161$ [14, 20, 36]. The chitosan dissolution was performed in a closed reactor under mechanical stirring at 4 °C for one day. The resulting chitosan solution was then placed in centrifuge syringes (Optimum®, Nordson EFD, USA) to remove air bubbles by repetitive centrifugations (5 min at 5000 rpm) and was extruded between two plastic foils with holds to control the thickness of the final gels (1.5 mm). The upper plastic foil was removed and the flattened chitosan solution was placed in a 1 M NaOH coagulation bath until the gelation process was completed. Gel disks were then cut with a biopsy punch of 11 or 25 mm diameter and washed several times in distilled water to reach deionized water pH. The obtained hydrogel disks were stored in distilled water prior to use.

3.2.5 SEM on chitosan aerogels

Hydrogel samples were firstly changed for 100% alcogel by immersing hydrogels into successive ethanol baths (10, 30, 50, 70, 90, and 100% ethanol in water) for 30 min each. Aerogels were obtained by exchange between ethanol and CO_2 supercritic fluid using an automated critical point dryer (EM CPD300, Leica). 20 exchange cycles were needed followed by a very slow CO_2 degassing at 37 °C. Samples were then carbonated and imaged using an scanning electronic microscope (Merlin Compact, Zeiss). To visualize the impact of a normal stress on the gel structure, precisely weighted loads was applied on top of the hydrogels prior to aerogel formation.

3.2.6 Observation of hydrogels and FRAP experiments by confocal laser scanning microscopy (CLSM)

CLSM micrographs of the hydrogels were obtained using a laser scanning confocal microscope (Zeiss 510 LCM) with a 10 x 0.3NA dry neofluor objective. Chitosan hydrogels were incubated with 0.6 mg/mL 40 kDa dextran-FITC fluorescent probes in a HEPES buffer (0.1 M HEPES, 150 mM NaCl and pH 7.4) for 24 h in a dark container at 4 °C. Excitation was conducted at 488 nm at 3% laser intensity (excitation laser source was set at 50%) and emission collected from 505 to 670 nm. The photomultiplicator (PMT) gain was set at 525. Pictures were taken in a fluorescent probe bath on both sides and on the side of a gel slice. Imaging, gel porosity, and macromolecule diffusion under stress were recorded by Fluorescence Recovery After Photobleaching (FRAP) technique[37] at a depth of 100 µm. In each experiment, small hydrogel disks were cut from chitosan gel membranes to get 5 mm diameter and 1.5 mm thick pieces and were incubated in 0.6 mg/mL 40 kDa dextran-FITC buffered solution (0.1 M HEPES, 150 mM NacL and pH 7.4) for 24 h to ensure complete homogenization. The gels were then mounted in CLSM and immersed in the fluorescent probe buffered solution. For FRAP experiment under load, each dextran-FITC concentration was fixed at 0.6 mg/mL and PMT gain was kept constant at 525. To ensure the recording of a 2D diffusion (in the focal plan) and the use of a mathematical fit, a full cylinder was bleached after intense photobleaching (100% laser intensity)[37]. In this case, the cylindrical bleaching volume avoids diffusion in the third dimension. 512x512 pixels images of a confocal xy plan (100 µm above the bottom of the plate, 15 µm of thickness) were scanned at 3 % laser initial intensity ($I < 0$) (15 pre-bleach scan images). At $t = 0$, a circle of 55 µm diameter is bleached with 50 iterations (about 10 s total) at 100 % laser intensity (I_0). A total of about 500 images scans (acquisition time < 1 s each) were collected for each sample. 5 repetitions were done per experiment. For diffusion under stress experiments, weights were deposited on a cover glass directly on top of the disks. To measure the diffusion coefficients, the gels were left to equilibrate 5 min prior to FRAP measurements. The transitory state was also recorded.

3.2.7 Mechanical properties by Dynamic Mechanical Analysis

Gel samples were die-cut with a 12 mm diameter punch and placed in a compression module. An aqueous bath was mounted to maintain complete hydration of gel disks and also water recovery after unconfined compression at room temperature. Firstly, a series of creep/recovery experiments were performed under constant stress using a DMA (DMA 800, TA Instrument). An initial preload of 0.02 N was applied to measure the sample thickness.

Then, a constant load was applied for 5 min and the gel length was monitored as a function of time. After 5 min of gel creep, the load was removed (set to initial value of 0.02 N) and the gel was free to re-swell. The gel length recovery was then monitored as a function of time for 5 min. This cycle was repeated several times with increasing loads upon creep from 0.05 to 2 N (corresponding to stresses from 0.5 to 20 kPa). Data were fitted using the Maxwell's approach taking into account the sum of different phenomena of specific response time via a sum of exponentials.

3.2.8 Tribological properties

Due to the process of gelation, physical chitosan hydrogel disks offered a bilayered structure. To assess friction properties of chitosan hydrogels on both sides, die-cut gel disks were tested by putting into contact either SZ/SZ or DZ/DZ configurations. A low-load tribometer consisting of an upper mobile part applying a sinusoidal motion and a servo-controlled load (to avoid the relaxation effect of the gel) and a lower immobile part sensing the normal and lateral forces was used. A cantilever spring (linking the upper mobile part and a pin where the 11 mm diameter gel disk is glued) transmitted a vertical load to the bottom surface. A nut allowed the pin to rotate to find a flat contact between the gels. The lower immobile part was equipped with lateral and normal force sensors. The lower 25 mm diameter gel was glued within a bath mounted on top of the lower immobile part. To glue the gels on metallic lower and upper parts, gels were slightly dried on the non-studied sides and deposited on waterproof glue (Superglue 3 Power Flex, Loctite). The bath was immediately filled with 0.1 M HEPES pH 7.4 buffer and left to incubate for 1 h. Both gels were brought into slight contact to ensure flat contact and the nut was tightened. The friction force and normal forces were measured as average values in the middle of the stroke (represented by green rectangles in Fig. 3.7) to avoid any edge effect due to the direction and speed changes and to ensure that the dynamic friction coefficient is assessed.

Normal force friction test

Upper and lower gels were brought into contact. A fixed 1 Hz oscillation frequency was applied along with a 5 mm lateral motion. Normal Force was successively increased from 0.05 N to 10 N (from 500 Pa to 100 kPa). Friction runs were performed over 250 cycles for each load.

Wear resistance

To assess wear, only 2.5 $\%_{w/w}$ chitosan hydrogels were used at 1 Hz oscillation frequency, 5 mm lateral motion and 3 N (~ G') normal forces for 10000 cycles. At the end of the test, the hydrogels were detached from the metallic parts, slightly dried on the studied surface using compressed air, analyzed qualitatively by a digital microscope (VHX-1000, Keyence) and quantitatively by interferometry (ContourGT-K 3D, Bruker).

3.2.9 Rheological characterization

Chitosan hydrogel disks were characterized for their rheological properties using an AR2000 rheometer (TA Instruments, USA). A parallel plate geometry was mounted with a water trap to limit water evaporation during measurement. Viscoelastic properties were performed at 1% gel deformation in frequency sweep mode in the linear domain (n = 5).

3.2.10 Stress-strain curves

Stress-strain curves were recorded for each gel using a Shimadzu AG-X+ 10 kN tensile tester. Load/Unload cycles were applied on top of a gel with increasing strain (10, 20, 30, 50, 70, and 80% of initial gel thickness) and the resulting stress is recorded. The compression plates were lubricated with mineral oil to avoid barreling effects. A compression study was performed following the same procedure as for the stress-strain curve except that a linear strain at a rate of 0.6 mm/min was applied on top of the gels. Water exudation was directly observed by the means of a camera.

3.2.11 Osmotic pressure assessments

Chitosan gel osmotic pressure was evaluated to determine the gel permeability using Eq. 5. The gel osmotic pressure determinations were carried out after de-swelling the gels by the dialysis bag method described elsewhere[38-39]. The gel disks were positioned at the contact of semi permeable regenerated cellulose membranes (MWCO 2 kDa, spectrum lab) and the sealed bags were immersed in an aqueous polyvinylpyrrolidone solution ($8.7\ 10^{-2}$ mg/mL, Mw = 29 kDa, Sigma-Aldrich) with a known osmotic pressure equal to 30.5 kPa and buffered with HEPES at 0.1 M and pH 7.4 at constant room temperature. After equilibrium is reached (4 days), gels are removed, weighed and viscoselastic measurements are performed using an AR2000ex rheometer to assess the shear moduli.

3.3 Results

3.3.1 Structure of chitosan hydrogels

The "one-pot" fabrication process facilitates the manufacturing of chitosan physical gels with controlled architecture (Fig. 3.1). The process allows obtaining a two-layered structure as depicted in figure schematic 1A. During the gelation process, the

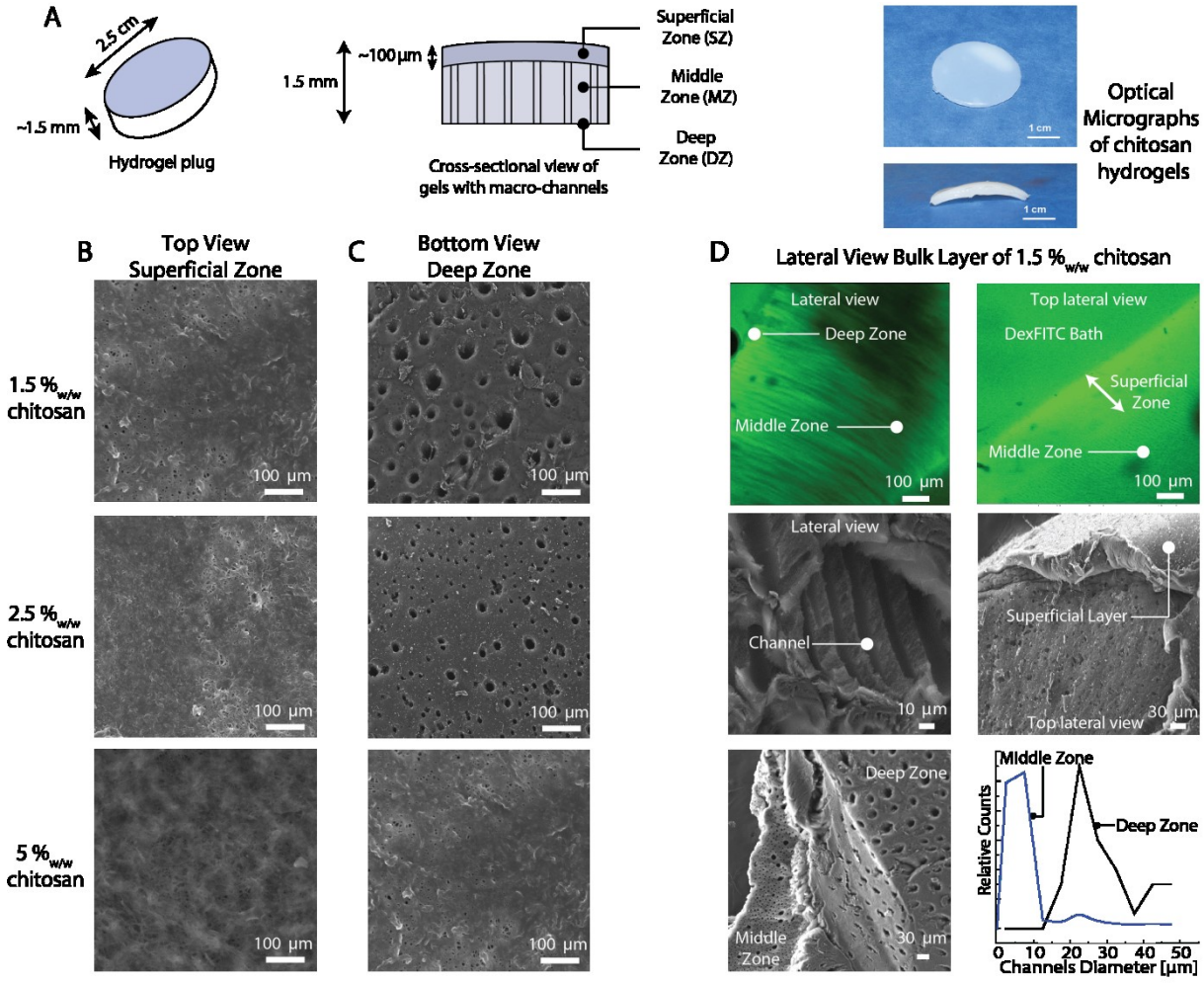

Figure 3.1. *Structural understanding of physical chitosan hydrogels. (A) Scheme of gel disk, cross-sectional view of chitosan gels owning or not macro-channels, and optical micrographs of hydrogel disks. SEM pictures of chitosan hydrogels after CO2 supercritical drying as a function of chitosan concentration showing (B) the superficial zone (top view) exhibiting a dense structure and (C) the deep zone (bottom view) of hydrogels showing macro-porosity. (D) CLSM and SEM pictures of a cross-section of 1.5 %w/w chitosan gel showing aligned channels perpendicularly to superficial zone. 40 kDa Dextran-FITC was added to the gel*

solution to visualize the gel structure by CLSM.

acidic chitosan solution in direct contact with the basic solution quickly forms a dense gel membrane[21] forming the superficial zone (SZ) of the gel (Fig 3.1B). Directly following the formation of the SZ, the middle zone (MZ) of the gel exhibits perpendicularly aligned channels (capillaries) of 10-25 µm in diameter (Fig. 3.1C-D) depending on the gel concentration. These channels were found to be densely packed throughout the gel thickness from the upper part of the MZ down to the deep zone (DZ) (Fig 3.1C). The size of the channels decreased with increasing chitosan concentration, C_p, from 20 µm at 1.5 $\%_{w/w}$ chitosan gel to 10 µm for 2.5 $\%_{w/w}$ chitosan gel and no apparent channels were observed in the 5 $\%_{w/w}$ chitosan gel (Fig. 3.1C). To gain more insights on the structure of the bilayered hydrogel, vertical slices of 1.5 $\%_{w/w}$ chitosan gel, parallel to the channels, were imaged by confocal microscopy and SEM (Fig. 3.1D). The MZ exhibits vertically aligned channels while the SZ appeared as a dense layer of about 100 µm in thickness. Throughout the MZ and DZ, the distribution of the channel diameters was bimodal (Fig. 3.1D). In the vicinity of the membrane (upper region of the MZ), a majority of 5 µm channels and few 20 µm channels were observed. In deeper regions (DZ), the channels appeared larger with a diameter ranging between 20 and 40 µm. At a finer size scale, in order to measure the nanoporosity of the gels, we quantified the diffusion coefficient of dextran-FITC probes embedded in the gel by fluorescent recovery after photobleaching (FRAP). When the probe size is close to the mesh size of the gel or internal gel porosity, its diffusion is expected to be significantly lowered (see the fluorescent probes sizes in Table 3.1). The mesh size for 1.5 $\%_{w/w}$ and 2.5 $\%_{w/w}$ chitosan gels were measured in the SZ and MZ and they ranged between 40 and 80 nm while the porosity of the 5 $\%_{w/w}$ hydrogels ranged between 10 and 40 nm (Fig. 3.2).

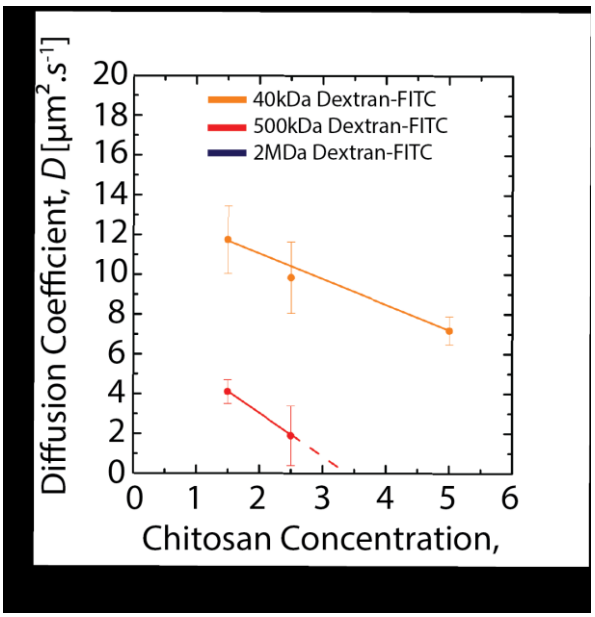

Figure 3.2. *Diffusion properties of chitosan hydrogels using different dextran-FITC probe sizes. 2 MDa Dextran-FITC diffusion was not detected by the FRAP technique.*

Table 3.1: Fluorescent probe characteristics (molecular weight (Mw), dispersity (PdI) and radius of gyration (Rg)) in HEPES buffer pH 7.4 NaCl 50mM.

Fluorescent probe	Mw (g/mol)[a]	PdI[a]	Rg (nm)[a]	Rg ($Rg=0.025*Mw^{0.5}$)[b]
40kDa DexFITC	3.85×10^4	1.31	8	5
500kDa DexFITC	4.68×10^5	1.81	22.5	17.7
2MDa DexFITC	1.81×10^6	1.50	41.2	35.4

[a] measured by GPC; [b] from literature[40]

3.3.2 Poroelastic properties of structured chitosan hydrogels

To gain more insight into the fluid transport properties inside the gels under normal stress, we performed a series of FRAP experiments at different applied normal loads. A normal load was applied by depositing a weight on top of the gel immersed in a 40 kDa dextran-FITC fluorescent buffer.

At rest (no load, $\sigma = 0$), the diffusion coefficients of 40 kDa dextran probes were 12 $\mu m^2/s$ for C_p = 1.5 and 2.5 $\%_{w/w}$ and decreased to 8 $\mu m^2/s$ for C_p = 5 $\%_{w/w}$ (Fig 3.3A). Under weak normal loading ($\sigma < \sigma_c$, σ_c being a critical stress at which diffusion within the gel matric is drastically reduced), the diffusion coefficient was firstly weakly impacted. At $\sigma > \sigma_c$, the diffusion coefficient of the probe drastically decreased and could not be measured. The value of σ_c was estimated at the slope transition (Fig. 3.3A). The values were σ_c = 2-8 kPa for C_p = 1.5% w/w and σ_c = 8-10 kPa for C_p = 2.5% w/w chitosan gels. The transition was much smoother for C_p = 5% w/w chitosan gels which complicated the determination of σ_c (estimated between 10 - 25 kPa).

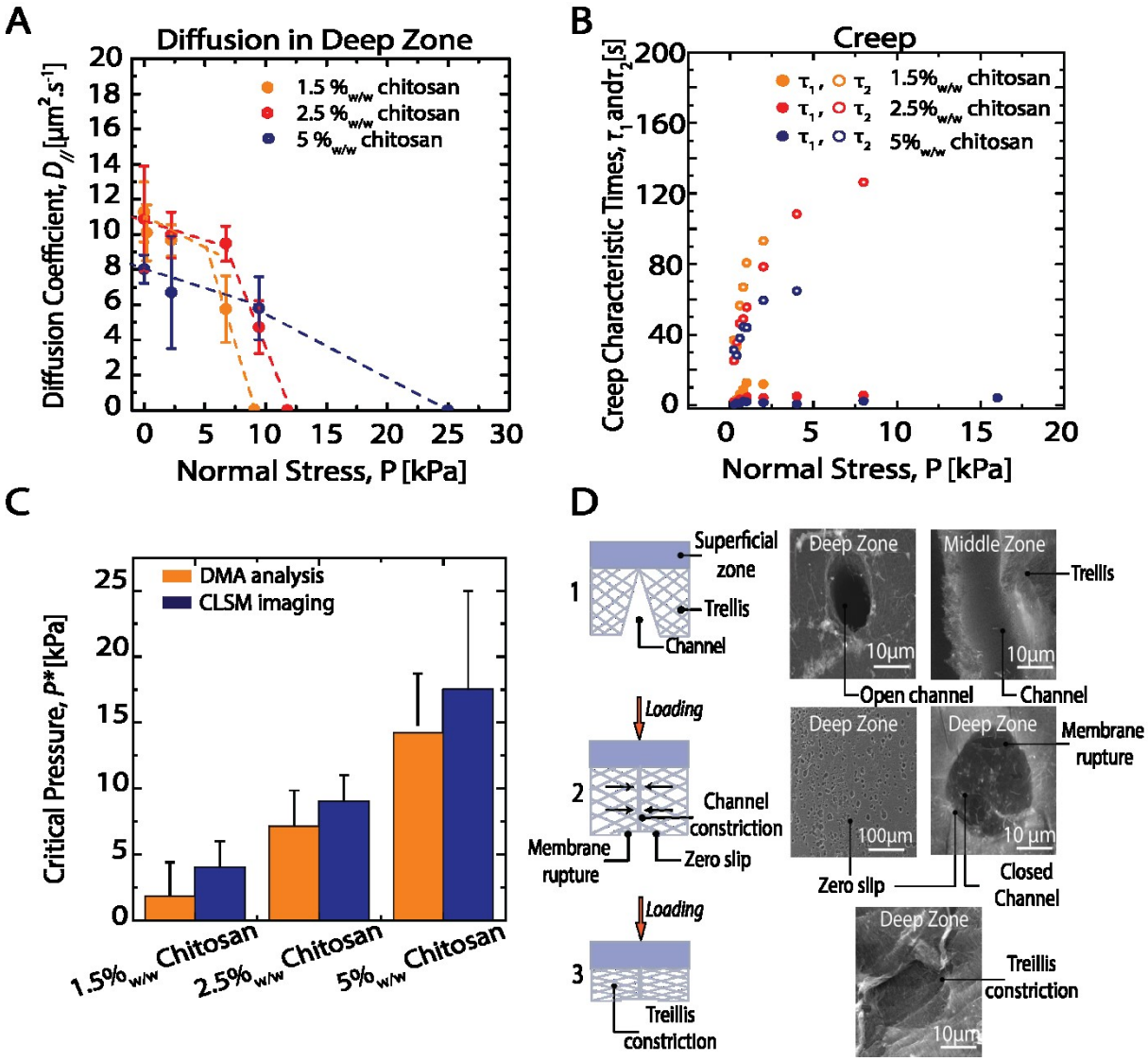

Figure 3.3. *(A) Diffusion coefficients of 40kDa Dextran-FITC embedded in chitosan gels as a function of normal stress (error bars represents standard deviations of n=5 independent measurements). (B) Characteristic creep times, τ_1 and τ_2, as a function of applied normal. (C)*

Comparison of the gel critical pressure, σ_c, between Dynamic Mechanical Analysis and Confocal Laser Scanning Microscopy. (D) Schematic and SEM micrographs of 2.5% $_{w/w}$ chitosan hydrogel nano- and micro- porosity (basal view) evolution under stress: (D1) unloaded gel with open channel and normal trellis-like structure, (D2) normally loaded gel (σ = 5 kPa) showing channel constriction, and (D3) normally loaded gel (σ = 50 kDa) showing channel and trellis constriction.

To characterize the mechanical behavior of the structured gels, we performed creep/recovery tests at increasing normal stress on fully immersed chitosan gels using Dynamic Mechanical Analyzer (DMA) (Fig. 3.3B and Fig. 3.4A). This study allows to measure the characteristic times for creep and recovery at different loads. Initially, at $\sigma < \sigma_c'$ (σ_c' being a critical stress at which the gels does not fully recover or reach the steady state after an applied strain), the gels exhibited full elastic creep and recovery after addition and release of the normal pressure. Above σ_c' (σ_c' = 1.8 kPa for C_p = 1.5 % $_{w/w}$, σ_c' = 7.1 kPa, for C_p = 2.5 %$_{w/w}$, and, σ_c' = 14.2 kPa for C_p = 5 %$_{w/w}$), gels were not able to reach the steady creep regime or recover completely (Fig. 3.4A). This first observation showed that $\sigma_c \sim \sigma_c'$ for all the gels tested indicating a strong correlation between the mechanical and transport properties of these gels (Fig 3.3C). The creep/recovery responses were fitted using the Voigt model for creep:

$$\varepsilon(t) = \varepsilon_{elast} + \sum_i^{\infty} \varepsilon_{ci}\left(1 - \exp\left(-\frac{t}{\tau_{ci}}\right)\right) \qquad \text{Eq.1}$$

where $\varepsilon(t)$, ε_{elast}, ε_{ci}, are the gel deformation with time, the initial gel thickness and the gel thickness at ith creep step, respectively, and τ_{ci}, is the characteristic time of the ith creep step. Concerning the recovery process:

$$\varepsilon(t) = \varepsilon_{\infty} + \sum_i^{\infty} \varepsilon_{ri}\left(1 - \exp\left(-\frac{t}{\tau_{ri}}\right)\right) \qquad \text{Eq. 2}$$

where ε_{∞} is the non-recoverable deformation at the end of the recovery step, ε_{ri} is the amplitude of the ith recovery component, and τ_{ri}, is the characteristic time of the ith recovery component.

In practice, two exponential terms were sufficient to adequately describe both the creep and recovery responses (i = 2), yielding to two characteristic times for creep, τ_{c1} and τ_{c2}, and recovery, τ_{r1} and τ_{r2}, and their corresponding amplitudes. Thus, these observations evidenced two different deformation regimes. A first process occurred with a characteristic time τ_{c1} and

τ_{r1} of about 5-10 s for creep and recovery, independently of chitosan concentration (full symbols in Fig 3.3B and Fig. 3.4B). During this first stage, at least 95% of the gel thickness deformation occurred at $\sigma < \sigma_c$. This was followed by a slower process with a characteristic time τ_{c2} and τ_{r2}, ranging from 30 to 100 s, responsible for less than 5% of the gel deformation (in the investigated creep and recovery time ranges).

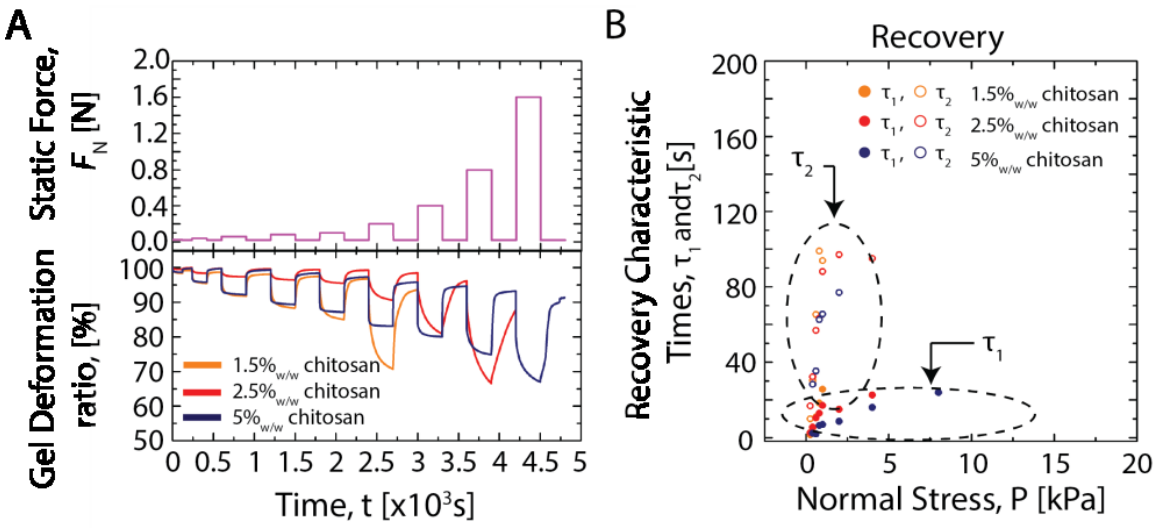

Figure 3.4. *(A) Creep/recovery cycles with increasing load of chitosan hydrogels assessed by DMA and (B) characteristic times of chitosan hydrogels during recovery.*

To understand the nature of these 2 distinct deformation regimes, 1.5%$_{w/w}$ chitosan gels were imaged by SEM at $\sigma < \sigma_c$ (Fig. 3.3D1), at $\sigma > \sigma_c$ (Fig. 3.3D2), and $\sigma >> \sigma_c$ (Fig. 3.3D3). At $\sigma < \sigma_c$, the initial gel structure was not affected by the applied normal stress. The hydrogel still exhibited open pores and channels. At $\sigma > \sigma_c$, the channels were fully filled with the polymer matrix. The opening of the pores in the DZ were still noticeable due to the adhesion of the gel to the glass substrate during sample preparation for SEM (creating a zero slip boundary). At $\sigma >> \sigma_c$, the nanoporosity collapsed leading to the closure of the nanoporosity, referred to as "treillis constriction" in Figure 3.3D3.

Finally, the mechanical properties of chitosan hydrogels were assessed by a tensile tester in compression mode. Figure 3.5 displays a typical loading/unloading true stress-strain curve (σ_v-ε_v curve). All gels appeared to exhibit a highly dissipative behavior characterized by a pronounced hysteretic loop. The dissipation ratio, defined as the ratio of the area under the hysteretic loop to the stress-strain tensile curve, reached values close to 1 above $\varepsilon_v = 50$ %, which is indicative of a plastic behavior with no strain or stress recovery. At lower strain, $\varepsilon_v <$

20 to 50%, recovery was still observed (Fig. 3.5). We noticed that the plastic behavior of the gels appeared at stresses close to σ_c for each gel, indicating a close relationship between the water expulsion and irreversible polymer chain rearrangements in the hydrogel structure.

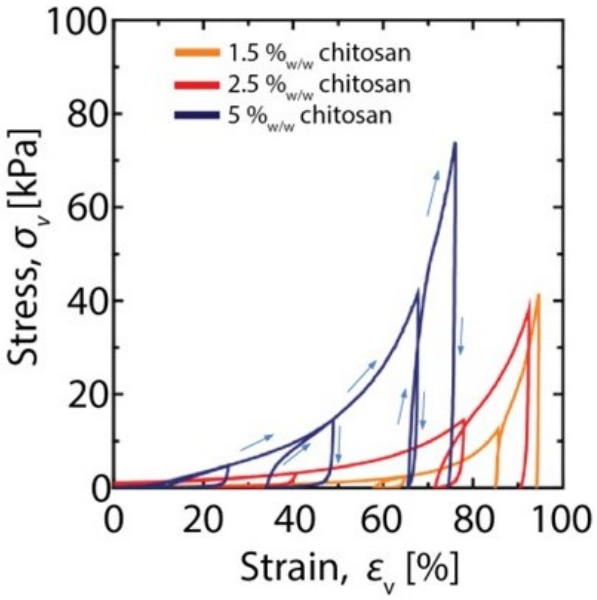

Figure 3.5. S*tress versus strain curves of chitosan hydrogels*

3.3.3 Tribological properties of chitosan hydrogels

To establish the relationship between the gel microstructure and the lubrication and wear resistance, we performed a series of tribotests at different loads using two hydrogels plugs as tribo pair. Gel/gel tribological measurements were performed in a geometry of contact plane/plane on a homemade tribometer in both SZ/SZ and DZ/DZ configurations (Fig. 3.6). No adhesion between the hydrogels nor stiction spikes were measured throughout the tribological experiments as shown in figure 3.7. Figure 3 represents the tangential force, F_t, as a function of applied normal force, F_N, at a constant sliding velocity of 5 mm/s. The gels were immersed in HEPES buffer at pH 7.4. In the configuration where the two SZ were facing each other, the Amontons coefficient of friction (CoF), μ, was $\mu = 0.38 \pm 0.02$, independently of the gel concentration (Fig 3.6A). When the configuration was changed to DZ/DZ configuration (Fig 3.6B), the measured CoF at low load was firstly very close to the SZ/SZ configuration, and reached a lower value of $\mu = 0.18 \pm 0.01$ at $\sigma > \sigma_c$, about half the SZ/SZ CoF value. Moreover, we noticed that experiments performed in the DZ/DZ configuration presented severe damage at normal pressures close to the elastic compression modulus, G', of

each gel (Fig. 3.8A-B). For comparison purposes, the elastic moduli measured for the present chitosan physical hydrogels were G' = 10 kPa for C_p = 1.5 $\%_{w/w}$, G' = 30 kPa for C_p = 2.5 $\%_{w/w}$, and G' = 100 kPa for C_p = 5 $\%_{w/w}$ (Fig. 3.8B). Such severe damage was *never* observed in the SZ/SZ configuration.

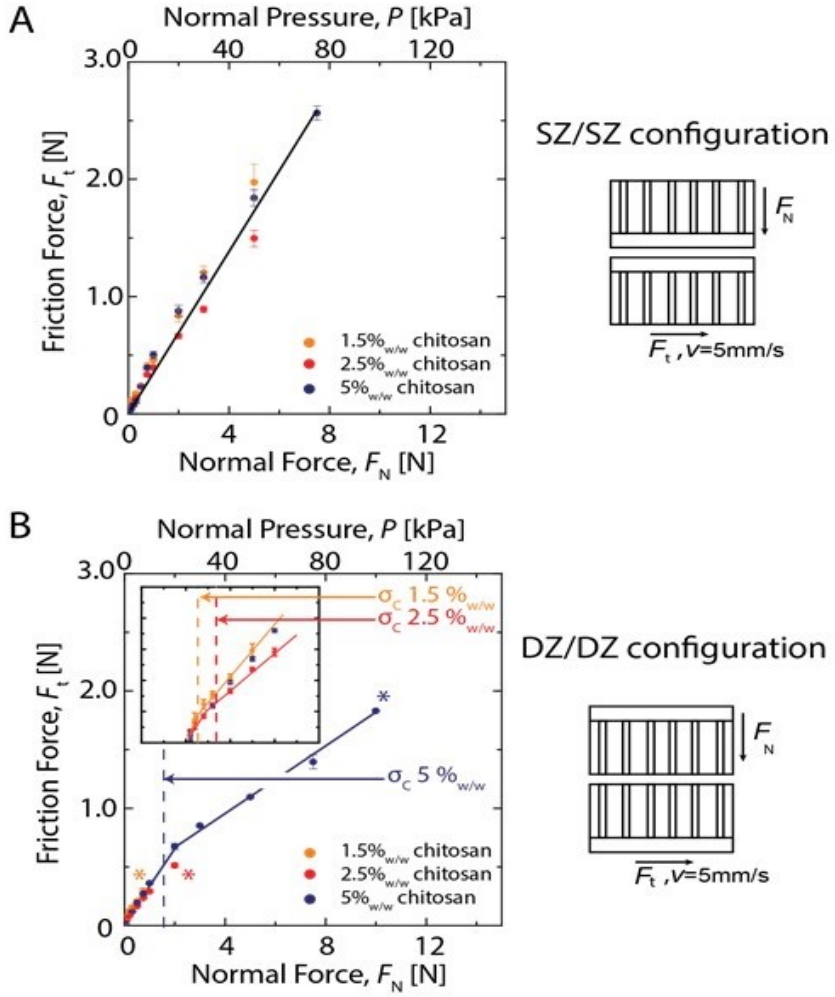

Figure 3.6. *(A) Schemes representing the contact configurations used in the friction experiments (SZ/SZ and DZ/DZ). Friction force, F_t, as a function of normal force, F_N, (B) SZ/SZ contact and (C) DZ/DZ contact measured by low-load tribometer. * highlights the pressure at which damage occurs in the DZ/DZ configuration.*

The lubrication and transport of lubricant/solvent between the contact zone and the bulk hydrogel were analyzed in the framework of the repulsion-adsorption model[41-42]. Accordingly, the friction force of a gel on a solid substrate was written as:

$$F_t = \frac{\eta . \nu}{\xi_g + \sqrt{K_{gel}}} \qquad \text{Eq.3}$$

where ν is the sliding speed, η is the viscosity of the lubricant film of thickness ξ_g, and K_{gel} is the permeability of the hydrogel to the lubricant. Upon loading and shear, the gel is excreting a thin film of lubricant maintaining the surfaces apart. Derived expressions can be used to scale the impact of the gel interfacial properties (Eq. 4) [41], in order to extract the interfacial fluid viscosity:

$$F_t \cong \eta . \nu . \left(\frac{E}{\tau}\right)^{1/3} . \frac{\frac{\sigma}{E}}{1 + \frac{\frac{\sigma}{E}}{\left(1+\frac{\sigma}{E}\right)^{\frac{1}{3}}}} \qquad \text{Eq. 4}$$

where σ is the normal pressure. The Poisson's ratio was assumed to be close to 0.5, and therefore, the elastic modulus, *E,* was close to 3 × G For Example, the 1.5 $\%_{w/w}$ chitosan gel owned a shear modulus *G* = 10 kPa, its elastic modulus was assumed to be E = 3 × G = 3 × 10 = 30 kPa. Equation 3 can also be derived to equation 5 substituting the gel permeability, yielding:

$$F_t = \frac{\eta . \nu}{\xi . \left(1 + \frac{\Pi_0}{\sigma}\right)} \qquad \text{Eq. 5}$$

where Π_0 is the gel osmotic pressure and $\xi \cong \sqrt{K_{gel}}$ is the correlation length of the polymer solution.

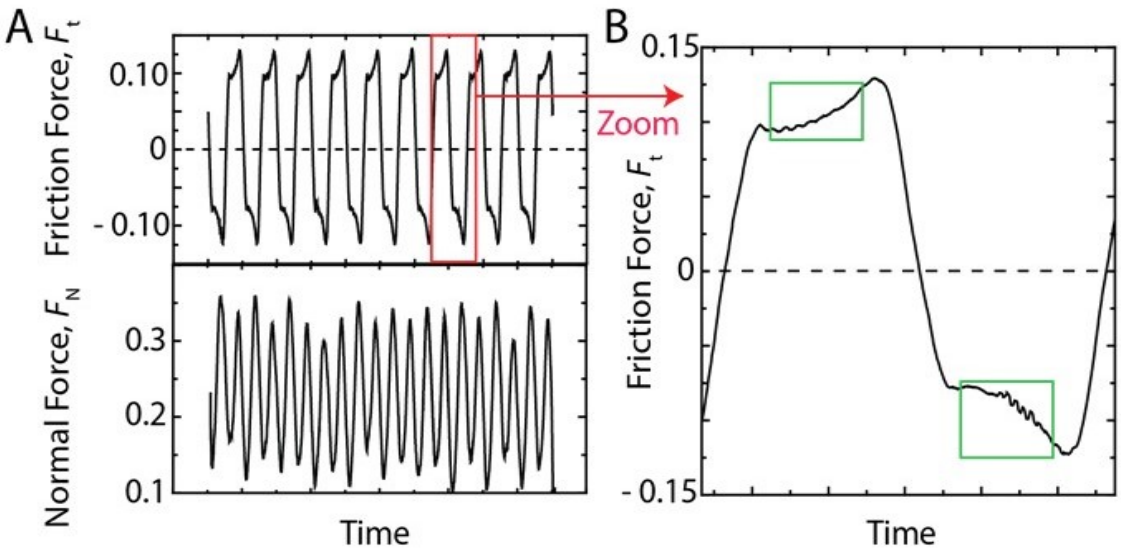

Figure 3.7. *(A) Typical friction and normal forces profiles for 2.5 %$_{w/w}$ chitosan gels on the DZ/DZ configuration at a speed of v = 5 mm/s and (B) zoom in the friction profile showing no stiction in the friction signal. These data correspond to that of Figure 3B for the chitosan gel at 2.5 %$_{w/w}$ at P = 3 kPa. Green rectangles represent the areas where the friction/normal forces were measured.*

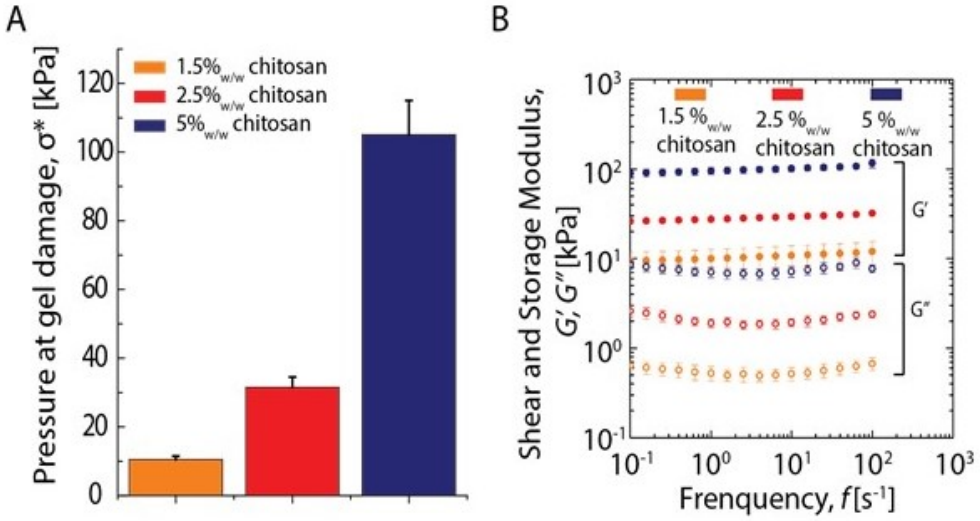

Figure 3.8. *(A) Pressure at gel damage measured for the chitosan hydrogels on the DZ/DZ configuration and (B) shear and storage moduli of chitosan hydrogels.*

Analysis of friction data in figure 3.6 with equations 4 and 5 showed good agreement with the repulsive gel on solid substrate model for both configurations (Fig. 3.9A-B).

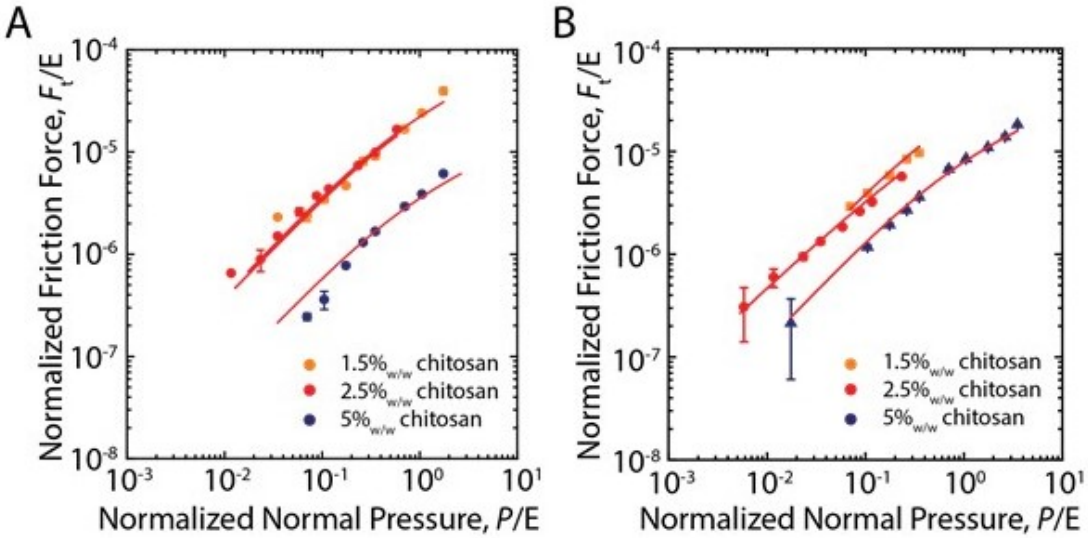

Figure 3.9. *Friction forces as a function of normal pressure for (A) SZ/SZ configuration and (B) DZ/DZ configuration. Red lines are fitting obtained from Eq. 1.*

The viscosity of the hydrodynamic lubrication film for the DZ/DZ configuration was η = 0.8 to 1.7 mPa.s which is close to water viscosity (Table 3.2). In the SZ/SZ configuration, η was close ranging from η = 0.9 to 2.4 mPa.s. It is noteworthy that the viscosity systematically increased when C_p decreased, suggesting a higher amount of polymer chains within the interfacial hydrodynamic film. The values of gel permeabilities, K_{gel}, in the DZ/DZ configuration were significantly higher than SZ/SZ and decreased with increasing C_p (Table 3.2). To give more insights in the lubrication process related to a higher gel permeability, compression studies on the chitosan gels were performed. Water exudation was systematically observed on the DZ side and appeared at pressures very close to the critical pressures, σ_c, previously discussed (3.10 ad Fig. 3.3C).

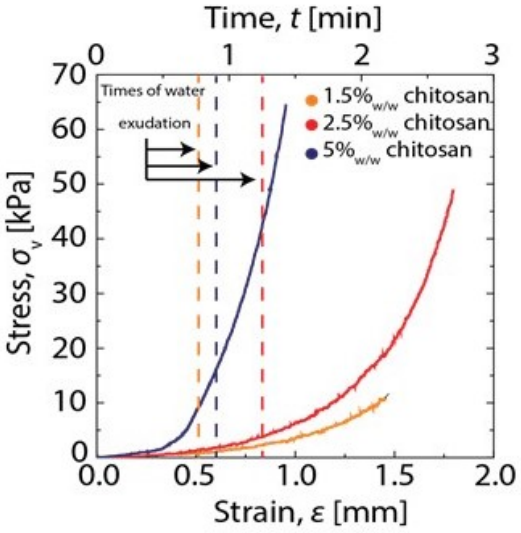

Figure 3.10. *Compression study of chitosan hydrogels showing the critical strains for exudation of water for different chitosan hydrogels.*

Table 3.2: Mechanical and thermodynamic properties of chitosan gel and fitted results using equation 4 and 5.

System	Elastic Modulus (Pa)[a]	Interstitial film viscosity, η (mPa.s)[b]		Permeability of the gel, K_{gel} (m^2)[c]	
		DZ/DZ	SZ/SZ	DZ/DZ ×	SZ/SZ ×

				10^{-12}	10^{-12}
1.5 $\%_{w/w}$ chitosan	3×10^4	1.7	2.4	10.56 (±0.38)	2.96 (±0.21)
2.5 $\%_{w/w}$ chitosan	9×10^4	1.0	1.8	4.53 (±0.01)	0.76 (±0.44)
5 $\%_{w/w}$ chitosan	3×10^5	0.8	0.9	1.80 (±0.05)	0.15 (±0.04)

[a] fitting using Eq. 4; [b] fitting using Eq. 5

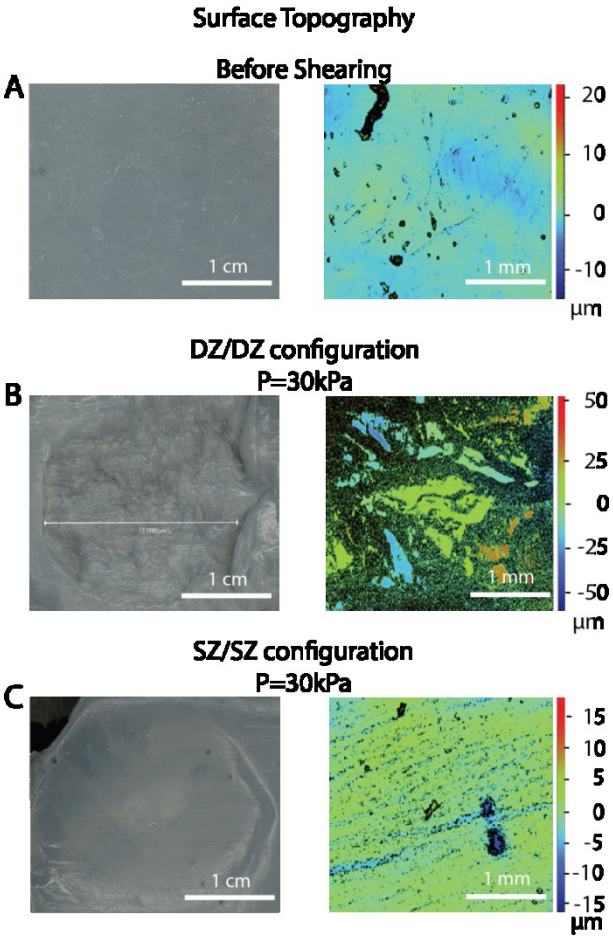

Figure 3.11. *2.5%$_{w/w}$ chitosan gel wear pictures taken by a digital microscope and using an interferometer. The gel surface is slightly dried to make streaks or fractures appear. (A) Intact gel before wear experiment, gel wear pictures in a (B) DZ/DZ configuration at 100% G' (P = 30 kPa) showing gel destruction, and (C) SZ/SZ configuration at 100% G' showing few damage. The black areas are due to large changes in heights. As a consequence, wear is*

so high that the interferometric method is unable to measure accurately the actual roughness.

We analyzed the surface topography of the 2.5 $\%_{w/w}$ chitosan hydrogels after tribotesting to assess their resistance to wear. Figure 3.11 shows 2.5 $\%_{w/w}$ chitosan gel topography using optical microscopy and light interferometry to quantify changes in roughness before and after tribo experiment. The initially intact gel exhibited a smooth surface (Fig. 3.11A). After applying a normal stress of 100% of the value of *G*' (~30 kPa) for the 2.5 $\%_{w/w}$ chitosan hydrogel, severe wear damage appeared on the DZ/DZ contact only (Fig. 3.11B). Wear damage was directly observable by digital microscopy *via* the presence of large variations of the surface profile in figure 3.11B, matching the black areas reported in the optical interferometry images**.** In the SZ/SZ, the gel surface demonstrated fewer signs of wear even though CoF in this configuration was higher (Fig. 3.11C). This could be explained by the weaker elastic compressive modulus of the DZ compared to the SZ even over 1.5 mm of gel thickness due to the gelation process[21]. These qualitative observations were confirmed by the quantitative assessment of surface roughness, S_a, using interferometry (Fig. 3.12). Figure 5 represents the surface roughness of chitosan gel samples after shearing the surface for 10^4 cycles at a normal load of 30 kPa. The values of the surface roughness obtained from interferometry followed the previous trend observed with optical microscopy. Indeed, a low increase of surface roughness on the SZ from 0.7 to 1.1 µm with the applied pressure was noticed. In contrast, a drastic increase of S_a with the DZ/DZ configuration was observed from 4 µm to higher than 12 µm due to gel erosion and fracture at σ = 30 kPa (the final roughness is a lower bound estimation of the exact value due to large variations of the surface height in the black regions in Figure 3.11B). In spite of the significant damage observed by microscopy imaging, the evolution of the CoF throughout the wear test was constant, meaning that tangential forces remained constant at a fixed normal force.

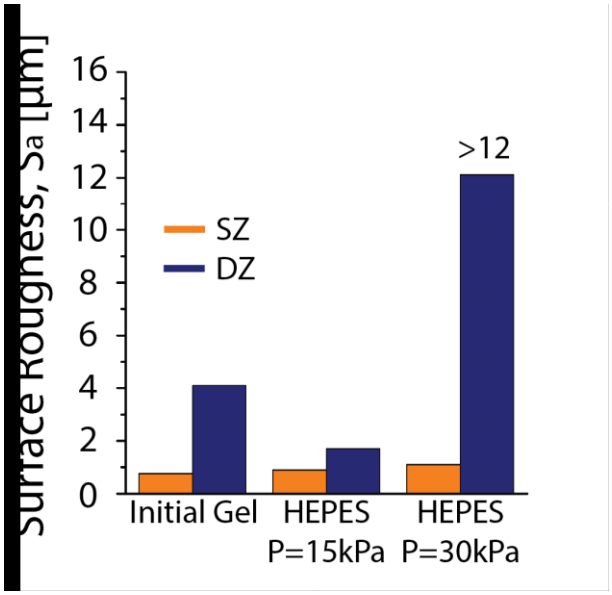

Figure 3.12. *Quantitative analysis of gel roughness after 10^4 cycles at 5mm/s and under an applied load equals to100% of elastic modulus of 2.5 $\%_{w/w}$ chitosan hydrogel (30 kPa) in 0.1M HEPES buffer pH 7.4. The analyzed area was 20% of the total wear track.*

3.4 Discussions

The one-pot gelation process allowed for the formation of a structured chitosan hydrogel mimicking naturally occurring features found in cartilage[43-44] such as the superficial membrane (SZ) and the middle zone composed of vertically aligned channels. The formation of these microstructures is the result of a two-steps process: first, the rapid gelation of chitosan chains at the interface between the chitosan solution and the base solution and second, a slower gelation regime occurring deeper within the gel leading to partial disentanglements and formation of channels. Recent reports have shown that chitosan hydrogels exhibit such a multi-layered structure that depends on the kinetics of the gelation process[13, 21, 45]. A similar multi-layered structure has also been reported for different natural polymer, such as collagen[46] and alginates[47].

The transport properties of the structured gels exhibit similarities to those observed in natural cartilage. The diffusion coefficient of polymeric probes obtained in our study were close to that deduced from similar experiments carried out on articular cartilage using a 70 kDa dextran-FITC fluorescent probe. Fetter *et al*. obtained a diffusion coefficient parrallel to the cartilage surface of 34 $\mu m^2/s$[48], while Greene *et al*. measured a diffusion coefficient of 3.8 $\mu m^2/s$[49]. Our results show that under normal load, the 40 kDa dextran-FITC probe diffusion in the layered gel was close to the NMR and FRAP studies from Greene *et al*.[49]. These authors also reported a constant value of the diffusion coefficient below a critical stress and an abrupt drop of diffusion above this stress[49]. The authors explained such behavior to result from the compression of a treillis-like structure with channels distributed vertically. Upon compression at $\sigma < \sigma_c$, the collapsing channels do not impact macromolecule diffusion inside the matrix. At higher compression (at $\sigma > \sigma_c$), the treillis constriction leads to a drastic decrease of the probe diffusion. In our study, this phenomenon was observed at C_p = 1.5 and 2.5 $\%_{w/w}$ and was less pronounced for the 5 $\%_{w/w}$ chitosan gel which does not present these channels.

Our results showed that the layered microstructure of the gels lead to peculiar poroelastic properties, observed only in natural materials similarly structured.

In addition, we observed two mechanical regimes separated by a critical pressure, σ_c, which depends on C_p. At $\sigma < \sigma_c$, the gels were found to behave as viscoelastic materials with short characteristic creep and recovery times. In this regime, the porosity of the gels was not affected by the load as shown by probe diffusion measurements. Below σ_c, the channels provide enough free volume to facilitate fluid transport. Interestingly, for the gels that did not

present microchannels (but still exhibited the superficial membrane), these changes in mechanical properties were still apparent around σ_c, but were less pronounced in terms of transport properties (diffusion). This observation confirms that the channel structure has a prominent role on fluid transport and polymer diffusion rather than on the mechanical properties. Above σ_c, microchannels were found to be obstructed, limiting fluid flow within the polymer matrix. Beyond this regime, the hydrogels suffered irreversible mechanical changes and plastic deformations.

The tribological behavior of the gels was not controlled by their mechanical properties since the CoF was independent of C_p for each configuration tested. At $\sigma < \sigma_c$, the CoF was independent of the configuration ($\mu \sim 0.3$), while at $\sigma > \sigma_c$, we observed that $\mu_{SZ/SZ} > \mu_{DZ/DZ}$. The observed friction change on the DZ/DZ configuration at $\sigma > \sigma_c$ is attributed to the hydrogel deformation, the microchannel closure and the water exudation to the surface leading to a more efficient lubrication. Our results show for the first time a correlation between the gel permeability and the COF suggesting that the friction dissipation at the hydrogel interface involves exudation via liquid pressurization. This is in agreement with the results of Khosla *et al.* who showed a drastic drop of CoF for porous PDMS surfaces sliding in water due to the creation of pressurized water pockets able to feed the hydrodynamic lubrication film[50].

The gel wear resistance was found to be governed by the hydrogel layered-structure since the SZ/SZ configuration exhibited significantly less wear than the DZ/DZ configuration. Therefore, the gel membrane present at the SZ acts as a protective layer which mechanical and transport properties are very different from those of the gel bulk[51].

In a nutshell, our observations echo many studies performed of natural materials such as structured tissues. The developed chitosan gels therefore offer a unique opportunity to study and rationalize dynamic mechanical processes occurring in such tissues under controlled conditions.

3.5 Conclusion

The present work shows that structuring allows controlling wear and lubrication independently without the necessity of changing material or lubricant composition. Bioinspiration is thus a promising route to design efficient cartilage substitutes by taking advantage of the natural structures found in living tissues. A better attention should be paid to the transport and tribological properties of hydrogels, besides the choice of the polymer and the focus on the mechanical properties, to ensure adequate response and sustainability *in vivo*. Further studies are ongoing to improve the lubrication and anti-wear properties of soft and porous materials by using synthetic synovial fluids interacting synergistically and dynamically with such hydrogels[52].

Acknowledgements

XB acknowledges the financial support from CHIR (CRC and Bridge grants) and NSERC (Discovery grant). JF is grateful to the Arthritis Society (TGP-16-183) and to the French Embassy for financial supports (Frontenac scholarship). We thank Agnes Crépet (IMP) and Pierre Alcouffe (IMP) for their technical assistance in size exclusion chromatography and scanning electron microscopy, respectively. We are also indebted to Matthieu Guibert (LTDS) for the low-load tribometer design and fabrication and Thomas Malhomme (LTDS) for wear characterization by interferometer. The help of Béatrice Burdin (Centre Technologique des Microstructures) for CLSM study implementation is also acknowledged.

Conclusion générale du chapitre III

À travers ce chapitre, nous avons déterminé les propriétés tribologiques de substituts hydrogels structurés sous forme d'assemblages multicouches, résultant des conditions de neutralisation et de la cinétique de diffusion dans les hydrogels. Nous avons appris que la friction et l'usure sont des phénomènes distincts puisque la face DZ (zone profonde, la plus tendre et la plus poreuse) qui donnait le CoF le plus faible montrait une usure plus élevée. Nous avons également déterminé que pour obtenir les plus faibles CoF, le gel a besoin d'une contrainte critique qui permet l'exsudation de l'eau vers le contact. Cette sécrétion permet une lubrification hydrodynamique du contact alors que les macromolécules restent piégées dans la matrice polymérique, à l'image des complexes aggrécane/HA[53-54]. Lors de cette étude, nous avons mis en place un test d'usure original par mesure de la rugosité de surface après friction permettant une mesure quantitative simple et rapide de ce paramètre crucial et peu étudié jusqu'à présent.

En perspectives à l'étude structurelle, mécanique et tribologique menée, il serait opportun d'envisager des moyens de renforcement des hydrogels de chitosane *a posteriori* afin d'améliorer leurs propriétés mécaniques pour atteindre un module élastique de l'ordre du MPa tout en conservant leurs bonnes propriétés structurelles et de diffusion des hydrogels.

Références

1. Vilela, C. A.; Correia, C.; Oliveira, J. M.; Sousa, R. A.; Espregueira-Mendes, J.; Reis, R. L., Cartilage Repair Using Hydrogels: A Critical Review of in Vivo Experimental Designs. *ACS Biomaterials Science & Engineering* **2015,** *1* (9), 726-739.
2. Matricardi, P.; Di Meo, C.; Coviello, T.; Hennink, W. E.; Alhaique, F., Interpenetrating Polymer Networks polysaccharide hydrogels for drug delivery and tissue engineering. *Advanced Drug Delivery Reviews* **2013,** *65* (9), 1172-1187.
3. Gong, J. P.; Katsuyama, Y.; Kurokawa, T.; Osada, Y., Double-Network Hydrogels with Extremely High Mechanical Strength. *Advanced Materials* **2003,** *15* (14), 1155-1158.
4. Kaneko, D.; Tada, T.; Kurokawa, T.; Gong, J. P.; Osada, Y., Mechanically Strong Hydrogels with Ultra-Low Frictional Coefficients. *Advanced Materials* **2005,** *17* (5), 535-538.
5. Gong, J. P., Friction and lubrication of hydrogels-its richness and complexity. *Soft Matter* **2006,** *2* (7), 544-552.
6. Kakugo, A.; Gong, J.; Osaka, Y., Friction and lubrication of hydrogel. *Seibutsu Butsuri* **2007,** *47* (4), 253-258.
7. Gong, J. P., Why are double network hydrogels so tough? *Soft Matter* **2010,** *6* (12), 2583-2590.
8. Haque, M. A.; Kurokawa, T.; Gong, J. P., Super tough double network hydrogels and their application as biomaterials. *Polymer* **2012,** *53* (9), 1805-1822.
9. Yashima, S.; Takase, N.; Kurokawa, T.; Gong, J. P., Friction of hydrogels with controlled surface roughness on solid flat substrates. *Soft Matter* **2014,** *10* (18), 3192-3199.
10. Mao, J.; Zhao, L.; De Yao, K.; Shang, Q.; Yang, G.; Cao, Y., Study of novel chitosan-gelatin artificial skin in vitro. *Journal of biomedical materials research. Part A* **2003,** *64* (2), 301-8.
11. Kim, T. H.; Park, I. K.; Nah, J. W.; Choi, Y. J.; Cho, C. S., Galactosylated chitosan/DNA nanoparticles prepared using water-soluble chitosan as a gene carrier. *Biomaterials* **2004,** *25* (17), 3783-3792.
12. Rinaudo, M., Chitin and chitosan: Properties and applications. *Progress in Polymer Science* **2006,** *31* (7), 603-632.
13. Ladet, S. G.; Tahiri, K.; Montembault, A. S.; Domard, A. J.; Corvol, M. T. M., Multi-membrane chitosan hydrogels as chondrocytic cell bioreactors. *Biomaterials* **2011,** *32* (23), 5354-5364.
14. Fiamingo, A.; Montembault, A.; Boitard, S.-E.; Naemetalla, H.; Agbulut, O.; Delair, T.; Campana-Filho, S. P.; Menasché, P.; David, L., Chitosan Hydrogels for the Regeneration of Infarcted Myocardium: Preparation, Physicochemical Characterization, and Biological Evaluation. *Biomacromolecules* **2016,** *17* (5), 1662-1672.
15. Jin, R.; Moreira Teixeira, L. S.; Dijkstra, P. J.; Karperien, M.; van Blitterswijk, C. A.; Zhong, Z. Y.; Feijen, J., Injectable chitosan-based hydrogels for cartilage tissue engineering. *Biomaterials* **2009,** *30* (13), 2544-2551.
16. Croisier, F.; Jérôme, C., Chitosan-based biomaterials for tissue engineering. *European Polymer Journal* **2013,** *49* (4), 780-792.
17. Rami, L.; Malaise, S.; Delmond, S.; Fricain, J.-C.; Siadous, R.; Schlaubitz, S.; Laurichesse, E.; Amedee, J.; Montembault, A.; David, L.; Bordenave, L., Physicochemical modulation of chitosan-based hydrogels induces different biological responses: Interest for tissue engineering. *Journal of Biomedical Materials Research Part A* **2014,** *102* (10), 3666-3676.
18. Kaderli, S.; Boulocher, C.; Pillet, E.; Watrelot-Virieux, D.; Rougemont, A. L.; Roger, T.; Viguier, E.; Gurny, R.; Scapozza, L.; Jordan, O., A novel biocompatible hyaluronic acid-chitosan hybrid hydrogel for osteoarthrosis therapy. *International journal of pharmaceutics* **2015,** *483* (1-2), 158-68.
19. Mohan, N.; Mohanan, P. V.; Sabareeswaran, A.; Nair, P., Chitosan-hyaluronic acid hydrogel for cartilage repair. *Int. J. Biol. Macromol.* **2017**.

20. Sereni, N.; Enache, A.; Sudre, G.; Montembault, A.; Rochas, C.; Durand, P.; Perrard, M. H.; Bozga, G.; Puaux, J. P.; Delair, T.; David, L., Dynamic Structuration of Physical Chitosan Hydrogels. *Langmuir* **2017,** *33* (44), 12697-12707.
21. Nie, J.; Lu, W.; Ma, J.; Yang, L.; Wang, Z.; Qin, A.; Hu, Q., Orientation in multi-layer chitosan hydrogel: morphology, mechanism, and design principle. *Sci. Rep.* **2015,** *5*, 7635.
22. Faivre, J.; Sudre, G.; Montembault, A.; Benayoun, S.; Banquy, X.; Delair, T.; David, L., Bioinspired Microstructures of Chitosan Hydrogel Provide Enhanced Wear Protection. *Soft Matter* **2018**, 2068-2076.
23. Green, J. J.; Elisseeff, J. H., Mimicking biological functionality with polymers for biomedical applications. *Nature* **2016,** *540* (7633), 386-394.
24. Montembault, A.; Tahiri, K.; Korwin-Zmijowska, C.; Chevalier, X.; Corvol, M. T.; Domard, A., A material decoy of biological media based on chitosan physical hydrogels: application to cartilage tissue engineering. *Biochimie* **2006,** *88* (5), 551-564.
25. Puppi, D.; Chiellini, F.; Piras, A. M.; Chiellini, E., Polymeric materials for bone and cartilage repair. *Progress in Polymer Science* **2010,** *35* (4), 403-440.
26. Hsieh, F.-Y.; Tseng, T.-C.; Hsu, S.-h., Self-healing hydrogel for tissue repair in the central nervous system. *Neural Regeneration Research* **2015,** *10* (12), 1922-1923.
27. Hoare, T. R.; Kohane, D. S., Hydrogels in drug delivery: Progress and challenges. *Polymer* **2008,** *49* (8), 1993-2007.
28. Hamidi, M.; Azadi, A.; Rafiei, P., Hydrogel nanoparticles in drug delivery. *Advanced Drug Delivery Reviews* **2008,** *60* (15), 1638-1649.
29. Latreille, P.-L.; Alsharif, S.; Gourgas, O.; Tehrani, S. F.; Roullin, V. G.; Banquy, X., Release kinetics from nano-inclusion-based and affinity-based hydrogels: A comparative study. *Colloids and Surfaces A: Physicochemical and Engineering Aspects* **2017,** *529*, 739-749.
30. El-Sherbiny, I. M.; Yacoub, M. H., Hydrogel scaffolds for tissue engineering: Progress and challenges. *Global Cardiology Science & Practice* **2013,** *2013* (3), 316-342.
31. Naleway, S. E.; Porter, M. M.; McKittrick, J.; Meyers, M. A., Structural Design Elements in Biological Materials: Application to Bioinspiration. *Adv. Mater.* **2015,** *27* (37), 5455-5476.
32. Lin, P.; Zhang, R.; Wang, X.; Cai, M.; Yang, J.; Yu, B.; Zhou, F., Articular Cartilage Inspired Bilayer Tough Hydrogel Prepared by Interfacial Modulated Polymerization Showing Excellent Combination of High Load-Bearing and Low Friction Performance. *ACS Macro Lett.* **2016,** *5* (11), 1191-1195.
33. Liu, M.; Zeng, X.; Ma, C.; Yi, H.; Ali, Z.; Mou, X.; Li, S.; Deng, Y.; He, N., Injectable hydrogels for cartilage and bone tissue engineering. **2017,** *5*, 17014.
34. Hao, T.; Wen, N.; Cao, J. K.; Wang, H. B.; Lü, S. H.; Liu, T.; Lin, Q. X.; Duan, C. M.; Wang, C. Y., The support of matrix accumulation and the promotion of sheep articular cartilage defects repair in vivo by chitosan hydrogels. *Osteoarthritis and Cartilage 18* (2), 257-265.
35. Hirai, A.; Odani, H.; Nakajima, A., Determination of degree of deacetylation of chitosan by 1H NMR spectroscopy. *Polymer Bulletin* **1991,** *26* (1), 87-94.
36. Montembault, A.; Viton, C.; Domard, A., Physico-chemical studies of the gelation of chitosan in a hydroalcoholic medium. *Biomaterials* **2005,** *26* (8), 933-943.
37. Blonk, J. C. G.; Don, A.; Van Aalst, H.; Birmingham, J. J., Fluorescence photobleaching recovery in the confocal scanning light microscope. *Journal of Microscopy* **1993,** *169* (3), 363-374.
38. Geissler, E.; Horkay, F.; Hecht, A. M., Osmotic and scattering properties of chemically crosslinked poly(vinyl alcohol) hydrogels. *Macromolecules* **1991,** *24* (22), 6006-6011.
39. Horkay, F.; Basser, P. J., Ionic and pH effects on the osmotic properties and structure of polyelectrolyte gels. *Journal of polymer science. Part B, Polymer physics* **2008,** *46* (24), 2803-2810.
40. Andrieux, K.; Lesieur, P.; Lesieur, S.; Ollivon, M.; Grabielle-Madelmont, C., Characterization of Fluorescein Isothiocyanate-Dextrans Used in Vesicle Permeability Studies. *Analytical Chemistry* **2002,** *74* (20), 5217-5226.
41. Gong, J. P.; Kagata, G.; Iwasaki, Y.; Osada, Y., Surface friction of polymer gels: 1. Effect of interfacial interaction. *Wear* **2001,** *251* (1–12), 1183-1187.
42. Gong, J. P.; Kagata, G.; Osada, Y., Friction of Gels. 4. Friction on Charged Gels. *The Journal of Physical Chemistry B* **1999,** *103* (29), 6007-6014.

43. ap Gwynn, I.; Wade, S.; Kaab, M. J.; Owen, G. R.; Richards, R. G., Freeze-substitution of rabbit tibial articular cartilage reveals that radial zone collagen fibres are tubules. *J. Microsc.* **2000,** *197* (Pt 2), 159-72.
44. ap Gwynn, I.; Wade, S.; Ito, K.; Richards, R. G., Novel aspects to the structure of rabbit articular cartilage. *European cells & materials* **2002,** *4*, 18-29.
45. Ladet, S.; David, L.; Domard, A., Multi-membrane hydrogels. *Nature* **2008,** *452* (7183), 76-79.
46. Furusawa, K.; Sato, S.; Masumoto, J.-i.; Hanazaki, Y.; Maki, Y.; Dobashi, T.; Yamamoto, T.; Fukui, A.; Sasaki, N., Studies on the Formation Mechanism and the Structure of the Anisotropic Collagen Gel Prepared by Dialysis-Induced Anisotropic Gelation. *Biomacromolecules* **2012,** *13* (1), 29-39.
47. Maki, Y.; Ito, K.; Hosoya, N.; Yoneyama, C.; Furusawa, K.; Yamamoto, T.; Dobashi, T.; Sugimoto, Y.; Wakabayashi, K., Anisotropic Structure of Calcium-Induced Alginate Gels by Optical and Small-Angle X-ray Scattering Measurements. *Biomacromolecules* **2011,** *12* (6), 2145-2152.
48. Fetter, N. L.; Leddy, H. A.; Guilak, F.; Nunley, J. A., Composition and transport properties of human ankle and knee cartilage. *Journal of Orthopaedic Research* **2006,** *24* (2), 211-219.
49. Greene, G. W.; Zappone, B.; Zhao, B.; Soderman, O.; Topgaard, D.; Rata, G.; Israelachvili, J. N., Changes in pore morphology and fluid transport in compressed articular cartilage and the implications for joint lubrication. *Biomaterials* **2008,** *29* (33), 4455-4462.
50. Khosla, T.; Cremaldi, J.; Erickson, J. S.; Pesika, N. S., Load-Induced Hydrodynamic Lubrication of Porous Films. *ACS Appl. Mater. Interfaces* **2015,** *7* (32), 17587-17591.
51. Murakami, T.; Yarimitsu, S.; Sakai, N.; Nakashima, K.; Yamaguchi, T.; Sawae, Y.; Suzuki, A., Superior lubrication mechanism in poly(vinyl alcohol) hybrid gel as artificial cartilage. *Proceedings of the Institution of Mechanical Engineers, Part J: Journal of Engineering Tribology* **2017**, 1350650117712881.
52. Faivre, J.; Shrestha, B. R.; Burdynska, J.; Xie, G.; Moldovan, F.; Delair, T.; Benayoun, S.; David, L.; Matyjaszewski, K.; Banquy, X., Wear Protection without Surface Modification Using a Synergistic Mixture of Molecular Brushes and Linear Polymers. *ACS Nano* **2017,** *11* (2), 1762-1769.
53. Seror, J.; Merkher, Y.; Kampf, N.; Collinson, L.; Day, A. J.; Maroudas, A.; Klein, J., Normal and Shear Interactions between Hyaluronan–Aggrecan Complexes Mimicking Possible Boundary Lubricants in Articular Cartilage in Synovial Joints. *Biomacromolecules* **2012,** *13* (11), 3823-3832.
54. Roughley, P. J.; Mort, J. S., The role of aggrecan in normal and osteoarthritic cartilage. *J Exp Orthop* **2014,** *1*, 8.

Chapitre IV - Conception et caractérisations d'un fluide lubrifiant bioinspiré pour la lubrification et la protection de l'usure d'hydrogels

-Chapitre IV-

Conception et caractérisations d'un fluide lubrifiant bioinspiré pour la lubrification et la protection de l'usure d'hydrogels

Introduction générale du chapitre IV

À l'instar du cartilage qui requiert les molécules du liquide synovial pour réduire le frottement et protéger sa structure contre l'usure, la principale idée de ce chapitre est montrer l'intérêt d'un fluide synovial synthétique (mime polymérique de l'aggrécane avec de l'HA) pour le frottement d'hydrogels physiques de chitosane. Afin de bien discriminer les effets de chaque composant du fluide synovial synthétique sur les propriétés des hydrogels, les effets de la masse molaire de HA, des concentrations de HA et de l'écouvillon moléculaire seront analysés, à la fois en friction et en usure. Pour une meilleure compréhension des mécanismes de friction des gels avec les liquides synoviaux bioinspirés, des balayages en forces normales à vitesse constante et en vitesses à force normale constante ont été réalisés couvrant des gammes de trois ordres de grandeur. Concernant les forces normales appliquées, nous avons été limités par les propriétés mécaniques des gels de chitosane utilisés puisque nous avons précédemment montré qu'à une pression normale comparable au module élastique G' du gel, celui-ci était endommagé[1]. Jusqu'à présent, peu d'études se sont intéressées à la fabrication d'un additif lubrifiant pour applications biomédicales. L'idée est, dans cette étude, de déterminer à quel point nos fluides synoviaux synthétiques sont capables de garantir l'intégrité de surfaces d'hydrogel fragiles, mais jouant le rôle de modèles des tissus biologiques.

Cette étude a fait l'objet d'un article dans le journal de l'American Chemical Society, *Biomacromolecules*, publié le 21 novembre 2018 et intitulé : *Lubrication and Wear Protection of Micro-Structured Hydrogels using Bioinspired Fluids*. Le polymère dibloc utilisé dans cette étude a été synthétisé et caractérisé par mes soins au sein du laboratoire du Pr Xavier Banquy. La fabrication et la caractérisation des gels ont été réalisées au sein du laboratoire IMP avec le Dr Guillaume Sudre, le Dr Alexandra Montembault et moi-même.

Les expérimentations tribologiques ont été effectuées au LTDS par mes soins avec l'aide de Thomas Malhomme pour les mesures interférométriques.

Lubrication and Wear Protection of Micro-Structured Hydrogels using Bioinspired Fluids

Jimmy Faivre[1,2], Alexandra Montembault[1], Guillaume Sudre[1], Buddha Ratna Shrestha[2], Guojun Xie[3], Krzysztof Matyjaszewski[3], Stéphane Benayoun[4], Xavier Banquy[2], Thierry Delair[1], Laurent David[1*]*

[1]*Ingénierie des Matériaux Polymères, IMP- CNRS UMR 5223, Université de Lyon, Université Claude Bernard Lyon 1, 15 Boulevard Latarjet, 69622 Villeurbanne Cedex, France*

[2]*Canadian Research Chair in Bioinspired materials, Faculty of Pharmacy, Université de Montréal, Montréal, Qc, Canada*

[3]*Center for Macromolecular Engineering, Department of Chemistry, Carnegie Mellon University, Pittsburgh, PA, USA*

[4]*Laboratoire de Tribologie et Dynamique des Systèmes, CNRS UMR 5513, Ecole Centrale de Lyon, 36 Avenue Guy de Collongue, 69134 Ecully Cedex, France*

Abstract

We report the fabrication and the use of a bioinspired synovial fluid acting as a lubricant fluid and anti-wear agent at soft and porous chitosan hydrogel tribopairs. This synthetic synovial fluid is composed of sodium hyaluronate (HA) and a bottle-brush polymer (BB) having a polycationic attachment group and polyzwitterionic pendant chains. 2.5 $\%_{w/w}$ chitosan hydrogel plugs are organized in a bilayered structure exposing a thin and dense superficial zone (SZ), covering a porous deep zone (DZ) and exhibiting microchannels perpendicularly aligned to the SZ. Using a low-load tribometer, the addition of HA lubricating solution at the hydrogel-hydrogel rubbing contact drastically decreased the coefficient of friction (CoF) from $\mu = 0.20 \pm 0.01$ to $\mu = 0.04 \pm 0.01$ on the DZ configuration and from $\mu = 0.31 \pm 0.01$ to $\mu = 0.08 \pm 0.01$ on the SZ surface when increasing HA concentration from 0 to 1000 µg/mL and its molecular mass from 10 to 1500 kDa, similar to what was found when using BB polymer alone. When combining the BB polymer and the 1500 kDa HA, the CoF remained stable at $\mu = 0.04 \pm 0.01$ for both studied contact configurations, highlighting the synergistic interaction of the two macromolecules. Hydrogel wear was characterized by assessing the final gel surface roughness by the means of an interferometer. Increasing HA concentration and molecular weight plus the addition of BB polymer lead to a dramatic surface wear protection with a final gel surface roughness of the hydrogels similar to the untested gels. In brief, BB polymer in combination with high molecular weight HA is a potential lubricating fluid as well as a wear resistant agent for soft materials lubrication and wear protection.

Graphical Abstract

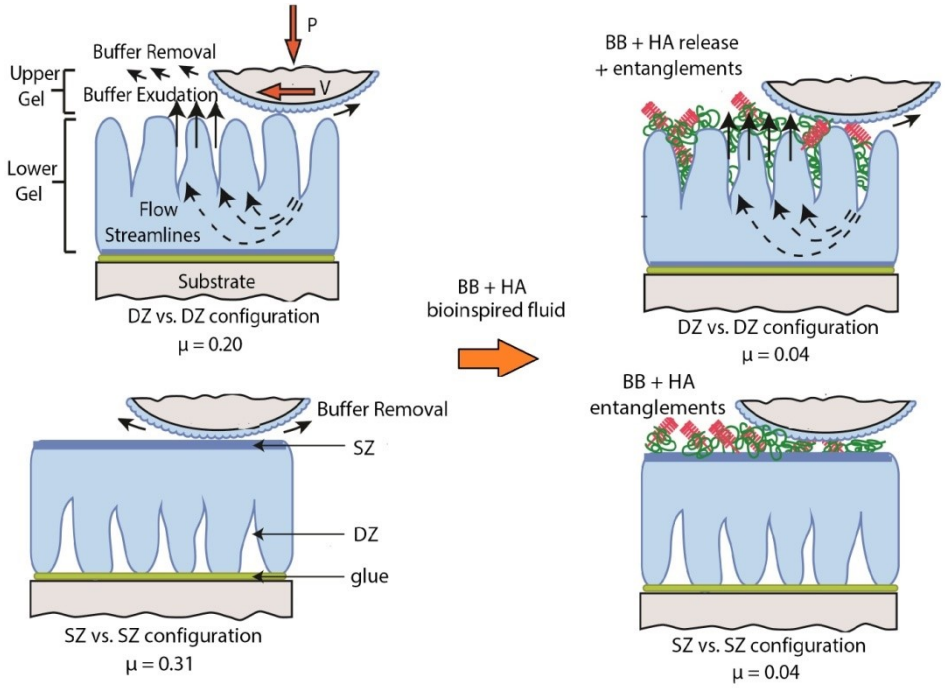

Keywords: hydrogel lubrication, wear resistance, chitosan, bottlebrush polymer, hyaluronic acid

4.1 Introduction

Hydrogels are of growing interest for tissue engineering as scaffolds since they can structurally and mechanically mimic the tissues and embed growth factors as well as chondrocytes to support joint regeneration[2-4]. However, few *in vivo* studies have characterized the potential lubrication properties and wear protection abilities of hydrogels despite its paramount importance for tissue engineering sustainability. For instance, in healthy diarthrodial joints, the cartilage and the synovial fluid act in synergy to provide low coefficient of friction (CoF) and excellent wear protection[5-9]. This synergy leads to efficient multiple modes of lubrication, depending on the spatio-temporal configuration of the joint during the motion process[10]. The excellent wear resistance is due to the fluid pressurization within the cartilage[11] and the presence of aggrecan (Agg)-hyaluronic acid complexes which increase the osmotic pressure within the collagen matrix which helps supporting the load[12-13]. Moreover, the formation of a thin macromolecular layer on the cartilage surface under load avoids the cartilage surfaces from rubbing on each other. To ameliorate lubrication and alleviate mechanical erosion of soft synthetic materials used as *in vivo* tissue substitutes, different bio-inspired strategies have been described in the literature. Indeed, the friction forces of hydrogels surfaces can be modulated *via* their surface porosity[14], topography[15-16] or the presence of highly hydrated moieties on polymer groups[17-18]. For instance, Lin *et al*. showed a CoF of $\mu = 0.15$ by using bilayered hydrogels made of a mixture of acrylamide, acrylic acid and diacrylamide exposing a highly porous superficial layer compared to a denser structure with a CoF of $\mu = 0.35$ [14]. The insertion of hydrophilic [2-(methacryloyloxy)ethyl] trimethylammonium chloride as part of the gel matrix drastically reduced the CoF to 0.05 thanks to the higher water trapping capability of the charged polyelectrolyte. The design of vertical pores or fibers at hydrogel surfaces is another technique to allow better lubrication due to water exudation upon compression and thus the formation of a lubricating hydrodynamic film[1, 16], a technique which can be combined with highly hydrophilic monomers[19]. To drastically decrease CoF, another method is to directly graft polyelectrolyte brushes at the gel surface. For example, poly(sodium 4-styrene sulfonate) grafted to poly(hydroxyethyl methacrylate) (p(HEMA)) lowered by almost an order of magnitude the CoF of p(HEMA) hydrogels[20]. The friction can also be decreased upon addition of a lubricating fluid either composed of surfactants[21], lipids, or naturally-occurring or bioinspired proteoglycans[22], which are known to be responsible for the lubrication and wear protection of

eyes, joints or mucous membranes. Nevertheless, the tools used for the tribological measurement such as tribometers or rheometers, the geometry of the probe (pin or ball on disc), the contact area or the nature and roughness of opposing geometry (glass, metal or hydrogel), highly affects the results and hence should be meticulously described in order to be comparable to other studies.

On the other hand, the interest on wear protection of soft materials is growing since it is essential to ensure the integrity of the hydrogels scaffolds to fully sustain the physiological conditions (pressure, shear, inflammation). The main route to limit wear initiation to hydrogels is to strengthen the scaffold *via* crosslinking[23] or interpenetrated networks[24-25]. An interesting alternative is called the "sacrificial bond principle"[26] which is based on the insertion of weak bonds inside the initial gel matrix. When a crack propagates in the gel, the weaker bonds break first and dissipate a large amount of energy[27]. Finally, the total energy needed to damage the hydrogels is drastically increased by several orders of magnitude compared to their counterparts without any sacrificial bonds.

In the present study, we emphasize on the design of lubricating fluids which are able to lubricate *and* reduce wear at soft multilayered chitosan hydrogels. These lubricating fluids were previously proven to reduce both friction and wear of stiff and non porous mica surfaces with CoF of $\mu \sim 0.02$ up to pressures of several megaspascals[28], matching physiological conditions. Contrary to mica surfaces, poroelastic chitosan hydrogels more closely mimic soft tissues, but suffer from frictional abrasion at low stresses impeding their uses *in vivo*[1]. By using a low-load tribometer and light interferometry, we show that the addition of high molecular weight hyaluronic acid (HA) and bottlebrush (BB), polymer at the interface between the two sliding chitosan gel tribopairs significantly lowered both the CoF and wear for both studied surface topographies. BB polymers represent novel polymeric architecture with very densely grafted side chains[29] which are typically prepared by atom transfer radical polymerization[30]. This unique architecture resembles the proteoglycan lubricin structure which is involved in the lubrication of the synovial joints. Since the synovial fluid also contains hyaluronic acid and phospholipids (DPPC)[31] the combination of HA with a synthetic BB polymer composed of pendant phospholipids moieties[32] mimics the macromolecular structure and composition of synovial fluid. This leads to the concept of bioinspired synovial fluids. This work demonstrates the potentiality of this lubricant and anti-wear fluid to help hydrate physiological surfaces such as in the case of dry eye syndrome or tissue substitutes

such as contact lenses or cartilage substitutes to keep and extend their tribological properties *in vivo*.

4.2 Experimental Section

4.2.1 Materials

Chitosan (M_w = 6.04.10^5, M_w/M_n 1.6, DA 4.5%, from squid pen chitin) was purchased from Mahtani Chitosan Pvt. Ltd (batch type 114). Sodium hyaluronates of different molecular weights were obtained from Lifecore Biomedical (Minneapolis, USA). Acetic acid, ammoniac hydroxide, and HEPES were supplied by Sigma-Aldrich. NaOH pellets, NaCl, and absolute anhydrous ethanol were obtained from Carlo Erba Reagents. Methyl methacrylate (MMA, 99%, Sigma-Aldrich), 2-(trimethylsilyloxy)ethyl methacrylate (HEMA-TMS, 96%, Sigma-Aldrich) and 2-(dimethylamino)ethyl methacrylate (DMAEMA, 98%, Sigma-Aldrich) were passed through a column filled with basic alumina prior to use. 2-Methacryloyloxyethyl phosphorylcholine (MPC, 97%, Aldrich) was recrystallized from acetonitrile and dried under vacuum overnight at room temperature before polymerization. Copper(I) bromide (Cu^IBr, 99.999%, Sigma-Aldrich), copper(II) bromide ($Cu^{II}Br_2$, 99.999%, Sigma-Aldrich), copper(I) chloride (Cu^ICl, ≥99.999% trace metals basis, Alfa Aesar), copper(II) chloride ($Cu^{II}Cl_2$, ≥99.999% trace metals basis, Sigma-Aldrich), 2,2′-bipyridyl (bpy, 99%, Sigma-Aldrich), 4,4′-Dinonyl-2,2′-dipyridyl (dNbpy, 97%, Sigma-Aldrich), potassium fluoride (KF, 99%, Sigma-Aldrich), tetrabutylamonium fluoride (TBAF, 1M solution in THF, Sigma-Aldrich), bromoisobutyryl bromide (BBiB, 98%, Sigma-Aldrich), α-bromoisobutyryl bromide (98%, Sigma-Aldrich), bromoethane (98%, Alfa Aesar), tris(2-pyridylmethyl)amine (TPMA) (98%, Sigma-Aldrich), and tributyltin hydride (97%, Sigma-Aldrich) were used without any additional purification. Solvents were used as received.

4.2.2 Chitosan hydrogels fabrication

Prior to gel fabrication, chitosan was purified by filtration on Millipore membranes of decreasing porosity (membrane porosities of successively 3, 0.8, and 0.45µm). 2.5 $\%_{w/w}$ multilayered chitosan physical hydrogels were fabricated according to previously published procedure[1]. In short, 2.5$\%_{w/w}$ solution was prepared by dissolving chitosan purified powder with a stoichiometric amount of acetic acid in water. The chitosan solution was then centrifuged at 5000 rpm for 10 min to remove air bubbles. The solution was then extruded and deposited on a plastic foil and pressed with a metal plate with 1.5 mm wedges to maintain the same thickness in all gels (i.e. 1.5 mm). The viscous chitosan film was then placed in a NaOH coagulation bath at 1 mol/L until the completion of the gelation process. The resulting gel disks were cut with a punch to final diameters of 11 and 21mm. The gel disks were washed in

pure water to reach neutral pH. The nano and micro structure of physical 2.5%$_{w/w}$ chitosan hydrogel were assessed by confocal microscopy (CLSM) and Scanning Electron Microscopy (SEM).

4.2.3 BB Polymer synthesis

In the following section, we describe the synthesis of the BB polymer of final composition **[(PBiBEM$_{552}$-*g*-PMPC$_{45}$)-*stat*-MMA$_{338}$] - *b* - (PqDMAEMA$_{93}$-*stat*-PMMA$_{153}$)** whose structure is inspired by our previously published references [32-34].

Synthesis of P(HEMA-TMS)-*stat*-PMMA (A block (Fig. 4.1 A)): A dried round bottom flask was charged with BBiB (3.4 µL, 0.023 mmol), dNbpy (112.8 mg, 0.276 mmol), HEMA-TMS (10.0 mL, 45.9 mmol), MMA (4.9 mL, 45.9 mmol) and anisole (3.0 mL). The solution was bubbled with argon for 30'. $Cu^{I}Br$ (0.0158 g, 0.110 mmol), and $Cu^{II}Br_2$ (0.0061 g, 0.028 mmol) were charged in a dried 50 mL round bottom flask and 3 argon-vacuum cycles were performed to remove oxygen. The flask was sealed, and then immersed in an oil bath at 40 °C. After bubbling, the monomer solution was injected into the catalyst solution. Reaction was stopped after 14 h via exposure to air, reaching the degree of polymerization of the product 500. The monomers consumption was calculated from ^{1}H NMR spectra by the integration of MMA and HEMA-TMS vinyl groups signal (C*H*H=C-CH$_3$, 6.11 ppm or 5.56 ppm) against the internal standard (anisole, *o*,*p*-Ar-H, 6.91 ppm). The product **A** was purified by three precipitations from methanol, dried under vacuum overnight at room temperature, and analyzed by GPC and ^{1}H NMR spectroscopy. The ratio of PMMA (*s*, broad, CO-O-C*H*$_3$, 3.54-3.68 ppm) to P(HEMA-TMS) (*s*, broad, OCO-C*H*$_2$, 3.90-4.17 ppm) signals gave the polymer composition.

Synthesis of (PDMAEMA-*stat*-PMMA)-*b*-[P(HEMA-TMS-*stat*-PMMA] (BA diblock (Fig. 4.1 A)): A dried round bottom flask was charged with **A block** (1.0 g, 0.0094 mmol), dNbpy (70 mg, 0.17 mmol), DMAEMA (1.2 mL, 7.0mmol), MMA (0.75 mL, 7.0 mmol) and anisole (4.0 mL). The solution was bubbled with argon for 30'. $Cu^{I}Cl$ (0.0074 g, 0.0752 mmol), and $Cu^{II}Cl_2$ (0.0010 g, 7.46 µmol) were charged in a dried 25 mL round bottom flask and 3 argon-vacuum cycles were performed to remove oxygen. The flask was sealed, and then immersed in an oil bath at 60 °C. After bubbling, the monomer solution was injected into the catalyst solution. Reaction was stopped after 48 h via exposure to air. The product was diluted in dichloromethane, passed through a neutral alumina column, concentrated under vacuum and precipitated twice from hexanes and water. The solvent was removed under vacuum and the

product was dried overnight under vacuum at room temperature. The structure of the polymer was determined by ^{1}H NMR from the ratio of selected polymer signals: PMMA (*s*, broad, CO-O-C*H*$_3$, 3.54-3.68 ppm),P(HEMA-TMS) (*s*, broad, O-Si(C*H*$_3$)$_3$, 0.11-0.21 ppm) and PDMAEMA (*m*, C*H*$_2$-NMe$_2$, 2.55-2.65 ppm).

Synthesis of [PBiBEM-*stat*-PMMA]-*b*-(PqDMAEMA-*stat*-PMMA) (BA-Macroinitiator (BA-MI)): BA diblock (0.1840 g), potassium fluoride (0.030 g, 0.52 mmol) and 2,6-di-*tert*-butylphenol (0.0090 g, 0.0439 mmol) were placed in a 20 ml round bottom flask. The flask was sealed, flushed with argon, and finally anhydrous THF (7 mL) was added. The mixture was cooled in an ice bath to 0 °C, tetrabutylammonium fluoride solution in THF (1M, 0.44 mL, 0.44mmol) was injected into the flask, followed by a drop-wise addition of 2-bromoisobutyryl bromide (0.121 g, 65 µL, 0.526mmol). After the addition, the reaction mixture was allowed to reach room temperature and stirring was continued for 24 h. The solution was passed through a short column filled with basic alumina, precipitated into hexanes and then methanol:water (70:30, v/v%) three times. The filtrate was dried under vacuum overnight at room temperature.

Synthesis of [(PBiBEM-*g*-PMPC)-*stat*-MMA]-*b*-(PDMAEMA-*stat*-PMMA) (BAC polymer (Fig. 4.1 A)): A dry 10 mL round bottom flask was charged with polymer **BA-MI** (2mg), 2-methacryloyloxyethyl phosphorylcholine (MPC)(0.2540 g, 0.860mmol), 2,2'-bipyridyl (bpy) (22 mg, 14.23 µmol), Cu^{I}Cl (6 mg, 60 µmol), and copper (II) chloride (Cu^{II}Cl$_2$) (1 mg, 7.40 µmol). A dry 10 mL round bottom flask was charged with methanol (3.0 mL) and anisole (500 µL). The solution was bubbled with argon for 15 min. The flask was sealed, and then immersed in an oil bath at 50 °C. After bubbling, the solvent solution was injected into the catalyst/monomer solution. Time of reaction was determined thanks to MPC conversion measurement by ^{1}H NMR to reach a DP of 45. Reaction was then stopped via exposure to air achieving PMPC diblock brush. The resulting brush was purified by ultrafiltration against MeOH under pressure using regenerated cellulose membrane (Millipore) with a pore size molar mass cut-off of 30,000 Da. Molecular weights were not determined as polymer was neither soluble in THF nor in DMF.

Synthesis of [(PBiBEM-*g*-PMPC)-*stat*-MMA]-*b*-(PqDMAEMA-*stat*-PMMA) (BB polymer)): BAC was placed in 20 mL vial and dissolved in methanol (10 mL). The solution was cooled in an ice bath to 0 °C, followed by a slow addition of bromoethane (0.5mL, 6.7

mmol). The reaction was stirred at room temperature for the next 48 h. The solvent and the unreacted bromoethane were evaporated under gentle pressure and solvent was exchanged for water by ultrafiltration. The polymer was freeze-dried and stored at -20°C in a dark container. The quantitative quaternization of -NMe_2 groups of **BB polymer** was determined by ^{1}H NMR.

4.2.4 Equipment and Analysis

Proton nuclear magnetic resonance (^{1}H NMR) spectroscopy was performed using Variant 400 MHz spectrometer. In all cases, deuterated chloroform ($CDCl_3$) was used as a solvent, except for PMPC ABA which was analyzed using deuterated water (D_2O). ^{1}H chemical shifts are reported in ppm downfield from tetramethylsilane (TMS) in deuterated chloroform and from 3-(trimethylsilyl) propane sulfonate sodium salts in deuterated water. Apparent molecular weights and molecular weight distributions measurements of polymers were measured by gel permeation chromatography (GPC, Waters 1525 system 35°) using Phenogel columns (guard, 10^5, 10^4, and 10^3 Å), with THF or DMF as eluent at 35 °C at a constant flow rate of 1.00 mL/min, and differential refractive index (RI) detector (Waters, 2414). The apparent number-average molecular weights (M_n) and molecular weight distribution (M_w/M_n) were determined with a calibration based on linear poly(styrene) (PS) standards (Polyscience).

AFM measurements were collected using a multimode Atomic Force Microscopy (AFM) with a NanoScope V controller (Bruker) in PeakForce QNM mode. Silicon tips (on nitride cantilever) with resonance frequency of 50-90 kHz and spring constant of ~0.4 N/m were used. The samples were dissolved in water and deposited on freshly cleaved mica.

4.2.5 Formulation of synthetic synovial fluids

10.0 mg of different molecular mass HA (10, 60, 500, and 1500 kDa) were dissolved with magnetic stirring in 10 mL 0.1M HEPES buffer pH 7.4 in a glass vial. The solution was then immediately poured in the tribometer bath immersing chitosan hydrogels during wear test. For tests with B-B polymer, 100 or 400 µg/mL solutions of B-B polymer were prepared in the same buffer with or without HA. Solutions were homogenized with a vortex for 1 min. Surfaces were then let to equilibrate for 1 h prior to the measurements.

4.2.6 Tribology tests on hydrogel tribopairs

A low load tribometer was used to assess frictional properties of chitosan gels in presence of artificial synovial fluids. The 11 mm gel disk was glued on the top mobile part on an aluminum pin and was able to rotate and be adjusted *via* a ball joint to obtain a flat contact between both gels. The 21 mm gel disk was glued on a metallic immobile metal surface. Typically, the two gel disks were pressed against each other reaching the set load and the mobile part was driven to oscillate at a frequency of 1 Hz with an amplitude of 5 mm from 500 to 1000 cycles. Normal and tangential forces were recorded and analyzed using a home-made labview software. Gels were glued on the mobile top part and immobile bottom part with Loctite Super Glue 3 power flex gel (from Loctite, waterproof and suited for porous materials). Two different configurations of the gel disks were characterized: 1) SZ on SZ flat contact and 2) DZ on DZ flat contact. During the experiments, the disks were fully immersed in the synthesized synovial fluid. Friction force (F_t) measurements were firstly performed as a function of the sliding velocity (v) with a constant load (F_n = 0.3 N) (0.3 N corresponding to a stress of 3 kPa which represents 10 % of elastic shear modulus of the gel G' determined at a frequency of 1Hz) and at an amplitude of 5 mm. This normal load was chosen to avoid the destruction of the gel under shearing at the DZ/DZ configuration which was systematically noticed at a pressure close to the shear modulus[1]. The number of cycles was increased to adapt the length of the experiments throughout the friction experiments as a function of sliding velocity since we covered three decades of velocities from 0.1 to 100 mm/s. In a second step, the effect of normal force was assessed at a sliding frequency of 1 Hz and an amplitude of 5 mm for 250 cycles. The range of applied normal forces was between 0.05 N and 5 N. Finally, wear of the gel disks was evaluated after shearing the surfaces for 10^4 cycles (at F_n = 3 N, P = 30 kPa ~~– G'~~, and v = 5 mm/s). Wear was visualized using a digital microscope (VHX-1000, Keyence) for optical micrographs and an interferometric microscope (Contour GT-K 3D Bruker). Surface roughness was characterized by the arithmetical mean height (S_a) of the surface and was quantified using vision 64 software (Bruker). The surface analyzed for the roughness measurements represented 20% of the total contact area. Prior to wear visualization, samples were dried by blowing compressed air to improve imaging contrast.

4.2.7 Correlation with physiological conditions

All experimental setups and parameters were adjusted to match physiological conditions as often as possible. pH was adjusted to 7.4 as in human fluids. The sliding frequency was in the range of 0.01 to 100 mm/s, similar to normal knee, eyelid or airways cilium motion speed[35-39],

with a displacement of 5 mm. The gel on gel plate geometry was placed in a bath filled with synthetic fluids in order to match natural synovial joints (i.e. cartilage on cartilage contact within synovial fluid) or eyes/eyelids/contact lenses function. Finally, the physical chitosan gel layered-structure composed of a thin superficial zone supported by a network of channels of few micrometers in diameter and perpendicularly orientated to the superficial zone was previously mechanically studied[40] and was proven to be an interesting tribological surface model to mimic natural tissues.

4.3 Results & Discussions

4.3.1 Experiment Design

The bioinspired synovial fluid was formulated using a BB polymer and HA in a buffered solution. The BB polymer is composed of three different blocks: a A block which is the polymer backbone bearing lateral chains, a polycationic B block - linked to the backbone - which provides attachment to negatively charged surfaces and the lateral C blocks - constituted of phosphoryl choline moieties acting as hydrophilic pendant chains (Fig. 1 A). The different constituents of the synthetic synovial fluids were introduced at concentrations close to natural joints for proteoglycans and HA. BB polymer concentration was 400 µg/mL whereas HA was used at concentrations ranging from 10 to 1000 µg/mL[41-43]. HA molecular mass was selected from 1.5 MDa, representing near physiological HA molecular mass, to 10 kDa which is close to degraded HA molecular weight[44]. The substrates used as tribopairs were 2.5 $\%_{w/w}$ chitosan hydrogels whose structure and mechanical behavior were previously characterized[1, 45-47]. The hydrogels were analyzed using confocal microscopy and SEM imaging (Fig. 1 B). They exhibited a bilayer structure with a first ~ 100 µm dense layer

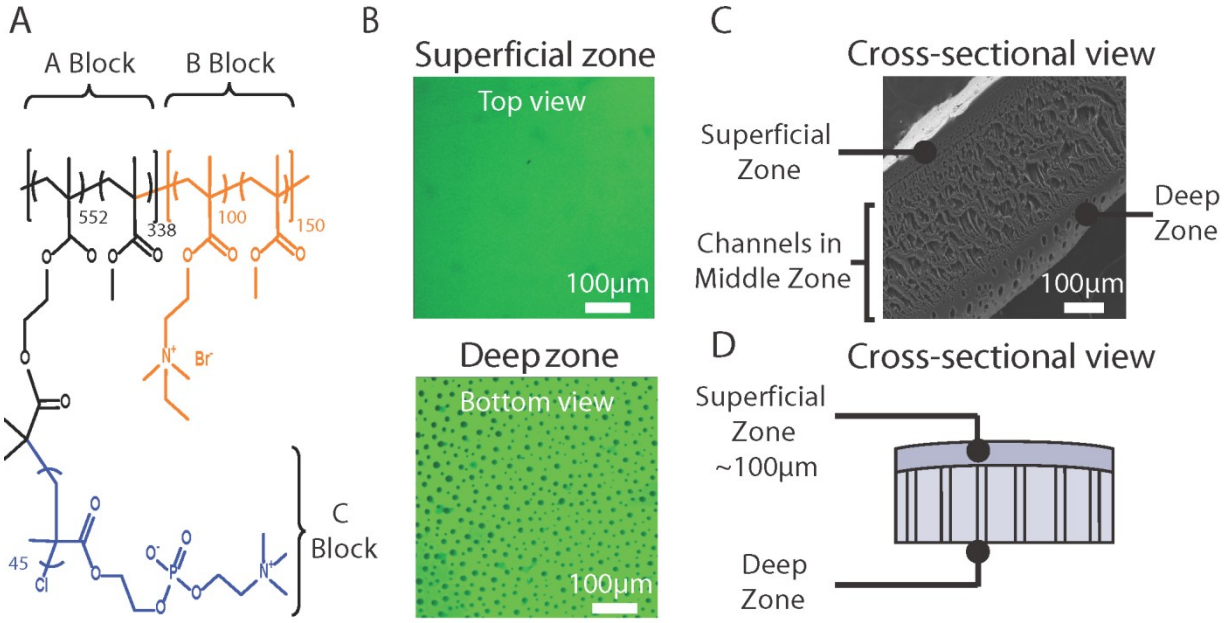

Figure 4.1. *(A) BB polymer structure showing the three different blocks used to build the polymer, and (B) confocal microscopy imaging of the top (superficial zone) and bottom (basal zone) of the hydrogel plug (C) scanning electron microscopy micrographs of the hydrogel cross-section showing the arrangement of the different layers and structures and (D) schematic of the chitosan hydrogel plugs structure used in this study.*

membrane called superficial zone (SZ). The SZ covered a deep zone (DZ) forming the majority of the gel disks composed of microchannels of ~ 10 µm in diameter, perpendicularly aligned to the SZ. These channels crossed the bottom of the gel as seen in the Fig. 1 B and were one millimeter long, reaching the bottom surface of the hydrogel plug.

4.3.2 Tribology of gel/gel contacts in HEPES buffer

The gel friction in an aqueous buffer was assessed in two different configurations: SZ/SZ and DZ/DZ configurations (Fig. 4.2 A). The gel disks were placed into a home-made low-load tribometer and fully immersed in a 0.1 M HEPES, 150 mM NaCl at pH 7.4. Buffered conditions were privileged since pH is known to impact the chitosan gel mechanical properties and consequently its tribological properties. In particular, a decrease of pH below or close to the pKa of amine groups of chitosan ($pK_{a\ chitosan}$ = 6.2) could trigger the chitosan chains dissolution and gel weakening. Friction forces, F_t, as a function of normal forces, F_N, were measured at a constant sliding velocity v = 5 mm/s (Fig. 4.2 B) and as a function of sliding velocity, v, at a constant normal pressure of P = 3 kPa (Fig. 4.2 C). To assess the speed effect, the normal pressure was set constant at 3 kPa, of the chitosan gel since it has been previously shown that our chitosan hydrogels at a concentration of 2.5%w/w were structurally altered at normal stresses close to 30 kPa.[1]

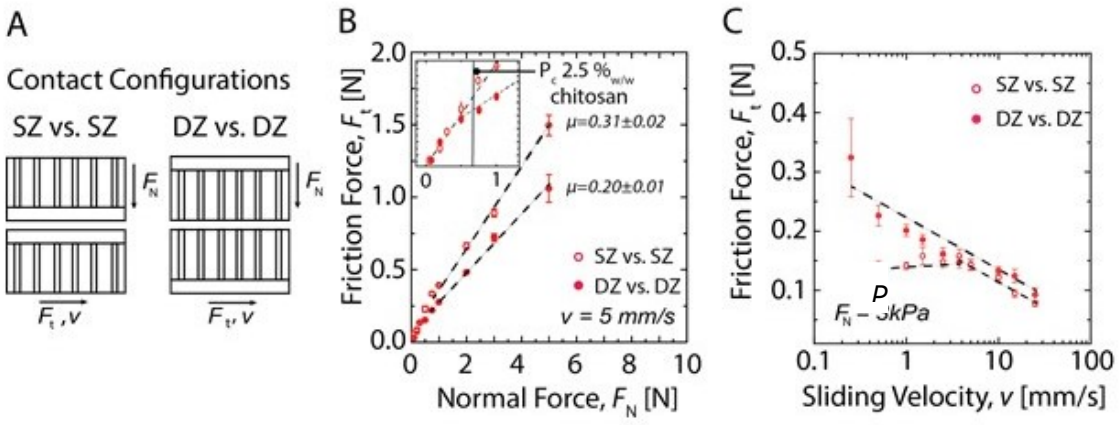

Figure 4.2. *Tribological characterization of gel on gel flat contact in 0.1 M HEPES buffer at pH 7.4. (A) Schematic of the configurations tested (B) Friction force, F_t, as a function of applied normal force, F_N, at v = 5 mm/s for both configurations, inset is an expanded view between 0 to 1 N in order to highlight the transition between DZ and SZ configurations at the*

critical pressure P_c and (C) Friction force, F_t, as a function of sliding velocity, v, at P = 3kPa for both configurations.

The CoF, also denominated μ and defined as $\mu = F_t/F_N$, was higher for the SZ/SZ configuration ($\mu = 0.31 \pm 0.02$) compared to the DZ/DZ configuration ($\mu = 0.20 \pm 0.01$, Fig. 4.2 B) in the high normal force range. No stick-slip behavior was observed in the present study as already reported for multilayered chitosan hydrogels tribopairs[1]. Such difference was observed at an applied normal pressure $P_c > 6$ kPa (~ 0.6 N) (see inset Fig. 4.2 B) while at $P < P_c$, both configurations exhibited similar CoF. We previously demonstrated that the gelation process allowed the formation of a dense gel layer in the SZ characterized by a low permeability to water exudation, while the deeper zone, DZ, is composed of micron-sized channels perpendicularly aligned to the SZ[1]. The low permeability of the SZ limits the formation of a hydrodynamic water film at the rubbing contact leading to a high CoF. On contrary, at the DZ/DZ contact, the CoF was initially similar to the SZ/SZ configuration for a pressure lower than a critical pressure ($P < P_c$). At $P > P_c$, the slope deviated to achieve a lower CoF which was due to the water exudation due to the microchannels closure into the contact from the more permeable DZ gel side.[1] This exudation was responsible for the creation of a sustainable fluid film throughout the experiment and thus improved lubrication.

Figure 4.2 C presents the friction force as a function of the sliding velocity between two chitosan hydrogels. Both configurations exhibited different behavior when increasing the sliding velocity. Indeed, the friction force on the DZ/DZ configuration decreased monotonously with the velocity possibly indicating the presence of a mixed lubrication regime[10] since hydrogels are rough and deformable materials whereas, for the SZ/SZ configuration, the friction force was constant at $v < 5$ mm/s^{-1} and then decreased monotonically at $v > 5$ mm/s, merging toward the friction force of the DZ/DZ configuration. The behavior of the SZ/SZ configuration friction is explained by the transition from the boundary lubrication at low velocity to the mixed lubrication regime at higher velocity[48].

4.3.3 Lubrication with synthetic synovial fluids - Effect of the applied normal force F_N

In order to elucidate the role of the synthetic synovial fluid on the hydrogels lubrication, we firstly immersed the chitosan gels in solutions of 1 mg/mL HA of different molecular mass (10, 60, 500, and 1500 kDa) during 1 h and then tested them on the tribometer (Fig. 4.3 A-C). HA was used as a comparative lubricating fluid for two reasons. First, HA has a key role in

the joint lubrication since it binds Agg to form a Agg/HA complexes within the cartilage, osmotically increasing the compressive modulus of cartilage as well with synovial fluid's lubricin and phospholipids to immobilize these molecules onto the shearing contact[6, 22, 49-54]. Secondly, HA is commercially used as a viscosupplement fluid for patient suffering from painful joints such as in the case osteoarthritis or directly in the eye for patients suffering from dry eye syndrom or wearing contact lenses[55-59].

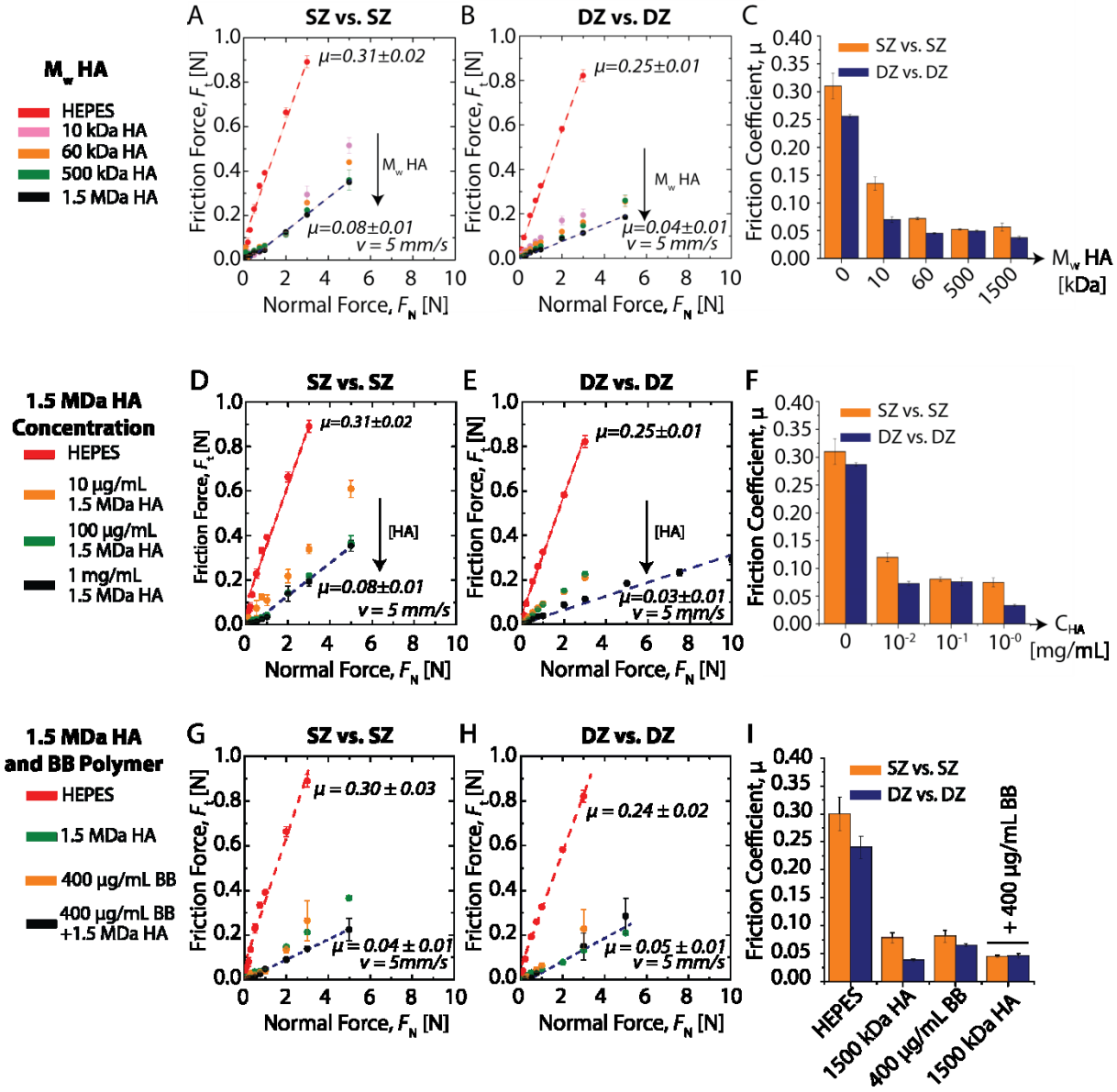

Figure 4.3. *Measurement of the friction force, F_t, as a function of normal force, F_N, between two hydrogel plugs in presence of solutions of different molecular weights HA in the (A) SZ/SZ configuration and (B) DZ/DZ configuration. (C) Evolution of the coefficient of friction μ as a function of HA molecular weights for SZ/SZ and DZ/DZ configurations. (D) F_t as a*

function of F_N at different HA concentrations in the SZ/SZ configuration and the (E) DZ/DZ configuration. (F) The resulting CoF as a function of HA concentration for SZ/SZ and DZ/DZ configurations. (G) Impact of BB and HA mixtures on the friction force F_t between two hydrogel plugs in the SZ/SZ configuration and (H) DZ/DZ configuration. (I) Corresponding CoF as a function of the lubricant composition.

In both SZ/SZ and DZ/DZ configurations, the presence of HA led to a drastic decrease of the CoF compared to pure HEPES buffer (Fig. 4.3 A and B). Once again, the DZ/DZ configuration exhibited a slightly lower CoF, $\mu = 0.04 \pm 0.01$ for 1.5 MDa HA at $P > P_c \sim 6$ kPa in comparison with the SZ/SZ configuration exhibiting $\mu = 0.08 \pm 0.01$. The lowest HA molecular mass (10 and 60 kDa) had significantly higher CoF than the highest molecular weights in both configurations (Fig. 4.3 C).

We then investigated the effect of high molecular weight HA concentration on the frictional behavior of chitosan gels. The gels were immersed in 1.5 MDa HA solutions of different concentrations (0, 10, 100, and 1000 µg/mL) for 1 h prior to tribo-experimentation. As seen in Fig. 4.3 D-F, increasing HA concentration tended to decrease the CoF by one order of magnitude in both hydrogels configurations. On the SZ/SZ configuration, the CoF reached, once again a higher value ($\mu = 0.08 \pm 0.01$) than the DZ/DZ configuration, slightly merging toward gel/gel rubbing in HEPES alone for the lowest HA concentrations suggesting that low Mw HA is depleted from the contact during shearing. On the DZ/DZ configuration, the CoF remained low at $\mu = 0.04 \pm 0.01$ for $P > P_c$. These observations can be rationalized using the trapping mechanism recently reported in natural articular cartilage.[8] This mechanism considers that high molecular weight HA molecules are partially traps in cartilage collagen network under high compression which transiently immobilizes them at the interface, right where they are needed for lubrication and wear protection. A similar behavior was observed in the present system. In the DZ/DZ configuration, high molecular weight HA was effectively trapped in the pores of the interface, allowing higher lubrication compared to low molecular weight HA or to the SZ/SZ configuration. This mechanism is facilitated by the relative size of the hydrogel channels diameter (10 microns) protruding at the interface in the DZ/DZ configuration and the radius of gyration of HA molecules ($R_g = 154 \pm 12$ nm at 1.5 MDa buffered saline).

The BB polymer alone presented a similar behavior to high molecular HA, which is not surprising since BB is also a high molecular weight polymer (Mw ≈ 10^7 g/mol, Fig. 4.3 G and H). At a concentration of 400 µg/mL, the CoF of the BB polymer solution was $\mu = 0.08 \pm 0.01$ in the SZ/SZ configuration compared to 0.05 ± 0.01 in the DZ/DZ configuration.(Fig 4.3 G-I). Finally, the BB polymer at 400 µg/mL was mixed to the 1.5 MDa HA solution and tribogically tested on both hydrogel configurations. To increase interaction with 1.5 MDa HA, a small polycationic attachment group (Fig. 4.1 A, B block) was grafted on a linear domain to mimic proteoglycan attachment groups onto HA. Figure 4.3 G shows that the CoF in SZ/SZ configuration (which was systematically the highest, independently of the HA used) was lowered using the macromolecules mixture ($\mu = 0.04 \pm 0.01$), reaching values similar to those observed for the DZ/DZ configuration (Fig 4.3 H) with the 1.5 MDa HA at 1 mg/mL. In contrast, the effect of the mixture was unnoticeable in the DZ/DZ configuration since no significant differences in CoF were observed compared to 1.5 MDa HA at 1 mg/mL alone. Therefore, the BB polymer combined with high molecular weight HA allows to obtain a CoF that is independent of the hydrogel configuration, smearing out the effect of the interface structure.

The last observation indicates that the synergistic interaction between HA and the BB polymer allows the lubricant to remain in the shear contact even in the absence of any surface pores. We previously showed that BB polymers without any polycationic side block could entangle with HA macromolecules under confinement creating a strongly cohesive lubricating interfacial film.[33] The presence of a polycationic side block in the BB polymer we used in this study drastically enhances the interaction between both polymers even under low applied load which helps maintaining them in the interfacial contact even under high shear conditions.

4.3.4 Lubrication with synthetic synovial fluids - Effect of the sliding velocity v

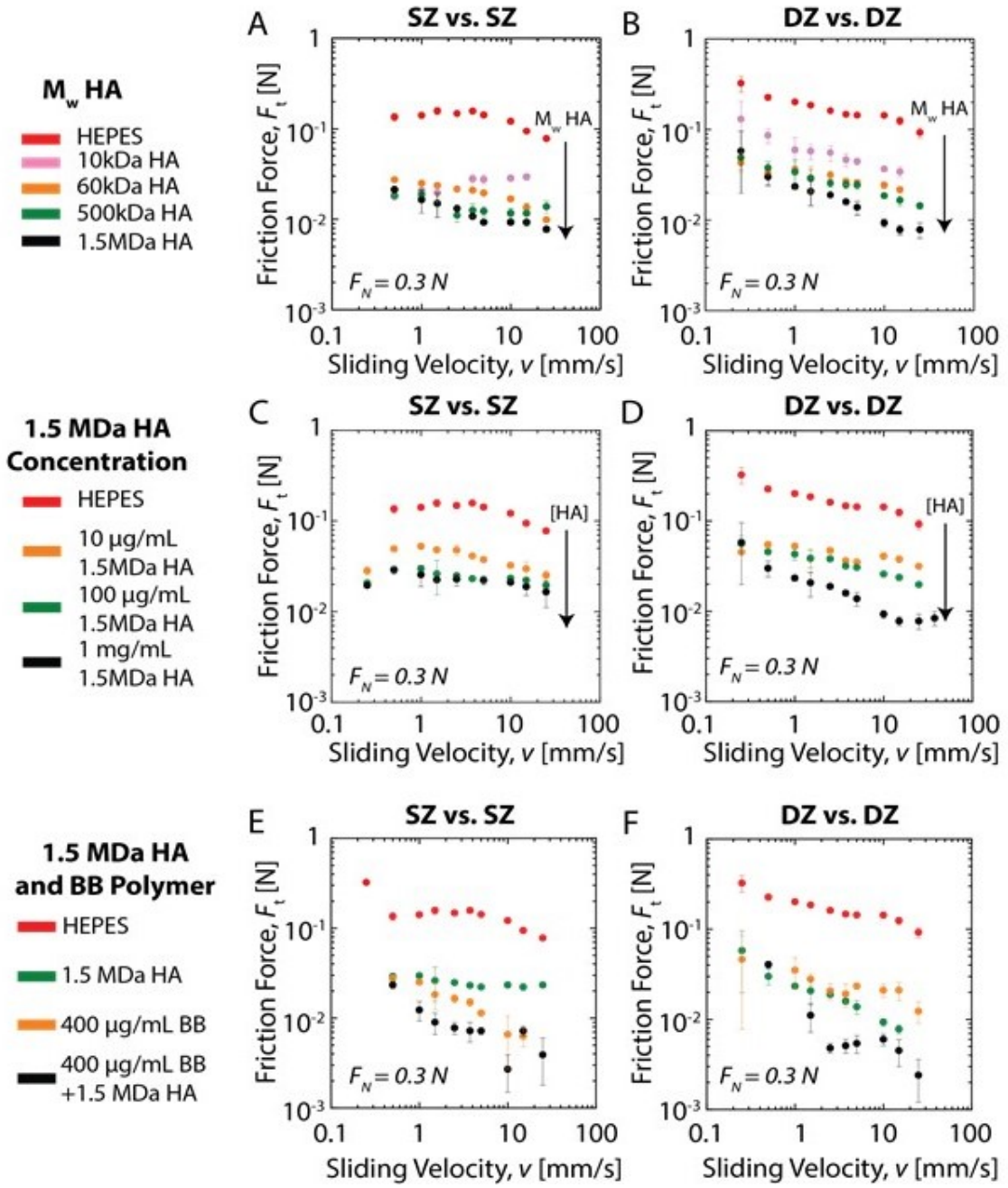

Figure 4.4. *Measurement of the friction force, F_t, as a function of the sliding velocity, v, to assess the effect of HA molecular mass (10, 60, 500 and 1500 kDa) at a fixed concentration of 1 mg/mL for the (A) SZ/SZ configuration and (B) DZ/DZ configuration. Measurement of F_t vs. v to assess the effect of HA concentration for the (C) SZ/SZ configuration and (D) DZ/DZ configuration. Measurement of F_t vs. v to assess the effect of 1.5 MDa HA at 1 mg/mL in combination with BB polymer for the (E) SZ/SZ configuration and (F) DZ/DZ configuration. Gels were immersed for 1 h in the synthetic synovial fluids prior to start the tribotests.*

The effect of the sliding velocity on the friction forces for the chitosan hydrogels plugs in the SZ/SZ and DZ/DZ configurations using different lubricating fluids is presented in Fig. 4.4. In these experiments, the applied normal load was set constant at P = 3 kPa < P_c. In both configurations and for each lubricating system, the friction force was decreased by one order of magnitude when HA, BB or HA and BB mixture were used compared to HEPES buffer only, suggesting a substantial role of these polymers on the lubrication at the gel/gel interface. Concerning the effect of HA molecular weight (Fig. 4.4 A-B), both configurations showed different behaviors upon increasing the sliding velocity. The SZ/SZ configuration exhibited a friction force almost independent of the velocity for low sliding velocities[60-61], indicating the mechanism of boundary lubrication regime, since the friction forces did not depend on the physical properties of the gel nor on the lubricant viscosity, but only on the chemical composition of the surface/adsorbed molecules (Fig. 4.4 A). The DZ/DZ configuration exhibited a monotonous decrease of the friction force suggesting a mixed lubrication mechanism due to the mixed load support by the lubricating film and local asperities on the hydrogels contact[48]. At low velocity, the friction force was slightly lower on the SZ/SZ configuration than the DZ/DZ configuration for low molecular weight HA. This might be due to the larger roughness of the DZ surface (see latter in the wear study section) which could lead to a higher friction[48]. This difference readily vanished upon increasing the sliding velocity and the friction force became even lower on the DZ/DZ configuration at v > 10 mm/s (Fig. 4.4 B). Increase of HA concentration tended to dramatically decrease the friction force (Fig. 4.4 C-D) independently of the hydrogel configuration used. The evolution of the friction force with the sliding speed measured at different HA concentrations of 1.5 MDa HA shows that boundary lubrication is the dominating regime in the SZ/SZ configuration while a mixed lubrication is possibly occurring in the DZ/DZ configuration.

The effect of the sliding velocity in presence of BB polymer alone is presented in Fig. 4.4 E-F. On both configurations, the frictions forces decreased monotonously with the increase of the sliding velocity and where lower in the SZ/SZ configuration than in the DZ/DZ configuration. This behavior has been reported for similar systems composed of grafted pMPC brushes[62]. This monotonous behavior was conserved when BB polymer was mixed with high molecular weight HA. However, the friction forces of the mixture were systematically lower than HA or BB alone at sliding speed greater than 1 mm/s which indicates a synergy between both polymers (Fig. 4.4 E-F). At low sliding speed, it appears

that the friction forces of HA, BB polymer and their mixture converge toward a high value friction force that depends on the testing configurations.

4.3.5 Hydrogel wear protection with synthetic synovial fluids - visualization and characterization

The structural integrity of the chitosan hydrogels surfaces was systematically monitored to highlight the role of the bioinspired synovial fluid on wear protection. The evaluation of wear debris volume was not possible in set up configuration we used, therefore wear damage was first qualitatively analyzed by the means of a digital microscope and quantitatively analyzed after tribotesting using interferometric microscopy. For wear experiments, hydrogels were mounted in the same SZ/SZ and DZ/DZ configurations as in the lubrication study. Imaging of the hydrogel plugs was performed after 10000 cycles of back and forth motion at an applied pressure P = 30 kPa in an aqueous solution fixed at pH 7.4 with a constant sliding speed of 5 mm/s at a frequency of 1 Hz. It was previously shown that multilayered chitosan hydrogels under shearing suffered from destruction at a pressure close to their shear modulus at the DZ/DZ configurations. Images of the 21 mm hydrogel plugs are shown in Fig. 4.5. The 11 mm hydrogel plugs displayed similar surface features after wear tests and were not presented for clarity. These images show that without any lubricant macromolecules, the chitosan gels displayed severe surface damage when tested in the DZ/DZ configuration and showed surface polishing / abrasion in the SZ/SZ configuration. Interferometric images on damaged surfaces presented large dark areas indicating the presence of deep crevices far too high to be measurable by this technique. Lubricating fluids containing HA at 1 mg/mL, exhibited M_w - dependent wear protection in the DZ/DZ configuration. High molecular mass HA solution (M_w = 1.5 MDa) protected the hydrogel plugs significantly more than low molecular mass HA (M_w = 10 kDa) in the DZ/DZ configuration while differences in wear protection in the SZ/SZ configuration were much less significant. These observations highlight the important role of the hydrogel interfacial structure in controlling wear initiation and propagation in presence of linear polymer lubricants. As seen in Fig. 5, the BB polymer alone was able to protect the hydrogel plugs very similarly to high molecular weight HA solutions with only few defects appearing on both tested configurations. The mixture of BB polymer along with high molecular mass HA (M_w = 1.5 MDa) showed very little wear on both SZ and DZ surfaces compared to the initial surfaces.

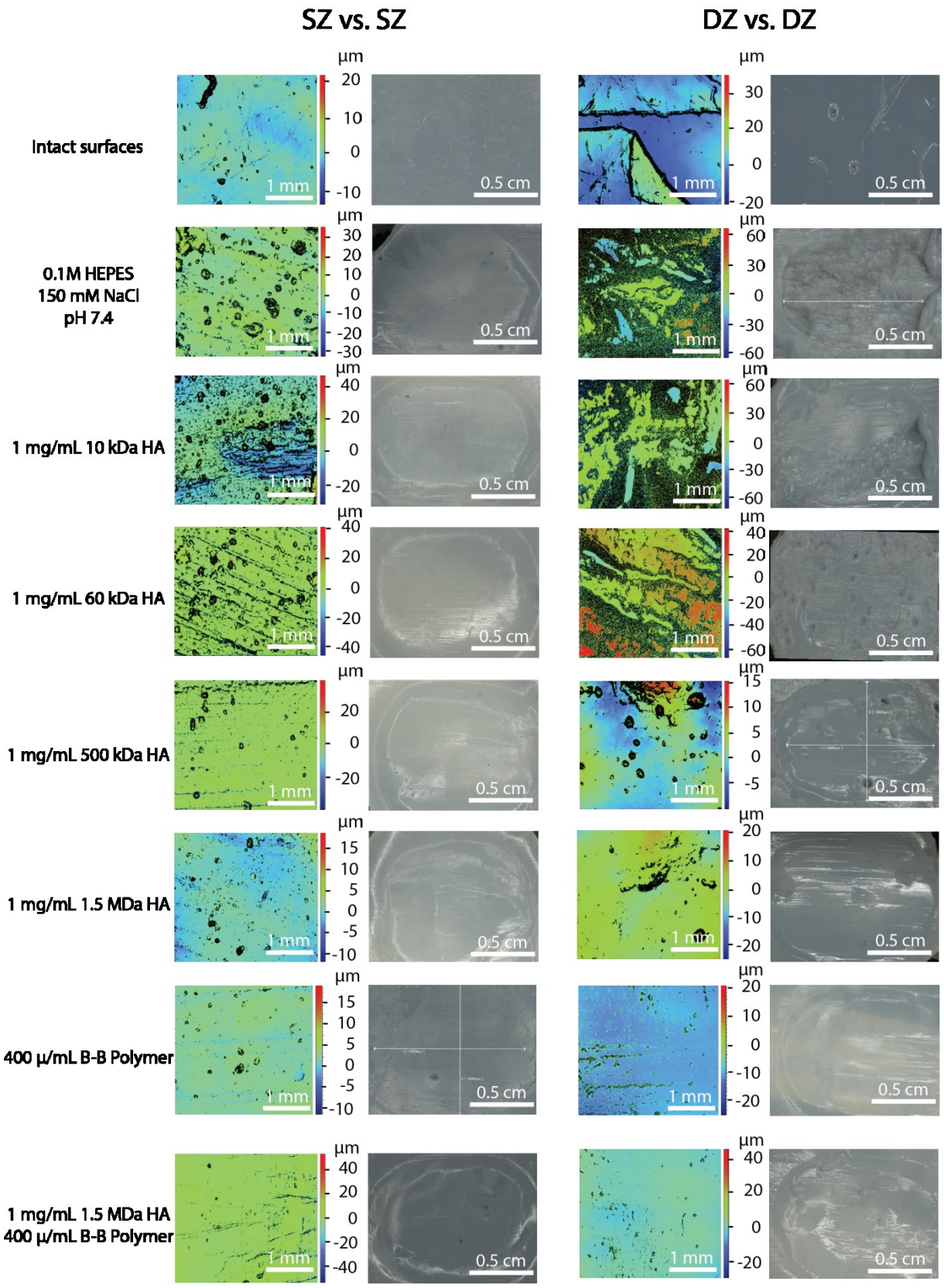

Figure 4.5. *Interferometric and digital imaging of chitosan hydrogel plugs after 10^4 cycles at P = 30 kPa, v = 5 mm/s and a frequency of 1 Hz using different fluid compositions and*

hydrogels configurations. Certain panels are reproduced from Ref. [1] with permission from the Royal Society of Chemistry.

Using optical interferometry, the roughness in the wear tracks was evaluated after tribotesting (Fig. 4.6). The arithmetical mean height of the whole gel surfaces, S_a, was used as the parameter characterizing the roughness before and after wear tests. This parameter corresponds to the absolute difference of the height of each point of a surface to the arithmetical mean of the gel surface. Before wear tests, the initial roughness of the chitosan hydrogel plugs (Intact surfaces in Fig. 4.6) was higher on the DZ side (S_a = 4 µm) than on the SZ side (S_a = 0.8 µm). When using only HEPES as a lubricating fluid, the final roughness of the chitosan hydrogels was significantly higher on both configurations since S_a increased to 2.5 µm on the SZ side and was impossible to measure on the DZ side due to strong damage of the gel (S_a >> 16 µm). When using HA-based fluids, the final gel roughness was significantly smaller than HEPES and decreased with HA molecular weight. Upon the addition of the BB polymer to the high molecular weight HA solution, the final roughness was finally equal to the initial value for the SZ/SZ configuration and lower than the initial value for the DZ/DZ configuration, possibly due to surface heterogeneities leveling upon gel rubbing.

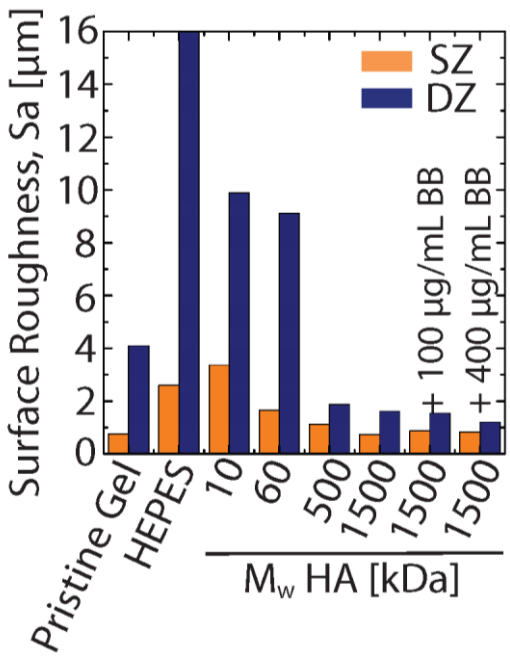

Figure 4.6. *Quantitative wear assessment by the means of surface roughness, S_a, of gel sample after wear experiment as a function of immersion bath composition for both contact configuration measured by interferometry*

4.4. Conclusions

The present study shows that a lubricating fluid composed of BB polymer and high molecular weight HA is able to efficiently provide concomitantly wear protection of soft and porous materials and decrease the CoF, for different surface topographies or structures. These results anticipate the potential use of such lubricating fluid for various biomedical applications such as joints viscosupplementation or eyes and contact lenses hydration and lubrication.

Acknowledgements

JF is grateful to the Arthritis Society, the Faculté des études supérieures et postdoctorales from the Université de Montréal and the French Embassy (Frontenac scholarship) for financial supports. BRS thanks the financial support of GRUM. XB acknowledges the financial support from the Canada research chair program and NSERC (Discovery grant). XB and GS are grateful for the financial support of the FRQNT-CFQCU (Samuel de Champlain grant). KM Acknowledges support from NSF (DMR 1501324). We thank Agnes Crépet (IMP) and Pierre Alcouffe (IMP) for their technical assistance in size exclusion chromatography and scanning electron microscopy, respectively. The help of Matthieu Guibert (LTDS) for the low-load tribometer design and fabrication, Thomas Malhomme (LTDS) for wear analysis by interferometry, and Béatrice Burdin (Centre Technologique des Microstructures) for CLSM study implementation is also acknowledged.

Conclusion générale du chapitre IV

Comme présenté dans le chapitre II, nous avons pu observer que l'HA de haut poids moléculaire accompagné de l'écouvillon moléculaire à une concentration de l'ordre de 100-400 µg/mL donnent des résultats tribologiques prometteurs à la fois sur des surfaces dures non poreuses de mica[32-34] et sur substrats poroélastiques d'hydrogels physiques de chitosane. Ces analyses correspondent à des échelles de mesure de la friction totalement différentes (de l'ordre micrométrique pour le SFA et macroscopique pour le tribomètre). Nous avons constaté que la topographie de l'hydrogel au niveau du contact importe peu, le fluide synovial inspiré est capable de garantir à la fois un faible CoF et une bonne protection à l'usure. Cela permet d'envisager une multitude d'applications biomédicales pour notre formulation, là où des protéoglycanes ou des glycoprotéines sont requis pour le bon fonctionnement des muqueuses et des séreuses. Ainsi, toutes les muqueuses déficientes par la composition et la quantité de mucus ou nécessitant une réhydratation du mucus, une lubrification ou une protection contre les frottements pourraient bénéficier de ce fluide bioinspiré. Nous pouvons penser à des solutions buvables pour la xérostomie, des collyres pour la xérophtalmie, des solutions salines pour les lentilles cornéennes, des injections intra-articulaires pour des problèmes de synovie ou d'arthrose, la lubrification pour la pose de stents, etc.

Références

1. Faivre, J.; Sudre, G.; Montembault, A.; Benayoun, S.; Banquy, X.; Delair, T.; David, L., Bioinspired Microstructures of Chitosan Hydrogel Provide Enhanced Wear Protection. *Soft Matter* **2018**, 2068-2076.

2. Spiller, K. L.; Maher, S. A.; Lowman, A. M., Hydrogels for the Repair of Articular Cartilage Defects. *Tissue Eng., Part B* **2011,** *17* (4), 281-299.

3. Montembault, A.; Tahiri, K.; Korwin-Zmijowska, C.; Chevalier, X.; Corvol, M. T.; Domard, A., A material decoy of biological media based on chitosan physical hydrogels: application to cartilage tissue engineering. *Biochimie* **2006,** *88* (5), 551-564.

4. Makris, E. A.; Gomoll, A. H.; Malizos, K. N.; Hu, J. C.; Athanasiou, K. A., Repair and tissue engineering techniques for articular cartilage. *Nat. Rev. Rheumatol.* **2015,** *11* (1), 21-34.

5. Greene, G. W.; Banquy, X.; Lee, D. W.; Lowrey, D. D.; Yu, J.; Israelachvili, J. N., Adaptive mechanically controlled lubrication mechanism found in articular joints. *Proc. Natl. Acad. Sci. U. S. A.* **2011,** *108* (13), 5255-5259.

6. Das, S.; Banquy, X.; Zappone, B.; Greene, G. W.; Jay, G. D.; Israelachvili, J. N., Synergistic interactions between grafted hyaluronic acid and lubricin provide enhanced wear protection and lubrication. *Biomacromolecules* **2013,** *14* (5), 1669-1677.

7. Greene, G. W.; Zappone, B.; Zhao, B.; Soderman, O.; Topgaard, D.; Rata, G.; Israelachvili, J. N., Changes in pore morphology and fluid transport in compressed articular cartilage and the implications for joint lubrication. *Biomaterials* **2008,** *29* (33), 4455-4462.

8. Greene, G. W.; Zappone, B.; Soderman, O.; Topgaard, D.; Rata, G.; Zeng, H.; Israelachvili, J. N., Anisotropic dynamic changes in the pore network structure, fluid diffusion and fluid flow in articular cartilage under compression. *Biomaterials* **2010,** *31* (12), 3117-3128.

9. Forster, H.; Fisher, J., The Influence of Loading Time and Lubricant on the Friction of Articular Cartilage. *Proc. Inst. Mech. Eng., Part H* **1996,** *210* (2), 109-119.

10. Jahn, S.; Seror, J.; Klein, J., Lubrication of Articular Cartilage. *Annu. Rev. Biomed. Eng.* **2016,** *18* (1), 235-258.

11. Ateshian, G. A., The role of interstitial fluid pressurization in articular cartilage lubrication. *J. Biomech.* **2009,** *42* (9), 1163-1176.

12. Klein, J., Molecular mechanisms of synovial joint lubrication. *Proc. Inst. Mech. Eng., Part J* **2006,** *220* (8), 691-710.

13. Balazs, E. A., The role of hyaluronan in the structure and function of the biomatrix of connective tissues. *Struct. Chem.* **2009,** *20* (2), 233-243.

14. Lin, P.; Zhang, R.; Wang, X.; Cai, M.; Yang, J.; Yu, B.; Zhou, F., Articular Cartilage Inspired Bilayer Tough Hydrogel Prepared by Interfacial Modulated Polymerization Showing Excellent Combination of High Load-Bearing and Low Friction Performance. *ACS Macro Lett.* **2016,** *5* (11), 1191-1195.

15. Yashima, S.; Takase, N.; Kurokawa, T.; Gong, J. P., Friction of hydrogels with controlled surface roughness on solid flat substrates. *Soft Matter* **2014,** *10* (18), 3192-9.

16. Khosla, T.; Cremaldi, J.; Erickson, J. S.; Pesika, N. S., Load-Induced Hydrodynamic Lubrication of Porous Films. *ACS Appl. Mater. Interfaces* **2015,** *7* (32), 17587-17591.

17. Gong, J. P., Friction and lubrication of hydrogels-its richness and complexity. *Soft Matter* **2006,** *2* (7), 544-552.

18. Singh, A.; Corvelli, M.; Unterman, S. A.; Wepasnick, K. A.; McDonnell, P.; Elisseeff, J. H., Enhanced lubrication on tissue and biomaterial surfaces through peptide-mediated binding of hyaluronic acid. *Nat. Mater.* **2014,** *13* (10), 988-995.

19. Zhang, R.; Feng, Y.; Ma, S.; Cai, M.; Yang, J.; Yu, B.; Zhou, F., Tuning the Hydration and Lubrication of the Embedded Load-Bearing Hydrogel Fibers. *Langmuir* **2017,** *33* (9), 2069-2075.

20. Ohsedo, Y.; Takashina, R.; Gong, J. P.; Osada, Y., Surface Friction of Hydrogels with Well-Defined Polyelectrolyte Brushes. *Langmuir* **2004,** *20* (16), 6549-6555.

21. Kamada, K.; Furukawa, H.; Kurokawa, T.; Tada, T.; Tominaga, T.; Nakano, Y.; Gong, J. P., Surfactant-induced friction reduction for hydrogels in the boundary lubrication regime. *J. Phys.: Condens. Matter* **2011,** *23* (28), 284107.

22. Samsom, M.; Iwabuchi, Y.; Sheardown, H.; Schmidt, T. A., Proteoglycan 4 and hyaluronan as boundary lubricants for model contact lens hydrogels. *J. Biomed. Mater. Res. B Appl. Biomater.* **2017**, 1329-1338.

23. McGann, M. E.; Bonitsky, C. M.; Jackson, M. L.; Ovaert, T. C.; Trippel, S. B.; Wagner, D. R., Genipin crosslinking of cartilage enhances resistance to biochemical degradation and mechanical wear. *J. Orthop. Res.* **2015,** *33* (11), 1571-1579.

24. Liao, I. C.; Moutos, F. T.; Estes, B. T.; Zhao, X.; Guilak, F., Composite Three-Dimensional Woven Scaffolds with Interpenetrating Network Hydrogels to Create Functional Synthetic Articular Cartilage. *Adv. Funct. Mater.* **2013,** *23* (47), 5833-5839.

25. Yasuda, K.; Ping Gong, J.; Katsuyama, Y.; Nakayama, A.; Tanabe, Y.; Kondo, E.; Ueno, M.; Osada, Y., Biomechanical properties of high-toughness double network hydrogels. *Biomaterials* **2005,** *26* (21), 4468-4475.

26. Nakajima, T., Generalization of the sacrificial bond principle for gel and elastomer toughening. *Polym. J.* **2017,** *49* (6), 477-485.

27. Kolmakov, G. V.; Matyjaszewski, K.; Balazs, A. C., Harnessing labile bonds between nanogel particles to create self-healing materials. *ACS Nano* **2009,** *3* (4), 885-892.

28. Faivre, J.; Shrestha, B. R.; Xie, G.; Olszewski, M.; Adibnia, V.; Moldovan, F.; Montembault, A.; Sudre, G.; Delair, T.; David, L.; Matyjaszewski, K.; Banquy, X., Intermolecular Interactions between Bottlebrush Polymers Boost the Protection of Surfaces against Frictional Wear. *Chem. Mater.* **2018,** *30* (12), 4410-9.

29. Lee, H.-i.; Pietrasik, J.; Sheiko, S. S.; Matyjaszewski, K., Stimuli-responsive molecular brushes. *Prog. Polym. Sci.* **2010,** *35* (1), 24-44.

30. Matyjaszewski, K., Atom Transfer Radical Polymerization (ATRP): Current Status and Future Perspectives. *Macromolecules* **2012,** *45* (10), 4015-4039.

31. Schmidt, T. A.; Gastelum, N. S.; Nguyen, Q. T.; Schumacher, B. L.; Sah, R. L., Boundary lubrication of articular cartilage: Role of synovial fluid constituents. *Arthritis & Rheumatism* **2007,** *56* (3), 882-891.

32. Banquy, X.; Burdyńska, J.; Lee, D. W.; Matyjaszewski, K.; Israelachvili, J., Bioinspired Bottle-Brush Polymer Exhibits Low Friction and Amontons-like Behavior. *J. Am. Chem. Soc.* **2014,** *136* (17), 6199-6202.

33. Faivre, J.; Shrestha, B. R.; Burdynska, J.; Xie, G.; Moldovan, F.; Delair, T.; Benayoun, S.; David, L.; Matyjaszewski, K.; Banquy, X., Wear Protection without Surface Modification Using a Synergistic Mixture of Molecular Brushes and Linear Polymers. *ACS Nano* **2017,** *11* (2), 1762-1769.

34. Faivre, J.; Shrestha, B. R.; Xie, G.; Delair, T.; David, L.; Matyjaszewski, K.; Banquy, X., Unraveling the Correlations between Conformation, Lubrication, and Chemical Stability of Bottlebrush Polymers at Interfaces. *Biomacromolecules* **2017**, 4002-4010.

35. Pan, Y.-S.; Xiong, D.-S.; Ma, R.-Y., A study on the friction properties of poly(vinyl alcohol) hydrogel as articular cartilage against titanium alloy. *Wear* **2007,** *262* (7), 1021-1025.

36. Choi, S. H.; Park, K. S.; Sung, M. W.; Kim, K. H., Dynamic and quantitative evaluation of eyelid motion using image analysis. *Med Biol Eng Comput* **2003,** *41* (2), 146-50.

37. Bentivoglio, A. R.; Bressman, S. B.; Cassetta, E.; Carretta, D.; Tonali, P.; Albanese, A., Analysis of blink rate patterns in normal subjects. *Mov. Disord.* **1997,** *12* (6), 1028-34.

38. Delmotte, P.; Sanderson, M. J., Ciliary Beat Frequency Is Maintained at a Maximal Rate in the Small Airways of Mouse Lung Slices. *Am. J. Respir. Cell Mol. Biol.* **2006,** *35* (1), 110-117.

39. Oldenburg, A. L.; Chhetri, R. K.; Hill, D. B.; Button, B., Monitoring airway mucus flow and ciliary activity with optical coherence tomography. *Biomedical Optics Express* **2012,** *3* (9), 1978-1992.

40. Dedinaite, A., Biomimetic lubrication. *Soft Matter* **2012,** *8* (2), 273-284.

41. Elsaid, K. A.; Fleming, B. C.; Oksendahl, H. L.; Machan, J. T.; Fadale, P. D.; Hulstyn, M. J.; Shalvoy, R.; Jay, G. D., Decreased lubricin concentrations and markers of joint inflammation in the synovial fluid of patients with anterior cruciate ligament injury. *Arthritis Rheum.* **2008,** *58* (6), 1707-1715.

42. Hilbert, B. J.; Rowley, G.; Antonas, K. N., Hyaluronic acid concentration in synovial fluid from normal and arthritic joints of horses. *Aust. Vet. J.* **1984,** *61* (1), 22-24.

43. Tamer, T. M., Hyaluronan and synovial joint: function, distribution and healing. *Interdiscip. Toxicol.* **2013,** *6* (3), 111-125.

44. Lee, D. W.; Banquy, X.; Das, S.; Cadirov, N.; Jay, G.; Israelachvili, J., Effects of molecular weight of grafted hyaluronic acid on wear initiation. *Acta Biomater.* **2014,** *10* (5), 1817-1823.

45. Nie, J.; Lu, W.; Ma, J.; Yang, L.; Wang, Z.; Qin, A.; Hu, Q., Orientation in multi-layer chitosan hydrogel: morphology, mechanism, and design principle. *Sci. Rep.* **2015,** *5*, 7635.

46. Fiamingo, A.; Montembault, A.; Boitard, S.-E.; Naemetalla, H.; Agbulut, O.; Delair, T.; Campana-Filho, S. P.; Menasché, P.; David, L., Chitosan Hydrogels for the Regeneration of Infarcted Myocardium: Preparation, Physicochemical Characterization, and Biological Evaluation. *Biomacromolecules* **2016,** *17* (5), 1662-1672.

47. Sereni, N.; Enache, A.; Sudre, G.; Montembault, A.; Rochas, C.; Durand, P.; Perrard, M. H.; Bozga, G.; Puaux, J. P.; Delair, T.; David, L., Dynamic Structuration of Physical Chitosan Hydrogels. *Langmuir* **2017,** *33* (44), 12697-12707.

48. Yashima, S.; Takase, N.; Kurokawa, T.; Gong, J. P., Friction of hydrogels with controlled surface roughness on solid flat substrates. *Soft Matter* **2014,** *10* (18), 3192-3199.

49. Kawano, T.; Miura, H.; Mawatari, T.; Moro-Oka, T.; Nakanishi, Y.; Higaki, H.; Iwamoto, Y., Mechanical effects of the intraarticular administration of high molecular weight

hyaluronic acid plus phospholipid on synovial joint lubrication and prevention of articular cartilage degeneration in experimental osteoarthritis. *Arthritis and rheumatism* **2003,** *48* (7), 1923-9.

50. Liu, C.; Wang, M.; An, J.; Thormann, E.; Dedinaite, A., Hyaluronan and phospholipids in boundary lubrication. *Soft Matter* **2012,** *8* (40), 10241-10244.

51. Chang, D. P.; Abu-Lail, N. I.; Guilak, F.; Jay, G. D.; Zauscher, S., Conformational Mechanics, Adsorption, and Normal Force Interactions of Lubricin and Hyaluronic Acid on Model Surfaces. *Langmuir* **2008,** *24* (4), 1183-1193.

52. Teeple, E.; Elsaid, K. A.; Jay, G. D.; Zhang, L.; Badger, G. J.; Akelman, M.; Bliss, T. F.; Fleming, B. C., Effects of supplemental intra-articular lubricin and hyaluronic acid on the progression of posttraumatic arthritis in the anterior cruciate ligament-deficient rat knee. *Am. J. Sports Med.* **2011,** *39* (1), 164-72.

53. Majd, S. E.; Kuijer, R.; Kowitsch, A.; Groth, T.; Schmidt, T. A.; Sharma, P. K., Both Hyaluronan and Collagen Type II Keep Proteoglycan 4 (Lubricin) at the Cartilage Surface in a Condition That Provides Low Friction during Boundary Lubrication. *Langmuir* **2014**, 14566-14572.

54. Bonnevie, E. D.; Galesso, D.; Secchieri, C.; Cohen, I.; Bonassar, L. J., Elastoviscous Transitions of Articular Cartilage Reveal a Mechanism of Synergy between Lubricin and Hyaluronic Acid. *PLOS ONE* **2015,** *10* (11), e0143415.

55. Masuko, K.; Murata, M.; Yudoh, K.; Kato, T.; Nakamura, H., Anti-inflammatory effects of hyaluronan in arthritis therapy: Not just for viscosity. *Int. J. Gen. Med.* **2009,** *2*, 77-81.

56. Bailleul, F., Regimens for intra-articular viscosupplementation. Google Patents: 2011.

57. Ammar, T. Y.; Pereira, T. A. P.; Mistura, S. L. L.; Kuhn, A.; Saggin, J. I.; Lopes Júnior, O. V., Viscosupplementation for treating knee osteoarthrosis: review of the literature. *Revista Brasileira de Ortopedia* **2015,** *50* (5), 489-494.

58. Samsom, M. L.; Morrison, S.; Masala, N.; Sullivan, B. D.; Sullivan, D. A.; Sheardown, H.; Schmidt, T. A., Characterization of full-length recombinant human Proteoglycan 4 as an ocular surface boundary lubricant. *Exp. Eye Res.* **2014,** *127*, 14-9.

59. Lambiase, A.; Sullivan, B. D.; Schmidt, T. A.; Sullivan, D. A.; Jay, G. D.; Truitt, E. R., 3rd; Bruscolini, A.; Sacchetti, M.; Mantelli, F., A Two-Week, Randomized, Double-masked Study to Evaluate Safety and Efficacy of Lubricin (150 mug/mL) Eye Drops Versus

Sodium Hyaluronate (HA) 0.18% Eye Drops (Vismed(R)) in Patients with Moderate Dry Eye Disease. *Ocul Surf* **2017,** *15* (1), 77-87.

60. Oogaki, S.; Kagata, G.; Kurokawa, T.; Kuroda, S.; Osada, Y.; Gong, J. P., Friction between like-charged hydrogels-combined mechanisms of boundary, hydrated and elastohydrodynamic lubrication. *Soft Matter* **2009,** *5* (9), 1879-1887.

61. Chang, D. P.; Abu-Lail, N. I.; Coles, J. M.; Guilak, F.; Jay, G. D.; Zauscher, S., Friction force microscopy of lubricin and hyaluronic acid between hydrophobic and hydrophilic surfaces. *Soft Matter* **2009,** *5* (18), 3438-3445.

62. Kobayashi, M.; Takahara, A., Tribological properties of hydrophilic polymer brushes under wet conditions. *Chem. Rec.* **2010,** *10* (4), 208-216.

Chapitre V - Discussions générales sur le projet de thèse

-Chapitre V-

Discussions générales sur le projet de thèse

Discussions sur le chapitre II - Conception d'une librairie de mimes polymériques lubrifiants

Objectif : *concevoir une librairie de mimes bioinspirés de l'aggrécane et de la lubricine et caractériser leur pouvoir lubrifiant à l'aide de l'appareil de forces de surface*

À travers notre premier objectif de recherche, nous nous sommes intéressés à la synthèse et à la caractérisation tribologique (friction et usure) d'écouvillons moléculaires dont la structure est inspirée de macromolécules lubrifiantes présentes dans les articulations synoviales : l'aggrécane et la lubricine. Pour rappel, la structure de telles macromolécules est composée d'un domaine central en mucine avec des chaines latérales très hydrophiles permettant une diminution de la friction et de groupements d'ancrage latéraux spécifiques permettant aux macromolécules de rester mobilisées dans les zones de contact[1].

Le principal avantage de tels écouvillons moléculaires est leur utilisation directe sans post-modifications ou réactions chimiques par simple physisorption de solution aqueuse de ces polymères sur des surfaces biologiques. La technique de synthèse par ATRP permet d'obtenir des structures polymériques originales et notamment des écouvillons moléculaires grâce à une polymérisation dite "vivante" aboutissant à des polymères à faibles dispersité[2]. Ces systèmes polymères requièrent néanmoins plusieurs étapes de synthèse pour obtenir structure et dimension de la lubricine et de l'aggrécane, ce qui pourrait limiter leur industrialisation. Contrairement aux brosses de polymère initiées sur des surfaces à l'aide d'un seul monomère, les écouvillons moléculaires sont généralement des copolymères à blocs[3-5], statistiques[6-9] ou des homopolymères fonctionnalisés[10-12]. Dans notre cas, la fabrication des écouvillons moléculaires nécessite trois étapes de polymérisation par ATRP (squelette central, domaines d'ancrage et chaines pendantes) et deux étapes de fonctionnalisation (déprotection du groupement OTMS/couplage de l'initiateur bromé, quaternisation du domaine d'ancrage) et donc cinq étapes de purification. La synthèse pourrait être plus rapide si les chaines pendantes polyzwitterioniques fonctionnalisées étaient disponibles commercialement, comme le PLL-g-PEG[6-7, 13] synthétisé avec des PEG fonctionnalisés commerciaux. De plus, l'utilisation de fonctions chimiques plus stables que des liaisons esters notamment au niveau des jonctions

squelette-chaines pendantes où les contraintes moléculaires sont les plus fortes, permettrait d'améliorer la stabilité des macromolécules, néanmoins les matériaux doivent rester biodégradables.

La gamme de CoF des articulations synoviales fréquemment citée dans la littérature s'étale typiquement entre 10^{-4} et 5.10^{-2}.[14] Une gamme de valeurs de CoF est généralement citée dans les études, car les méthodes pour les mesurer nécessitent soit de travailler *in situ* avec la présence des tissus, ou *in vitro* qui implique une altération très rapide du cartilage par un processus enzymatique[14], limitant la reproductibilité. Dans le cadre de notre étude, les CoF obtenus avec nos écouvillons moléculaires sont proches de 10^{-2}, ce qui se situe dans la partie haute de la gamme de CoF des articulations. Néanmoins, cette comparaison est à relativiser. En effet, les CoF de 10^{-3} des articulations synoviales ont été obtenus par le biais de la combinaison synergique du cartilage avec le fluide synovial avec un tribomètre particulier dans des conditions particulières qui s'éloignent de notre méthodologie. À titre de comparaison, le fluide synovial seul possède un CoF de 0.2 [15] beaucoup plus élevé que les articulations complètes (0.038 pour la lubricine seule[16] et ~ 0.5 pour l'HA greffé seul[17]), tous mesurés à l'aide du SFA avec des tribopaires de mica. Banquy *et coll*. ont par exemple montré que le liquide synovial, sur une surface de mica sous contrainte normale et sous cisaillement, se réorganise sous forme de gel composé de protéines, lipides et GAG puis rapidement sous forme d'agrégats donnant lieu à une grande protection contre l'usure (P* = 20 MPa), mais une friction assez élevée[15].

En comparaison avec les résultats de littérature obtenus avec d'autres systèmes polymériques physisorbés ou chemisorbés (voir Chapitre 1 - Introduction), nous nous situons dans la même gamme de CoF sur une grande gamme de pression et sur plusieurs décades de vitesse de cisaillement. Les systèmes naturels seuls, quant à eux, peinent à atteindre des CoF de 10^{-2} (voir chapitre 1) en utilisant le SFA avec des surfaces de mica. Pour obtenir cet ordre de grandeur de coefficient de friction, il faut généralement des combinaisons binaires comprenant aggrécane, lubricine, HA et/ou phospholipides. Ces résultats étant obtenus pour des pressions normales relativement faibles.

Ces résultats illustrent l'avantage de la bioinspiration afin de concevoir des systèmes lubrifiants capables de garantir une faible friction des surfaces étudiées. De plus, nous pouvons travailler efficacement en présence d'une force saline de 150 mM de NaCl à pH 7.4 grâce aux chaines polyzwiterioniques, globalement insensibles aux sels, sans altération des

propriétés lubrifiantes, contrairement à de nombreux systèmes polymériques chargés. Finalement, l'utilisation de notre polymère par simple adsorption physique sans modifications de surface permet une procédure simple, rapide et reproductible contrairement à la plupart des systèmes polymériques étudiés jusqu'à présent.

À travers ce projet de doctorat, nous nous sommes également efforcés à étudier les propriétés de protection contre l'usure de nos écouvillons moléculaires. Très peu d'études à visée biomédicale se sont intéressées à protéger les surfaces d'intérêt contre l'usure contrairement à l'amélioration de la friction, peut-être du fait de l'hypothèse qui n'est pas toujours vérifiée[18] qu'une excellente friction est synonyme de protection contre l'usure. Un contre-exemple est présenté dans le chapitre 3. La face DZ des hydrogels de chitosane possède une friction plus faible, mais une usure plus élevée que la face SZ de ce même gel. La protection contre l'usure est pourtant un paramètre au moins aussi important que la réduction de la friction puisqu'il en va de l'intégrité directe des surfaces exposées au contact. Le challenge de cet objectif était de trouver une méthode fiable et reproductible de détermination de l'usure puisqu'il existe très peu de méthodes référencées concernant les revêtements de polymères lubrifiants pour applications biomédicales. Le SFA nous a permis de remédier à ce problème *via* deux paramètres distincts mesurés simultanément : un changement abrupt de la friction dans les profils de friction, corrélé par l'observation des FECO (topographie des surfaces en contact et mesure de la distance de séparation des surfaces). Ainsi, nous avons pu déterminer les pressions à partir desquelles les films de polymères adsorbés rompent et pourraient engendrer l'usure du mica. Ces pressions allant de quelques atmosphères (~ 0.1 MPa) à plus de 14 MPa, dépendamment du nombre de groupements d'ancrage et de la combinaison avec HA. À titre de comparaison, l'articulation du genou des mammifères, quel que soit le poids de l'animal, supporte des variations de pressions normales allant de 0.1 à 20 MPa [14]. Finalement, le dernier paramètre étudié est la résistance du film polymérique à différentes vitesses de cisaillement. Grâce au SFA, nous avons été capables de travailler à très faibles vitesses (quelques nanomètres par seconde) et à des pressions de l'ordre du mégapascal avec une distance de séparation des surfaces de mica de l'ordre moléculaire[19-20]. Nous nous situons ainsi dans un régime de lubrification limite. Dans le cas des tests sur gels de chitosane, nous avons travaillé à des vitesses de l'ordre de quelques millimètres par seconde pour une protection contre l'usure et une friction similaire aux conditions obtenues avec les surfaces de mica[19]. Nous avons donc conçu des mimes polymériques lubrifiants opérant sur toute la gamme de

pressions physiologiques rencontrées chez les mammifères et sur une très large gamme de vitesse de cisaillement et de modules des matériaux formant la tribopaire.

Discussions sur le Chapitre III - Développement de substituts hydrogels multicouches et caractérisations structurales, physiques, mécaniques et tribologiques

Objectif : *développer un support poroélastique à base d'hydrogel et déterminer ses propriétés mécaniques, physiques et tribologiques*

Dans une seconde partie, nous nous sommes intéressés à la conception de substituts poroélastiques et inspirés architecturalement du cartilage. Les hydrogels sont une bonne première approximation de la structure du cartilage avec une matrice polymérique gonflée d'eau possédant des propriétés de fluage et de recouvrance[21], de transport de fluide[21], de culture cellulaire[22-23] semblables au cartilage. Le chitosane a été choisi comme matériau de l'hydrogel, car c'est un polysaccharide aux propriétés intéressantes déjà utilisé dans des applications biomédicales comme la réparation articulaire et l'ingénierie tissulaire[22, 24-29], le traitement des brûlures[30], la délivrance d'actifs[31-32] et d'autres applications[33-35]. Les hydrogels possèdent typiquement des modules élastiques (E) éloignés de ceux du cartilage. En effet, les modules E des hydrogels sont généralement compris entre 1 et 100 kPa alors que le module du cartilage est de l'ordre du MPa. Différentes alternatives existent néanmoins pour renforcer les hydrogels comme les réseaux interpénétrés[36-38] ou les composites[39-43]. Dans notre cas, nous avons étudié des gels de chitosane balayant une gamme de modules élastiques en cisaillement, G', de 10 à 100 kPa en jouant sur la concentration en polymère. En approximant $E \sim 3 \times G'$ pour un gel incompressible, nous n'atteignons encore pas les valeurs de modules du cartilage [21].

Néanmoins, le procédé de gélification utilisé pour le chitosane dans notre étude [21, 44-45] et également référencé pour le collagène [46-47] permet d'obtenir un hydrogel multicouche rappelant l'organisation des fibrilles de collagène dans le cartilage. Ceci nous a permis d'obtenir un second degré de bioinspiration de notre hydrogel à un cartilage naturel[21]. Afin d'améliorer la ressemblance au cartilage, il serait opportun d'augmenter les propriétés mécaniques de l'hydrogel sans pour autant toucher la structuration du gel par le biais par exemple de post-réticulations.

Les propriétés tribologiques d'un tel hydrogel physique de chitosane bicouche ont été étudiées sur les deux faces (superficielle : SZ et profonde : DZ). L'objectif était de mieux comprendre comment les caractéristiques de ces hydrogels influent la friction et la protection contre

l'usure des surfaces afin de développer des systèmes de lubrification plus performants. Les mécanismes tribologiques mis en jeu en fonction de la force normale et de la vitesse de cisaillement appliquées ont également été étudiés. Les gels de chitosane, globalement neutres, ne présentent pas d'aussi bonnes propriétés tribologiques (CoF de l'ordre de 10^{-1}, dans nos conditions d'études) que d'autres systèmes à base d'hydrogel contenant des zones très hydratées, des polyélectrolytes ou des brosses de polymères ($\mu = 10^{-4}$-10^{-2}) [48-49]. Néanmoins, le CoF de nos hydrogels se rapproche du CoF du cartilage seul ($\mu = 10^{-2}$-10^{-1})[50]. Forster *et al*. ont étudié au cours du temps et dans un milieu tamponné l'évolution du CoF du cartilage de condyle bovin contre un cylindre métallique ou de cartilage[50-52]. Un CoF de ~ 0.01 est initialement mesuré et augmente drastiquement et très rapidement à un CoF ~ 0.1 au bout de 5 min et de ~ 0.3 au bout de 45 min[50], ce qui nous rapproche du frottemement de gels de chitosane seuls. De manière intéressante, il est possible de travailler de manière très précise à différents régimes de lubrification selon la pression, la vitesse de cisaillement et le côté du gel de chitosane exposé. Un régime limite (forces de friction constantes en fonction de la vitesse de glissement) est observable sur la face SZ à faibles vitesses et à hautes pressions tandis qu'un régime mixte (forces de friction diminuant de manière monotone en fonction de la vitesse de glissement) est présent à vitesses plus élevées sur les deux faces[21], ce qui rend ces gels d'excellents modèles tribologiques.

Concernant l'étude d'usure, une méthode quantitative de sa caractérisation à été mise en place par mesure de la topographie et de la rugosité finale des hydrogels. La caractérisation de l'usure des gels est très peu étudiée, d'autant plus que les mécanismes mis en jeu, les propriétés viscoélastiques des substrats et le faible contraste entre l'eau et la matrice polymérique rendent les mesures standards inefficaces. Une fois encore, les gels de chitosane seuls n'offrent pas une grande résistance à l'usure puisque quelques cycles à une pression, P égale à G' suffit à détruire la face DZ et à former de nombreuses marques d'usure sur le côté SZ. La structuration du gel conduit cependant à de grandes disparités de comportement tribologique selon la surface en contact. En effet, la surface DZ, la plus perméable à l'eau et la plus déformable offre une meilleure friction alors que la surface SZ offre une meilleure protection contre l'usure. À l'image des premières couches du cartilage protégeant contre les forces de cisaillement l'intégrité des articulations[53-57], la fine couche SZ protège le gel contre l'usure sans pour autant assurer une bonne lubrification. Toujours en comparaison avec les articulations synoviales, une amélioration de la friction de la face SZ peut émerger de

l'addition d'un fluide lubrifiant immergeant le gel comme nous l'avons abordé à travers l'objectif 3.

Discussions sur le Chapitre IV - Conception et caractérisations d'un fluide lubrifiant bioinspiré pour la lubrification et la protection de l'usure d'hydrogels

*Objectif : améliorer les propriétés de friction **et** de résistance à l'usure du substitut de cartilage par l'ajout du fluide synovial bioinspiré*

Le dernier objectif nous a conduits à reformer une articulation synoviale synthétique inspirée de l'architecture des articulations naturelles. En immergeant les gels de chitosane structurés développés dans notre fluide synovial synthétique, il a été possible de retrouver des propriétés tribologiques des hydrogels proches de celles des articulations avec des CoF de 2.10^{-2} sur une large gamme de pressions et de vitesses de cisaillement (CoF identique à ce qui a été obtenu à l'aide des écouvillons moléculaires physisorbés sur des surfaces de mica à l'aide du SFA) et ce quelque soit la face du gel mis en contact. Les tests d'usure ont montré qu'il était possible de limiter voire prévenir l'usure des hydrogels même à des pressions égales à G'. Dans les articulations synoviales, le cartilage apporte les propriétés mécaniques tandis que le liquide synovial améliore les propriétés tribologiques. D'une manière similaire, la concentration et les conditions de neutralisation des hydrogels (SZ/DZ) conditionnent les propriétés mécaniques des matériaux et l'écouvillon moléculaire supplée par l'HA de haut poids moléculaire permet un ancrage sur la surface du gel et donc apporte de très bonnes propriétés tribologiques. Nous avons ainsi amélioré à la fois la lubrification d'hydrogels de chitosane **et** leur résistance à l'usure en s'inspirant des principales caractéristiques rencontrées dans les articulations synoviales. À notre connaissance, peu d'études sur ce sujet ont montré à la fois une amélioration positive de la friction et de l'usure d'hydrogels[58], et notamment en utilisant un fluide lubrifiant extérieur au gel. En effet, l'amélioration d'une des propriétés tribologiques est souvent au détriment de l'autre. Par exemple, Lin *et al.* ont montré que l'ajout du monomère de chlorure de [2-(méthacryloyloxy)éthyle] trimethylammonium dans la couche superficielle d'un gel d'acrylamide permet de diminuer le CoF de 0.35 à 0.05, mais cette couche est progressivement érodée par quelques milliers de cycles de friction comme le montre des clichés de microscopie électronique[59]. Notre démarche est donc originale et généralisable à divers types de surface (mica, hydrogel, etc.) permettant d'envisager des applications biomédicales très variées.

Références

1. Dedinaite, A., Biomimetic lubrication. *Soft Matter* **2012,** *8* (2), 273-284.
2. Sheiko, S. S.; Sumerlin, B. S.; Matyjaszewski, K., Cylindrical molecular brushes: Synthesis, characterization, and properties. *Progress in Polymer Science* **2008,** *33* (7), 759-785.
3. Banquy, X.; Burdyńska, J.; Lee, D. W.; Matyjaszewski, K.; Israelachvili, J., Bioinspired Bottle-Brush Polymer Exhibits Low Friction and Amontons-like Behavior. *J. Am. Chem. Soc.* **2014,** *136* (17), 6199-6202.
4. Lin, B.; Tieu, A. K.; Zhu, H.; Kosasih, B.; Novareza, O.; Triani, G., Tribological performance of aqueous copolymer lubricant in loaded contact with Si and coated Ti film. *Wear* **2013,** *302* (1), 1010-1016.
5. Lee, S.; Iten, R.; Müller, M.; Spencer, N. D., Influence of Molecular Architecture on the Adsorption of Poly(ethylene oxide)−Poly(propylene oxide)−Poly(ethylene oxide) on PDMS Surfaces and Implications for Aqueous Lubrication. *Macromolecules* **2004,** *37* (22), 8349-8356.
6. Morgenthaler, S.; Zink, C.; Stadler, B.; Voros, J.; Lee, S.; Spencer, N. D.; Tosatti, S. G., Poly(L-lysine)-grafted-poly(ethylene glycol)-based surface-chemical gradients. Preparation, characterization, and first applications. *Biointerphases* **2006,** *1* (4), 156-65.
7. Lee, S.; Spencer, N. D., Adsorption Properties of Poly(l-lysine)-graft-poly(ethylene glycol) (PLL-g-PEG) at a Hydrophobic Interface: Influence of Tribological Stress, pH, Salt Concentration, and Polymer Molecular Weight. *Langmuir* **2008,** *24* (17), 9479-9488.
8. Rosenberg, K. J.; Goren, T.; Crockett, R.; Spencer, N. D., Load-Induced Transitions in the Lubricity of Adsorbed Poly(l-lysine)-g-dextran as a Function of Polysaccharide Chain Density. *ACS Appl. Mater. Interfaces* **2011,** *3* (8), 3020-3025.
9. Morgese, G.; Cavalli, E.; Rosenboom, J.-G.; Zenobi-Wong, M.; Benetti, E. M., Cyclic Polymer Grafts That Lubricate and Protect Damaged Cartilage. *Angewandte Chemie International Edition* **2017**, n/a-n/a.
10. Samaroo, K. J.; Tan, M.; Andresen Eguiluz, R. C.; Gourdon, D.; Putnam, D.; Bonassar, L. J., Tunable Lubricin-mimetics for Boundary Lubrication of Cartilage. *Biotribology* **2017,** *9* (Supplement C), 18-23.
11. Samaroo, K. J.; Tan, M.; Putnam, D.; Bonassar, L. J., Binding and lubrication of biomimetic boundary lubricants on articular cartilage. *J. Orthop. Res.* **2017,** *35* (3), 548-557.
12. Raviv, U.; Frey, J.; Sak, R.; Laurat, P.; Tadmor, R.; Klein, J., Properties and Interactions of Physigrafted End-Functionalized Poly(ethylene glycol) Layers. *Langmuir* **2002,** *18* (20), 7482-7495.
13. Hartung, W.; Rossi, A.; Lee, S.; Spencer, N. D., Aqueous Lubrication of SiC and Si3N4 Ceramics Aided by a Brush-like Copolymer Additive, Poly(l-lysine)-graft-poly(ethylene glycol). *Tribol Lett* **2009,** *34* (3), 201-210.
14. Jahn, S.; Seror, J.; Klein, J., Lubrication of Articular Cartilage. *Annu. Rev. Biomed. Eng.* **2016,** *18* (1), 235-258.
15. Banquy, X.; Lee, D. W.; Das, S.; Hogan, J.; Israelachvili, J. N., Shear-Induced Aggregation of Mammalian Synovial Fluid Components under Boundary Lubrication Conditions. *Adv. Funct. Mater.* **2014,** *24* (21), 3152-3161.
16. Zappone, B.; Ruths, M.; Greene, G. W.; Jay, G. D.; Israelachvili, J. N., Adsorption, lubrication, and wear of lubricin on model surfaces: polymer brush-like behavior of a glycoprotein. *Biophys. J.* **2007,** *92* (5), 1693-1708.
17. Yu, J.; Banquy, X.; Greene, G. W.; Lowrey, D. D.; Israelachvili, J. N., The Boundary Lubrication of Chemically Grafted and Cross-Linked Hyaluronic Acid in Phosphate Buffered Saline and Lipid Solutions Measured by the Surface Forces Apparatus. *Langmuir* **2012,** *28* (4), 2244-2250.
18. Bronzino, J. D.; Schneck, D. J., *Biomechanics: principles and applications*. CRC press: 2002.
19. Faivre, J.; Shrestha, B. R.; Burdynska, J.; Xie, G.; Moldovan, F.; Delair, T.; Benayoun, S.; David, L.; Matyjaszewski, K.; Banquy, X., Wear Protection without Surface Modification Using a Synergistic Mixture of Molecular Brushes and Linear Polymers. *ACS Nano* **2017,** *11* (2), 1762-1769.
20. Faivre, J.; Shrestha, B. R.; Xie, G.; Delair, T.; David, L.; Matyjaszewski, K.; Banquy, X., Unraveling the Correlations between Conformation, Lubrication, and Chemical Stability of Bottlebrush Polymers at Interfaces. *Biomacromolecules* **2017**, 4002-4010.

21. Faivre, J.; Sudre, G.; Montembault, A.; Benayoun, S.; Banquy, X.; Delair, T.; David, L., Bioinspired Microstructures of Chitosan Hydrogel Provide Enhanced Wear Protection. *Soft Matter* **2018**, 2068-2076.
22. Montembault, A.; Tahiri, K.; Korwin-Zmijowska, C.; Chevalier, X.; Corvol, M. T.; Domard, A., A material decoy of biological media based on chitosan physical hydrogels: application to cartilage tissue engineering. *Biochimie* **2006,** *88* (5), 551-564.
23. Ladet, S. G.; Tahiri, K.; Montembault, A. S.; Domard, A. J.; Corvol, M. T. M., Multi-membrane chitosan hydrogels as chondrocytic cell bioreactors. *Biomaterials* **2011,** *32* (23), 5354-5364.
24. Croisier, F.; Jérôme, C., Chitosan-based biomaterials for tissue engineering. *European Polymer Journal* **2013,** *49* (4), 780-792.
25. Rami, L.; Malaise, S.; Delmond, S.; Fricain, J.-C.; Siadous, R.; Schlaubitz, S.; Laurichesse, E.; Amedee, J.; Montembault, A.; David, L.; Bordenave, L., Physicochemical modulation of chitosan-based hydrogels induces different biological responses: Interest for tissue engineering. *Journal of Biomedical Materials Research Part A* **2014,** *102* (10), 3666-3676.
26. Kaderli, S.; Boulocher, C.; Pillet, E.; Watrelot-Virieux, D.; Rougemont, A. L.; Roger, T.; Viguier, E.; Gurny, R.; Scapozza, L.; Jordan, O., A novel biocompatible hyaluronic acid-chitosan hybrid hydrogel for osteoarthrosis therapy. *International journal of pharmaceutics* **2015,** *483* (1-2), 158-68.
27. Mohan, N.; Mohanan, P. V.; Sabareeswaran, A.; Nair, P., Chitosan-hyaluronic acid hydrogel for cartilage repair. *Int. J. Biol. Macromol.* **2017**.
28. Hao, T.; Wen, N.; Cao, J. K.; Wang, H. B.; Lu, S. H.; Liu, T.; Lin, Q. X.; Duan, C. M.; Wang, C. Y., The support of matrix accumulation and the promotion of sheep articular cartilage defects repair in vivo by chitosan hydrogels. *Osteoarthritis and cartilage / OARS, Osteoarthritis Research Society* **2010,** *18* (2), 257-65.
29. Song, K.; Li, L.; Li, W.; Zhu, Y.; Jiao, Z.; Lim, M.; Fang, M.; Shi, F.; Wang, L.; Liu, T., Three-dimensional dynamic fabrication of engineered cartilage based on chitosan/gelatin hybrid hydrogel scaffold in a spinner flask with a special designed steel frame. *Materials science & engineering. C, Materials for biological applications* **2015,** *55*, 384-92.
30. Mao, J.; Zhao, L.; De Yao, K.; Shang, Q.; Yang, G.; Cao, Y., Study of novel chitosan-gelatin artificial skin in vitro. *Journal of biomedical materials research. Part A* **2003,** *64* (2), 301-8.
31. Kim, T. H.; Park, I. K.; Nah, J. W.; Choi, Y. J.; Cho, C. S., Galactosylated chitosan/DNA nanoparticles prepared using water-soluble chitosan as a gene carrier. *Biomaterials* **2004,** *25* (17), 3783-3792.
32. Pickenhahn, V. D.; Darras, V.; Dziopa, F.; Biniecki, K.; De Crescenzo, G.; Lavertu, M.; Buschmann, M. D., Regioselective thioacetylation of chitosan end-groups for nanoparticle gene delivery systems. *Chemical Science* **2015,** *6* (8), 4650-4664.
33. Rinaudo, M., Chitin and chitosan: Properties and applications. *Progress in Polymer Science* **2006,** *31* (7), 603-632.
34. Zhou, Y.; Liedberg, B.; Gorochovceva, N.; Makuska, R.; Dedinaite, A.; Claesson, P. M., Chitosan-N-poly(ethylene oxide) brush polymers for reduced nonspecific protein adsorption. *Journal of Colloid and Interface Science* **2007,** *305* (1), 62-71.
35. Fiamingo, A.; Montembault, A.; Boitard, S.-E.; Naemetalla, H.; Agbulut, O.; Delair, T.; Campana-Filho, S. P.; Menasché, P.; David, L., Chitosan Hydrogels for the Regeneration of Infarcted Myocardium: Preparation, Physicochemical Characterization, and Biological Evaluation. *Biomacromolecules* **2016,** *17* (5), 1662-1672.
36. Greene, G. W.; Zappone, B.; Banquy, X.; Lee, D. W.; Soderman, O.; Topgaard, D.; Israelachvili, J. N., Hyaluronic acid-collagen network interactions during the dynamic compression and recovery of cartilage. *Soft Matter* **2012,** *8* (38), 9906-9914.
37. Haque, M. A.; Kurokawa, T.; Gong, J. P., Super tough double network hydrogels and their application as biomaterials. *Polymer* **2012,** *53* (9), 1805-1822.
38. Matricardi, P.; Di Meo, C.; Coviello, T.; Hennink, W. E.; Alhaique, F., Interpenetrating Polymer Networks polysaccharide hydrogels for drug delivery and tissue engineering. *Advanced Drug Delivery Reviews* **2013,** *65* (9), 1172-1187.

39. Zhang, D.; Shen, Y.; Ge, S., Research on the friction and wear mechanism of Poly(vinyl alcohol)/hydroxylapatite composite hydrogel. *Science in China Series E: Technological Sciences* **2009,** *52* (8), 2474-2480.
40. Holloway, J. L.; Lowman, A. M.; VanLandingham, M. R.; Palmese, G. R., Interfacial optimization of fiber-reinforced hydrogel composites for soft fibrous tissue applications. *Acta Biomaterialia* **2014,** *10* (8), 3581-3589.
41. Chen, K.; Yang, X.; Zhang, D.; Xu, L.; Zhang, X.; Wang, Q., Biotribology behavior and fluid load support of PVA/HA composite hydrogel as artificial cartilage. *Wear* **2017,** *376-377*, 329-336.
42. Chen, K.; Liu, J.; Yang, X.; Zhang, D., Preparation, optimization and property of PVA-HA/PAA composite hydrogel. *Materials Science and Engineering: C* **2017,** *78*, 520-529.
43. Meng, Y.; Ye, L.; Coates, P.; Twigg, P., In Situ Cross-Linking of Poly(vinyl alcohol)/Graphene Oxide–Polyethylene Glycol Nanocomposite Hydrogels as Artificial Cartilage Replacement: Intercalation Structure, Unconfined Compressive Behavior, and Biotribological Behaviors. *The Journal of Physical Chemistry C* **2018**.
44. Sereni, N.; Enache, A.; Sudre, G.; Montembault, A.; Rochas, C.; Durand, P.; Perrard, M. H.; Bozga, G.; Puaux, J. P.; Delair, T.; David, L., Dynamic Structuration of Physical Chitosan Hydrogels. *Langmuir* **2017,** *33* (44), 12697-12707.
45. Nie, J.; Lu, W.; Ma, J.; Yang, L.; Wang, Z.; Qin, A.; Hu, Q., Orientation in multi-layer chitosan hydrogel: morphology, mechanism, and design principle. *Sci. Rep.* **2015,** *5*, 7635.
46. Furusawa, K.; Sato, S.; Masumoto, J.-i.; Hanazaki, Y.; Maki, Y.; Dobashi, T.; Yamamoto, T.; Fukui, A.; Sasaki, N., Studies on the Formation Mechanism and the Structure of the Anisotropic Collagen Gel Prepared by Dialysis-Induced Anisotropic Gelation. *Biomacromolecules* **2012,** *13* (1), 29-39.
47. Hanazaki, Y.; Masumoto, J.-i.; Sato, S.; Furusawa, K.; Fukui, A.; Sasaki, N., Multiscale Analysis of Changes in an Anisotropic Collagen Gel Structure by Culturing Osteoblasts. *ACS Applied Materials & Interfaces* **2013,** *5* (13), 5937-5946.
48. Kaneko, D.; Tada, T.; Kurokawa, T.; Gong, J. P.; Osada, Y., Mechanically Strong Hydrogels with Ultra-Low Frictional Coefficients. *Advanced Materials* **2005,** *17* (5), 535-538.
49. Gong, J. P., Friction and lubrication of hydrogels-its richness and complexity. *Soft Matter* **2006,** *2* (7), 544-552.
50. Forster, H.; Fisher, J., The Influence of Loading Time and Lubricant on the Friction of Articular Cartilage. *Proc. Inst. Mech. Eng., Part H* **1996,** *210* (2), 109-119.
51. Forster, H.; Fisher, J., The influence of continuous sliding and subsequent surface wear on the friction of articular cartilage. *Proceedings of the Institution of Mechanical Engineers. Part H, Journal of engineering in medicine* **1999,** *213* (4), 329-45.
52. Jin, Z. M.; Pickard, J. E.; Forster, H.; Ingham, E.; Fisher, J., Frictional behaviour of bovine articular cartilage. *Biorheology* **2000,** *37* (1-2), 57-63.
53. Buckley, M. R.; Gleghorn, J. P.; Bonassar, L. J.; Cohen, I., Mapping the depth dependence of shear properties in articular cartilage. *Journal of biomechanics* **2008,** *41* (11), 2430-7.
54. Buckley, M. R.; Bergou, A. J.; Fouchard, J.; Bonassar, L. J.; Cohen, I., High-resolution spatial mapping of shear properties in cartilage. *Journal of biomechanics* **2010,** *43* (4), 796-800.
55. Silverberg, J. L.; Dillavou, S.; Bonassar, L.; Cohen, I., Anatomic variation of depth-dependent mechanical properties in neonatal bovine articular cartilage. *Journal of Orthopaedic Research* **2013,** *31* (5), 686-691.
56. Buckley, M. R.; Bonassar, L. J.; Cohen, I., Localization of viscous behavior and shear energy dissipation in articular cartilage under dynamic shear loading. *Journal of biomechanical engineering* **2013,** *135* (3), 31002.
57. Henak, C. R.; Ross, K. A.; Bonnevie, E. D.; Fortier, L. A.; Cohen, I.; Kennedy, J. G.; Bonassar, L. J., Human talar and femoral cartilage have distinct mechanical properties near the articular surface. *Journal of biomechanics* **2016,** *49* (14), 3320-3327.
58. Milner, P. E.; Parkes, M.; Puetzer, J. L.; Chapman, R.; Stevens, M. M.; Cann, P.; Jeffers, J. R. T., A low friction, biphasic and boundary lubricating hydrogel for cartilage replacement. *Acta Biomaterialia* **2018,** *65*, 102-111.
59. Lin, P.; Zhang, R.; Wang, X.; Cai, M.; Yang, J.; Yu, B.; Zhou, F., Articular Cartilage Inspired Bilayer Tough Hydrogel Prepared by Interfacial Modulated Polymerization Showing Excellent

Combination of High Load-Bearing and Low Friction Performance. *ACS Macro Lett.* **2016,** *5* (11), 1191-1195.

Chapitre VI - Conclusions et Perspectives

-Chapitre VI-

Conclusions et Perspectives

Nous nous sommes intéressés au développement et à la caractérisation tribologique de substituts de cartilage et de liquide synoviaux dans l'objectif de trouver des solutions innovantes et originales aux problèmes liés à l'ostéoarthrite. Pour mener à bien ce projet, nous avons fondé notre raisonnement sur la bioinspiration qui consiste à prendre avantage du fonctionnement de systèmes tribologiques naturels et de les retranscrire sous forme de biomatériaux. Ainsi, nous avons développé i) une librairie d'écouvillons moléculaires polymériques, mimes de la lubricine et de l'aggrécane aux propriétés tribologiques remarquables, ii) conçu un hydrogel de chitosane à l'architecture semblable au cartilage et aux propriétés tribologiques originales et enfin iii) réunit ces deux composantes pour développer une articulation synthétique complète, en apportant la preuve de concept de la lubrification de ce modèle articulaire.

Grâce à une conception bioinspirée des polymères, il a été possible d'obtenir des substituts synoviaux synthétiques avec propriétés tribologiques semblables à celle des articulations synoviales, à savoir des CoF de l'ordre de 10^{-2} jusqu'à des pressions supérieures à 14 MPa et à diverses vitesses de cisaillement. Ces polymères peuvent être utilisés en milieu salin et voient leurs performances de résistance à l'usure améliorées en présence de groupements d'ancrage non spécifiques (polycations, liaisons hydrophobes) et la présence de HA de haut poids moléculaire. L'application en "tribo-supplémentation" de ces substituts synoviaux sera validée lorsque sa biocompatibilité et son efficacité auront été testées (annexe 2). S'il fallait améliorer les propriétés tribologiques de ces lubrifiants polymères, ma priorité serait la conception de groupements d'ancrage multiples (à l'aide d'un groupement initiateur d'ATRP multifonctionnel) et la conception de groupements d'ancrage spécifiques (à l'ECM : collagène, HA, etc., ou à d'autres surfaces : prothèses, surfaces chirurgicales, implants). Ceci permettrait d'augmenter l'affinité des polymères avec les surfaces d'étude. Cependant, il parait opportun de ne pas trop bouleverser le groupement central lubrifiant zwitterrionique, car celui-ci permet de garantir un faible CoF et de résister aux fortes concentrations salines du fait de sa neutralité globale et de la grande hydratation grâce aux charges locales.

Afin d'apprécier l'étendue des applications biomédicales possibles, il est opportun de s'intéresser, par exemple, aux applications de la lubricine. Aujourd'hui, la lubricine humaine

purifiée ou recombinante est utilisée en recherche, en préclinique et en clinique pour divers traitements. En effet, le traitement de nombreuses pathologies nécessite de rétablir une concentration saine de ce protéoglycane dans toutes les muqueuses. De plus, ce protéoglycane peut être utilisé pour hydrater, protéger contre l'usure, empêcher l'adsorption de protéines et de pathogènes (*antifouling*) sur des surfaces et lubrifier les surfaces biologiques. La lubricine apparait également comme un excellent traitement de "tribo-supplémentation"[1] chez le rat. Une solution ophtalmique de lubricine pour le traitement du syndrome des yeux secs (Lubris BioPharma LLC, USA) est en étude clinique de phase 2[2] et la lubricine est envisagée dans des lentilles cornéennes de nouvelle génération permettant un confort et une longévité augmentée[3-5]. D'autres traitements sont envisagés comme le traitement de la xérostomie, ou la cystite interstitielle. Nos écouvillons pourraient être utilisés pour toutes ces applications en évitant une éventuelle immunogénicité. Ils permettraient également de remplacer les mucines non synthétisées ou de compenser leur dégradation lors de pathologies puisque certains motifs de protéoglycanes sont sélectivement dégradés lors d'épisodes inflammatoires. Des traitements de surface antimicrobiens sont également une application prometteuse aux écouvillons moléculaires. Une étude récente menée par des collègues de l'Université de Tianjin et au sein du laboratoire du Pr Xavier Banquy a mis en évidence ces propriétés en revêtant des surfaces de silice par nos écouvillons moléculaires (article en cours de soumission). L'efficacité des mimes polymériques pour éviter l'adsorption de protéines (albumine, lysozyme, β-lactoglobuline) et de bactéries (*E.Coli*) a été démontrée sur des surfaces de silice, sur une gamme de pH allant de pH 2 à 8 et en présence de sel. Par simple trempage durant 30 minutes de la surface de silice dans une solution contenant le polymère, le revêtement est opérationnel. Ce revêtement pourrait être utilisable, par exemple, sur des instruments chirurgicaux comme les endoscopes. Avant de développer ces applications biomédicales, il faudra toutefois étudier les propriétés pharmacocinétiques de nos écouvillons moléculaires par différentes études in vitro et précliniques in vivo. Le plus grand questionnement reste, en effet, la stabilité du polymère en milieu inflammatoire. Des études préliminaires *in vivo* ont d'ores et déjà été effectuées en collaboration avec le Pr Florina Moldovan de l'hôpital Sainte Justine de Montréal et la compagnie Biomomentum Inc. (Laval, Canada) afin d'évaluer l'efficacité de notre fluide lubrifiant bioinspiré à ralentir l'avancée de l'OA chez le rat arthrosique (voir Annexe 2).

Dans le cadre de ce travail, pour la fabrication d'hydrogels multicouches, l'objectif était de développer un modèle reprenant des aspects structuraux du cartilage afin d'étudier son

comportement tribologique. La fabrication en une étape de gels de chitosane bicouches a permis d'obtenir une fine membrane superficielle (SZ) isotrope et dense, couvrant un volume plus perméable traversé par des microcanaux (DZ). Les propriétés tribologiques de tels gels sont gouvernées par la face exposée au contact. Ainsi, un contact DZ/DZ donne lieu a une diminution de la friction par rapport au contact SZ/SZ à partir d'une pression critique qui implique la fermeture des pores et l'exsudation de l'eau au niveau du contact. La fermeture des microcanaux et de la porosité s'accompagne du piégeage des macromolécules qui, à l'instar des complexes aggrécane-HA, pourraient augmenter la pression osmotique du substrat poroélastique. L'usure des hydrogels est également dictée par la structure de matériau constituant la tribopaire, car une structure hydrogel plus dense avec une aire de contact plus importante (côté SZ) donne lieu à moins d'usure qu'une face perméable (DZ) plus poreuse et rugueuse. Nous avons pu ainsi vérifier que friction et usure n'étaient pas des paramètres systématiquement reliés, contrairement au sens commun. De ce fait, il est important de savoir quel paramètre a le plus d'importance clinique (diminution de la friction, protection contre l'usure ou les deux en même temps) pour concevoir des matériaux et dispositifs adaptés à l'application envisagée.

La caractérisation approfondie des hydrogels physiques de chitosane ainsi que leur emploi original dans une étude tribologique ont montré qu'ils étaient des modèles tribologiques intéressants. Pour passer à une application concrète en ingénierie tissulaire de mosaicplastie (hydrogels utilisés comme substituts cartilagineux induisant la régénération du cartilage), l'idée principale serait d'améliorer les propriétés mécaniques des hydrogels tout en conservant leurs propriétés biologiques, de transport de fluide et tribologiques, peut-être en utilisant une réticulation ou un renfort de l'hydrogel. Une autre alternative également inspirée des articulations serait l'incorporation de macromolécules chargées, tels l'aggrécane ou nos écouvillons moléculaires directement au sein de la matrice hydrogel lors de la fabrication des gels. En effet, le piégeage de ces macromolécules fait augmenter la pression osmotique du cartilage[6] lorsque l'eau est chassée sous contrainte. L'application d'une contrainte et le début de l'usure pourraient aussi libérer des molécules lubrifiantes ce qui pourrait stopper et prévenir l'usure. Pratiquement, nous savons que notre écouvillon polymère résiste à une large plage de pH (entre pH 2 et 8, article en cours de soumission) ce qui permettrait de fabriquer nos hydrogels enrichis par le même procédé de gélification en ajoutant dans la solution acide de chitosane, l'écouvillon moléculaire. Par ailleurs, l'ajout de HA de haut poids moléculaire dans la solution de chitosane peut être effectuée par desalination[7].

La réunion d'un substrat hydrogel multicouche avec un liquide synovial synthétique a permis l'élaboration d'une articulation synthétique modèle. Il a été montré que la lubrification en film mince dépendait de la structuration des hydrogels et de la composition du fluide. Ainsi, le côté DZ imbibé dans du HA de haut poids moléculaires et à haute concentration, similaire aux conditions physiologiques, montre des propriétés lubrifiantes proches de celles des articulations saines contrairement au côté SZ moins perméable. Cependant, l'ajout d'écouvillon moléculaire a permis de diminuer le CoF du côté SZ vers des valeurs identiques au côté DZ, tout en améliorant drastiquement la résistance à l'usure des substrats hydrogels jusqu'à des pressions qui impliquent normalement leur destruction. Une étude plus fondamentale pourrait s'intéresser à la mécanistique de la lubrification de substituts porélastiques en localisant les macromolécules impliquées dans le matériau hydrogel sous contraintes et leur biodistribution dans l'hydrogel et le contact. En étudiant la localisation du HA et d'un écouvillon moléculaire, tous deux fluorescents, dans un hydrogel par microscopie confocale à fluorescence, il serait possible de comprendre comment ces macromolécules s'organisent de manière passive, puis sous contraintes normales et en cisaillement.

Finalement, un projet a été initié depuis février 2018 sur la fabrication de mimes polymériques de la lubricine, synthétisés cette fois-ci à partir d'un squelette de polysaccharide fonctionnalisé. L'objectif est de développer des boucles de polymères très hydratées, solubles à tout pH et en milieu salin, réalisables en très peu d'étapes de synthèses et avec des produits peu chers et biocompatibles. Les groupements d'ancrage peuvent être adaptés pour être spécifiques aux tribo-paires. Ces polyélectrolytes sont utilisables soit par dépôt d'une goutte de solution de polymère sur les tribo-paires ou directement intégrés dans un hydrogel pour en améliorer les propriétés tribologiques. Les tests tribologiques sont à ce jour en cours.

Références

1. Jay, G. D.; Fleming, B. C.; Watkins, B. A.; McHugh, K. A.; Anderson, S. C.; Zhang, L. X.; Teeple, E.; Waller, K. A.; Elsaid, K. A., Prevention of cartilage degeneration and restoration of chondroprotection by lubricin tribosupplementation in the rat following anterior cruciate ligament transection. *Arthritis and rheumatism* **2010,** *62* (8), 2382-91.
2. Lambiase, A.; Sullivan, B. D.; Schmidt, T. A.; Sullivan, D. A.; Jay, G. D.; Truitt, E. R., 3rd; Bruscolini, A.; Sacchetti, M.; Mantelli, F., A Two-Week, Randomized, Double-masked Study to Evaluate Safety and Efficacy of Lubricin (150 mug/mL) Eye Drops Versus Sodium Hyaluronate (HA) 0.18% Eye Drops (Vismed(R)) in Patients with Moderate Dry Eye Disease. *Ocul Surf* **2017,** *15* (1), 77-87.
3. Samsom, M. L.; Morrison, S.; Masala, N.; Sullivan, B. D.; Sullivan, D. A.; Sheardown, H.; Schmidt, T. A., Characterization of full-length recombinant human Proteoglycan 4 as an ocular surface boundary lubricant. *Exp. Eye Res.* **2014,** *127*, 14-9.
4. Samsom, M.; Iwabuchi, Y.; Sheardown, H.; Schmidt, T. A., Proteoglycan 4 and hyaluronan as boundary lubricants for model contact lens hydrogels. *J. Biomed. Mater. Res. B Appl. Biomater.* **2017**, 1329-1338.
5. Samsom, M.; Korogiannaki, M.; Subbaraman, L. N.; Sheardown, H.; Schmidt, T. A., Hyaluronan incorporation into model contact lens hydrogels as a built-in lubricant: Effect of hydrogel composition and proteoglycan 4 as a lubricant in solution. *J. Biomed. Mater. Res. B Appl. Biomater.* **2017**.
6. Lai, W. M.; Hou, J. S.; Mow, V. C., A triphasic theory for the swelling and deformation behaviors of articular cartilage. *Journal of biomechanical engineering* **1991,** *113* (3), 245-58.
7. Costalat, M.; Alcouffe, P.; David, L.; Delair, T., Macro-hydrogels versus nanoparticles by the controlled assembly of polysaccharides. *Carbohydrate Polymers* **2015,** *134*, 541-546.

Annexe 1 - Techniques expérimentales

-Annexe 1-

Techniques expérimentales

L'appareil de forces de surface (SFA)

Le SFA permet la mesure de forces d'interactions, F(D), entre deux surfaces composées généralement de mica épais de quelques microns collés sur des cylindres en verre entrecroisés et séparés d'une distance D[1-3]. Le mica est utilisé pour ces propriétés optiques intéressantes et car il est atomiquement plan. Grâce à cet appareil, il est possible de mesurer directement la résultante des forces d'interaction par le biais d'un ressort de raideur connue, la distance de séparation avec une précision subnanométrique (± 0.2 nm) et l'aire de contact grâce à une méthode interférométrique. Un faisceau de lumière blanche est dirigé perpendiculairement aux deux cylindres entrecroisés (Fig. A.1 et A.2). Les deux surfaces de mica sont revêtues d'une mince couche d'argent (face non exposée au contact) créant ainsi une chambre d'interférence par réflexions multiples. Le faisceau de lumière est ensuite dirigé dans un spectromètre qui permet, par diffraction, d'obtenir des franges d'interférence d'ordre chromatique égal (FECO) sur une caméra[4-5]. Les FECO représentent directement la topographie de la surface (Fig. A.3).

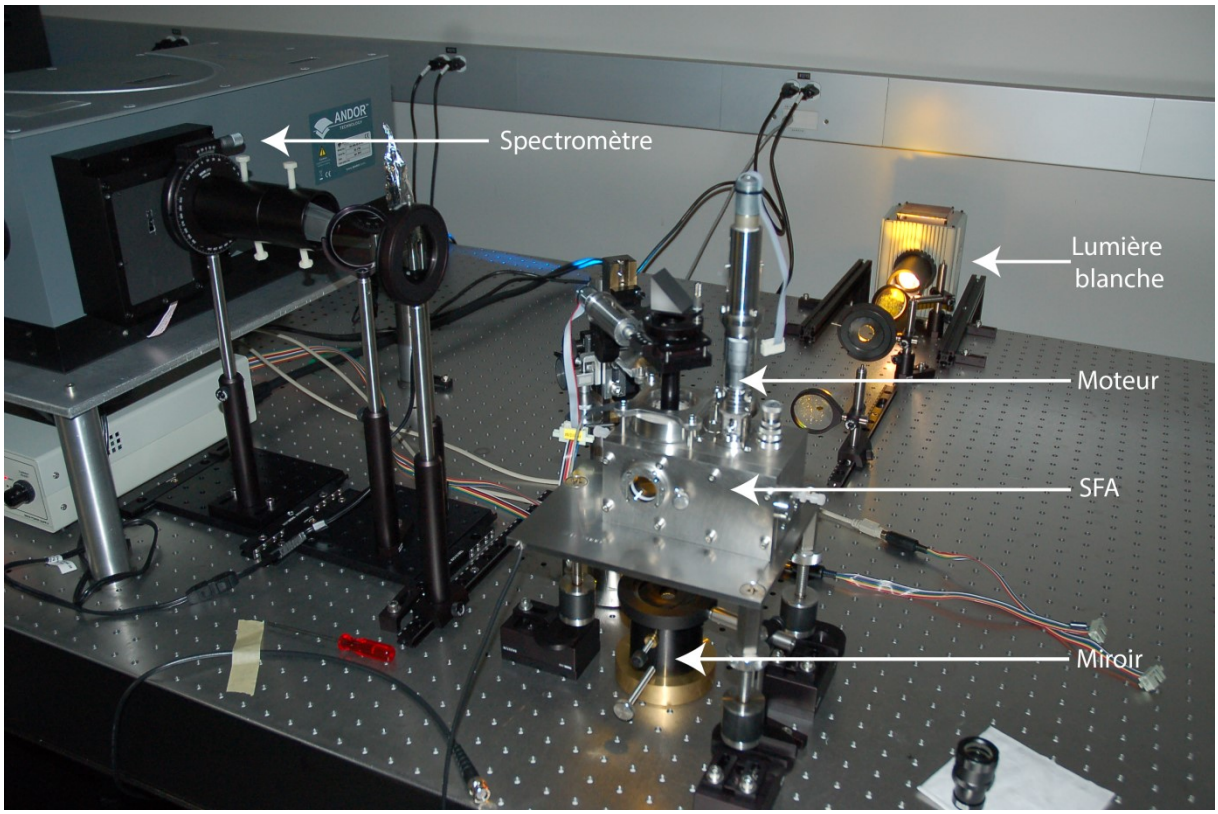

Figure A.1. *Photographie du montage de l'appareil de forces de surface (SFA 2000) utilisé lors de ces travaux de thèse.*

Pratiquement, les forces d'interaction, $F(D)$, sont mesurées à partir de $F(D) = 0$, pour des D très grands en supposant qu'à D très grand, il n'y a plus d'interaction entre les deux surfaces (intervalle utile : de quelques millimètres jusqu'au contact moléculaire). Au cours de la mesure, la surface mobile inférieure se rapproche tout d'abord linéairement de la surface immobile supérieure à une vitesse constante de l'ordre de quelques nm/s à quelques mm/s, contrôlée par un moteur mécanique ou piézoélectrique, tant qu'il n'y a pas d'interactions (D diminue) (Fig. A.2). À partir d'une certaine distance, nommée D_{onset}, des forces d'interaction commencent à intervenir aboutissant à une déflexion du ressort portant la surface inférieure : c'est la portée des interactions de notre système. Cette déflexion peut rapprocher les surfaces plus rapidement que la consigne attribuée au moteur, on a alors une force globale adhésive. Dans le cas inverse, si les surfaces se rapprochent moins vite que la consigne attribuée au moteur, on a une force globale répulsive La distance à laquelle D = 0 est déterminée dans une enceinte balayée d'azote avec les surfaces de mica pures avant introduction de l'échantillon à étudier. L'échantillon peut être :

- introduit directement au niveau du contact

- introduit par immersion complète de la chambre de mesure du SFA

- greffé sur les surfaces de mica par greffage physique ou chimique.

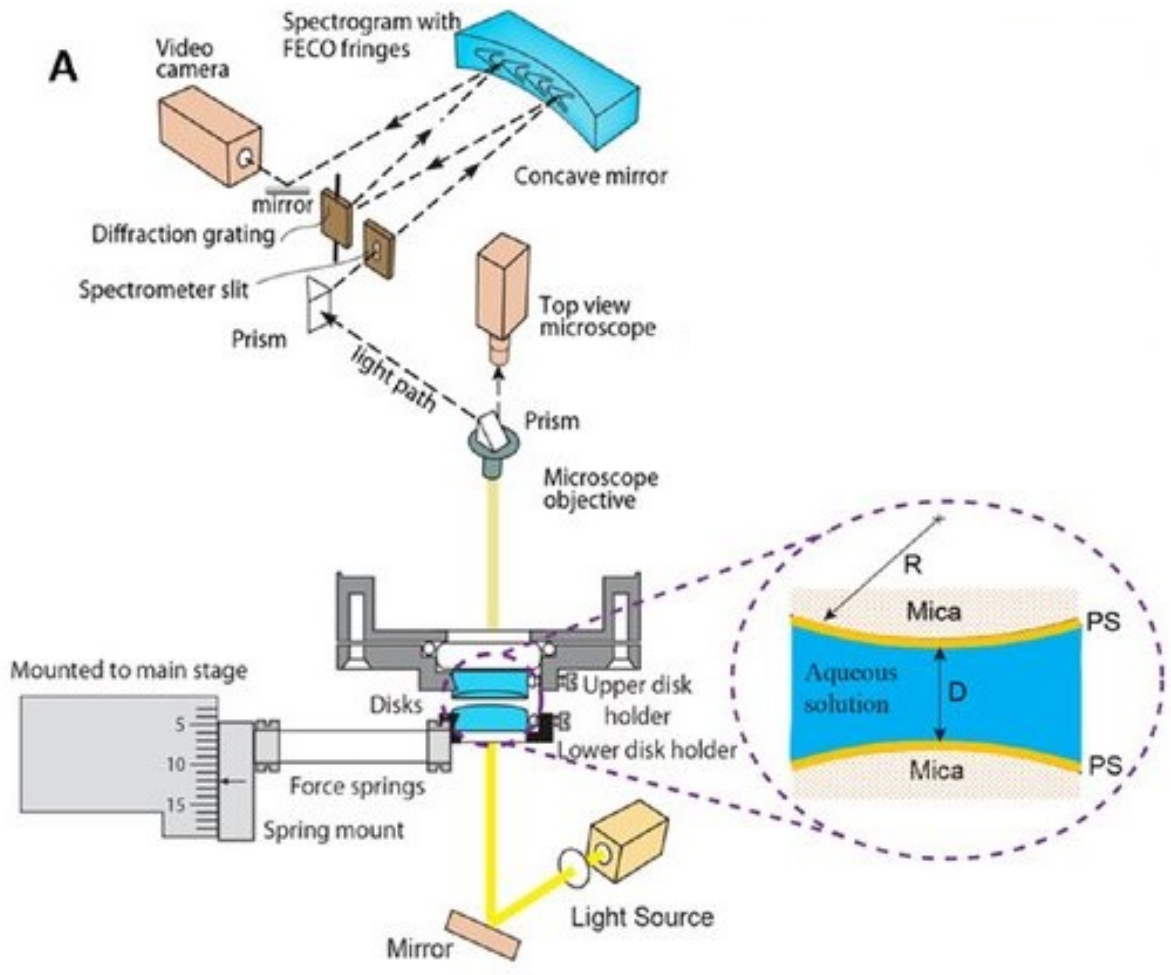

Figure A.2. *Schéma du SFA tiré de la référence[6].Un faisceau de lumière blanche est dirigé perpendiculairement aux cylindres entrecroisés sur lesquels des surfaces de mica argenté sont collées. Les réflexions multiples dans la chambre d'interférence sont dirigées dans un spectromètre où la mesure précise de la longueur d'onde des FECO est prise.*

La distance de séparation D est obtenue par le biais de l'équation 1[1]:

$$tan\left(\frac{2\pi\mu D}{\lambda_n^D}\right) = \frac{2\overline{\mu}\, sin\left[\dfrac{1-\frac{\lambda_n^0}{\lambda_n^D}}{1-\frac{\lambda_n^0}{\lambda_{n-1}^0}}\,\pi\right]}{\left(1+\overline{\mu}^2\right)cos\left[\dfrac{1-\frac{\lambda_n^0}{\lambda_n^D}}{1-\frac{\lambda_n^0}{\lambda_{n-1}^D}}\,\pi\right] \pm (\overline{\mu}^2-1)} \qquad \text{(Eq. 1)}$$

avec $\overline{\mu}$ = μ_{mica} / μ, où μ_{mica} représente l'indice de réfraction du mica à la longueur d'onde λ_n^D et μ, l'indice de réfraction du milieu entre les deux surfaces à la longueur d'onde λ_n^D. Le signe $\pm$ se réfère aux franges impaires (ordre n) et paires (ordre n-1), respectivement. Les exposants 0 et D se reportent aux longueurs d'onde lorsque les surfaces sont en contact ou séparées d'une distance D, respectivement.

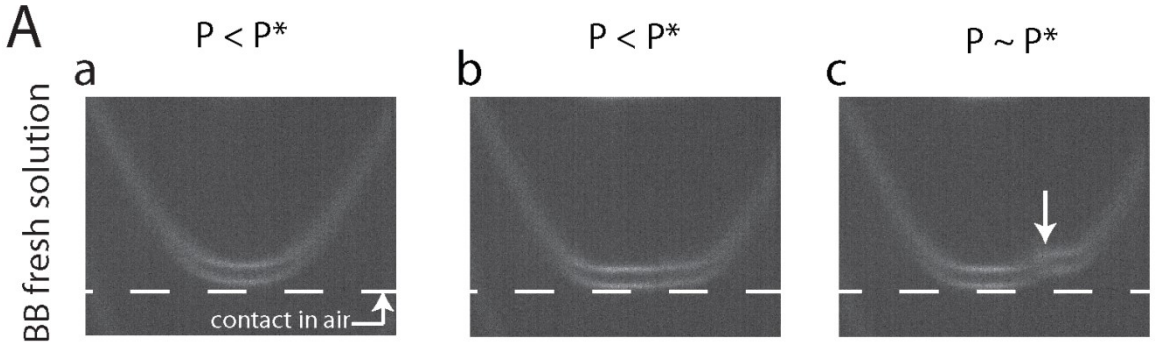

Figure A.3. *Le système étudié est un contact mica-mica en présence de polymère BB. (a) À faible pression, les deux surfaces se rapprochent, mais la frange conserve sa forme arrondie, ce qui signifie que le mica ne s'est pas déformé et qu'il n'y a pas de contact. (b) La pression est plus grande et le mica se déforme, néanmoins, la frange n'est pas superposée à la ligne blanche ce qui signifie qu'il y a contact des deux surfaces de mica sur une couche très mince de matériel polymérique (de l'ordre de quelques nanomètres). La ligne pointillée représente la position de la frange d'interférence lors du contact mica/mica, D = 0. (c) A haute pression, le film de polymères BB rompt et endommage les surfaces de mica aboutissant à de l'usure (marqué par une flèche blanche). Franges issues de la référence*[7].

Afin de faciliter l'estimation de la force d'interaction entre deux surfaces, la géométrie composée de deux cylindres entrecroisés permet de relier directement la force *F*(D) à l'énergie de surface *E*(D) mesurée entre deux plans à la distance de séparation D. La relation, appelée approximation de Derjaguin, s'écrit :

$$F(\mathrm{D}) = 2\pi \mathrm{R}\, E(\mathrm{D}) \qquad \text{(Eq. 2)}$$

avec R, le rayon moyen des cylindres utilisés (généralement de rayon R = 2 cm).

Ainsi, il est possible d'obtenir graphiquement l'énergie de surface entre les deux surfaces d'étude en reportant le rapport F(D)/R, permettant ainsi de comparer les résultats avec d'autres techniques expérimentales.

La SFA permet également l'étude tribologique d'un échantillon entre les deux surfaces de mica. Un moteur piézoélectrique met en mouvement la surface inférieure dans un mouvement de va-et-vient à une fréquence fixée. La force de friction, F_t, transmise de la surface inférieure à la surface supérieure est détectée par des jauges de contrainte placées au niveau du support de la surface supérieure immobile. La force normale, F_N, est mesurée par la déflexion du ressort de la surface inférieure grâce à des capteurs de force. Les forces et la distance de séparation des surfaces sont enregistrées simultanément. Il est alors possible de remonter au coefficient de friction, $\mu = F_t / F_N$, à la pression $P = F_N / S$, avec S, l'aire de contact, à la topographie du contact et la visualisation de l'usure obtenue par les FECO.

Le tribomètre faible charge

Dans le cadre de ce projet de thèse, une collaboration a été mise en place avec le LTDS à l'École Centrale de Lyon avec le Pr Stéphane Benayoun afin de caractériser tribologiquement les substituts hydrogels accompagnés des fluides synoviaux synthétiques. Avec l'aide de Matthieu Guibert (LTDS), un tribomètre appliquant de faibles forces normales a été développé pour caractériser plus finement ces matériaux viscoélastiques fragiles en totale immersion (Fig. A.4) comme pourrait l'être une articulation. Le support supérieur est relié par des ressorts de faibles raideurs à des moteurs permettant des mouvements latéraux et verticaux à vitesses constantes. La partie inférieure immobile est composée d'un bain d'immersion, permettant de travailler dans un liquide, monté sur des capteurs d'efforts latéraux et de force normale permettant la mesure simultanée de F_t et F_N grâce à un logiciel LabVIEW® développé au LTDS. Ce tribomètre nous permet de travailler sur des gammes de forces normales entre 0.05 et 10 N et des vitesses de cisaillement allant de 0.01 à 100 mm/s. Du fait du caractère viscoélastique des hydrogels, sous cisaillement et contrainte, ils se déforment en permanence, changeant ainsi significativement la force normale appliquée initialement. Afin de garantir une force normale constante durant l'analyse, le support

supérieur est asservi pour s'ajuster en tout temps à une valeur consigne de force normale transmise au support inférieur.

Pour étudier un contact gel-gel plan, un des gels possède un diamètre inférieur à l'autre afin d'avoir une course gel-gel en tout temps. L'alignement des deux gels est effectué par contact des deux surfaces et ajustement d'une rotule du support supérieur. Pratiquement, le gel de faible diamètre est collé (glue Loctite Powerflex 3) sur le support en aluminium de la partie supérieure et le gel plus large est collé dans le bain d'immersion. Les surfaces sont préalablement légèrement asséchées du côté non étudié avec un Kimwipe® avant d'être collées. Les surfaces sont laissées à reposer durant une dizaine de secondes avant d'être immergées dans le bain d'immersion.

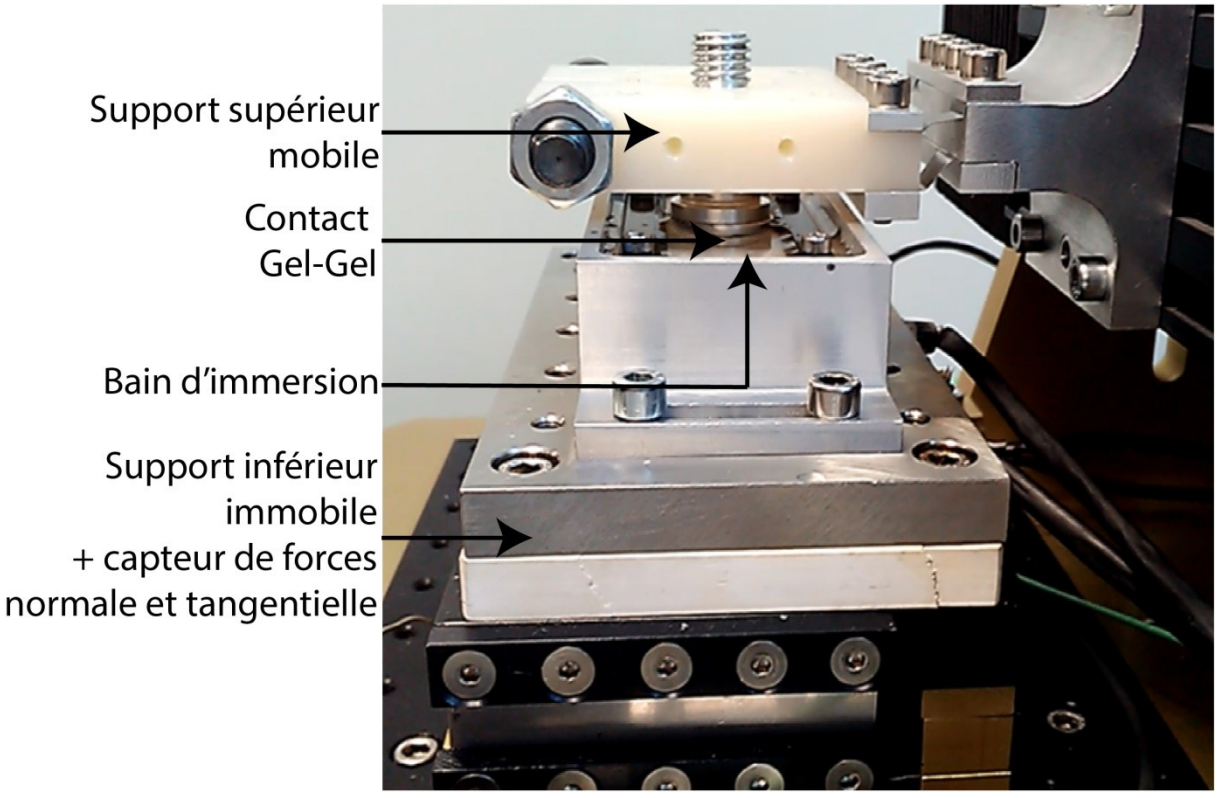

Figure A.4. *Photographie du tribomètre faible charge conçu au LTDS et utilisé lors de ces travaux de thèse.*

Références

1. Israelachvili, J. N., Thin film studies using multiple-beam interferometry. *J. Colloid Interface Sci.* **1973,** *44* (2), 259-272.
2. Israelachvili, J.; Min, Y.; Akbulut, M.; Alig, A.; Carver, G.; Greene, W.; Kristiansen, K.; Meyer, E.; Pesika, N.; Rosenberg, K.; Zeng, H., Recent advances in the surface forces apparatus (SFA) technique. *Rep. Prog. Phys.* **2010,** *73* (3).
3. Israelachvili, J. N.; McGuiggan, P. M., Adhesion and short-range forces between surfaces. Part I: New apparatus for surface force measurements. *J. Mater. Res.* **1990,** *5* (10), 2223-2231.
4. Heuberger, M.; Luengo, G.; Israelachvili, J., Topographic Information from Multiple Beam Interferometry in the Surface Forces Apparatus. *Langmuir* **1997,** *13* (14), 3839-3848.
5. Tadmor, R.; Chen, N.; Israelachvili, J. N., Thickness and refractive index measurements using multiple beam interference fringes (FECO). *Journal of Colloid and Interface Science* **2003,** *264* (2), 548-553.
6. Xie, L.; Shi, C.; Cui, X.; Zeng, H., Surface Forces and Interaction Mechanisms of Emulsion Drops and Gas Bubbles in Complex Fluids. *Langmuir* **2017,** *33* (16), 3911-3925.
7. Faivre, J.; Shrestha, B. R.; Xie, G.; Delair, T.; David, L.; Matyjaszewski, K.; Banquy, X., Unraveling the Correlations between Conformation, Lubrication, and Chemical Stability of Bottlebrush Polymers at Interfaces. *Biomacromolecules* **2017**.

Annexe 2 - Études préliminaires *in vitro* et *in vivo*

-Annexe 2-

Études préliminaires *in vitro* et *in vivo*

Des études préliminaires de cytotoxicité *in vitro* et d'efficacité *in vivo* ont été effectuées au cours de ce projet. Ces études sont toujours en cours au moment de l'écriture et ne sont pas encore formatées pour être présentées dans le corps de ce manuscrit.

Études in vitro

Des études de cytotoxicité de notre fluide lubrifiant bioinspiré ont été effectuées sur des ostéoblastes, synoviocytes, et des chondrocytes humains, d'un patient atteint d'arthrose. Les cellules ont été cultivées dans des plaques multipuits puis incubées durant 48 h avec les différents polymères du fluide lubrifiant : 1.5 MDa HA à 1 mg/mL, le polymère BB sans groupement d'ancrage à 100 µg/mL et un mélange de ces deux polymères aux mêmes concentrations. Le test a été répété de 3 à 6 fois pour chaque système. Un dosage de la lactate dihydrogénase (LDH), permettant d'évaluer la lyse des cellules (Fig. B.1), et un dosage au sel de tétrazolium (MTT), permettant d'observer l'activité cellulaire (Fig. B.2), ont été effectués.

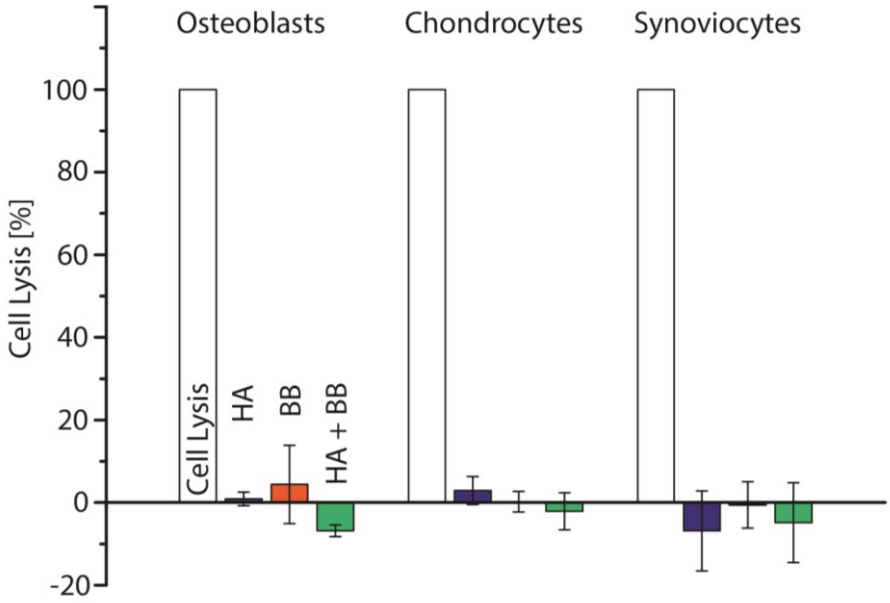

Figure B.1. *Résultats du test LDH de cytotoxité sur 3 lignées de cellules différentes incubées avec HA (bleu), BB (orange) et un mélange HA+BB (vert).*

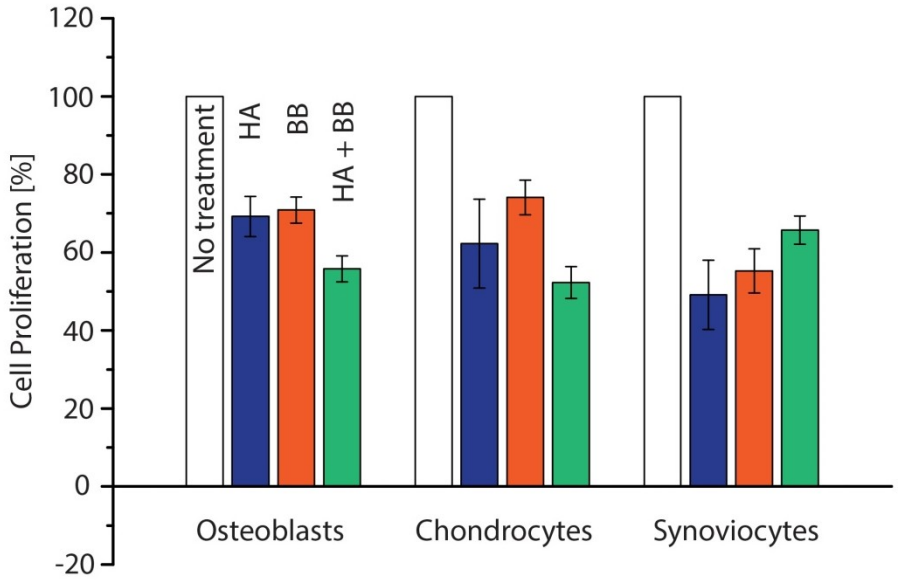

Figure B.2. *Résultats du test MTT mesurant l'activité cellulaire sur 3 lignées de cellules différentes incubées avec HA (bleu), BB (orange) et un mélange HA+BB (vert).*

Les résultats du test LDH indiquent que les polymères testés n'induisent par de mort cellulaire après incubation de 48 h sur les trois différentes lignées cellulaires.

Les résultats du test MTT montrent que les 3 systèmes polymériques HA, BB et HA+BB possèdent les mêmes effets sur l'activité mitochondriale des cellules testées. Ainsi BB et BB+HA ne n'interfèrent pas plus sur l'activité des cellules que HA qui est une molécule naturellement présente dans le corps et est utilisée cliniquement dans divers traitements comme la viscosupplémentation. La différence systématique d'environ 30-40 % entre les polymères et le contrôle sans traitement est expliquée par le fait que les polymères, dissous dans une solution isotonique, ont introduit, de par leurs charges, des ions supplémentaires (sodium hyaluronate et chaines polyzwitterioniques), rendant la solution hypertonique. Cette solution hypertonique a donc certainement contrarié l'activité mitochondriale des cellules.

Études in vivo

Des tests d'efficacité préliminaires chez le rat ont été menés en collaboration avec le laboratoire de Pr Moldovan de l'hôpital Ste Justine et l'entreprise Biomomentum Inc. avec l'aide du Dr Éric Quenneville et Dr Sotcheadt Sim. Le jour 0, l'OA a été induite dans les genoux gauches de rats Lewis adultes mâles par ACLT (CHI) selon une procédure publiée[1]. Les genoux droits n'ont pas été opérés (CTL) pour comparer les deux articulations. Un groupe contrôle sans opération chirurgicale a fait parti de l'étude. Après une semaine de convalescence (J+7) durant laquelle l'OA s'est initiée, une première injection intra-articulaire

de 50 µL de HA ou HA+BB a été effectuée sous anesthésie à l'isoflurane. Les solutions de polymères ont été préparées à 1 mg/mL de 1.5 MDa HA et 100 µg/mL de BB dans du 10mM PBS, 150 mM NaCl pH 7.4 et stérilisées. L'opération a été renouvelée à J+14. À J +30, les animaux ont été euthanasiés sous anesthésie. Les articulations du genou ont été analysées par microtomographie pour mesurer l'espace interosseux (Fig. B.4). Les pattes ont ensuite été méticuleusement disséquées pour analyse des condyles (fémurs) par machine d'indentation-compression en aveugle (Mach-1, Biomomentum Inc., Laval, Canada). Cette technique permet de faire une cartographie très précise en module élastique du cartilage, qui sonde l'intégrité du cartilage, et en épaisseur du cartilage[2]. Le condyle est tout d'abord photographié et des références sont placées afin de faire correspondre l'image aux cartographies en module ou en épaisseur. Une cinquantaine de points sont définis sur le cartilage pour l'indentation. L'appareil va tout d'abord mesurer la courbure de l'échantillon en sondant 4 points autour du point de mesure afin de corriger la courbure dans le calcul du module. Ensuite, l'indenteur (de diamètre 0.25 mm) mesure le module du cartilage à ce point et répète l'opération sur toute la surface (Fig. B.3).

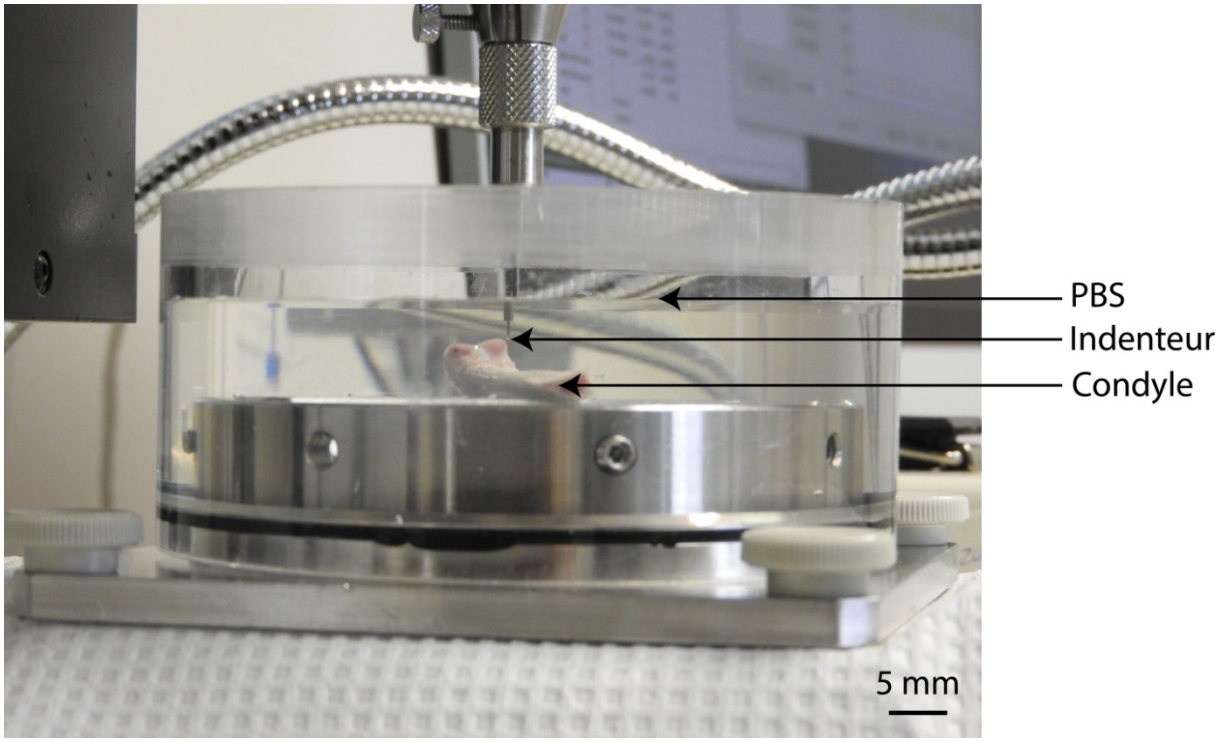

Figure B.3. *Photographie du montage d'indentation-compression pour la lecture du module élastique de condyles de rats.*

L'indenteur est ensuite remplacé par une aiguille très fine qui va permettre la mesure de l'épaisseur du cartilage à chaque point d'indentation. Lorsque l'aiguille pénètre le cartilage, un premier changement de pente sur la force selon l'axe vertical est mesuré. Lorsque l'aiguille pénètre l'os, qui possède un module plus élevé que le cartilage, un second changement de pente apparait. La distance parcourue verticalement corrigée par la courbure de l'échantillon en ce point permet une mesure précise de l'épaisseur. Les articulations sont ensuite fixées dans le paraformaldéhyde à 0.4 % puis décalcifiées (RDO Rapid Decalcifier) avant montage dans un bloc de paraffine pour analyses histologiques. Des coupes de 5 µm d'épaisseur colorées à la Safranine O qui colore les protéoglycanes en rouge, au Fast Green FCF qui colore les protéines en vert et au kit d'hématoxyline de fer Weigert qui colore les noyaux en noir ont été effectuées et montées à l'aide de Permount (Fig. B.4). Ces coupes ont été analysées au microscope optique. Des tests ultérieurs d'immunohistochimie sont également en cours concernant la détection de collagène de type II et d'autres molécules d'intérêt.

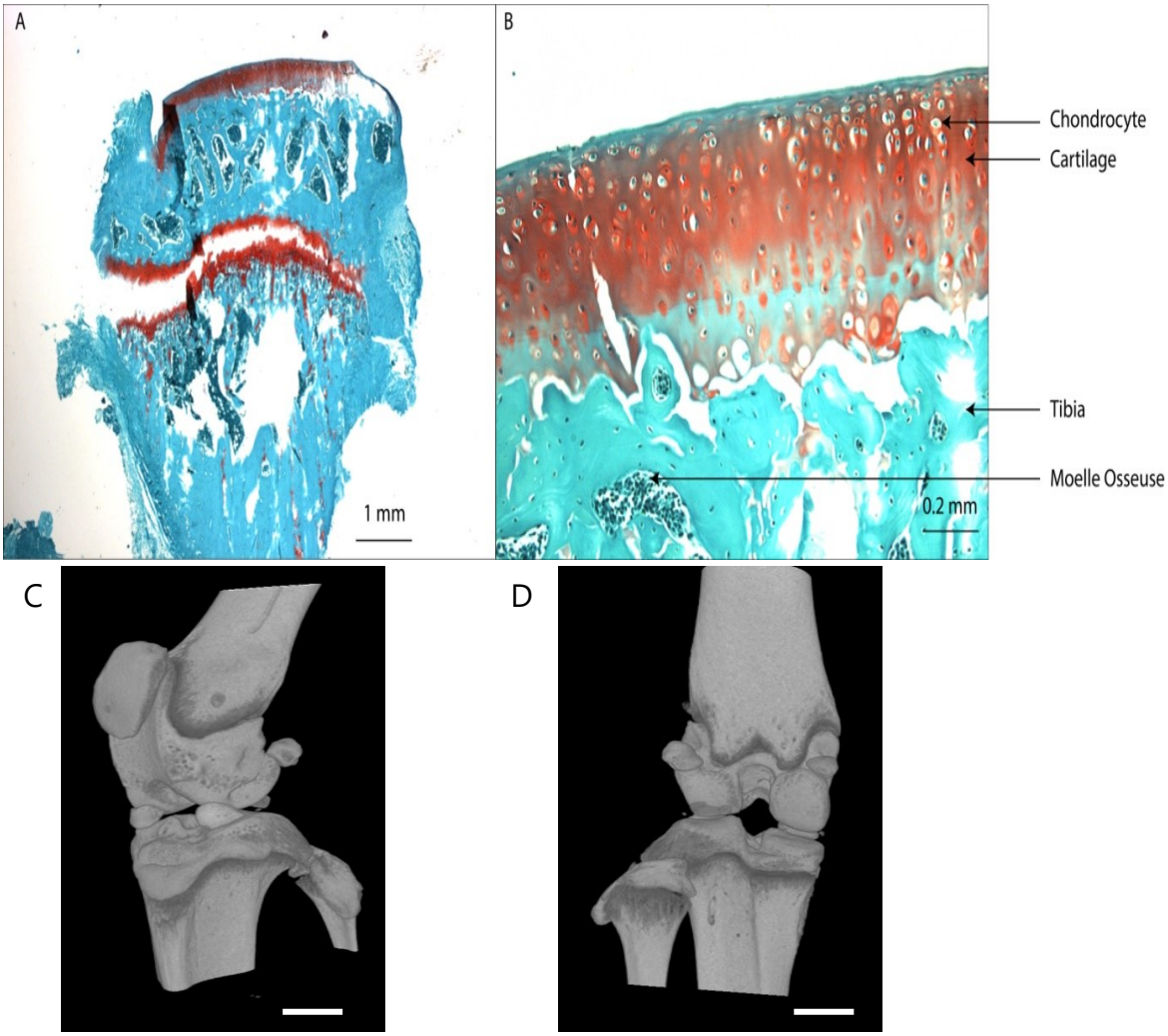

Figure B.4. *Photographie au microscope optique d'un plateau tibial de rat montrant les*

différentes colorations obtenues. (A) photographie d'un plateau complet montrant l'os en bleu, le cartilage (riche en protéoglycane) sur la partie supérieure ainsi que la zone de croissance au milieu de l'os.Les amas de cellules foncées constituent la moelle osseuse, (B) grossissement de 10 fois de l'image (A) montrant les chondrocytes organisés dans le cartilage. (C) Image en microtomographie de l'avant d'une articulation du genou pris de 3/4 face. La partie supérieure est le fémur avec la rotule, la partie inférieure est le tibia et le péroné. Le cartilage n'étant pas visualisé aux rayons X, cette technique permet la mesure de la distance interosseuse et l'observation du rétrécissement du cartilage comme dans le cas de l'OA. (D) Image en microtomographie de la même articulation prise à l'arrière de l'articulation. La barre d'échelle représente 2 mm.

Les résultats sont en cours de mesure pour l'histologie et de traitement pour la microtomographie et l'indentation-compression au sein du laboratoire du Pr Moldovan. Les résultats préliminaires en indentation-compression montre que le cartilage de fémur de rat est épais de ~ 100 µm et possède un module élastique moyen de 2.4 ± 1.4 MPa. La figure B.5 A montre que les condyles en position médiale postérieure (mpc) pour le traitement avec HA seul et sans traitement (voire la figure B.5 B) sont des zones aux modules élastiques beaucoup plus faibles que leurs contrôles sains et que le traitement avec HA+BB. Chaque rat possède des caractéristiques biologiques différentes (épaisseur et module du cartilage,) de ses articulations, la perte de module élastique a ainsi été calculée par rapport au genou non chirurgié pour chaque rat (n=5) afin de normaliser les résultats. Malgré les grandes variations obtenues entre chaque rat, une première tendance se dessine puisque sans traitement ou avec traitement avec HA seul, une perte de module élastique du cartilage d'environ 40 % a été observée (35 ± 5 % pour le sans traitement, 42 ± 35 % pour le traitement à HA) contrairement au traitement avec HA+BB qui présente une perte de 2 ± 39 %). Ces résultats sont bien entendu très préliminaires et nécessitent une augmentation du nombre de répétitions et une corrélation avec les autres expériences effectuées sur ces articulations.

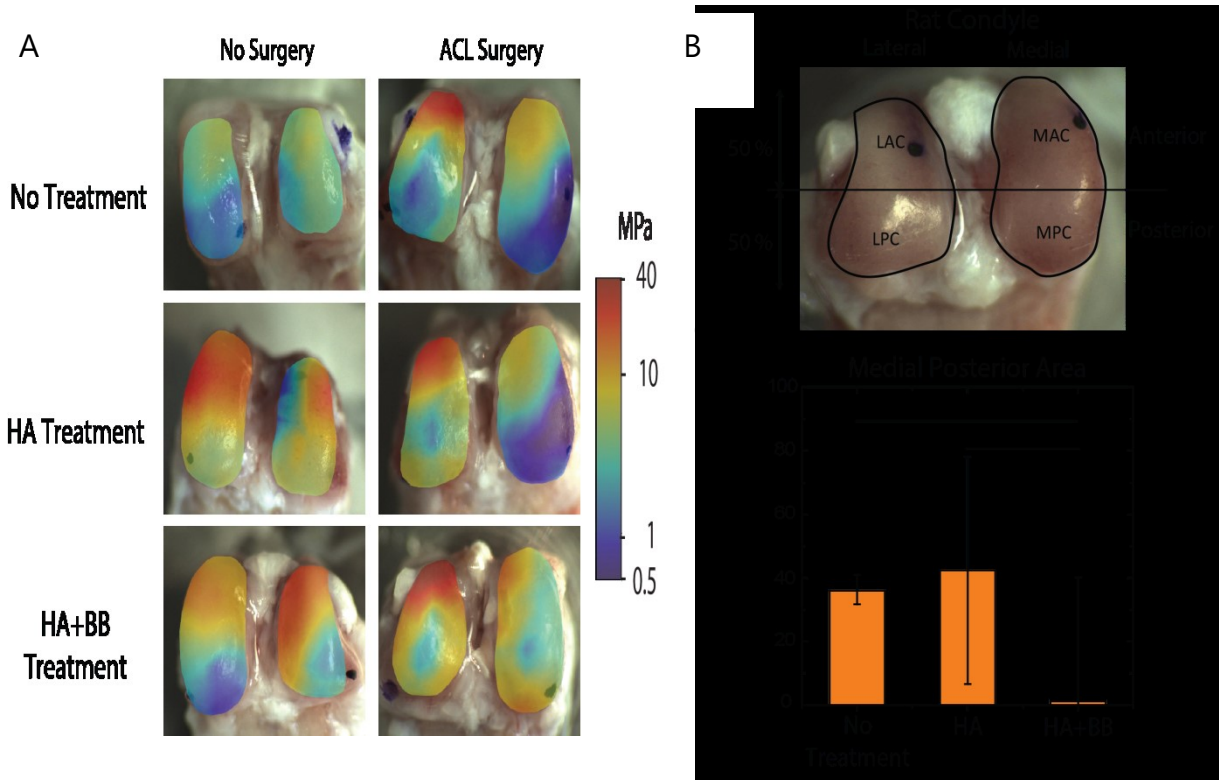

Figure B.5. *Résultats obtenus lors du test d'indentation-compression. (A) Cartographie en module de quelques articulations (contrôle et chirurgie) après induction de l'OA sans traitement, avec injection de HA et de HA+BB ; (B) profils d'un condyle de rat et définition des quatre zones d'intérêt (médial/latéral, antérieur/postérieur) ; (C) perte de module élastique des articulations chirurgiées par rapport à l'articulation saine dans la zone médiale postérieure du condyle (mpc).*

Références

1. Kaufman, G. N.; Zaouter, C.; Valteau, B.; Sirois, P.; Moldovan, F., Nociceptive tolerance is improved by bradykinin receptor B1 antagonism and joint morphology is protected by both endothelin type A and bradykinin receptor B1 antagonism in a surgical model of osteoarthritis. *Arthritis Res. Ther.* **2011,** *13* (3), R76.
2. Sim, S.; Chevrier, A.; Garon, M.; Quenneville, E.; Lavigne, P.; Yaroshinsky, A.; Hoemann, C. D.; Buschmann, M. D., Electromechanical probe and automated indentation maps are sensitive techniques in assessing early degenerated human articular cartilage. *J. Orthop. Res.* **2017,** *35* (4), 858-867.